



# First principles and proceedings of action-FRET : probing the molecular conformation of gas phase proteins and macro-ions

Geoffrey Knight

## ► To cite this version:

Geoffrey Knight. First principles and proceedings of action-FRET : probing the molecular conformation of gas phase proteins and macro-ions. Theoretical and/or physical chemistry. Université de Lyon, 2017. English. NNT : 2017LYSE1232 . tel-01767996

**HAL Id: tel-01767996**

**<https://theses.hal.science/tel-01767996>**

Submitted on 20 Apr 2018

**HAL** is a multi-disciplinary open access archive for the deposit and dissemination of scientific research documents, whether they are published or not. The documents may come from teaching and research institutions in France or abroad, or from public or private research centers.

L'archive ouverte pluridisciplinaire **HAL**, est destinée au dépôt et à la diffusion de documents scientifiques de niveau recherche, publiés ou non, émanant des établissements d'enseignement et de recherche français ou étrangers, des laboratoires publics ou privés.



N°d'ordre NNT :  
2017LYSE1232

## **THESE de DOCTORAT DE L'UNIVERSITE DE LYON**

opérée au sein de  
**L'Université Claude Bernard Lyon 1**

**Ecole Doctorale N° ED 52 -  
EDPHAST**

**Spécialité de doctorat :**  
**Discipline :** Physical chemistry

Soutenue publiquement le 13/11/2017, par :  
**Geoffrey D. Knight**

---

# **First principles and proceedings of action-FRET. Probing the molecular conformation of gas phase proteins and macro-ions.**

---

## **2017**

Devant le jury composé de :

Gerbaux, Pascal  
Charles, Laurence  
Pouilly, Jean-Christophe  
Demesmay, Claire

Chercheur qualifié FRS/FNRS  
Professeur  
Maître de conférences  
Professeur

Université de Mons  
Université Aix-Marseille  
Université Caen Normandie  
Université de Lyon

Rapporteur  
Rapporteuse  
Examineur  
Présidente

Dugourd, Philippe  
Macaleese, Luke  
Davesne, Dany

Directeur de recherche  
Chargé de recherche CNRS  
Professeur

Université de Lyon  
Université de Lyon  
Université de Lyon

Directeur de thèse  
Co-directeur de thèse  
Invité

---

# UNIVERSITE CLAUDE BERNARD - LYON 1

## **Président de l'Université**

Président du Conseil Académique

Vice-président du Conseil d'Administration

Vice-président du Conseil Formation et Vie Universitaire

Vice-président de la Commission Recherche

Directrice Générale des Services

**M. le Professeur Frédéric FLEURY**

M. le Professeur Hamda BEN HADID

M. le Professeur Didier REVEL

M. le Professeur Philippe CHEVALIER

M. Fabrice VALLÉE

Mme Dominique MARCHAND

## ***COMPOSANTES SANTE***

Faculté de Médecine Lyon Est – Claude Bernard

Directeur : M. le Professeur G. RODE

Faculté de Médecine et de Maïeutique Lyon Sud – Charles Mérieux

Directeur : Mme la Professeure C. BURILLON

Faculté d'Odontologie

Directeur : M. le Professeur D. BOURGEOIS

Institut des Sciences Pharmaceutiques et Biologiques

Directeur : Mme la Professeure C. VINCIGUERRA

Institut des Sciences et Techniques de la Réadaptation

Directeur : M. X. PERROT

Département de formation et Centre de Recherche en Biologie Humaine

Directeur : Mme la Professeure A-M. SCHOTT

## ***COMPOSANTES ET DEPARTEMENTS DE SCIENCES ET TECHNOLOGIE***

Faculté des Sciences et Technologies

Directeur : M. F. DE MARCHI

Département Biologie

Directeur : M. le Professeur F. THEVENARD

Département Chimie Biochimie

Directeur : Mme C. FELIX

Département GEP

Directeur : M. Hassan HAMMOURI

Département Informatique

Directeur : M. le Professeur S. AKKOUCHE

---

Département Mathématiques	Directeur : M. le Professeur G. TOMANOV
Département Mécanique	Directeur : M. le Professeur H. BEN HADID
Département Physique	Directeur : M. le Professeur J-C PLENET
UFR Sciences et Techniques des Activités Physiques et Sportives	Directeur : M. Y. VANPOULLE
Observatoire des Sciences de l'Univers de Lyon	Directeur : M. B. GUIDERDONI
Polytech Lyon	Directeur : M. le Professeur E. PERRIN
Ecole Supérieure de Chimie Physique Electronique	Directeur : M. G. PIGNAULT
Institut Universitaire de Technologie de Lyon 1	Directeur : M. le Professeur C. VITON
Ecole Supérieure du Professorat et de l'Education	Directeur : M. le Professeur A. MOUGNIOTTE
Institut de Science Financière et d'Assurances	Directeur : M. N. LEBOISNE

# Acknowledgements

First and foremost, I would like to thank my advisor, Dr. Philippe Dugourd who deserves my immeasurable gratitude. I thank him for all his contributions of time, ideas and funding that made my PhD possible. I am also thankful for the excellent example he has provided as a successful physicist and research group leader. The members of the group have contributed immensely to my personal and professional time at Lyon. The group has been a source of friendships as well as good advice and support. To all of the group members that have indirectly or directly participated in the success of this research mission, thank you: Antoine Rodolphe, Bertorelle Franck, Comby-Zerbino Clothilde, Mathilde Bouakil, Florian Trichard, Halim Mohammed Abdul, Macaleese Luke, Moncayo Martin Samuel, Motto-Ros Vincent, Rayane Driss, Caroline Bourgeois, Clothilde Zerbino, and Soleilhac Antonin. It is also a coincidental and tremendous pleasure to have worked alongside Kulesza Alexander and Daly Steven. At this laboratory group, I have also grown a kind appreciation to Frank Bertorelle, his practice, and knowledge in wet chemistry. All my thanks also to Chirot Fabien, for his help and advice. Many thanks also to Clément Capitain that I have come to meet lately in my final year, the same goes to Alexandre Resplandy and Marine Leprince. Thank you for being there. I also deeply appreciate the company and discussions with a past graduate student now onto their next research mission, Anne-Laure Simon.

Regarding the administration and help in settling in France, I thank Kervella Delphine, Sylvie Flores and all members of the Ulys team. For this dissertation I would also like to thank doctoral school directors Christophe Dujardin and Dany Davesne. Lastly, I would like to thank my family for all their affection and encouragement. For my parents who raised me with a love of science and supported me in all my aims and goals. Thank you. I also look forward to resuming on with LASERs and chemistry.

Geoffrey Knight, 16 Juin 2017.

# Abstract

In this thesis, I discuss the application and development of mass spectrometry (MS) - LASER coupled techniques for the characterization and measurement of trapped biomolecules in the gas phase. In broad terms, this thesis demonstrates the potential and perspectives of action-FRET a novel structural biology tool amenable to the gas phase. The fundamentals rely on a well attested resonance quantic process known as Förster resonance energy transfer (FRET). As of yet it has been a widely utilized method to scrutinize molecular structure in solution. The motivation has been to transpose this occurrence to the instrumental settings of a mass spectrometer, its gas confinement and, in doing so, overcome the earlier limitations of the technique and stride into the theoretical and experimental study of well determined systems as well as those whose structure were presently undetermined - all without the influence of the environment of a solvated medium.

The first chapter of this thesis offers a general overview on peptides and proteins plus how they can be studied. Subsequent chapters include how the work carried out herein adds towards their study, moving the technique towards a gold standard of native mass spectrometry (native MS).

In the second chapter, a treatment of the synthetic steps and preparations is given detailing the mechanistics of the reactions at play and above all outlining the experimental procedures and providing any information on any observations made.

The third chapter describes, and is devoted to an introduction of the instrumental setup outlaid as it stands giving an account on the LASER, optical pieces and the mass spectrometer employed throughout the course of this thesis, effectively setting the premises of thought and understanding for subsequent chapters and methodology.

Chapter four presents energy transfer, in particular to the Foster Resonance Energy Transfer and furthermore outlines the developed technique central to the mass spectrometry method to look at donor-acceptor chromophores espoused to biomolecular systems and their photofragments — what is nicknamed as action-FRET.

Chapter five reviews and discusses the study of a macromolecule: Ubiquitin, by action-FRET. The first gas phase experiment on the protein to have ever been realised. The information and content gathered from this adapted experiment is compared to work found elsewhere giving an appraisal on the potential of action-FRET and providing an idea to what future insights the technique could bring.

In chapter six the reader is introduced to the project of establishing action-FRET in the negative mode of the mass spectrometer's ionization source as opposed to its positive mode. Suitable pairs of donor-acceptor chromophores to validate the energy transfer under a negative regime were explored. These were profiled and characterized before being adapted to a biomolecular

---

system. The results provide a different flavor of complimentary structural and conformation information, the first of its kind for negative mode action-FRET.

The seventh and final chapter is devoted to future developments. The conclusive work tends to grant a further understanding of neurodegenerative diseases that afflict our societies. Chiefly that of the likes of Alzheimer's: it's the mechanism of action pertinent to other neurodegenerative pathologies; Parkinson's, Huntington's but also prion diseases or amyloid neuropathy. In doing so a contribution is presented on a way to trace a strategy in how to tackle and treat such diseases.

## Keywords

FRET, action-FRET, ubiquitin, amyloid-beta protein, mass spectrometry, LASER, conformation.

## Résumé

Mon travail de thèse aborde différents développements physico-chimiques qui reposent sur le principe de transfert d'énergie par résonance de Foster (FRET). Le but est de parvenir à étudier et caractériser des assemblages moléculaires ainsi que des changements structuraux de biomolécules (ou macro-ions) en phase gazeuse. Le transfert d'énergie par résonance de type Förster est un procédé par lequel de l'énergie s'échange de manière non radiative entre un chromophore dit donneur dans un état excité et un second chromophore accepteur en proximité directe. Conventionnellement, cette technique permet de localiser et déterminer l'écart entre deux molécules (de l'ordre de 10 à 100nm). Principalement utilisée pour étudier des systèmes biologiques, des résultats marquants ont été obtenus sur l'étude de système tel que l'appareil de Golgi, le cytosquelette ou les membranes cellulaires. Elle n'est cependant appliquée qu'à des systèmes en phase liquide. Il nous a paru intéressant de transposer cette technique en phase gazeuse, en utilisant la capacité des spectromètres de masse à sélectionner, isoler et activer des espèces moléculaires, nous permettant d'obtenir de nouvelles informations structurales.

Une grande partie de ma thèse a consisté à premièrement, valider le concept de FRET en phase gaz puis à développer et optimiser, la technique FRET dit 'd'action'. L'Action-FRET est une technique d'analyse par couplage de spectrométrie de masse et spectroscopie LASER mise au point par l'équipe SpectroBio afin d'étudier les molécules isolées en phase gazeuse. A travers ce dispositif, je me suis particulièrement investi à contrôler, étudier et caractériser l'évolution des conformations de biomacromolécules d'intérêt biochimique et biologique.

Dans une première partie je ferai une courte introduction générale sur les fondamentaux des protéines, de leur composition et élaboration en entités structurales complexes, diverses et fonctionnelles. La manière dont les protéines s'arrangent successivement en niveaux structural quaternaire est aussi décrite. La deuxième partie est consacrée à une présentation des chromophores utilisés. Je présente ensuite leurs utilisations et détaille la synthèse des édifices moléculaires produits pour réaliser les expériences de FRET. Ceux-ci sont constitués de composés biologiques (peptides ou protéines), couplés aux chromophores, (donneur-accepteur). Dans le contexte de ce chapitre se trouve également une discussion sur les mécanismes et produits utilisés lors de l'étape de conjugaison qui permet d'obtenir les composants désirés.

En troisième partie vient un chapitre qui relate le fonctionnement des appareils utilisés dans le montage expérimental; le LASER et le spectromètre de masse. La méthode de couplage est décrite et spécifiée, détaillant comment les appareils commerciaux ont été modifiés pour interagir avec l'un avec l'autre. Avec ce nouveau montage, un suivi de la signature optique de FRET appartenant aux protéines entières greffées et à différents états de charge a été possible.

Le quatrième chapitre est dédié dans les premières sections à la théorie et l'état de l'art en ce qui concerne le FRET. Les éléments emblématiques et leurs applications en solution de ces dernières années et les travaux plus récents en phase gazeuse y sont présentés. Par ailleurs, nous avons voulu démontrer dans ce chapitre que nos diverses manipulations ont l'avantage critique de ne pas dépendre d'une mesure de l'émission de lumière suite au transfert résonant d'énergie. A la place, on dispose de la fragmentation spécifique de l'ion piégé du chromophore à travers l'analyse de masse conventionnelle du spectromètre de masse pour détecter et quantifier une manifestation de FRET. Nous démontrerons aussi la possibilité cette méthode appliquée à la biologie moléculaire. Proprement dit, nous étudierons les protéines amyloïde beta d'Alzheimer et montrerons comment leurs conformations jouent sur l'évolution, le développement et



---

la formation de fibrilles pathogéniques qui sont les promoteurs de nombreuses maladies tel que Parkinson, Huntington mais aussi les maladies de prion, certains diabètes ou amyloïde neuropathique. Au cours de ma thèse une collaboration avec des chercheurs de Mons a aussi vu le jour. Ensemble, une étude d'action-FRET sur des complexes supramoléculaires entre une protéine d'Alzheimer (greffée avec un donneur) et la molécule de beta cyclodextrine (greffé avec un accepteur) a été menée. L'avantage de cette technique a été le contrôle stœchiométrique et la capacité d'observer le système en isolé tout en et en sélectionnant l'état de charge voulu.

Les résultats de mon travail de recherche m'ont ensuite conduit à m'intéresser à une protéine d'intérêt biologique, l'ubiquitine. Pour cela, nous avons comparé la version naturelle avec des versions mutantes, greffés avec les chromophores pour devenir compatible à l'étude de FRET d'action en phase gazeuse. Nos résultats démontrent d'une part que les profils de conformation structurale de l'ubiquitine varient et dépendent du solvant utilisé pour l'électrospray. En effet, il y a une corrélation entre le solvant utilisé et les états de charges observables en spectroscopie de masse. Deuxièmement, nous confirmons qu'il est possible de mesurer l'inter-distance entre chromophores et valider, comme anticipé, une évolution de cette distance en accord avec l'augmentation de charges portées par la protéine. En effet la protéine se déroule et se déploie au fur et à mesure qu'elle gagne en états de charge. Finalement, des efforts ont été mis dans le développement de la technique de 'FRET d'action' en mode négatif. Il a notamment fallu développer des chromophores compatibles avec la polarité négative. Différents chromophores maleimides ont été étudiés et testés en tant que paire donneur-accepteur, puis dans un second temps implémenté sur des oligopeptides de longueurs différentes. Malgré tout, le travail sur l'utilisation de la technique demeure un défi, présentant des effets indésirables majeurs même et ce en dépit d'un travail assidu. Cette méthode ne se montra pas aussi stable que le FRET d'action en mode positif. Cependant, ce champ exploratoire reste large et pourrait faire ses preuves, et être tout aussi réussie que le FRET en mode positif qui contribue à l'amélioration de la connaissance de la bio-structure de protéines en isolation hors influence de son environnement biologique.

Dans un deuxième temps, plusieurs essais et amélioration du protocole de préparation d'échantillon de peptides ont fait partie de mon projet doctoral et ceux-ci ont contribué aux travaux d'IMS de l'équipe. Cette facette a pris une grande place dans mon travail : mettre aux points des synthèses de greffages reproductibles à haut rendement qui se limitent à des solvants compatibles avec la spectrométrie de masse. Au cours de cette investigation nous avons aussi caractérisé une série de chromophores potentiellement utiles pour l'étude native des biomolécules en piège à ions, dont l'éosine et l'éosine maleimide.

En conclusion, à travers ce manuscrit sont consignés les travaux expérimentaux de FRET dans un sens général mais aussi plus précisément, et avec le développement de l'action FRET. Cette rédaction apporte aussi une preuve de l'utilité du FRET en tant que technique pour étudier les distances de substances de manière empirique sur une échelle nanométrique. Il est espéré que le futur développement de nouveaux fluorophores et techniques de transfert d'énergie et de charge permettront de mieux appréhender les systèmes impliqués dans les travaux et thématiques de recherche prochaine.

# Contents

<b>Acknowledgements.....</b>	<b>iv</b>
<b>Introduction .....</b>	<b>xiii</b>
<b>Abstract.....</b>	<b>v</b>
<b>Keywords.....</b>	<b>vi</b>
<b>Résumé .....</b>	<b>vii</b>
<b>Contents .....</b>	<b>ix</b>
<b>List of symbols and abbreviations .....</b>	<b>xv</b>
<b>List of Tables.....</b>	<b>xviii</b>
<b>List of Figures.....</b>	<b>xix</b>
<b>List of Equations.....</b>	<b>xxiii</b>
<b>Chapter 1      Introduction.....</b>	<b>2</b>
1.1    Systems.....	3
1.1.1 Peptides and proteins.....	3
1.2    On the spectroscopy of peptides and proteins.....	8
1.2.1 Nuclear magnetic resonance.....	9
1.2.2 X-ray crystallography .....	9
1.2.3 Small angle X-ray scattering (SAXS).....	10
1.2.4 Circular dichroism (CD) spectroscopy .....	11
1.3    References :.....	14
<b>Chapter 2      Synthetic preparations. ....</b>	<b>16</b>
2.1    From chemical substrates to target compounds.....	16
2.2    Peptides and chromophores. ....	20
2.3    Synthesis .....	23
2.4    References :.....	28
<b>Chapter 3      Instruments. ....</b>	<b>30</b>
3.1    Mass spectrometry and the mass spectrometer.....	30
3.1.1 Electrospray ionization (ESI).....	32
3.1.2 The Detectors for MS.....	33
3.1.3 MS excitation and fragmentation methods .....	33

---

3.2	The mass spectrometer, LTQ Velos .....	35
3.2.1	Ion polarity modes .....	37
3.2.2	Electrospray ionization .....	37
3.2.3	Mass analyzer .....	38
3.2.4	Principle of the linear quadrupole ion trap .....	44
3.2.5	Summary of Mass Analyzer Operation .....	47
3.2.6	Ion detection system .....	48
3.2.7	Helium damping gas in the mass analyser .....	48
3.3	LASER source .....	49
3.3.1	Legend to Horizon OPO Layout .....	52
3.3.2	Horizon optical parametric oscillator blueprint .....	53
3.5	Installations .....	54
3.5.1	LTQ Velos and LASER UV-Vis coupling set-up. ....	55
3.5.3	LASER alignment .....	57
3.6	References : .....	58
<b>Chapter 4</b>	<b>FRET.....</b>	<b>60</b>
4.1	Types of energy transfer .....	60
4.1.1	FÖSTER .....	60
4.1.2	Foster Radius .....	65
4.1.3	Dexter or Electron Exchange Energy Transfer .....	65
4.1.4	Radiative coupling in atomic systems .....	67
4.3	Conventional FRET — Applications. ....	68
4.3.1	Selected applications of FRET in solution .....	68
4.4	Gas phase mass spectrometry & action FRET .....	86
4.4.1	Gas phase mass spectrometry .....	86
4.4.2	Action spectroscopy .....	88
4.4.3	Action FRET .....	88
4.5	Experimental and data analysis techniques .....	89
4.5.1	Inspection of the MS spectrum .....	89
4.5.2	Measuring fragmentation .....	90
4.5.3	On building FRET frameworks .....	91

---

4.5.4	Extracting FRET data .....	96
4.5.5	FRET efficiency determination .....	96
4.6	Studying amyloid-beta (12-28) alloforms using action-FRET .....	97
4.7	Action-FRET in application. Second study.....	109
4.8	References :.....	120
<b>Chapter 5</b>	<b>Ubiquitin. ....</b>	<b>126</b>
5.1	Ubiquitin's identity .....	126
5.1.1	Function and mechanism .....	127
5.2	Ubiquitin in the gas phase.....	127
5.3	Ubiquitin FRET in the condensed state.....	129
5.5	Action-FRET on Ubiquitin in the gas phase.....	130
5.5.1	Method.....	130
5.5.2	Results and discussion .....	132
5.6	On FRET efficiency determination: Ubiquitin framework.....	138
5.7	References :.....	142
<b>Chapter 6</b>	<b>Negative action FRET.....</b>	<b>144</b>
6.1	Honing into negative action-FRET. Introduction. ....	144
6.1.1	Mass Spectrometry and Optical Spectroscopy.....	144
6.1.2	Experimental.....	145
6.1.3	Results and discussion .....	146
6.1.4	Conclusion.....	151
6.2	A case of action-FRET II in the negative mode.....	151
6.2.1	Materials and methods.....	152
6.2.2	Results and discussion .....	152
6.2.3	Conlusion.....	167
6.3	Outline on encountered difficulties. ....	167
6.4	References :.....	168
<b>Chapter 7</b>	<b>Future developments. ....</b>	<b>170</b>
7.1	Conclusion and general perspectives .....	170
7.1.1	Conclusion.....	170
7.1.3	Future developments.....	171



---

# Introduction

The early use of Förster Resonance Energy Transfer (FRET) to study conformation in the liquid phase has proven particularly useful and is a well-tested and accurate structural tool. However, differentiating molecules of interest with no bias or interference from neighbouring interactions is a challenge which has yet to be solved. This problem has fuelled the recent development of transposing FRET to mass spectroscopy techniques. My doctoral research has focused on progressing with this recent technological advancement.

The research undertaking has taken to address the challenge to study trapped biological molecules in the solvent-free confinement within a mass spectrometer. The advantage of the approach is that it allows to select and follow the conformational changes and evolution of biomolecules (peptides and proteins e.g. ubiquitin) in gas phase isolation without any undesirable influence that would be found in its direct solution environment. Towards this end, we have developed a custom built coupled laser mass spectrometry interface to a workstation. Whereby a beam of tuneable coherent light is deviated and aimed through the back electrode of the dual linear ion trap so to interact and excite ions of interest within the cavity of the mass spectrometer. This enabled us to study the photophysics of the trapped ions and their conformation, and report on their findings.

The Gaseous ions in question are formed using electrospray ionization (ESI). From the multiple charge states that are produced and by selecting and isolating the species of interest, ejecting all others, it is then possible to examine different charge states of a molecule and donor acceptor built frameworks individually. These are then taken to interact photo-physically with the tuneable laser whose energy induces changes in quantum states and dissociation of the trapped species. A produced photon pulse enters the first cell of a dual linear ion trap such as to react with a pair of donor acceptor chromophores (dyes) pre-assembled onto the protein or peptide molecule.

The action spectroscopy, the spectrometric evolution of the breakdown of the acceptor as a function of wavelength, giving unique specific photofragments is detected and registered to report a FRET efficiency. The technique was nicknamed as action-FRET and has the unique advantage in that it sidesteps the need to monitor fluorescence unlike other spectroscopy methods. By this way, the early objective which was to build the proof of principle of action-FRET and elucidate the molecular conformations of small alanine peptide of differing chain length using Rhodamine 575 and QSY7 donor acceptor pair of chromophores, was validated.

This action-FRET developed technique was then taken to reach the more challenging goal to study biomolecules of biological interest: first ubiquitin and then the amyloid beta protein. These biomolecules of greater three dimensionalities are described in this thesis. Information on both ubiquitin and Alzheimer proteins, on their spatial geometry and conformation as a function of charge state were determined.

---

In a later experiment, the objective of scrutinising amyloid beta protein complex with amino- $\beta$ -cyclodextrin in gas confinement was established. It has also provided real term answers to the structural arrangement of an amyloid protein segment in a host-guest interaction with a cyclodextrin molecule in gas isolation. Finally, efforts were made to test and validate the action-FRET technique in the negative mode (specifically looking at peptides; CAC, CA<sub>3</sub>DA<sub>3</sub>C and CA<sub>3</sub>DA<sub>3</sub>DA<sub>3</sub>C). During this research, we came across many difficulties, mainly in the synthesis and isolation of the compounds of interest needed to generate the ion products of a desired charge state with sufficient spectral quality to carry out experimental manipulations.

In summary, the aim of this dissertation has been to demonstrate and give results on isolated species in gas confinement and study their action spectroscopy response in rapport to the FRET mechanism which has the advantage to provide an overview insight on the intrinsic properties and characteristics of biomolecular systems without bias and without perturbations that would have existed in the condensed medium. As with the gas phase action spectroscopy approach any bias or interference from neighbouring species, ensemble average or molecular biochemical effects are insignificant. The work carried out herein is important as action-FRET provides the development of a new quantitative structural tool that can glean new light on biomolecules in the interest of structural biology and biochemistry which are not accessible or not as directly available when using conventional biochemical approaches. Action-FRET also has its interest as it is useful to validate the mechanisms and distance structural relationships developed by computer molecular dynamics models produced by group co-researchers.

---

# List of symbols and abbreviations

A	Acceptor specific fragmentation yield
AC	Alternating current
AChR	Acetylcholine receptor
ALCP	Absorbance of left circularly polarized light
Amu	Atomic masse unit
AR	Anti reflective
ARCP	Absorbance of right circularly polarized light
ATP	Adenosine triphosphate
BBO	Beta barium borate <i>i.e.</i> $\beta$ -BaB <sub>2</sub> O <sub>4</sub>
BODIPY	4,4-difluoro-4-bora-3a,4a-diaza-s-indacene
C4	Butyl-type hydrocarbon chain with four carbon atoms
CA	Collisional activation
CAD	Collisionally activated dissociation
cAMP	Cyclic adenosine monophosphate
CCS	Collision cross section
CD	Circular dichroism
CyD	Cyclodextrin
CFP	Cyan fluorescent protein
CID	Collision induced dissociation
CMR	Mean residue concentration
CP	Consensus peptide
CPU	Central processing unit
CRM	Charge residue model
CTMR	5-carboxytetramethylrhodamine
DABCYL	4-{(E)-[4-(Dimethylamino)phenyl]diazenyl}benzoic acid
DC	Direct current
DHP	Dihydropyridine
DMBODIPY	[( <i>-</i> )-1,4-dihydro-2,6-dimethyl-4-2-(2-trifluoromethylphenyl)-3,5-pyridinedicarboxylic acid 2-[4,4-difluoro-5,7-dimethyl-4-bora-3a,4a-diaza-3-(s-indacene)propionylamino]ethylethylester)]
DMSO	Dimethyl sulfoxide
DNA	Deoxyribonucleic acid
DNP	2,4-dinitrophenyl
DTT	Dithiothreitol
ECD	Electron capture dissociation
EDANS	5-[(2-Aminoethyl)amino]-1-naphthalenesulfonic acid
EGF	Epidermal growth factors
ESI	Electrospray ionisation
EET	Excitation energy transfer



---

FAM	Fluorescein amidite
FRET	Fluorescence or Föster resonance energy transfer
FT-ICR	Fourier transform ion cyclotron resonance
FWHM	Full width at half maximum
GFP	Green fluorescent protein
GMP	Guanosine monophosphate
G-proteins	Guanine nucleotide-binding proteins
GPCR	G protein-coupled receptors
HCD	High energy collisional activation dissociation
HIV-1 PR	Human immunodeficiency protease
HOMO	Highest occupied molecular orbital
HPLC	High-performance liquid chromatography
IADANS	8-Hydroxy-9-oxo-9H-xanthen-2-yl $\beta$ -D-glucopyranosiduronic acid
IASF	Intensity of acceptor specific fragmentation
IEM	Ion evaporation model
IgE	Immunoglobuline E
IMS	Ion mobility spectroscopy
ITIC	Intensity of the total ion count or chromatogram
IRMPD	Infrared multiple photon dissociation
LCMO	Low mass cutoff
LID	Laser induced dissociation
LIT	Linear ion trap
LTQ	Linear trap quadrupole
LUMO	Lowest unoccupied molecular orbital
LY	Lucifer Yellow CH
MD	Molecular dynamics
MS	Masse spectrometry or mass spectroscopy
m/z	Masse ratio of a charged ion
NBD	7-nitro-2, 1, 3-benzoxadiazol-4-yl
NMR	Nuclear magnetic resonance
nsL-TP	Nonspecific lipid transfer protein
OPO	Optical prametric oscillator
Pdb	Protein databank
PCR	Polymerase chain reaction
PC-TP	Phophatidylcholine-specific transfer protein
PEG	Polyethylene glycol(s)
Q00	First quadrupole piece
Q0	Second quadrupole piece
Q1	Octapole
QSY	Carboxylic acid succinimidyl ester, nomenclature varies for specific versions
R575	Carboxyrhodamine 575 C <sub>5</sub> -maleimide

---

REACH	Resonance Energy-Accepting Chromoprotein
REMD	Replica exchange molecular dynamics
Rf	Radio frequency
ROX	Carboxy X-rhodamine
SAXS	Small angle X-ray scattering
SNP	Single nucleotide polymorph
smFRET	Single molecule FRET
STR	Short tandem repeats
SUMO	Small ubiquitin like modifier
TC	Transfer close
TCEP	Tris(2-carboxyethyl) phosphine
TDI	Template directed dye terminator incorporation
TI	Transfer initialise
TIC	Total ion count
TO	Transfer dwell
TOF	Time of flight
TAMRA	6-carboxy-tetramethyl-rhodamine
Ubc	Ubiquitin carrier protein
UBI	Ubiquitin, associated to ubiquitin mutant
Ubl	Ubiquitin-like modifier protein
UV	Ultraviolet
UV-Vis	Ultraviolet visible
Ve	Voltage
YAG	Yttrium aluminium garnet
YFP	Yellow fluorescent protein
XRF	X-ray fluorescence spectroscopy
EDXRF	Energy dispersive X-ray fluorescence spectroscopy
WDXRF	Wavelength dispersive X-ray fluorescence spectroscopy
$\lambda_A$	Excitation wavelength of the acceptor
$\lambda_D$	Excitation wavelength of the donor
$\Phi$	Fluence

# List of Tables

Table 2.1.1. Reaction conditions for QSY9-CA3DA3C-ATTO514. ....	19
Table 2.2.1. The catalogue of chromophores used in the research theme. ....	21
Table 2.2.2. Peptides. ....	22
Table 2.3.1. Available solvents used in experiments. ....	26
Table 3.2.1. Characteristics of the LTQ Velos. ....	46
Table 3.3.1. OPO items. ....	52
Table 4.1.1. Typical values of $R_O$ [10]. ....	65
Table 4.3.1. Energy transfer parameters and spectroscopic constants. ....	73
Table 4.5.1. Catalogue of expected $m/z$ values and calculated exact mass of species of interest. ....	89
Table 4.6.1. Summary compiling the measured and calculated collision cross sections and action FRET data. ....	100
Table 5.6.1. Major fragment peaks observed in the LID mass spectrum of [d-UBI-a +8H] <sup>10+</sup> initiated by photon irradiation at either 545 nm or 505 nm. ....	139
Table 6.2.1. Absorption maxima ( $\lambda_{\max}$ ) in the gas and solution phase and fluorescence maxima ( $\lambda_{\text{fl}}$ ) for QSY9 and ATTO514 where available. ....	152
Table 6.2.2. The fragmentation species. ....	158
Table 6.2.3. The structures of the breakdown species. ....	158
Table 6.2.4. Peak position, height and area for donor and acceptor and the FRET efficiency scores. ....	166

# List of Figures

Figure 1.1.1. The $\alpha$ position on an amino-acid residue. ....	4
Figure 1.1.2. The amino-acid zwitterion. ....	4
Figure 1.1.3. Protein derived amino acids and their letter codes. ....	5
Figure 1.1.4. Peptide coupling, the condensation reaction. ....	6
Figure 1.1.5. The torsional angles in the backbones of proteins. ....	6
Figure 1.1.6. Coercive structural interactions. ....	7
Figure 1.1.7. The structural levels of proteins. ....	8
Figure 1.2.1. Far UV CD spectra profiling various sorts of secondary structure. ....	12
Figure 3.1.1. The set-out of a Mass Spectrometer instrument. ....	31
Figure 3.1.2. Pictorial representation of the electrospray ionization (ESI). ....	33
Figure 3.2.1. The Thermo Scientific LTQ Velos. ....	35
Figure 3.2.2. Functional layout of the linear ion trap. ....	36
Figure 3.2.3. LTQ Velos mid-section mass filtering ion optics. ....	37
Figure 3.2.4. A functional representation of the ESI. ....	38
Figure 3.2.5. Pictorial diagram of a linear quadrupole. ....	40
Figure 3.2.6. Cross section of a quadrupole. ....	40
Figure 3.2.7. Stability diagram for a linear quadrupole analyzer. ....	42
Figure 3.2.8. Upper half of region I of the linear quadrupole. ....	42
Figure 3.2.9. $U/V = \text{constant}$ linked scan. ....	43
Figure 3.2.10. A pictorial depiction of the hyperbolic linear ion trap ....	44
Figure 3.2.11. Ion ejection paths, radial and axial. ....	45
Figure 3.2.12. An ion 'Scan out' representation. ....	47
Figure 3.3.1. Horizon OPO and Surelite laser. ....	49
Figure 3.3.2. Beta barium borate harmonic crystal. ....	51
Figure 3.3.3. Functional layout of the Horizon OPO. ....	53
Figure 3.5.1. The LASER-MS appliance. ....	54
Figure 3.5.2. A brief outline on the setup used to modulate power. ....	55
Figure 3.5.3. A panel illustrating the synchronisation between the triggering from the MS computer, the shutter mechanics, and the laser wave pulsing. ....	56

---

Figure 4.1.1. FRET described in a Jablonski diagram.....	61
Figure 4.1.2. The spectra of a pair of fluorescent dyes .....	61
Figure 4.1.3. Spectral excitation-adsorption bands.....	62
Figure 4.1.4. Angles describing the orientation of the dipoles .....	63
Figure 4.1.5. Functional mechanisms – Energy level diagrams .....	66
Figure 4.3.1. Illustration on the procedure for measuring unfolding rates by energy transfer .....	69
Figure 4.3.2. Figures on F-actin .....	70
Figure 4.3.3. Fluorescence energy transfer figure.....	71
Figure 4.3.4. Equilibrium binding properties and pharmacological profile of DMBODIPY-DHP binding to L-type $\text{Ca}^{2+}$ channels using FRET .....	72
Figure 4.3.5. Time evolution of a doubly labelled DNA .....	75
Figure 4.3.6. FRET in the context of DNA hybridisation .....	76
Figure 4.3.7. Operation of the molecular beacons.....	77
Figure 4.3.8. Chemiluminescence induced by differently coloured molecular beacons to the addition of a target.....	78
Figure 4.3.9. Double labelled probe: 16-base oligodeoxyribonucleotide.....	79
Figure 4.3.10. Illustrative diagram of model used to fit the FRET data.....	80
Figure 4.3.11. Linear correlation between fusion index and $\Delta R'$ .....	82
Figure 4.3.12. Voltage sensitive FRET mechanism.....	83
Figure 4.3.13. Quenching of the EDANS fluorophore .....	84
Figure 4.3.14. Fractional saturation of Zn (CP-L-F) as a function of Zn (II) added .....	85
Figure 4.4.1. The mechanism of evolution in prior to ESI of the structure of a globular protein (e.g. cytochrome c, ubiquitin).....	87
Figure 4.5.1. Spectrum: QSY7-amino- $\beta$ -cyclodextrin FullMS.....	90
Figure 4.5.2. QSY7-AAK <sup>+</sup> QSY7-CID (normalised collision energy of 27) and LID .....	91
Figure 4.5.3. Breakdown sites of the acceptor chromophore QSY .....	92
Figure 4.5.4. Acceptor, QSY7-AAK <sup>+</sup> optical action spectrum.....	92
Figure 4.5.5. QSY9 solution absorption spectrum.....	93
Figure 4.5.6. Donnor, Rh6G-AAK <sup>+</sup> optical action spectrum. ....	94
Figure 4.5.7. (Rh6G-AAK-Rh6G) <sup>2+</sup> optical action spectrum.....	95

---

Figure 4.5.8. (Rh6G-AAK-QSY7) <sup>2+</sup> optical action spectrum .....	95
Figure 4.6.1. CCS plotted against FRET efficiency .....	100
Figure 4.6.2. Representative conformations .....	101
Figure 4.6.3. The Ramachandran plot for poly alanine. ....	102
Figure 4.6.4. Ramachandran plots .....	103
Figure 4.6.5. Ramachandran plots .....	104
Figure 4.7.1. Selected host-guest partners for experimentation .....	109
Figure 4.7.2. Action spectrum of mass selected [amino-β-CyD-QSY] <sup>+</sup> . ....	111
Figure 4.7.3. Gas phase fragmentation mass spectra .....	112
Figure 4.7.4. CID (normalised collision energy set at 15, 10) mass spectra of binary complexes .....	113
Figure 4.7.5. LID mass spectra (545nm excitation) of binary complexes containing Rh-CAβ and amino-β-CyD-QSY7 as the guest and the receptor, respectively .....	114
Figure 4.7.6. LID (505nm) of mass selected [AβC-Rh575+H] <sup>2+</sup> ions irradiated with a single laser pulse (2mJ). ....	115
Figure 4.7.7. LID (505nm) mass spectrum of mass selected [AβC-Rh575+H] <sup>3+</sup> ions irradiated with single laser pulse (5mJ). ....	115
Figure 4.7.8. Action spectra .....	116
Figure 4.7.9. Branching ratio .....	117
Figure 4.7.10. Branching ratio .....	118
Figure 5.1.1. Seventy-six residue long ubiquitin (X-ray, 1.5Å, monomer state) adapted from swiss-model .....	126
Figure 5.5.1. Ubiquitin mutant and chromophores .....	131
Figure 5.5.2. Bovine Ubiquitin erythrocyte mutant. ....	131
Figure 5.5.3. Circular dichroism signal .....	133
Figure 5.5.4. Mass spectrum following ESI of bovine ubiquitin .....	135
Figure 5.5.5. Collision cross section figure .....	136
Figure 5.5.6. Collision cross section results .....	137
Figure 5.6.1. Mass spectra of mass-selected [d-Ubi-a +8H] <sup>10+</sup> ions .....	138
Figure 5.6.2. Experimental FRET efficiency .....	140
Figure 5.6.3. FRET efficiency as a function of charge state .....	140

---

Figure 5.6.4. Representative folds of doubly grafted ubiquitin. Native like (†) and extended (‡) forms.....	141
Figure 6.1.1. Eosin-Y cystein negative mode fragmentation pathways, CID (top) and LID (bottom) at 490nm. ....	147
Figure 6.1.2. Action optical spectrum for EYM 1-, 2- and NBD-CYS. ....	148
Figure 6.1.3. Linear dependence of the fragmentation of CAADAAEAA with power. A one photon process. ....	149
Figure 6.1.4. Action optical spectrum for NBDmaleimide-CAKAC-Eosin.	150
Figure 6.1.5. FRET efficiency against charge state .....	150
Figure 6.2.1. Optical action spectra of [ATTO514] <sup>-</sup> and [QSY9] <sup>-</sup> .....	153
Figure 6.2.2. ATTO514-CAA (yellow curve) and QSY9-CAA (purple curve) normalized optical spectra. ....	154
Figure 6.2.3. Excitation and emission spectrum for ATTO514 in solution.	154
Figure 6.2.4. Optical absorption spectra of [ATTO514,QSY9] <sup>2-</sup> dimer overlaid against optical absorption spectra of [ATTO514] <sup>-</sup> and [QSY9] <sup>-</sup> .....	155
Figure 6.2.5. QSY-CAA LID and CID figure .....	157
Figure 6.2.6. Bond breaking sites of QSY9 molecule. ....	159
Figure 6.2.7. Comparing the [QSY-CAA] <sup>-</sup> spectra. ....	160
Figure 6.2.8. Branching ratio of the fragmentation efficiency .....	161
Figure 6.2.9. a) d-CAC-a (2- ) normalized optical spectra reserved to the <i>m/z</i> 625 specific photofragment b) loss of QSY9 <i>m/z</i> 980 c) loss of ATTO514 <i>m/z</i> 874. ....	162
Figure 6.2.10. Peptide ion optical spectra .....	163
Figure 6.2.11. Peptide ion optical spectra .....	164
Figure 6.2.12. Mobility profiles.....	166

---

# List of Equations

Equation 3.2.3.1 - Potential relations .....
Equation 3.2.3.2 - Potential relations .....
Equation 3.2.3.3 - Description of the electrical bias .....
Equation 3.2.3.4 - Mathieu expression.....
Equation 3.2.3.5 - Mathieu expression.....
Equation 3.2.3.6 - Identity of some terms.....
Equation 4.1.1.1 - Föster's relationship for molecular interaction.....
Equation 4.1.1.2 - Description of the orientation factor .....
Equation 4.1.2.1 - Description of the $R_0$ term.....
Equation 4.1.3.1 - Treatment of the Dexter process.....
Equation 4.5.2.1 - Fragmentation yield .....





# Chapter 1 Introduction.

The bullion of this dissertation: Foster resonance energy transfer (FRET), is a technique used to provide structural information on biomolecules and its setting. It is important to assimilate and recall on what is known in this arena, on molecular biochemistry. This priority is focused on in chapter one. The section sets out to give the essential background knowledge on proteins, their function and make up, together with a comprehensive on current methods of their structural analysis and spectroscopic characterization.

There is a mounting understanding that it is not only important to define a protein's structure but to also develop an idea on how this structure or conformer of the biomolecule evolves from primary all the way to quaternary structural arrangements (*cf.* structural organization of a real protein, transthyretin). An insight on gas-phase spectroscopic developments such as action spectroscopy is presented later, in chapter four, bringing about a way to address the problematic: finding ways in unveiling intrinsic biomolecular properties (also in gas isolation).

## 1.1 Systems

### 1.1.1 Peptides and proteins

Proteins routed from the Greek προτειος, “ranked first”, are complex molecules that play a major role, if not the most important, in the function and chemistry of living things. They are a class of natural polymers that make up, arguably, near 15% of our bodies with relative molar masses ranging from 6000 to 1,000,000 grams per mole [1]. Each biopolymer can fulfill a myriad of specialised or general tasks and purposes essential to the survival of bio-organisms. A brief review of these are underscored in the section below [2, 3].

- 1 . **Structure.** Cartilage, hair, wool, fingernails and claws are mainly protein. Viruses have an exterior layer of protein, shelling a nucleic acid core. Similarly, specialized proteins such as actin provide fundamental skeletal architecture to cells. Proteins called histones are fixated tightly to DNA, helping to fold and furl the DNA in an orderly fashion in chromosomes.
- 2 . **Motility.** Proteins are the principal substituents of muscle and permit the muscle to contract. Sperm movement is the result of protein filaments tightening in their tails. Protein structural change also governs chromosome motility important to cell division.
- 3 . **Catalysis.** The catalysis of chemical reactions by enzymes conditioned in biologics are almost always proteins.
- 4 . **Transport.** The obvious function of transport membrane proteins. Proteins that allows a controlled passage of substrates and ions to the cell. Another protein, hemoglobin is famously known to carry oxygen from the lungs to other tissues. By the same token the protein transferrin transports iron in blood plasma from the intestines (where the iron is absorbed) to the spleen (storage) and finally to the liver and bone marrow for synthesis.
- 5 . **Storage.** There are a variety of proteins that coordinate [4, 5] and stock ionic trace elements, among others. As mentioned above ferritin is responsible in dealing with iron.
- 6 . **Energy transformation and storage.** Useful work is derived from the chemical energy that is made available by muscle proteins such as myosin.
- 7 . **Protection.** A function managed by a class of their own, antibodies. These proteins tackle foreign substances and pathogens. They fixate themselves to those substances or cells termed antigens, providing us with immunity to a variety of diseases. Other protective proteic species, such as interferon exist with their own mode of action.
- 8 . **Control.** As hormones, insulin or glucagon for example, proteins are key in the transmission and control of chemical information that directs the metabolism of living organisms.
- 9 . **Buffering.** As proteins hold both acidic and basic functional groups exposed on their side chain, they tend to neutralise both acids and bases. Effectively purveying the buffering of blood and tissues.

The simplest structural entity or repeat unit (-mer) of the polymer that makes up a protein chain is an  $\alpha$ -amino-acid. Amino acids are fundamental building blocks that contain both a carboxylic group, an amino group and the side chain, the R substituent, one of about 20 groups. The  $\alpha$ -amino acids are the most important class of these compounds, Figure 1.1.1.

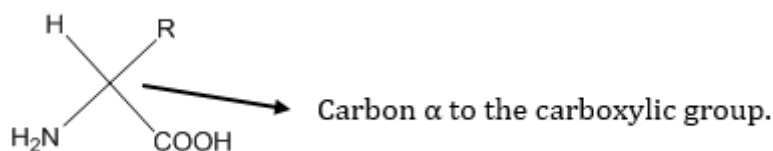


Figure 1.1.1. The  $\alpha$  position on an amino-acid residue.

They are zwitterionic by nature and also amphoteric *i.e.* they contain both an acidic (-COOH) group as well as a basic (-NH<sub>2</sub>) group. In aqueous conditions at a specific pH solution (the isoelectric point) an amino acid exists mainly as the zwitterion, see Figure 1.1.2.

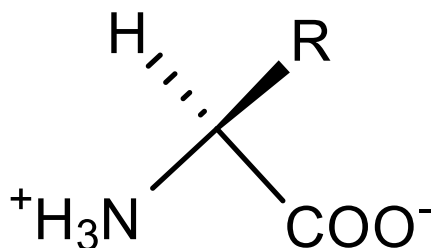


Figure 1.1.2. The amino-acid zwitterion.

These species are also chiral, with the single exception of the amino acid glycine. They have the same basic structure holding a stereocentre at the  $\alpha$  carbon. By convention they are more commonly referred as having an L- as opposed to a D-configuration. A catalogue of the 20 amino acids that are assembled under nucleic acid control in the synthesis of proteins are shown in Figure 1.1.3. below.

## Introduction

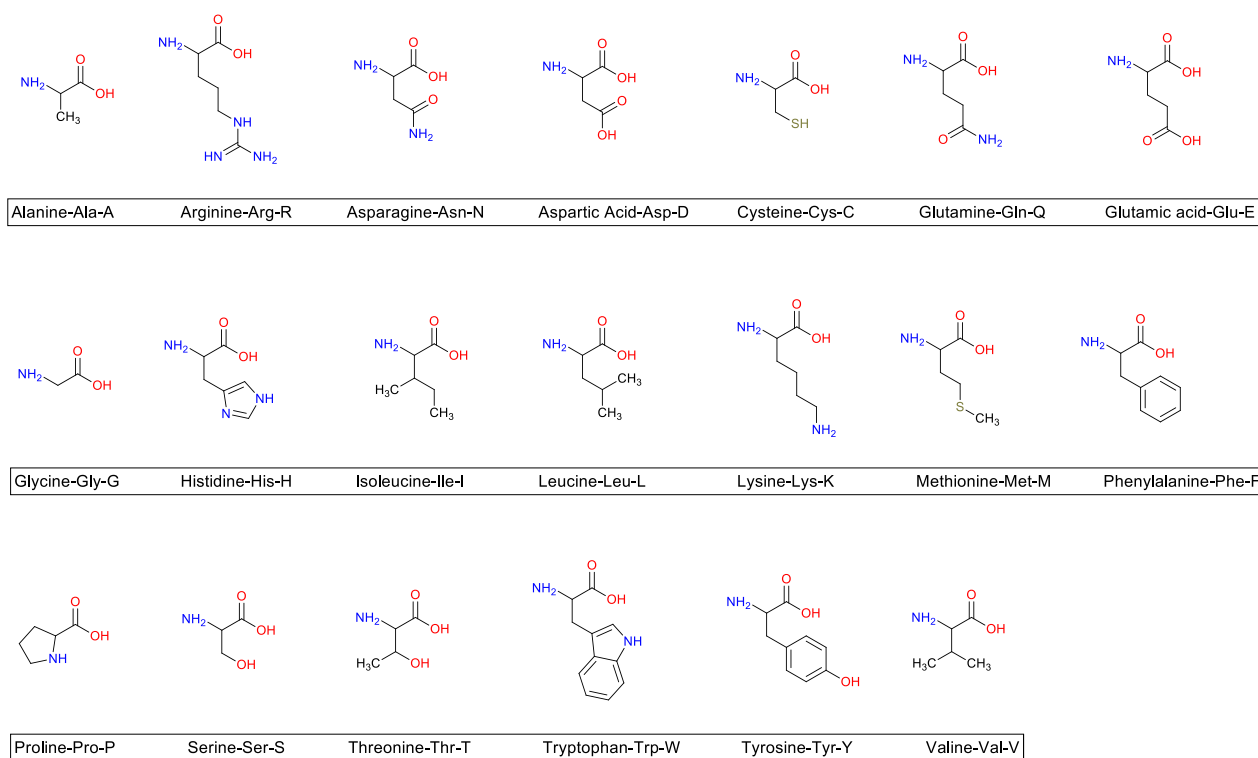


Figure 1.1.3. Protein derived amino acids and their letter codes.

Depending on the side chain group, the amino acids can be sub-divided into four classes: the polar and apolar and the basic and acidic. Comparing the side chains, apolarity is a property intrinsic to high carbon and hydrogen content amino acids and conversely amino acids with R groups with nitrogen and oxygen atoms will be polar. Again, depending on the availability of electron withdrawing groups and free electron pairs or protic groups among other sterical or electronic effects, an amino acid would respectably be basic or acidic. These essential features are important as they greatly affect the three dimensional structure of the protein and its propensity in being hydrophilic or hydrophobic, globular or fibrous [2].

Proteins are the fruit of the condensation reactions (giving of  $\text{H}_2\text{O}$ ) between amino acids forming amide bonds, Figure 1.1.4.

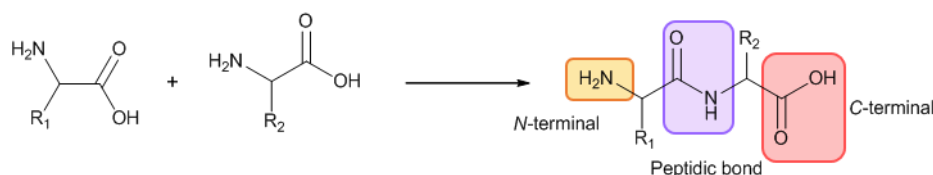


Figure 1.1.4. Peptide coupling, the condensation reaction.

The coupling reaction continues past the dipeptide stage, string along in a linear sequence of amino acids, until lengthening and yielding into protein. Strictly speaking, this means a chain of more than about fifty amino-acid residues. 'Peptide' is the appropriate nomenclature reserved for molecules with fewer amino acid residues than this.

Fully built up proteins and their systems show several echelons of structural architecture: a primary, secondary, tertiary and quaternary [2, 3]. The primary structure makes reference to the linear sequence of the amino acid chain with an understanding that the right is a carboxyl terminus and the left terminus is the free primary amine end. A sequence of amino acids connected by peptide bonds form a polypeptide chain with each amino acid unit in a polypeptide called a residue [2, 3]. In singular cases, the residues may reticulate into a network, a primary structure in which cross-links bond different chains (*cf.* cross-linked polyacrylamide). When primary structure is disrupted, one refers to what is commonly known as: degradation [6]. A natural property of the polymer are its torsional angles of its backbone named  $\phi$  (phi),  $\psi$  (psi) and  $\omega$  (omega) [7]. These dimensionalities are presented here below, Figure 1.1.5.

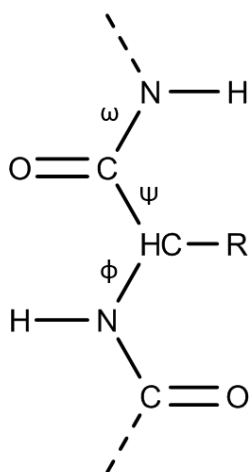


Figure 1.1.5. The torsional angles in the backbones of proteins.

The secondary structure encompasses in part the conformations that are energetically favoured by available bond rotations depending on hydrogen bonding between the lone pairs of the oxygen atoms in the carbonyl group pertaining to the peptidic backbone chain and the hydrogens bonded to the nitrogen of another amino acid of the polypeptide. This is how  $\alpha$ -helix, pleated sheets or  $\beta$ -sheets and finally structural arrangements come around. They are a result of intrachain (within a given protein chain) hydrogen bonding. The random-coil is a “wastebasket” conformational architecture that describes packet protein assembly, it is used to make the distinction from a total unraveled arrangement. Nevertheless, this does not exempt them from high control or specificity. Other structural denomination such as the “hairpin loop” that match well how residues arrange themselves have become popular within the community [2, 3]. From an informative standpoint, the loss of secondary structure is called denaturation [6]. The third echelon of order depicts how the various secondary structural folds come together giving the final geometry of the protein molecule [3]. This tertiary structure is given shape by a collection of interactions: ionic bonding (a), hydrogen bonding (b), covalent bonds (c), London dispersion forces between nonpolar groups and dipole-dipole interactions (e) [2]. These stabilizing forces, discussing the bonding types in this text are illustrated in Figure 1.1.6.

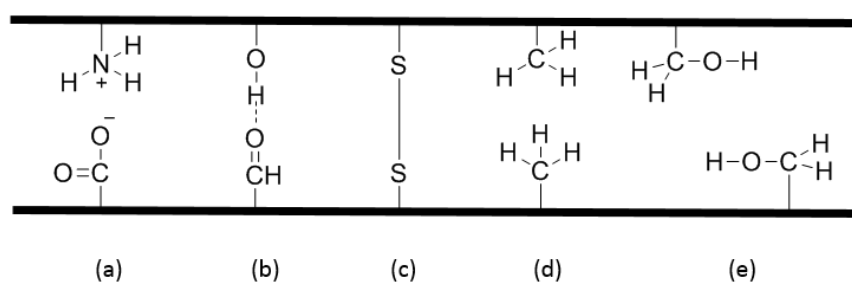


Figure 1.1.6. Protein interactions: (a) ionic bonding, (b) hydrogen bonding, (c) covalent bonds, (e) London dispersion forces between nonpolar groups and dipole-dipole interactions.

It is important to underline the importance of cysteine as it frequently stabilizes tertiary structure through disulfide bond formation. The thiol groups oxidise and react together to form a –S-S– covalent bond, effectively stapling the protein into shape. Other key specific chemistries spur the design of a protein, notably, the coordination of metals, linking of auxiliary components like haem, or compounds such as carbohydrates, phosphates groups, or lipids. Furthermore, acetylation, hydroxylation, methylation and carboxylation play a crucial role in the fate of a protein’s tertiary shape.

Finally, quaternary structure refers to the montage of multiple folded protein subunits and how they order themselves in three dimensional space [2, 3]. It is predominantly made feasible through interchain (between protein chains) hydrogen bonding. Organizations of the type denominate dimers and grander oligomeric complexes or indeed molecular machines. For example, haemoglobin, DNA polymerase and ion channels are recognized assemblies to have quaternary structure. In the same line of logic, the ribosome is a molecular machine that, bears quaternary structure. An overall outline of how the four echelons of structure stifle progressively

into structure is resumed in Figure 1.1.7 below. This representation is unique as it depicts the hierarchical structure of a real protein: transthyretin.

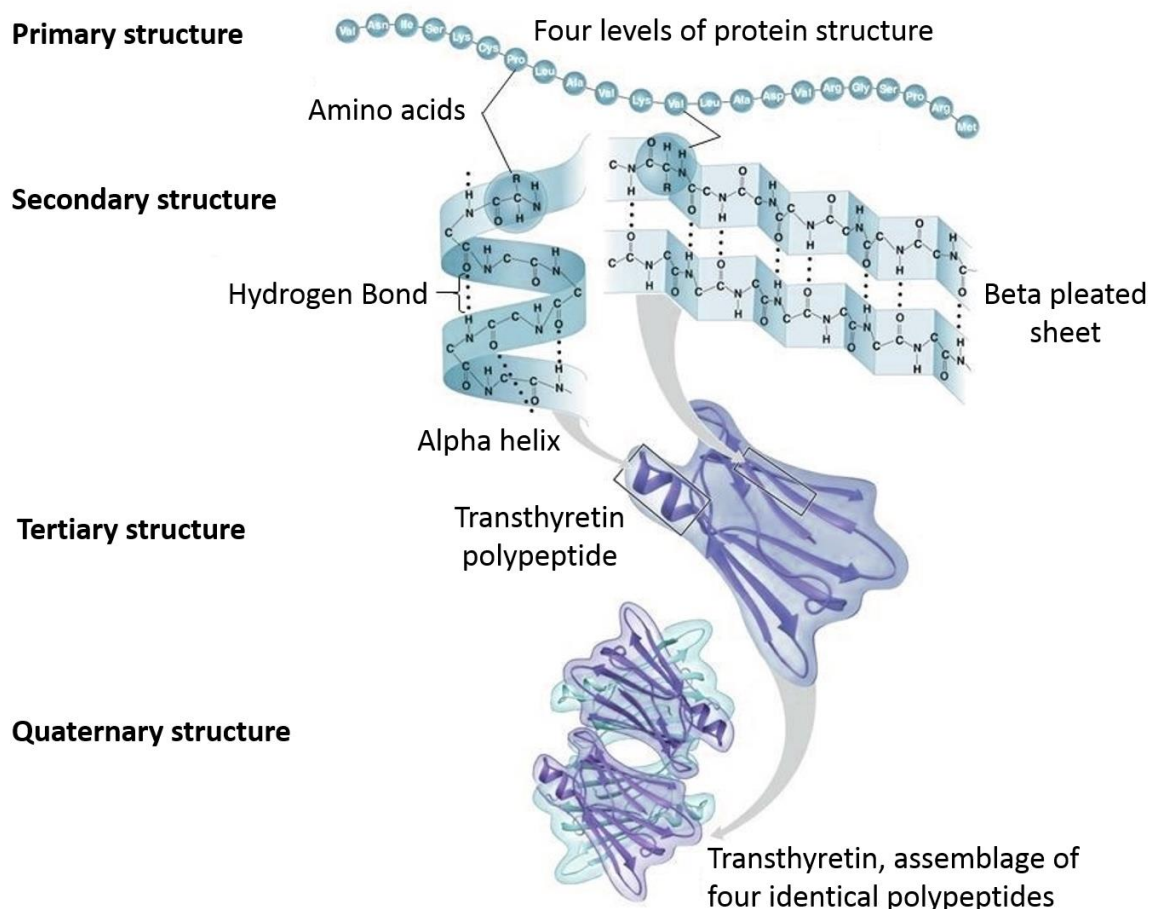


Figure 1.1.7. The structural levels of proteins.

## 1.2 On the spectroscopy of peptides and proteins

Peptides and proteins are biological macromolecules, they are the main actors in the makeup of life be it in the context of prospering diversity or in pathological disease. The question of their size, identity, composition and conformation (that weighs critically on function) has been revealed by spectroscopy. The principal and popular techniques that consign this field are:

mass spectrometry (MS) [5, 8-11], nuclear magnetic resonance (NMR) [3, 5, 8], X-ray crystallography [3, 5, 8, 12], small angle X-ray scattering (SAXS) [12, 13], circular dichroism (CD) spectroscopy [5, 6, 12]. The last four techniques are each a massive field in their own *i.e.* NMR, X-ray crystallography, SAXS, CD spectroscopy. Nevertheless, a brief overview of these is sectioned here.



### 1.2.1 Nuclear magnetic resonance

Fully as praiseworthy the technique has become to be, there have been six Nobel prizes awarded up till now to researchers dedicated to the subject. Today, the most well-known application of this spectroscopic method is magnetic resonance imaging or MRI. In a nutshell, NMR exploits the physical observation that nuclei in a magnetic field absorb and re-emit electromagnetic radiation. From this principle the magnetic properties of certain atomic nuclei can be used to assess intimate information about the structure, dynamics, reaction state and chemical environment of molecules. The first NMR instrument made available commercially was released in 1961 and gradual improvements in magnet technology have been made reaching ever stronger field strengths needed to uncover yet finer details on analytical compounds [8]. Nowadays, more than ever, it comes in a wide range of geometries and serves different purposes. One –dimensional NMR is routinely used by chemists to examine and identify inter-atomic structures in molecules. Two-dimensional techniques are deployed to determine how various atoms (their spins) relate to each other, most often in larger molecular frameworks. Time domain NMR spectroscopic methods are used to assay molecular dynamics in solutions. Furthermore, solid state NMR spectroscopy is useful in ascribing the molecular structure of solids. Other scientists have developed NMR methods for measuring diffusion coefficients [14]. The NMR technique finds a connection with the work of this thesis in that it was time ago used to unveil and assign the sequence and secondary structure of human ubiquitin [15]. In spite of recent advancements, sensitivity remains a limitation. In effect, as an alternating magnetic field is subjected on the sample, typically by radiofrequency radiation, the nuclei spin states change and as they relax back down in the absence of the field they emit the signals that define the species at study [8]. The pitfalls lie in the magnitude of energy difference between the spin states that is very minuscule. This means that the population differences between the spin states are also intricately small. In summary, NMR can somewhat be of an insensitive technique as only a small proportion of the nuclei generate a feedback that can be used to work out information on the analyte [16]. Another major bottleneck is achieving the required sample purity for analysis and even then, interpretation can prove difficult. Also, as new applications and markets are continuously found, NMR remains a professional instrument with a prohibitive cost (purchase and maintenance) and limit's it from being a democratic instrument, at the reach for many [16].

### 1.2.2 X-ray crystallography

Life around us comes in manner shapes and forms but the broadest categories admittedly take in amorphous and crystalline solids. X-ray crystallography can be set up to determine the physico-chemical composition of the latter range of objects. Its value stems from its non-destructive and potential for identification in a sample. Typical applications areas include paint, glass, pottery, ceramics, metals and alloys, soil, plastics and fabrics. The fundamental knowledge is gained by subjecting the crystalline solids (those that present a high internal arrangement of their components) to X-ray radiation. X-ray radiation that are wavelengths of the order of 0.001nm to 10nm and are the product of electrons decelerating or transitioning from an energy level to another within the shell of an atom [17]. The dispersed X-rays give a

unique diffraction pattern, in other words the light and dark areas on the detectors occur because the waves deflected from various atoms reinforce or cancel each other out. As the distance traveled after defraction depends on the distance between the atoms, the diffraction pattern can be used to determine how atoms are coordinated in space to one another. The technological advancement noticed its true significance when it led to the groundbreaking elucidation of DNA's structure in 1953. Pleasingly, from then on, the last decades have seen several variations of the technique (e.g. X-ray fluorescence spectroscopy (XRF), energy dispersive XRF crystallography (EDXRF) or even wavelength dispersive XRF (WDXRF) [17]). X-ray crystallography today continues to make huge impacts and produce motivating data in the discipline of biochemistry and the physical sciences. What is important to take on from this section is that the initial step of generating the diffraction pattern is moved on to a workflow that starts with elucidating the basic structural shape, more accurately phase information is solved. Then, the next step consists in taking the interpretative data to produce an electron density map, the model is taken to build up. Finally, the preliminary model is refined repetitively against the raw data, to a closing model where it is made sure no electron density rests unaccounted. The final model's quality is weighed with a percentage known as the R-factor, it is an expression of the agreement between the model and the data (typically between 0.15 and 0.20) [4]. This widely adaptive method that is X-ray crystallography is disadvantaged however in that firstly it is limited to scrutinising crystalline solids, liquid samples needing considerable sample preparation. These are taken to solidify through chemical treatment. In a second part, it still remains difficult to interpret, resolution can be an issue especially as the repeating unit of the crystal becomes larger and more complex. The difficulty also in obtaining crystals that diffract at high resolution exists, also it is important to realise that some protein molecules have resisted all attempts to crystallize them [4].

### 1.2.3 Small angle X-ray scattering (SAXS)

Small scattering of X-rays is a powerful diffraction method for examining the structure of matter. This analytical technique based on elastic scattering is used in various themes of work in science and technology, notably condensed matter physics, molecular biology and biophysics, polymer science and metallurgy. Take for example the combined efforts lead of by Hurley *et al.* [18]. The instrument that is SAXS crucially provides structural information at lower resolution (global shape of the protein, as well its quaternary and tertiary structures). The technique is geared towards molecular species in the order of 10-1000Å in size, making it a valuable not only to look at proteins but also macromolecular assemblages [12].

In a second part the instrument or measurements also play to extract feedback on:

- Radius of gyration.
- Molecular weight.
- Maximum particle dimension.
- Oligomeric state and organization in solution.
- Amount of native flexibility or unfoldedness.
- Visualisation of disordered regions that fall short to X-ray crystallography.
- Low resolution molecular envelope.

The methodology of SAXS relies on the study of scattered patterns of radiation that are the result of the influence a primary beam of light by a sample. This diffraction pattern associated to the superatomic lattice lies in a small angle region ( $0.1\text{-}10^\circ$ ), hence the name of the method. In this way, it is possible to derive back structural and spatial characteristics of a substance with a resolution determined by the wavelength of the radiation. Although limited to  $\sim 10\text{ \AA}$  resolution, SAXS can deliver a wealth of structural information on biomolecules in solution and is compatible with a wide range of experimental conditions. This is especially advantageous when other techniques, such as conventional crystallography, cannot be used. Furthermore, advanced use of SAXS can provide unique insight into biomolecular behavior that can only be observed in solution, such as large conformational changes and transient protein-protein interactions. Another major attraction has been the implementation of SAXS with synchrotron beamlines. In this way with the higher light densities it is possible to unveil different diffraction patterns, allowing further theoretical and experimental analysis of exquisite molecular substances or compounds. The projected work however suffers of a complex data analysis and the determination of a sample's make-up is not always straightforward. From a practical standpoint, the technique demands specialised working knowledge as many irregularities and operational choices are to be made in using the apparatus. Routine usage encounters difficulties related to the experimental device (e.g. spontaneous mechanical changes in instrument design, instability in beam dumping and electronic instability) but also real time variations of the analyte (*i.e.* temperature and destruction under radiation) [13].

#### 1.2.4 Circular dichroism (CD) spectroscopy

Circular dichroism is a major addition to visible and UV spectroscopy. Indeed, electronic spectra can reveal additional details of molecular structure when irradiating samples with polarized light, electromagnetic radiation with electric and magnetic fields that oscillate only in certain directions.

CD measures the difference in absorption of right and left circularly polarized light (cpl) by an analyte. The vector  $E$  that describes the electric field of cpl rotates about the direction of propagation once in each wavelength of the light. The electric vector can rotate either clockwise when looking towards the light source, corresponding to right-circularly polarized light (rcpl), or counterclockwise, left-circularly polarized light (lcpl). The apex of the electric vector of rcpl will describe a right-handed helix in space, whereas that of lcpl will generate a left-handed helix. To put it in another manner, cpl is chiral. Consequently, rcpl and lcpl will interact differently with a chiral molecule and exhibit different optical properties. A CD signal can be either positive or negative. Mirror image molecules, or enantiomers, have CD spectra that are the same with exception of their sign that is opposite. CD is exhibited not only off intrinsically chiral (optically active) chromophores, but also if a chromophore becomes effectively chiral by being covalently bound to a nearby chiral centre or placed in an asymmetric environment [5].

The distinct advantage of CD spectra is their capability to acquire and determine the configuration of complexes by referring and contrasting them to the CD spectrum of a similar complex of known chirality. Also, due to the fact that individual monomer units are chiral as is the helix in its entirety and in a unique way, CD spectroscopy provides considerable wealth of knowledge on the secondary structure of macromolecules. In sum different  $\alpha$ -helices share sparingly specific CD spectra. The same applies for  $\beta$ -sheets and random coils as they too display unique distinguishable spectral attributes. What CD spectro-polarimeters do is measure the difference in absorbance between the L and R circularly polarised components ( $\Delta A = A_L - A_R$ ). These are returned in the form as degrees of ellipticity ( $\theta$ ) in degrees. It is worthy of mention that  $\theta = \tan^{-1}(b/a)$  with  $b$  and  $a$  representing the minor and major axes of the resulting ellipse.

CD is very important in molecular biology as the amount of secondary structure composition (% helix, sheet, turns, etc.) from the peptide bond region can be assessed. In effect, the different sorts of ordered secondary structure found in proteins draw characteristic CD spectral patterns in the far UV, Figure 1.2.1.

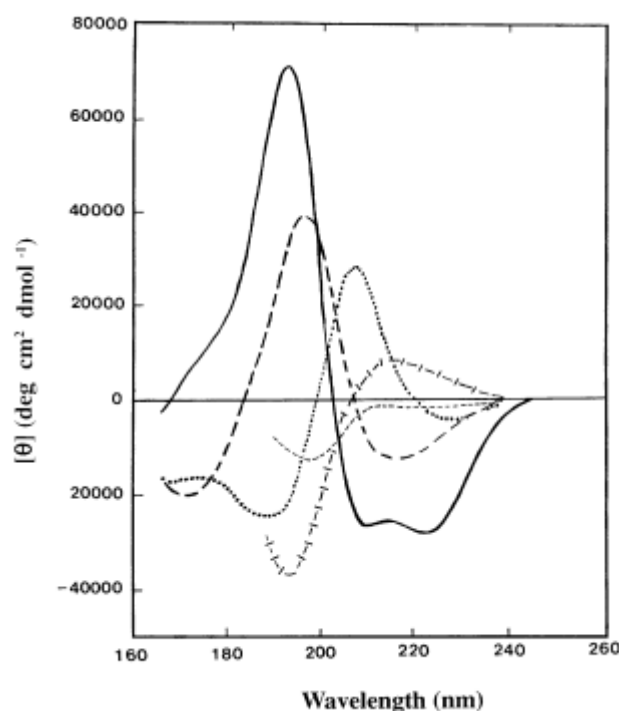


Figure 1.2.1. Far UV CD spectra profiling various sorts of secondary structure. Solid line,  $\alpha$ -helix; long dashed line, anti-parallel  $\beta$ -sheet; dotted line, type I  $\beta$ -turn; cross dashed line, extended  $3_1$ -helix or poly (Pro) II helix; short dashed line, irregular structure. Reprinted from Publication (Kelly SM, Jess TJ, Price NC: How to study proteins by circular dichroism. *Biochimica Et Biophysica Acta-Proteins and Proteomics* 2005, 1751:119-139). Copyright (2017), with permission from Elsevier.

It is important to bare in mind that CD in application to biological studies produces very small signals *i.e.* ellipticities are typically in the range of 10 mdeg, corresponding to a difference in absorbance ( $\Delta A (=A_L - A_R)$ ) of the order of  $3 \times 10^{-4}$ . It is therefore especially key to CD measurement to pay attention to the experimental conditions in order to ensure that meaningful data are obtained [19].

### Information available from CD studies of proteins

CD signals only arise where absorption of radiation takes place. Spectral profiles are ascribed to distinct structural characteristics of a molecule. The convenience of using CD in studies of proteins is that it uncovers complementary structural data of a sparse number of spectral regions. The photo-responsive relevant moiety chiefly includes the peptide bond (absorption below 240nm), aromatic amino acid side chains (260-320nm range of absorptions) and disulphide bonds (weak broad absorption bands around 260nm). The method has found equally useful in looking at flavins that are absorb over a wide spectral area. For example, pyridoxal-5'-phosphate absorbs at 300nm, flavins are sensitive to wavelengths of the 300nm to 500nm range (depending on oxidation state). Haem groups strongly respond to wavelengths around 410nm with other bands at 350nm and 650nm (depending on spin state and coordination of the central Fe ion). Lastly, induced CD signals may arise from ligands that acquire chirality when bound in an asymmetric framework such as that of a protein [19].

### 1.3 References :

1. Jones J: *Amino Acid and Peptide Synthesis*. 2 edn: Oxford University Press; 2002.
2. Zumdahl SS: *Chemical principles*. 3rd edn; 1998.
3. Berg JM, Tymoczko JL, Gregory J, Gatto J, Stryer L: *Biochemistry*. 8<sup>th</sup> edn; 2015.
4. Branden C-I, Tooze J: *Introduction to protein structure*. 2<sup>nd</sup> edn; 1999.
5. Creighton TE: *The physical and chemical basis of molecular biology*. Helvetian press; 2010.
6. Atkins P, Depaula, J.: *Atkins' physical chemistry*. 8th edn; 2006.
7. Holtje H.D. SW, Rognan D., Folkers G.: *Molecular Modeling. Basic principles and applications*. 3<sup>rd</sup>. edn: Wiley-VCH.; 2007.
8. Brodie R: *Spectroscopy product guide*. Royal society of chemistry; 2015.
9. Wysocki VH, Resing KA, Zhang QF, Cheng GL: **Mass spectrometry of peptides and proteins**. *Methods* 2005, **35**:211-222.
10. Strupat K: **Molecular weight determination of peptides and proteins by ESI and MALDI**. In *Mass Spectrometry: Modified Proteins and Glycoconjugates. Volume 405*. Edited by Burlingame AL. San Diego: Elsevier Academic Press Inc; 2005: 1-36: *Methods in Enzymology*.
11. Domon B, Aebersold R: **Review - Mass spectrometry and protein analysis**. *Science* 2006, **312**:212-217.
12. Kaltashov IA, Eyles SJ: *Mass spectrometry in biophysics*. Hoboken, New Jersey: Wiley; 2005.
13. Feigin LA, Svergun DI: *Structure analysis by small-angle X-ray and neutron scattering*. Plenum press; 1987.
14. Hornak JP: *The basics of NMR*. Rochester, NY.: Rochester Institute of Technology.; 1999.
15. Weber PL, Brown SC, Mueller L: **Sequential H-1-NMR assignments and secondary structure identification of human ubiquitin**. *Biochemistry* 1987, **26**:7282-7290.
16. Jeffries E: **Spinning into focus**. In *Chemistryworld*: Royal society of chemistry; 2014.
17. John R. Dean AMJ, David Holmes, Rob Reed, Allan Jones, Jonathan Weyers: *Practical skills in chemistry*. 2<sup>nd</sup> edn: Prentice Hall; 2011.
18. Boura E, Rozycki B, Herrick DZ, Chung HS, Vecer J, Eaton WA, Cafiso DS, Hummer G, Hurley JH: **Solution structure of the ESCRT-I complex by small-angle X-ray scattering, EPR, and FRET spectroscopy**. *Proceedings of the National Academy of Sciences of the United States of America* 2011, **108**:9437-9442.
19. Kelly SM, Jess TJ, Price NC: **How to study proteins by circular dichroism**. *Biochimica Et Biophysica Acta-Proteins and Proteomics* 2005, **1751**:119-139.



## Chapter 2 Synthetic preparations.

Particular attention is paid at this point of the manuscript to give a general overview and description of the synthetic routes taken to derivatise molecular species used and considered in the experimental studies of this doctoral project.

### 2.1 From chemical substrates to target compounds

The methodology in developing the target compounds and molecules used in this doctoral project rely on the same preparative and ligation synthetic steps. The synthetic goal remains to build a three-modular system by covalently binding two different FRET amenable chromophores together to a biomolecule. The criterion in the design of these frameworks are: i) the choice of chromophores ii) the choice in covalent bonding mechanism (chemistry) iii) what biomolecule to evaluate.

The basis of deciding which chromophores to select was already made in that it was decided to exploit what was already understood and determined on the optical responsiveness of QSY both in the literature and earlier MS exploratory experimentation and testing in the lab. The QSY chromophore was chosen to work as an acceptor chromophore for its quality to fragment and give clear unique dissociative fragmentation on laser irradiation. In the focus to finding a second donor chromophore that would meet and validate the spectral constraint, *i.e.* that the photophysics of the donor chromophore deposes an emission band that overlaps with the absorption band of the acceptor, rhodamine was select as the dye of choice. Note that this donor acceptor system was also used for their compatibility to ionize and produce quality spectra in the positive mode (to the individual chemistry of the dye, to the dye's charge prior to electrospray). For this reason, a different pair was used in the negative mode. In the negative mode, ATTO514 was used in pair with the QSY acceptor. QSY dyes ionizing well in both modes of the MS. In another developed negative mode exploratory experiment, a different pair of NBD and Eosine Y were used altogether.

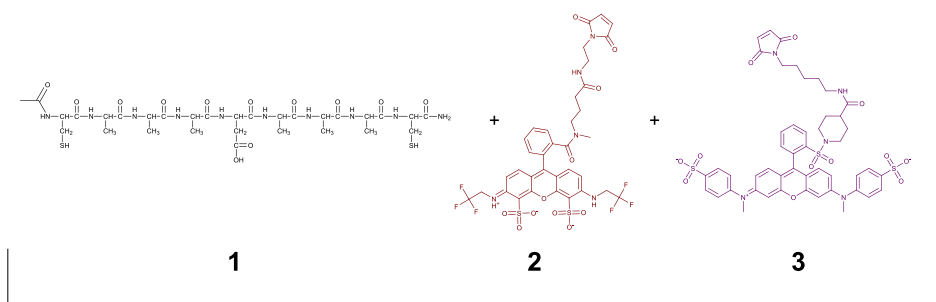
In terms of the favoured, appointed, chemistry in building the molecular frameworks, conjugate addition of thiols to the conjugate functional group of the maleimide (described later herein) is the major approach used in the covalent binding of chromophores to the biomolecule, be it a peptide or a protein. This reaction is chosen as it was first possible to commercially obtain versions of the chromophore that include the maleimide group for tethering. Secondly the reaction is irreversible under a wide range of conditions and pH. It should be noted that AAK tripeptide frameworks with chromophores were built for study, without thiols, this one binded to chromophores by amine nucleophilic substitution.



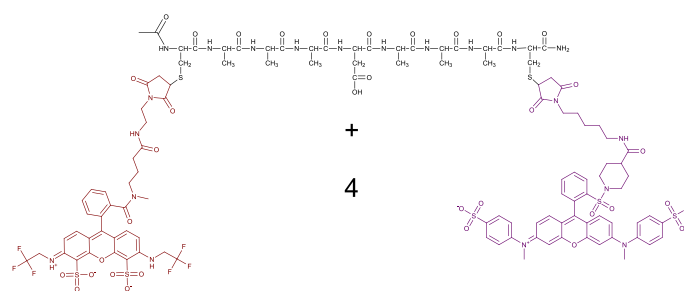
Finally, there was much more flexibility in determining what peptide or biomolecule to use. The choice was large as the only single precondition is that the molecule presents a or several nucleophilic groups (thiol or amine). In most of cases this meant selecting peptides or proteins with cystein amino acids. Cystein amino acids are residues that hold -SH mercaptan nucleophiles on their side chains. Peptide length selected varied depending on their intended use for experimentation.

So, to have an overall understanding of the preparative steps, let us point to an independent reaction scheme as an example. Here the one pot synthesis (1 hour) describes the dispatch of the QSY9-CA3DA3C-ATT0514 end-product (1), following page:

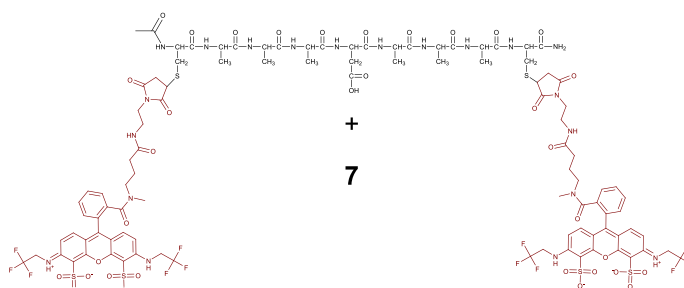
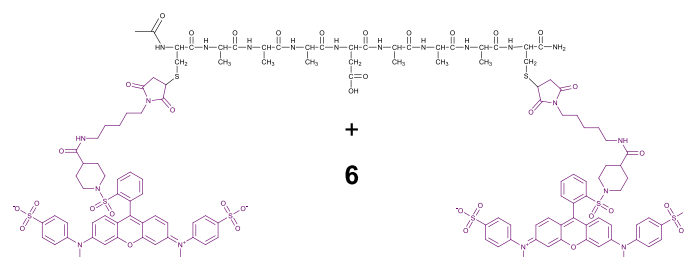
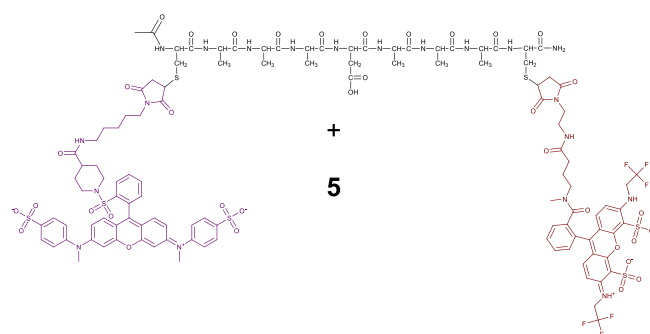
## Synthetic Preparations



1h



↑ Regioisomers ↓



(1)

Review below a table detailing the conditions used in taking through the above exemplified one pot synthesis.

QSY9-CA3DA3C-ATT0514 reaction conditions.	
Solvent	H <sub>2</sub> O or H <sub>2</sub> O:CH <sub>3</sub> OH (1:1). No buffer.
Concentration of peptide	0.0652mM
pH	6-7.5 (neutralization by addition of NH <sub>4</sub> OH)
Reaction crucible	Eppendorf
ATT0514	~ 0.064 mM used of the peptide
QSY9	~ 0.0012 mM used of the peptide (1:54 ratio to ATT0514)
Volume (general)	1ml cocktail mixture.

Table 2.1.1. Reaction conditions for QSY9-CA3DA3C-ATT0514.

All other molecular frameworks featured within this thesis are a variation of the above *cf.* method sections.

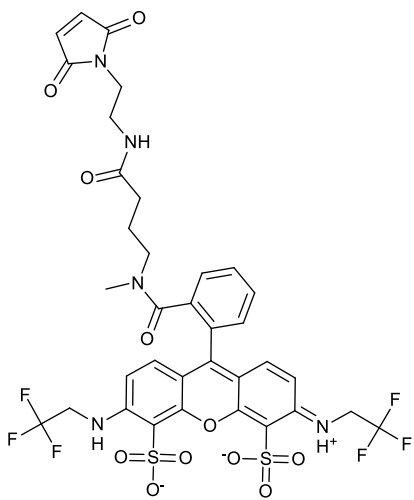
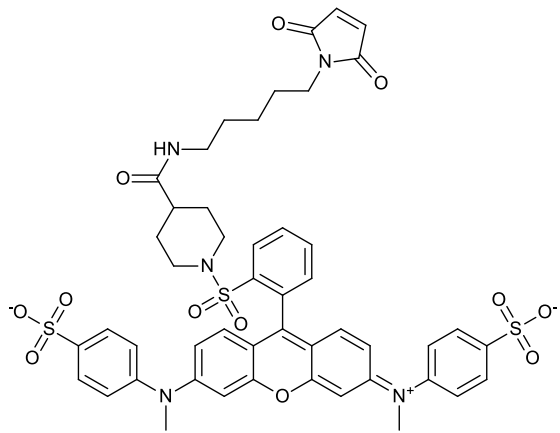
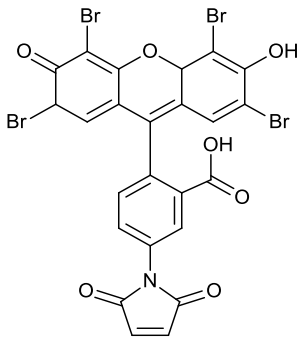
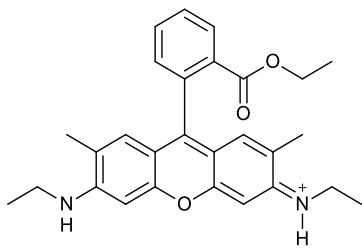
### Synthetic strategy

The grafting is based on the nucleophilic thiol covalent binding of the cysteine amino acid to the electrophilic maleimide group which is a thiol reactive probe. It is known that maleimides perform as excellent reagents for thio-selective modification, quantitation and analysis. The reaction end products are those where the thiol is added across the double bond of the maleimide to yield a thioether. It is important to take onboard that maleimides do not favorably react with methionine, histidine or tyrosine. Reactions with amines usually are only favoured at higher pH than that for the reaction of maleimides with thiols. Competitive reaction one must consider is the hydrolysis of the maleimide to an unreactive product, more so at pH higher than 8. Once formed the maleimide reacted to thioether can hydrolyse to an isomeric mixture of succinamic acid adducts. Alternatively they undergo cyclisation with adjacent amines to yield crosslinked products [1].

In the context of the preparations carried out in this thesis, the major difficulties encountered have been that of solubilizing the peptide, and with MS electrospray solvents available only. Secondary issues have included pH control, and general manipulation of the made-up sample, keeping the reaction products at an acceptable temperature that postpones oxidation.

## 2.2 Peptides and chromophores.

A review of the chromophores employed is available in Table 2.2.1. below.

<b>ATTO 514 Maleimide</b> Molecular formula: $C_{35}H_{30}F_6N_5O_{11}S_2^-$ Molecular weight: 990.0 Appearance: Red solid Supplier: Atto-Tec 	<b>QSY 9 C<sub>5</sub> Maleimide</b> Molecular formula: $C_{54}H_{62}N_6O_{12}S_3$ Molecular weight: 1083.3 Appearance: Purple solid Supplier: Sigma aldrich 
<b>Eosin Y</b> Molecular formula: $C_{20}H_8Br_4O_5$ Molecular weight: 647.9 Appearance: Yellow solid Supplier: 	<b>Rhodamine 6G</b> Molecular formula: $C_{28}H_{31}N_2O_3Cl$ Molecular weight: 479.0 Appearance: Magenta solid Supplier: Sigma aldrich 

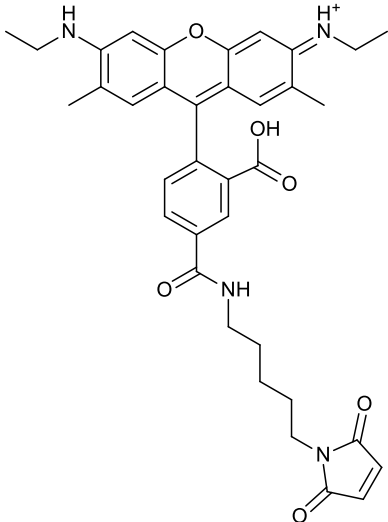
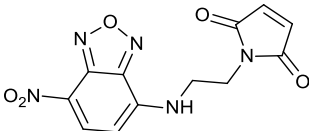
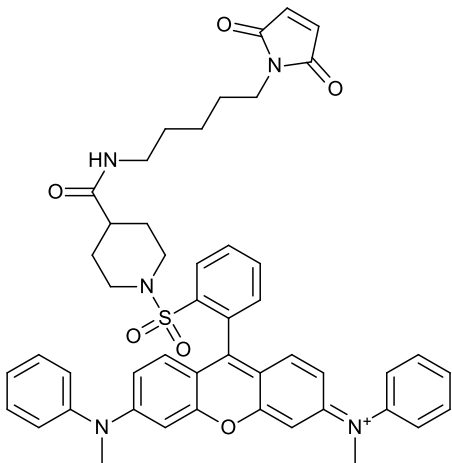
<p><b>Carboxyrhodamine 575 C<sub>5</sub>-maleimide</b></p> <p>Molecular formula: C<sub>31</sub>H<sub>26</sub>N<sub>3</sub>O<sub>7</sub><sup>+</sup>                      Molecular weight: 623.7                      Appearance: Magenta solid                      Supplier: Setareh biotech</p> 	<p><b>NBD Maleimide</b></p> <p>Molecular formula: C<sub>12</sub>H<sub>9</sub>N<sub>5</sub>O<sub>5</sub>                      Molecular weight: 303.2                      Appearance: Red solid                      Supplier: N/A.</p> 
<p><b>QSY 7 C<sub>5</sub> Maleimide</b></p> <p>Molecular formula: C<sub>48</sub>H<sub>48</sub>ClN<sub>5</sub>O<sub>6</sub>S                      Molecular weight: 823.0                      Appearance: Purple solid                      Supplier: Sigma Aldrich.</p> 	

Table 2.2.1. The catalogue of chromophores used in the research theme.

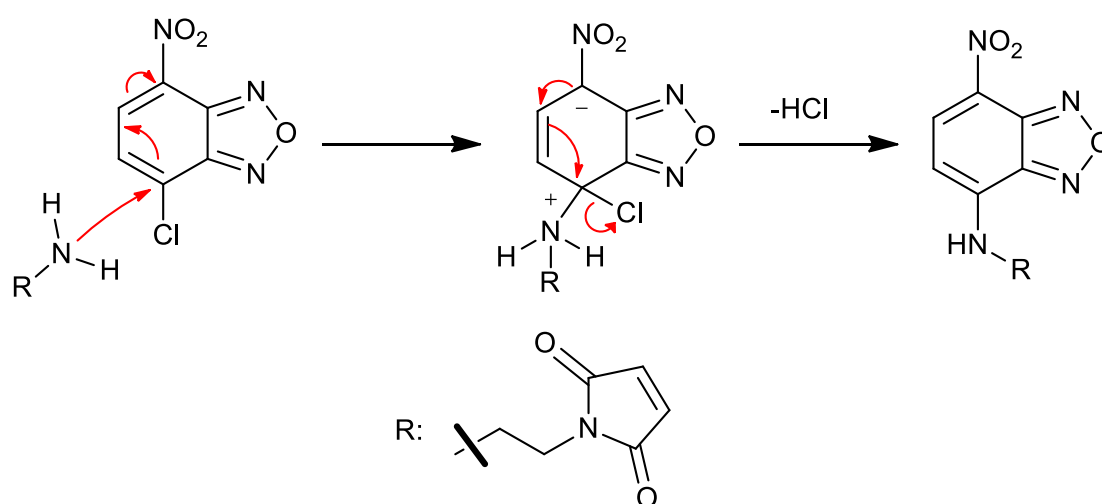
A review of the peptides employed is available in Table 2.2.2.

Peptides ordered from Genscript USA.	
CAKAC ~82 % purity Molecular weight: 494.63	CAADAAEAA ~82 % purity Molecular weight: 791.83
CAADAAEAAC ~82 % purity Molecular weight: 894.97	CAAADAAAC ~82 % purity Molecular weight: 765.86
CAA ~82 % purity Molecular weight: 263.32	

Table 2.2.2. Peptides.

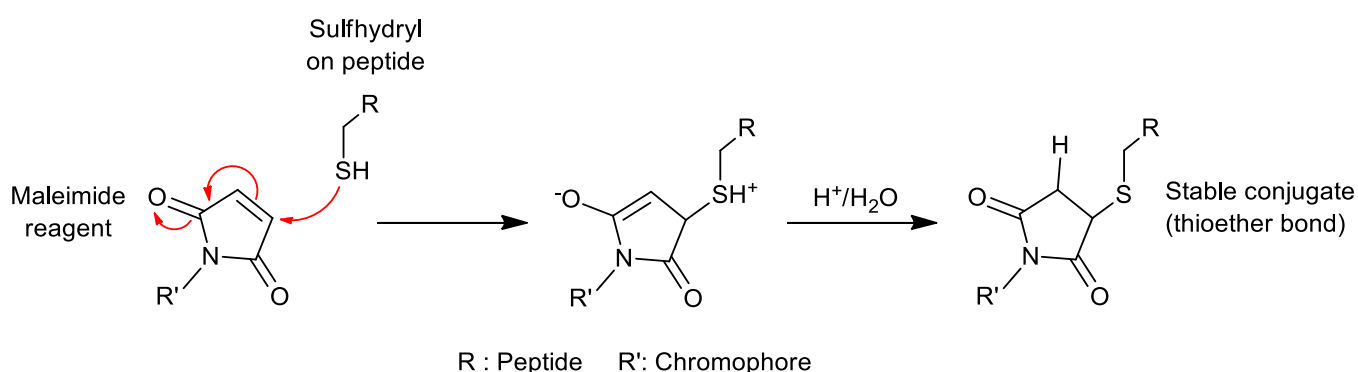
## 2.3 Synthesis

On building doubly grafted FRET frameworks with NBD Maleimide, the synthetic workplan was sparingly different. First the functionalization of the chromophore to bear a maleimide moiety for grafting was needed. Conversely other chromophores already came purchased with the maleimide ligation group on. The synthetic scheme on this reaction that is a nucleophilic substitution of NBD-Cl by N-(2-ethylamine/maleimide) is presented here, in summary, (2):



(2)

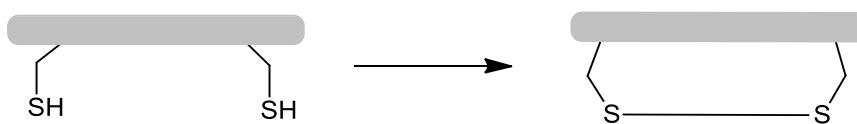
Altogether, the mainstay of these one pot preparations is the thiol tethering to the alkene functionality of the  $\alpha$ ,  $\beta$ -unsaturated carbonyl present in the maleimide of the optical-responsive (second) reaction component. This chemical process is a two-step reaction, it is an addition followed by a protonation: what is commonly referred to as a conjugate addition [2]. The maleimide group bonds favorably with the mercaptan or sulfhydryl group (in this context of the cystein residue of the peptide) when the pH of the reaction mixture is between pH 6.5 and 7.5; the end-product is a stable thioether linkage that is not reversible (*i.e.* the bond cannot be cleaved with reducing agents). In more alkaline conditions (pH >8.5), the reaction favors primary amines and also increases the rate of hydrolysis of the maleimide group to a non-reactive maleamic acid [3]. This is the summary mechanism (3):



(3)

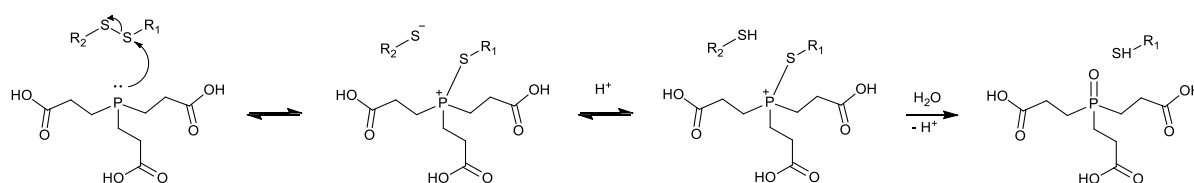


This procedure often does not carry out to completion alone due to the nature of the peptide used for our experiments. Indeed, the frameworks of interest are embedded with two cysteine residues such as to have in the synthetic design, by their thiol functionality, two grafting sites ready at hand. Incidentally, grafting reactions compete with disulfide bridge formation (4):



(4)

The undesirable disulfide bond formation is prevalent in virtually all preparative solutions of the peptide. It is only by introducing a phosphine reducing agent, Tris(2-carboxyethyl)phosphine (TCEP) that the thiol groups can be kept free for further work-up. So far as the mechanism of the TCEP agent is concerned, the disulfide reduction reaction involves the formation of a P-S bond followed by protonation and displacement of the P-S bond for a stronger P=O bond (575 kJ mol<sup>-1</sup>) that gives the phosphine oxide (5):



(5)

Other cleavage agents exist although these are claimed inferior to TCEP (e.g. 1,4-dithiothreitol (DTT) also known as Cleland's reagent or  $\beta$ -mercaptoethanol) [4]. In fact, TCEP presents a number of practical advantages over other sulfhydryl reducing agents [5-10]. (Interchem product sheet available: <http://www.interchim.fr/ft/2/242214.pdf>):

- It is selective.
- It does not reduce metals.
- Does not produce a pungent odor.
- Reductions are quick and quantitative (less than 5 minutes).
- It is effective in both alkaline and acidic conditions (pH 1.5-8, as opposed to DTT).
- It has proven to be more resistant to air oxidation and more hydrophilic.
- The reducing agent does need to be isolated before modifying the thiols.

Anyhow, the alternative reducing agent DTT cannot be used as its mechanism of action relies on mercaptan chemistry, any unreacted DTT during the reducing step can potentially react later down the synthesis and undesirably with the chromophores.

In the case of chromophore grafting to a protein, an HPLC preparation step of the precursor pretreated with TCEP was brought about so to separate the protein from its accompanying salts (buffer). Although not necessary (if not overshooting with TCEP) but still appreciable, the reacted TCEP and excess reducing agent was also observed to carry off with the rest of the HPLC eluent. A positive consideration as TCEP has been reports to react directly with the maleimide [9]. This crucial step affords the synthetic purity required to progress on to the 1, 4-conjugate addition of the photoactive component. The reader is directed to the respective methods of this thesis for more specific information on the featuring protein chromatography of this procedure. What is very important is that the HPLC treatment of crude protein allows us to observe the electrospray of protein of interest in a rich way so to give a wide distribution of charged states of the protein in question (chapter 5) that is not observable when the (crude) protein from its purchased vial is electrosprayed. We affectively assess protein purity with the MS spectral pattern on MS examination.

Reaction selectivity was additionally carefully considered by starting off with what is referred as capped peptides where possible. Whereby the *N*- and *C*- termini are acetylated (Ac) and amidated ( $-\text{CONH}_2$ ) respectively so to sidestep dimerization, cyclisation or disproportionate coupling to the peptide ends as opposed to the sulphhydryl associated to the side chain. It was also proceeded in this way so to prevent charge to localise at the termini and thus tend towards a more native like ionization. It is important emphasize that the reaction conditions for the actual grafting do require the pH criterion, *i.e.* that the liquid mixture be near pH 7. For this, dropwise additions of NaOH,  $\text{NH}_4\text{OH}$  base or  $\text{NH}_4\text{Ac}$  buffer were used.

Another constraint has been that of all the various conditions possible, the reaction substrates had to be carried through synthesis using only solvents compatible with the ionizing source (*cf.* electrospray sample preparation [11]) of the LTQ Velos mass spectrometer and made available in the laboratory. For reference these were:

Acetonitrile*	Water*	Methanol
*either solvent mixed with 0.05% trifluoroacetic acid (TFA)		

Table 2.3.1. Available solvents used in experiments.

### Purification of the made-up samples

Once the cocktail mixture made, the reaction crucible was left to react, for large synthetic targets (proteins), its contents were purified so as to separate the unreacted material with that of the product. It was first attempted to effectuate this by introducing the mixture onto small desalting columns and running them on a centrifuge. The MS spectrum on the eluent did not pass as satisfactory: a polluted spectra with an over redundancy of species detected, unuseable to the later steps of the research plan, selection of charged species cannot be done to our expectations. It was then decided to use HPLC. This afforded a pure sample of the desired of the species of interest (*e.g.* bovine ubiquitin protein). The HPLC setting was run for 10min at a 50:50 mobile mixture of acetonitrile, 1%TFA:  $\text{H}_2\text{O}$ , 1%TFA for 2min then moving to a 75:25 gradient start of

acetonitrile, 1%TFA: H<sub>2</sub>O, 1%TFA moving down to 20:80 mobile phase composition (acetonitrile, 1%TFA: H<sub>2</sub>O, 1%TFA) at the end of the run (10min). The wavelength for detection used was set at 220nm and flow rate was 1ml/min, 40°C, C4 column. A characteristic of the HPLC mode is that the C4 column is a bonded phase column, fitting in partition chromatography category.

With the electrospray constraint in mind, virtually all synthetic preparations were made in water, water methanol mixtures were employed for larger molecular frameworks. The acetonitrile played a major role however between analytical operations, to clean and elute prior byproducts, unreacted reagents and other undesirables away from the various the instrumental pieces. Whilst the acetonitrile has been useful for cleaning (electrospray source) it has not been comparable to water as a solvent because of water's attractive physical polar attributes and higher dielectric constant to acetonitrile, thus it was taken care to resolute where possible with water. To this end an air dryer spewer was set up so to recondition the HPLC eluted end-products to a water solution.

## 2.4 References :

1. Anon.: *The molecular probes handbook. A guide to fluorescent probes and labeling technologies*. 11th edn; 2010.
2. Sykes P: *Mechanism in organic chemistry*. 6<sup>th</sup>6th edn: Pearson. Prentice Hall; 1986.
3. Hermanson GT: *Bioconjugate Techniques*. 3<sup>rd</sup> edn; 2013.
4. Smith RD, Loo JA, Edmonds CG, Barinaga CJ, Udseth HR: **New developments in biochemical mass-spectrometry - electrospray ionization**. *Analytical Chemistry* 1990, **62**:882-899.
5. Levison ME, Josephson AS, Kirschenbaum DM: **Reduction of biological substances by water-soluble phosphines - gamma-globulin (IGG)**. *Experientia* 1969, **25**:126-+.
6. Mery J, Granier C, Juin M, Brugidou J: **Disulfide linkage to polyacrylic resin for automated fmoc peptide-synthesis - immunochemical applications of peptide resins and mercaptoamide peptides**. *International Journal of Peptide and Protein Research* 1993, **42**:44-52.
7. Han JC, Han GY: **A procedure for quantitative-determination of tris(2-carboxyethyl)phosphine, an odorless reducing agent more stable and effective than dithiothreitol**. *Analytical Biochemistry* 1994, **220**:5-10.
8. Getz EB, Xiao M, Chakrabarty T, Cooke R, Selvin PR: **A comparison between the sulfhydryl reductants tris(2-carboxyethyl)phosphine and dithiothreitol for use in protein biochemistry**. *Analytical Biochemistry* 1999, **273**:73-80.
9. Shafer DE, Inman JK, Lees A: **Reaction of tris(2-carboxyethyl)phosphine (TCEP) with maleimide and alpha-haloacyl groups: Anomalous elution of TCEP by gel filtration**. *Analytical Biochemistry* 2000, **282**:161-164.
10. Tyagarajan K, Pretzer E, Wiktorowicz JE: **Thiol-reactive dyes for fluorescence labeling of proteomic samples**. *Electrophoresis* 2003, **24**:2348-2358.
11. Strupat K: **Molecular weight determination of peptides and proteins by ESI and MALDI**. In *Mass Spectrometry: Modified Proteins and Glycoconjugates. Volume 405*. Edited by Burlingame AL. San Diego: Elsevier Academic Press Inc; 2005: 1-36: *Methods in Enzymology*.



## Chapter 3 Instruments.

Separate sections of this chapter discuss the instrumentation and equipment used and how they have been implemented together so to work in unison as a single workstation for the research investigation and experiments on the proteins and macro-ions of interest to this thesis. A short description on mass spectroscopy is offered detailing commonly used modern fragmentation techniques how it can be applied to determine protein structure. A second part provides the basic technical aspects of the LASER source used and its light separation piece.

### 3.1 Mass spectrometry and the mass spectrometer

Mass spectrometry (MS) looks at the production of gas-phase ions of the molecules drawn out by vaporization and electrospray of the sample without loss of information, without eliminating the analyte. Ionization occurs through the collisions between electrons and molecules in the gas phase, and the protonation or deprotonation of the molecule of interest M, to yield either  $[M+H]^+$  (positive mode) or  $[M-H]^-$  (negative mode) ions [1]. Charging may also be induced by adduction of small ions of the like of  $Na^+$ ,  $K^+$ , acetate or ammonium (dispatching  $[M+Na+H]^{2+}$  species for example) [2-4]. The mass spectrometer utilizes the ability of electric and magnetic fields to separate the charged particles on the basis of their mass to charge or mass to charge ratio ( $m/z$ ) [1]. These ions that are detected and set out to make the mass spectrum two-dimensional plot that relates the mass to charge ratio ( $m/z$ ) on the x-axis to the relative abundance (RA, %), in other words the number of ions (y-axis) [5].

Mass spectrometry, unlike other analytical spectroscopic techniques such as NMR, CD or X-ray, does consume the analyte. This is at the expense of ionizing the analyte and it being maneuvered across the mass analyser to strike the detector during analysis. In spite of this, the concerted opinion among the community is that it is considered a non-destructive technique as the amount of the analyte needed is in the low microgram range and often even in several orders of yet smaller dimension below.

The mass spectrometer itself consists of an inlet that leads to a device to volatilize and ionize the molecules into a beam of charged particles, a mass analyzer that separates ions of different mass-to-charge ratio ( $m/z$ ) and a detector supported with a data analyzer that records their relative intensity. There is a variety of ways to arrange these components to fashion MS instruments. Within this variety of class of components each have their own merits and disadvantages and tailored specification to suit particular sample types. For example, there is the quadrupole based mass spectrometer, the ion trap and the time of flight mass spectrometer. Some of these mass spectrometers designs can distinguish molecular fragment masses to six decimal places others are made to serve as bench top machines that can resolve masses of up to just  $m/z$  800. Each operate in a different manner, in layman's terms they spur the ions differently. Nevertheless, they all share the same design layout. Their components follow the same simple basic setup, common to all mass spectrometers. It should also be said that the *ion source*, a *mass analyser* and a *detector* are operated under high vacuum conditions [6]. An overview of how these are fixed together is available below, Figure 3.1.1.

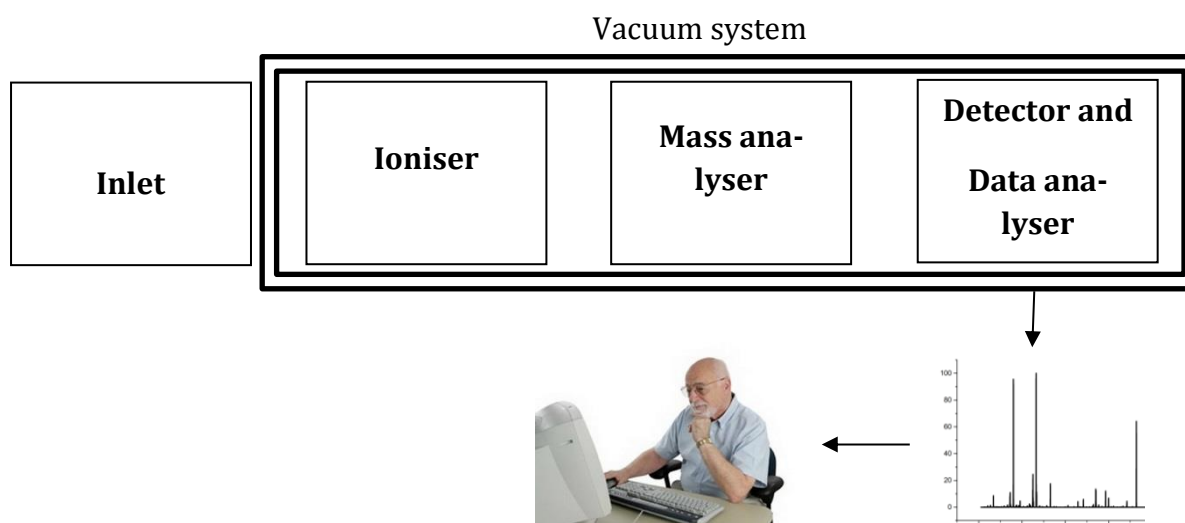


Figure 3.1.1. The set-out of a Mass Spectrometer instrument.

All of the methods produce a signal that in turn is profiled and computer generated to give the mass spectrum. The mass spectrum of a compound is employed to elucidate and give a first indication on the following chemical structural information [7]:

- Molecular ion mass. The detection of the intact ionized molecule . This can give an indication to the number of nitrogen atoms and the presence of chlorine and bromine atoms. This is used and key in determining the elemental composition of a chemical compound. Also, as long as only singly charged ions are observed ( $z=1$ ) the  $m/z$  scale directly represents the  $m$  scale.
- The most stable and major fragment, the base peak which is looked at to match molecular weight calculations. A key piece in resolving the structure of the molecule.
- A fragmentation pattern that can be exploited to confirm any reference to a repository of structures that have been databased.

### 3.1.1 Electrospray ionization (ESI)

The LTQ Velos source is one that implements an electrospray technique, a development of the 1980's [4, 8] which transforms species in solution into ions in the gas phase. The system relies on pumping sample from high-performance liquid chromatography or a (Hamilton) syringe through a stainless-steel capillary tube which is set at a high potential (2-5kV). The influence of this electric field induces the mixture to be sprayed from the capillary tube's apex. This action generates highly charged solvent and solute ion droplets that are further nebulized by blowing a carrier gas (N<sub>2</sub>) [7, 9-11]. These evaporate until coulombic explosion and the ensemble is lead to the high-vacuum system of the mass spectrometer via a nozzle-skimmer optical disposition. The electrospray and nozzle-skimmer arrangement are typically positioned at right or acute angles to one another. By ramping the potential that exists between the electrospray and nozzle-skimmer arrangement, the ions are pulled into the mass spectrometer in a way to riddle out desirable solute ions from unwanted extraneous material for example salts present in the sample mixture or mobile phase. An elucidation on how the ions are drawn to the gas-phase rests on two established models: the charge residue model (CRM) posited by Dole [10, 12] and the ion evaporation model (IEM) associated to Iribarne and Thomson [13]. The charged residue model considers the gas-phase ions to be produced as a result of continuous droplet fission down to the limit, where droplets bear only one excess ion. Conversely, the ion evaporation model claims that gas-phase ions detract directly from small droplets [4]. Even though great many papers have been published the exact transformative in gas phase ion formation is still debatable, recently it has been disputed that both models, in unison, play a part in the ejection of gas-phase ions [14]. The conclusive learning of this work is that IEM is valid for small inorganic ions and the CRM for large ions such as those that typify proteins.

The ESI device allows characterization of samples (*i.e.* heat-labile compounds or high molecular weight compounds) that are incompatible with the design of other, especially early, methods of ionization. ESI is particularly suitable in the analysis of polar compounds that easily tend to ionize in the condensed solution. These preformed ions typically also encompasses adduct ions, such as those formed between NH<sub>4</sub><sup>+</sup> ions of an ammonium acetate ESI solution and oxygen atoms associated to a polymer analyte. The range of molecular masses that ESI makes disposable to the LTQ mass spectrometers is of the order of 100 000 amu –plus. This makes it a method of choice when looking to work with biological polymers that are peptides, proteins and nucleotides, among others; pharmaceuticals and their metabolites; and industrial polymers *e.g.* polyethylene glycols [7].



The block diagram below shows the evolution from onset: ions solvated in highly charged droplets to ejected charged gaseous analyte species, Figure 3.1.2.

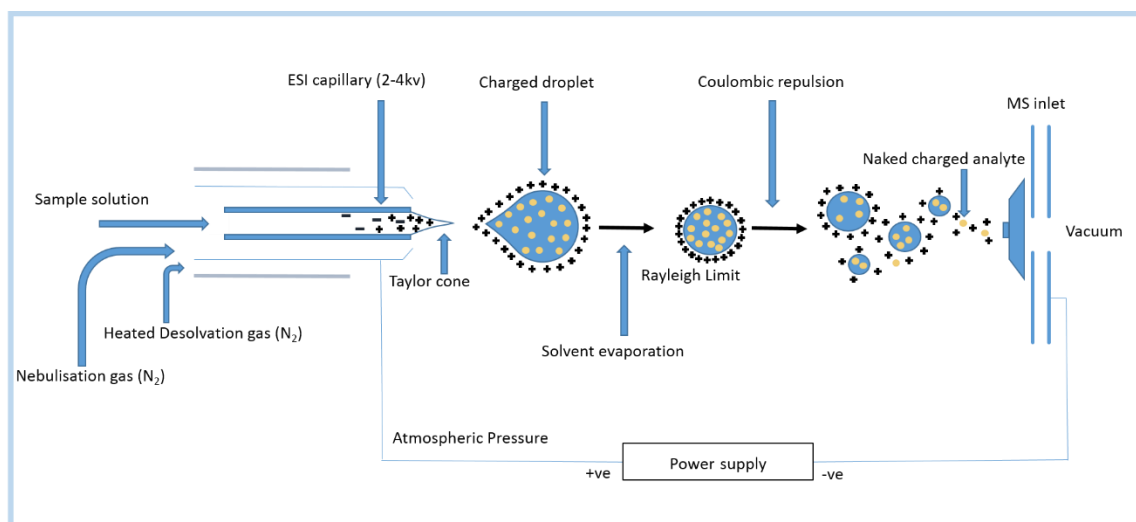


Figure 3.1.2. Pictorial representation of the electrospray ionization (ESI).

### 3.1.2 The Detectors for MS

Detectors for MS are devices that are employed to register ion hits and thus, the signal. This generated signal is then compounded through an acquisition system. To give a display of the analysis that has been taken in progress. It is important to say that these again come in different colors and manufacture designs but compared and contrasted well, can highlight certain points over others.

### 3.1.3 MS excitation and fragmentation methods

Fragmentation or excitation energies in ionization can be categorized in two groups depending their *modus operandi*: vibrational or electrical excitation.

#### Collision-induced dissociation

Collision-induced dissociation (CID) also known as collisionally activated dissociation (CAD) or collisional activation (CA). It is by far the most prevalent and widespread vibrational activation technique. The principle relies on passing the ion beam through a collision cell in a way that the ions brake on arrest with a collision gas (He, N<sub>2</sub> or Ar). Upon each activating collision, a portion the kinetic energy of the impact is converted into internal energy. The internal energy then accumulates engendering the ions to dissociate as a result [15]. The gas itself is regulated at a considerably higher pressure to that of the surrounding vacuum space. This is made possible by mounting a gas needle inlet to a tight compartment cell or ion trap montage purposed with two opposing faced openings — ion entrance and exit points which the ion beam can pass. Depending on the design of the instrument, a vacuum is applied in order to

create a differentially pumped space to manage the effusing gas. In this manner, an appreciation of the pressure can be gained with the aim of reproducing the pressure adjustment, however, the reading on the ion gauge will never reflect the true, real pressure within the instrumental piece [6]. Because of its breadth of application, collisional activation remains also the most popular activation approach, most certainly due in part to its understood mechanisms of action such as the mobile proton model [15]. This model that applies to peptides assumes that ionizing protons are initially located at basic sites such as the N-terminus. Upon collisional activation one or several of the ionization protons may shift to less basic sites of the polypeptide which encourages various charge-site-initiated mechanisms of backbone dissociation [15].

However, CID does present some disadvantages. First, energy deposition is a multi-step gradual process characterized to tend to a limit in the total energy imparted on the species. The higher statistical being low energy pathways of fragmentation. Consequently, collisional activation induces cleavage of the most labile bonds and causes structurally uninformative neutral losses of water, ammonia, or CO<sub>2</sub> in peptide and proteins [15]. Secondly, conventional low energy CID in in trap instruments arises from truncation of the lower  $m/z$  range. The low mass cutoff (LMCO) disadvantages the process as it disfavors the detection of shorter N-terminal and C-terminal fragment ions of peptides [15]. Hence the development of higher energy collisional deactivation (HCD) in ion traps. This higher energy deposition technique takes a second ion cell or multipole cavity so to avoid having the activation process being dependent of the trapping parameters, and as such prevents the low mass range to cutoff. Another disadvantage with CID is its shortcoming with post translational modifications such as phosphorylation. Collisional activation is a slow heating process that cause the weakest labile bonds to break, thus post translational modifications are given as neutral losses and this limits the utility of CID to site localize post translational modifications [15].

#### Infrared multiple-photon dissociation.

Infrared multiple-photon dissociation (IRMPD) is a technique used in mass spectroscopy to fragment molecules in gas-phase isolation for structural analysis of the parent chemical species.

In summary, an infrared laser is directed through a window into the vacuum of a mass spectrometer. The mechanism of fragmentation involves the absorption of numerous photons, on ions. The parent ions excite and are promoted into more energetic vibrational states. Bonds brake, giving a gas phase fragmentation of the parent ion. In the case of powerful laser pulses, the dissociation proceeds via inner-valence ionization of electrons.

### 3.2 The mass spectrometer, LTQ Velos

Thermo Fischer Scientific's LTQ Velos is a dual cell linear ion trap mass spectrometer that includes a syringe pump, an injection and diversion valve and an Ion Max ion source, Figure 3.2.1.



Figure 3.2.1. The Thermo Scientific LTQ Velos, part of Thermo Fischer Scientific.

An overview of the linear ion, quadrupole, trap and how it is interlocked with the other fundamental pieces of the instrument is given below, Figure 3.2.2 [16].

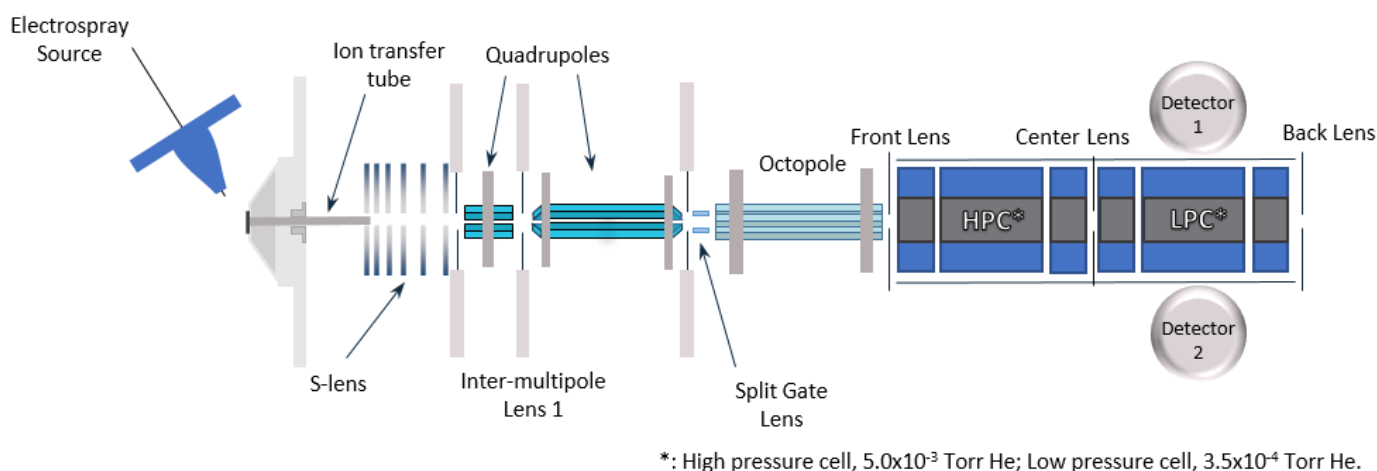


Figure 3.2.2. Functional layout of the linear ion trap. Adapted with permission from (Second TP, Blethrow JD, Schwartz JC, Merrihew GE, MacCoss MJ, Swaney DL, Russell JD, Coon JJ, Zabrouskov V: Dual-Pressure Linear Ion Trap Mass Spectrometer Improving the Analysis of Complex Protein Mixtures. *Analytical Chemistry* 2009, 81:7757-7765.). Copyright (2017) American Chemical Society.

The LTQ Velos in short consists of first an electrospray ionizer placed at a  $60^\circ$  angle so to deliver a stream of charged species or ions down the ion source interface entrance and ion transfer capillary. This first modular section then leads to a series of orderly spaced plates (*i.e.* the S-lens) that funnel the ion beam down to a collection of various multipole focusing optics that converge and filter the ions produced to the detector for signal processing. These are the Q00 Ion Optics, the Q0 Ion optics and the Q1 Ion Optics, Figure 3.2.3. The Q00 rf apparatus is an arrangement of four square thin metal bars, giving the so-called quadrupole device. An rf voltage is distributed along these poles, generating a quadrupole field that focuses the beam of charged particles and trains them along an z-axis and oriented towards the succeeding optics of the instrument. The ions then pursue their path towards the Q0 optical piece which is a second quadrupole with a 'U' topology, unique to the LTQ Velos and serves to filter out the neutrals. Next the ions are transmitted to the Q1 ion optics, an octapole downstream in the instrumental setting of the LTQ Velos. Their role is once more to transmit and gather the ions together as they shuttle towards the detectors. The octapole in question is as the name implies an arrangement of eight round-profile rods that work in a very similar manner to the previously mentioned quadrupoles. Both quadrupoles and octapole are subject to an increasing vacuum gradient that allows to curtain the ions to the linear ion trap cells of the LTQ Velos MS design. The pathway track of these charged analytes is also assisted and simultaneously controlled by a series of lenses subjected to an electrical potential that baffle both the vacuum and applied quadrupole guiding field of the mid-section of the MS system [7].

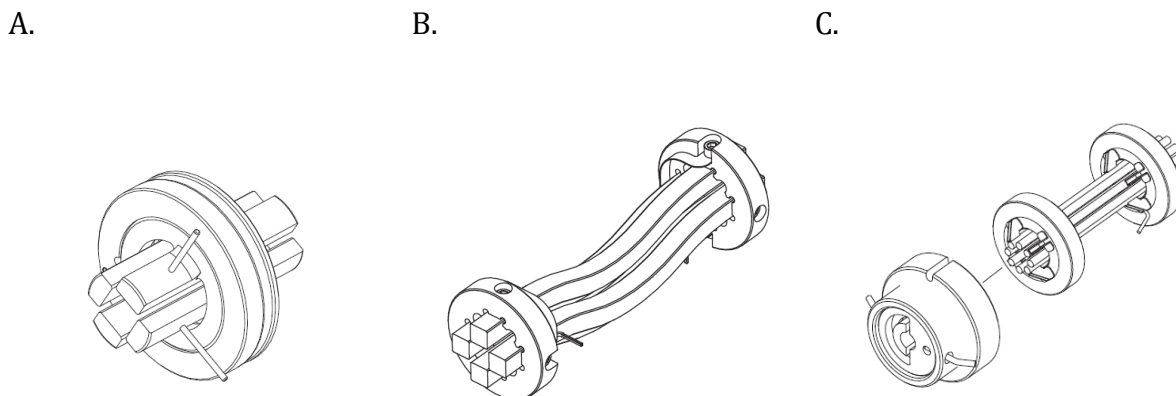


Figure 3.2.3. LTQ Velos mid-section mass filtering ion optics. (A) Q00 (B) Q0 (C) Q1. Adapted from (Scientific TF: **LTQ Series**. In *Hardware Manual*; 2009).

### 3.2.1 Ion polarity modes

This instrument as with other mass spectrometers of the LTQ series can operate in either the negative or positive mode that are more accurately known as the ion polarity modes. The MS system governs whether a positive or negative ion regime will be carried to the mass analyzer for mass evaluation. This is achieved by reversing the polarity of the potentials applied to the source and ion optics located between the source and the mass analyzer.

The insight gleaned from a positive-ion mass spectrum is different but consistent with that obtained from a negative-ion spectrum. The possibility to acquire both positive-ion and negative-ion spectral information during a single run greatly improves the capacity and depth to qualitatively analyze a sample [7].

### 3.2.2 Electrospray ionization

Continuing and recapitulating on the discussion on page 32, the workings of the ESI can be practically laid out as described:

1. The sample solution reaches the ESI needle which is supplied with a voltage.
2. The ESI needle sprays the sample solution into a fine aerosol of charged droplets with a potential at their surface.
3. Evaporation pins the system towards increasingly smaller and more electrically charged droplets.
4. The density of the electrical charge at the surface of the droplets hikes up to a critical point: the Rayleigh stability limit. Subsequently, the droplets divide into a smaller suspension because of the Coulombic repulsion that overtakes the surface tension. The process is designed to provide a continuous spray of droplet solution.
5. The Coulombic repulsion that affect the ions in these very small, highly charged droplets causes the sample ions to be transposed into the gas phase.
6. The analyte ions are guided through an ion transfer capillary and enter the MS detector for signal processing.

For the LTQ Velos, the ESI needle is angled at 60 degrees to the axis of the ion transfer capillary that carries ions into the MS detector. This instrumental layout protects the transfer capillary from any spoilage, see Figure 3.2.4. [7]. The ion sweep cone acts as a mechanical barrier that prevents large droplets and pollutants from entering the ion transfer capillary [7].

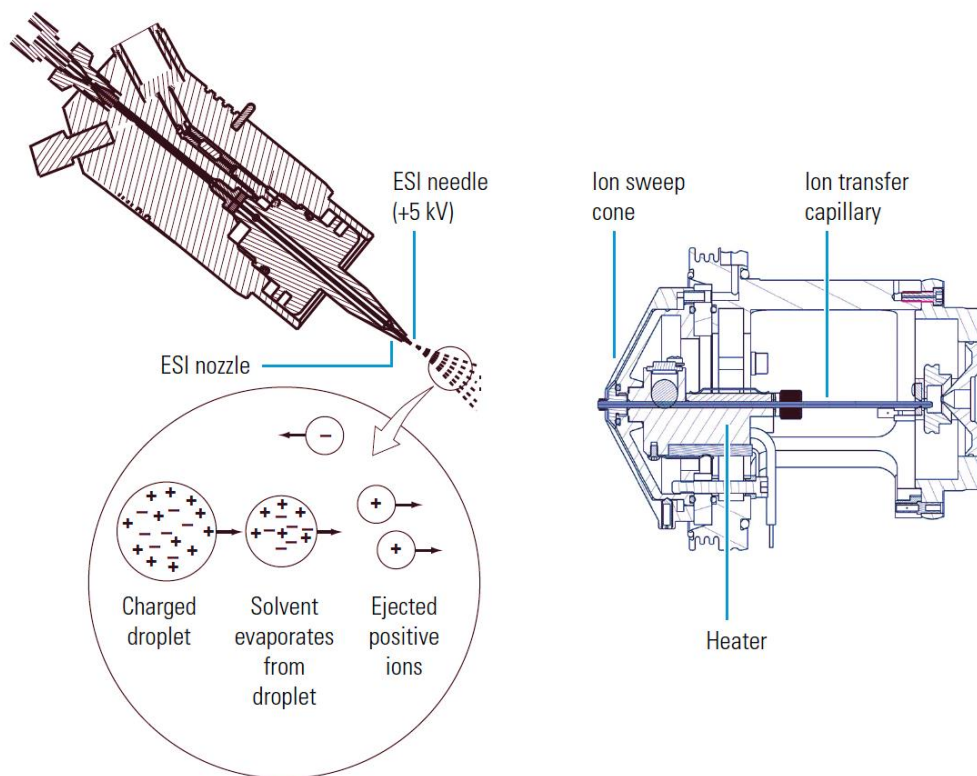


Figure 3.2.4. A functional representation of the ESI under the positive regime. Adapted from (Scientific TF: **LTQ Series**. In *Hardware Manual*; 2009).

### 3.2.3 Mass analyzer

Mass isolation, separation analysis and associated ion storage, ion separation, collision induced dissociation and ion ejection is discussed here. This section details the key constituent parts of the mass analyser, the voltages applied to its electrodes, the helium gas filling associated to the mass analyzer cavity and the workings of the mass analyzer in operation.

The LTQ Velos mass spectrometry technique's fundamentals rely on dual cell two-dimensional linear ion traps. Both linear ion traps are delimited with a front, central and back pierced lenses so as to let the ions travel through. The three lenses are there to provide potential conductance limits. The linear ion trap itself is built to hold four hyperbolic rods. The poles are spaced by slots in order to eject the ions during 'scan out'. The rods can be considered as two pairs of each, connected electrically. By the linear ion trap design, it is then possible to distribute three DC axial trapping voltages, uniquely, to each of the three lenses. An additional AC is set for the trap. A potential well can be created in this way, allowing to axially trap species of interest.

### Principle of the linear quadrupole

Before proceeding in describing the hyperbolic quadrupole linear ion traps it is well to look at the earlier groundwork principles of a quadrupole mass analyzer in greater detail. As mentioned above, the quadrupole consists of an arrangement of four electrode bars. These are of a hyperbolic or cylindrical geometry. The pairs of opposite electrodes are held at a same potential composed of a DC and AC element, consistent with the following equations [6]:

$$3.2.3.1 \quad -(U + V \cos \omega t)$$

$$3.2.3.2 \quad +(U + V \cos \omega t)$$

Here;

$U$	DC voltage applied continuously to the electrodes of a multipole.
$V$	Amplitude of the AC current with a given frequency applied to the electrodes of a multipole.
$\Omega$	A radiofrequency (rf), angular frequency.
$T$	Time

In a Cartesian space, the rods extend in the  $z$ -direction, Figure 3.2.5, and in the  $xy$ -plane can be viewed to feature a square geometry, Figure 3.2.6.

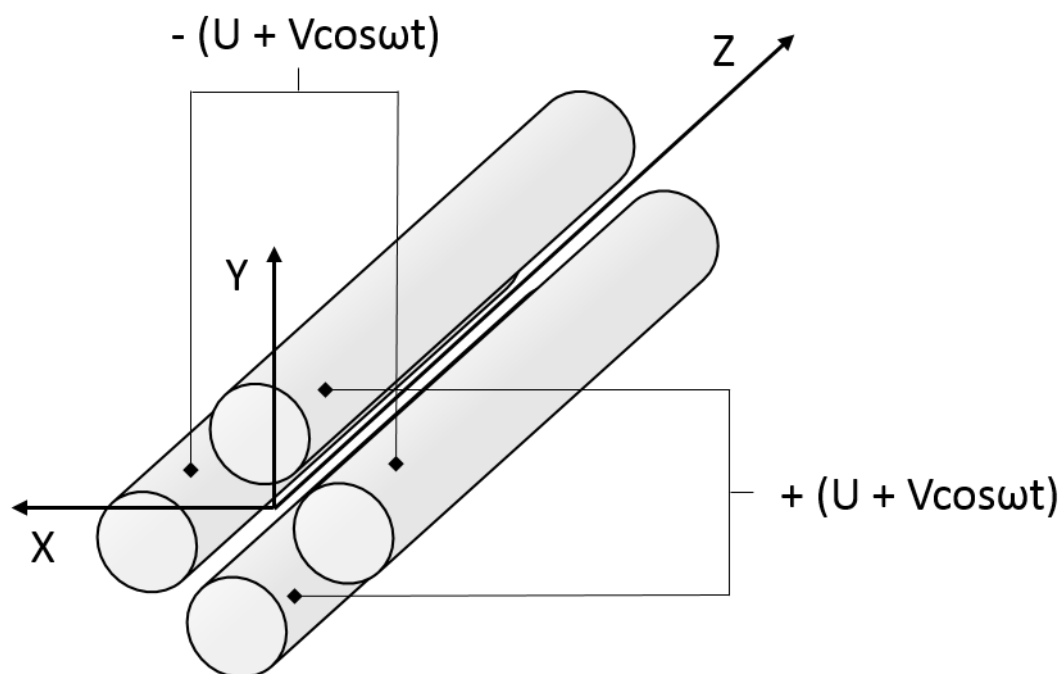
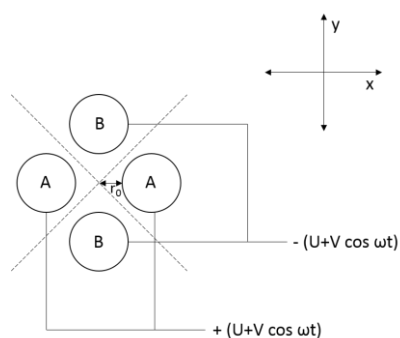


Figure 3.2.5. Pictorial diagram of a linear quadrupole in Cartesian space (Gross. JH: *Mass Spectrometry*.: Springer.; 2004.).

a.



b.

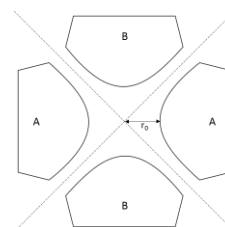


Figure 3.2.6. Cross section of a quadrupole (a) for the cylindrical variant and (b) for the hyperbolic profile of the rods. The asymptotes in dotted lines delineates a space where the electric field is zero (Gross. JH: *Mass Spectrometry*.: Springer.; 2004.).



Within these devices, the quadrupole becomes an “ion guide” if the DC component of the electric field is equal to zero (what is known as the “RF-only mode” of operation) ions are tracked down the axle in the z-direction by the set potentials. It can also be used as a “mass filter” device as it can selectively maintain stable trajectories for ions of certain  $m/z$  ratios, while making the others to become unstable. The quadrupole purposefully acts as a “tunable” mass filter that transits ions within a given  $m/z$  window.

The cluster of ions is paced through by a periodic attraction and repulsion in the x- and also y-directions in accordance to the sign of the electrical forces induced by the poles. The DC element of the electrical bias,  $U$  and the amplitude of the AC component  $V$  of a radiofrequency (rf) given the symbol  $\omega$  works to give a relation where the total potential  $\phi_0$ , which is the quadrupole potential (*i.e.* the difference between the potentials applied to the x-pair and the y-pair of electrodes [17]). The periodic potential can be elucidated by:

$$3.2.3.3 \quad \phi_0 = U + V \cos \omega t$$

Where the electrical field is close to, or, zero; *i.e.* along the dotted lines, for hyperbolic electrodes anyway and within the delimitation of  $2r_0$ , it is possible to guide the ions as to traverse the poles without impacting the rods provided it is stabilized by the electrical forces in the xy-planes. These conditions stem from the theory of the Mathieu equations [6] and depict the ion trajectories in question. Writing the differentials formulates;

$$3.2.3.4 \quad \frac{d^2x}{d\tau^2} + (a_x + 2q_x \cos 2\tau)x = 0$$

$$3.2.3.5 \quad \frac{d^2y}{d\tau^2} + (a_y + 2q_y \cos 2\tau)y = 0$$

Where  $a$ ,  $q$  and  $\tau$  are defined as ( $m_i$  is the mass of the ion,  $e$  the charge);

$$3.2.3.6 \quad a_x = -a_y = \frac{4eU}{m_i r_0^2 \omega^2}, \quad q_x = -q_y = \frac{2eV}{m_i r_0^2 \omega^2} \quad \tau = \frac{\omega t}{2}$$

For a said combination of specific  $U$ ,  $V$  and  $\omega$  the global ion motion may lead to a stable trajectory of ions of a said  $m/z$  ratio or ratio range that gun out the quadrupole leaving other unstable species to sheath off the mass analyzer. In simple terms, this path is mostly dependent as the magnitude of the rf voltage  $V$  and by the ratio  $U/V$ . These islet of stabilities, and under what conditions to find them, can be appreciated by plotting a graph with an ordinate as  $a$  (time invariant field) and the abscissa expressing  $q$  (time variant field) [6].

The relationship is of special interest as it is the stability diagram for two-dimensional quadrupole fields and reveals the existence by where: i) both x- and y- trajectories are stable, ii) either x- or y- trajectories are stable, and iii) no stable spurring of the ions takes place. See below, Figure 3.2.7.

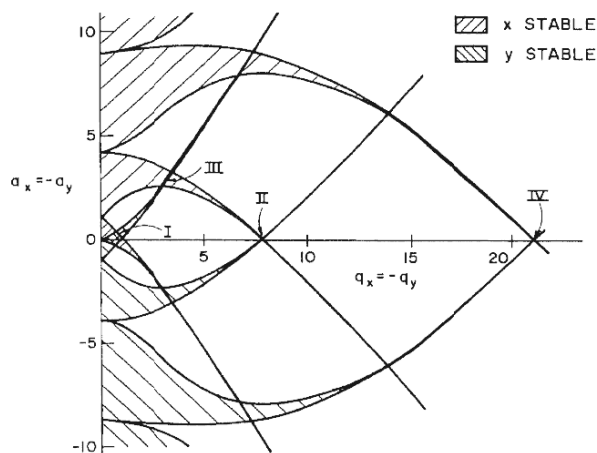


Figure 3.2.7. Stability diagram for a linear quadrupole analyzer depicting four stability regions (I-IV) corresponding to the x- and y-motions. Gross, JH: *Mass Spectrometry*.; Springer.; 2004.

For practical reasons, in the operational use of a MS instrument, region I is the only that applies to a routine working of the linear quadrupole, Figure 3.2.8.

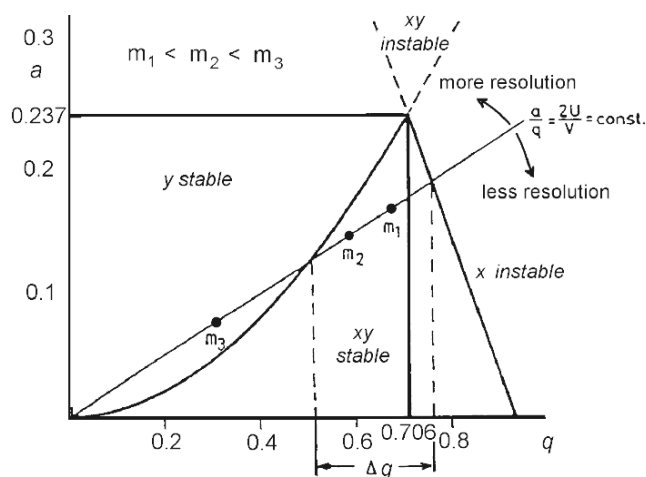


Figure 3.2.8. Upper half of region I of the linear quadrupole stability diagram. Gross, JH: *Mass Spectrometry*.; Springer.; 2004.

It is possible to tune the electricals of the linear quadrupole as to reach focal points that is to say where the ratio  $a/q$  would translate to the equality  $2U/V = 0.237/0.706 = 0.336$  pointing to the apex of the diagram. Conversely, lowering the said coefficient - in real terms reducing the  $U$  relative to  $V$ , it is possible to window of a range  $m/z$  ratios. In keeping this window small a sufficient resolution can be achieved. Gating a stable region of a width ( $\Delta q$ ) furnishes a given resolution. Modulating the magnitude of  $U$  and  $V$  at constant  $U/V$  ratio is how scanned ions of increasingly higher  $m/z$  values are brought about, Figure 3.2.9. [6, 18].

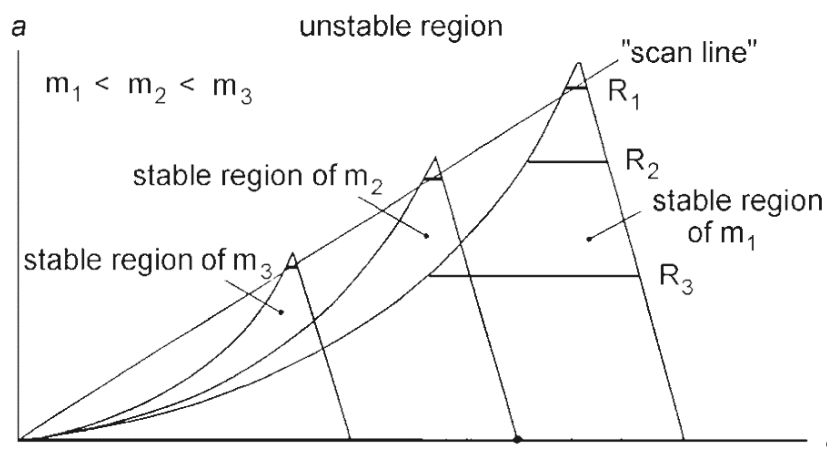


Figure 3.2.9.  $U/V$ =constant linked scan. Resolution levels are governed by the  $a/q$  coefficient. Higher  $a/q$  ratio translates into improved resolution and is represented by a steeper "scan line";  $R_1 > R_2 > R_3$ . Gross, JH: *Mass Spectrometry*.: Springer.; 2004.

### 3.2.4 Principle of the linear quadrupole ion trap

After having curtailed the ions through the various band-pass RF-only multipoles it is possible to halt the package of ions in a linear (quadrupole) ion trap (LIT). The linear ion trap typically consists of a front, center and back section, Figure 3.2.10. The flanking ion optics assure the admission and confinement or closure at the end of the longitudinal axis, they set a trapping potential that constrains the field to the central cell. This center section chambers the ion package prior to extracting them in an orderly fashion for mass analysis. Alternatively, the potential at the end aperture plates of the LIT can be switched in a way to provision portions of the chambered ions to other subsequent parts of an MS system such as FT-ICR or TOF analyzers. More information on these can be found elsewhere. Notice that as described above the LTQ Velos exercises all of its operations through a unified pair of hyperbolic quadrupoles, enhancing its dynamic range [8], sensitivity and capabilities in precursor selection and MS experiments [7, 8].

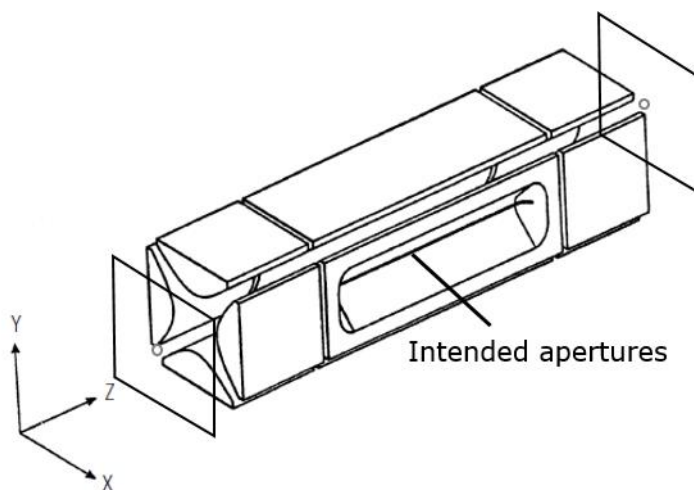


Figure 3.2.10. A pictorial depiction of the hyperbolic linear ion trap, displaying the ion exit slot and front and back sections (Gross. JH: *Mass Spectrometry*.: Springer.; 2004).

The LTQ Velos is a spectrometer with a dual-pressure linear ion trap [16], two hyperbole quadrupoles paired together. The dual-pressure linear ion trap consists of the two last quadrupoles. The first cell is held at a high pressure ( $\sim 5 \times 10^{-3}$  Torr). This first quadrupole is used to chamber precursor ions and convert them to product ions notably through CID. This first analyser cavity is also where MS/MS or higher order  $MS^n$  processes are executed. The second quadrupole of the dual-pressure linear ion trap is held at a lower pressure ( $\sim 4 \times 10^{-4}$  Torr) and is where the scan out of the ions is ran. In this way, by its dual cell instrumental geometry, it is possible to attain higher mass resolution for a given scan ran compared to previous MS trapping designs [16].

It is possible to describe some the basic principle of a hybrid rf/DC quadrupole-linear ion trap relevant to such a mass spectrometer. The principle is that ions are trapped in a linear ion trap by the rf voltage in the radial direction (see Figure 3.2.11) and the axial direction is controlled by the aperture plates which are DC biased. Motion at thermal velocities between the end aperture plates affect the ion motion in the axial direction, thus by modulating the DC potential of the plates it is possible to shuttle the ion packet from one linear ion trap quadrupole to the second one flanked by the detectors. Radial ion motion within a linear ion trap is governed by the solutions to the Mathieu equation [19]. For an ideal hyperbolic linear quadrupole, resonance excitation can occur when the frequency of an auxiliary AC field coincides that of the  $\omega$  angular frequency excitation. This results as an increase in radial amplitude of ion motion and eventual ejection from the trap, radially *i.e.* ions sheath out the intended apertures (last linear ion trap quadrupole) and are sent to the channeltron detectors. Application of an auxiliary AC field of appropriate amplitude and frequency to the rods of the ion trap efficiently provides this mass radial excitation [19].

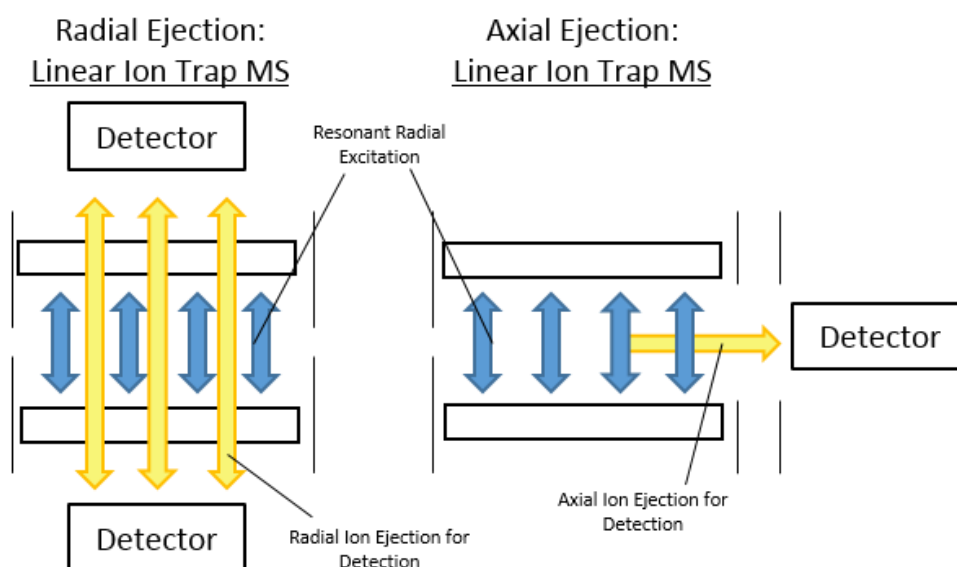


Figure 3.2.11. Ion ejection paths, radial and axial.

### On the superiority of hyperbolic shaped rods compared to cylindrical rods

The LTQ Velos conceives a collection of mass filters of cylindrical geometry, yet it configures an LIT of hyperbolic geometry. It is noteworthy to consider that this is because the cylindrical rods are advantageously much more straightforward to manufacture and are hence more democratic in cost versus the hyperbolic geometry [6, 17, 18]. However, hyperbolic poles do not have the disadvantage of engendering a reduction in the macromotion frequency in response to an arbitrary increased residence time of the ions within the quadrupole space. Also, slight inaccuracies with the mechanical shape of the quadrupole cause considerable losses of ion transmission and resolution. Experts in the field have addressed this by implementing the cylindrical assembly so as to proxy the hyperbolic field by installing the rods apart by  $r = 1.1468 r_0$  from each other ( $r$ , radius of the rod)[17]. Nevertheless, hyperbolic rods are in sum, superior and apply the transmission field more consistently and accurately, affording a higher resolution. This explains why they are saved to configure the mass analyzer of the MS system (as an LIT) [6].

Specification and characteristics of the LTQ Velos linear ion trap,  
Table 3.2.1.

Mass range	$m/z$ 15-200, $m/z$ 50-2000, $m/z$ 200-4000
Resolution	0.05 full width half maximum (FWHM) with Ultra zoom scan between $m/z$ 50-2000
Mass Accuracy	+/- 0.1 Da [20]
Scan power	MS <sup>n</sup> for n=1 through 10

Table 3.2.1. Characteristics of the LTQ Velos.

### 3.2.5 Summary of Mass Analyzer Operation

The process that occurs in the mass analyzer can be dotted down into four steps:

1. Ion storage
2. Ion isolation
3. Collision-induced dissociation
4. Ion scan out

The last step is carried out in the second chamber of the LTQ Velos that is neighboured by the detectors. Here the produced ions are scanned, the main rf voltage is increased incrementally and a resonance ejection ac voltage is applied in unison to the rods to assist ejection. This is how ions of greater  $m/z$  ratio are made progressively unstable and are ejected to impinge the detector saucers in an orderly fashion for signal processing, Figure 3.2.12 [7].

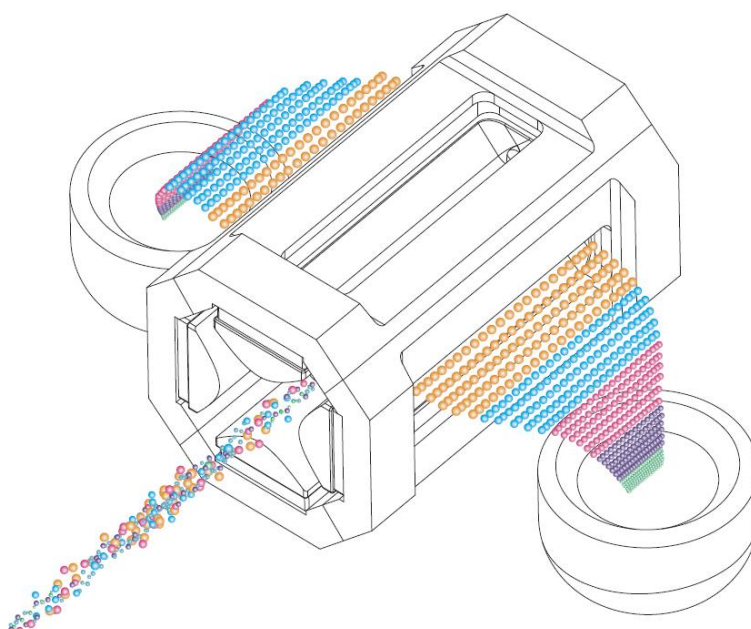


Figure 3.2.12. An ion 'Scan out' representation with ions exiting the trap to the detectors.  
Adapted from (Scientific TF: **LTQ Series**. In *Hardware Manual*; 2009).

### 3.2.6 Ion detection system

The ion detection system comprises of two flanking ion channeltron detectors (*vide supra*, Figure 3.2.12). These ion detection systems produce high signal-to-noise ratio and enable to change the voltage bias to either the positive ion or negative ion modes of operation. The channeltrons are based on a conversion dynode and an electron multiplier. The ion detection systems are situated on opposite to each other with respect to the second linear ion trap.

The conversion dynode can be described as a concave metal plate located at a right angle to the ion path. A positive potential for a negative ion channel and a negative potential for a positive ion channel are applied to the conversion dynode. On impact, the ions striking the conversion plate generate one or more secondary electrons. The curved surface of the dynode has an effect to converge these secondary electrons. These are then funneled down electrically to the electron multiplier. The conversion dynode also shields the vacuum manifold from the electric field that the conversion dynode produces.

The electron multiplier is fitted overhead to the cover plate of the vacuum manifold beside the mass analyzer. The electron multiplier comprises of a cathode and an anode. The cathode of the electron multiplier in essence is a funnel shaped resistor. The anode sits at the exit of the cathode. This anode fosters the electrons transmitted by the cathode. Secondary particles that bullet out from the conversion dynode hit the inner walling of the electron multiplier cathode with sufficient impact to eject electrons. These electrons in turn, strike the inner exposed space of the cathode further up. A snow ball effect is triggered as even more electrons discharge. This opens the possibility for a measurable current at the anode to be observed. The collected current by the anode is proportional to the number of secondary particles striking the cathode. The current that leaves the electron multiplier via the anode is saved by the data system. Altogether, the whole set up is designed in a way so that the orientation of the pieces prohibits any neutral undesirables to touch the conversion dynode or electron multiplier, considerably improving the signal to noise ratio [7].

### 3.2.7 Helium damping gas in the mass analyser

The mass analyzer cavity is pressurized with helium gas. Its role is one of a damping gas and collisional activation partner. The helium brakes and dims the kinetic energy of the ions through collisions and, having their amplitude of oscillation lowered, these then become amenable to trapping by the rf field in the mass analyzer and refocus to the center of the cavity of the trap. This is what is known as collisional cooling. Without helium it would be impossible to have the required sensitivity and mass spectral resolution for a commercial instrument.

When under the CID regime, the resonance excitation voltage drives the parent ions to collide with the helium atoms. Provided that the internal energy transfer from the impact is sufficient, the parent ion dissociates into one or more product ions.



### 3.3 LASER source

Continuum's Horizon OPO pumped by the third harmonic of a Surelite I Nd:YAG laser, Figure 3.3.1.



Figure 3.3.1. Horizon OPO and Surelite laser, in foreground and background respectively.

The light sources used throughout the course of this thesis have been the Panther EX OPO and a Horizon OPO (Continuum). Both are non-continuous, Q-switched lasers. The most routinely employed laser has been the most recent of the series, the Horizon OPO instrument, and will be the only one described in this thesis. The Horizon OPO comes as a three-piece product: a CPU and control board, the laser pump *i.e.* the Surelite laser piece and the optical parametric oscillator (OPO). The Surelite is the benchtop source - it houses together in order the integral parts that make up the “pump” in a nonlinear optical instrument. Crucially the box assembles the laser head module to the doubler and tripler crystals. The pump also comprises essential dichroics, polarizers and mirrors. The laser head itself shields in a rod, flashlamp and a coupling medium. The apparatus features a flashlamp that is mantled with a high brilliance magnesium oxide diffuser, in this way, high pumping efficiency, a reduced power consumption and low thermal loading is assured.

All of the components of the Surelite working in unison, it is possible by sum frequency generation to output a laser ray from the Nd:YAG fundamental wavelength (1064nm) all the way to its alternate second, third (532 nm, 355nm respectively). This is the result of streaming the fundamental beam either through a second crystal, a combination of a second with a third crystal. The harmonic crystals are located towards the end of the benchtop source. These are optimized as need be, using tuning knobs situated overhead and on the right of the exit port. The Surelite laser wave then proceeds with the last table-top component: the optical parametric oscillator. It is a separation package that when implemented confers the system to access a high-power output laser wave tunable to a range of colors in the UV-visible and near infrared (192-2750nm), see Figure 3.3.3.

The Horizon OPO instrument presents large improvements over other instruments such as the Panther EX OPO. Principally, there is no dip in the wavelength emission between 300-400nm due to improvements brought to the sum frequency generation. Another breakthrough has been that it can maintain a high pointing stability and does not need to realign throughout a step by step wavelength sweep or scan. Other specifications of the Horizon OPO include beam quality (5-7ns FWHM), beam pointing stability ( $<\pm 100\text{nm}$ ), a maximum energy of 2J, and a seamless freedom in drawing wavelengths of the vacuum ultraviolet region. The system is also equipped with ultra-resolution stepping motors for its Pellin Broca prism and crystals. All in all, the Horizon OPO has proven itself as a reliable source of stable light for our photophysical spectroscopy experiments [21].

## Rods

The laser head is laid out in a way to pump from an Nd +3 doped YAG garnet ( $\text{Y}_3\text{Al}_5\text{O}_{12}$ ). The degree of doping is in the order of 0.9 to 1.4%. The YAG rod ends are enhanced with hard dielectric antireflective coatings (AR). The rod length measures 115mm along and has a diameter width of 6mm or 9mm depending on specification of the product [21].

## Flashlamps

The linear flashlamps role is to pump the heads. The lamps are gas cells filled with xenon, they are pressurized at 1-3 atmospheres and are under a voltage polarity. The flashlamp reaches its discharge with a critical negative damped pulse (-1.8kV max) that lasts for the short period of 200 microseconds [21].

## Cooling

Both modules, flashlamps and rods are cooled by a circuit of distilled water [22].

## The optical parametric oscillator (OPO)

The Horizon OPO system is pumped by the input 355nm laser wave from the Nd:YAG garnet stimulated emission of the Surlite piece. The optical parametric process is a three-photon photophysical event whereby one photon from the pump laser wave drops out into a pair of less energetic ones [22]. The ‘daughter’ photons in general do not have the same energies. The higher energy photon generated is commonly termed as the signal whilst the lower energy photon is termed the idler, see Figure 3.3.2. To summarize, the input laser with frequency of  $\omega_p$  is converted to output waves of lower frequency ( $\omega_s, \omega_i$ ) as a response to what is referred to a second-order nonlinear optical interaction. This relationship gives us the following equation:  $\omega_s + \omega_i = \omega_p$ . This theoretical treatment tells us that there is an energy conversion process that can be understood as the reverse of the sum frequency generation; in other words, in reverse, two photons combine to form a third, more energetic photon. During this whole photophysical process, energy and momentum vectors are conserved, this is achieved by the optical properties of the transparent beta-barium borate (BBO) crystal. This material is the nonlinear parametric element, depicted in Figure 3.3.2. In effect, at certain angles; the idler and/or signal photons have polarizations orthogonal to the pump photon. Then the frequency dependent refractive index of the crystal changes the three laser wave’s velocities in a way that maintains their linear momentum. Tuning between such crystal birefringent axis angles, that conserve momentum, is known as phase matching. The technique that produces and determines the particular pair of signal and idler frequencies.

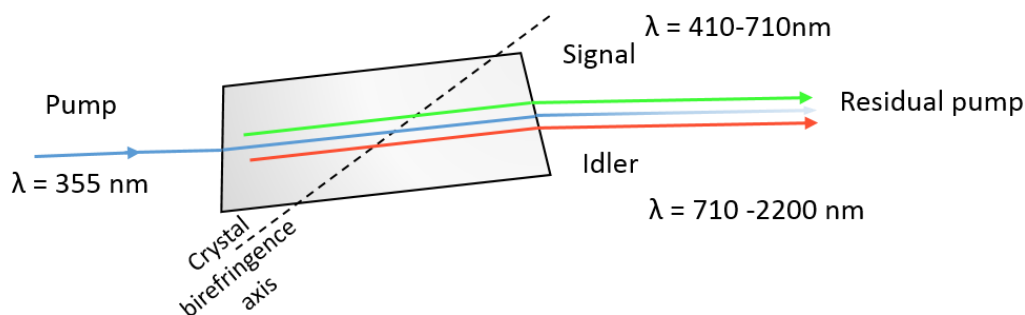


Figure 3.3.2. Beta barium borate harmonic crystal.

## 3.3.1 Legend to Horizon OPO Layout

Item	Description
1, 2, T1	Mirror dichroics, 355nm
3	Lens
4	Lens
5	Window
6	Porro prism
7	Half wave plate 355
8	Injection pump mirror
9	#1 Crystal BBO type-1
10	#2 Crystal BBO type-1
11	Mirror
12	Window
13 (A)	Polarizer
14 (B)	Half wave plate broadband signal
15	Window - Inquire manufacturer
16	Crystal, BBO
17 (C)	Waveplate UV broadband
18	Mirror
19	Crystal, BBO
20	Window - Inquire manufacturer
21	Pellin Broca
22	Mirror, 1064nm
23	Mirror, 1064nm
24	Half wave plate 1064
25 (D)	Beam dump assay
26	Pellin Broca
27, 28	Prism 90 degree

Table 3.3.1. OPO items.

The Horizon OPO illustrated above is an optical dispatching unit that serves to convert the high spatial coherent input of the pump wave into an output of mid-band radiation. The laser output is of the visible or near infrared part of the electromagnetic spectrum that would otherwise be impossible or difficult to obtain with a conventional laser based system. The OPO consists essentially of an optical resonator and a nonlinear optical crystal that treat the incoming pump waves. The mirrors and Pellin Broca then ensure that the generated parametric output the signal and idler is directed to their respective exits.

## 3.3.2 Horizon optical parametric oscillator blueprint

Signal/ Idler (for longer waves e.g infrared)

Output

400nm-2750nm

UV Output Output

192nm-400nm

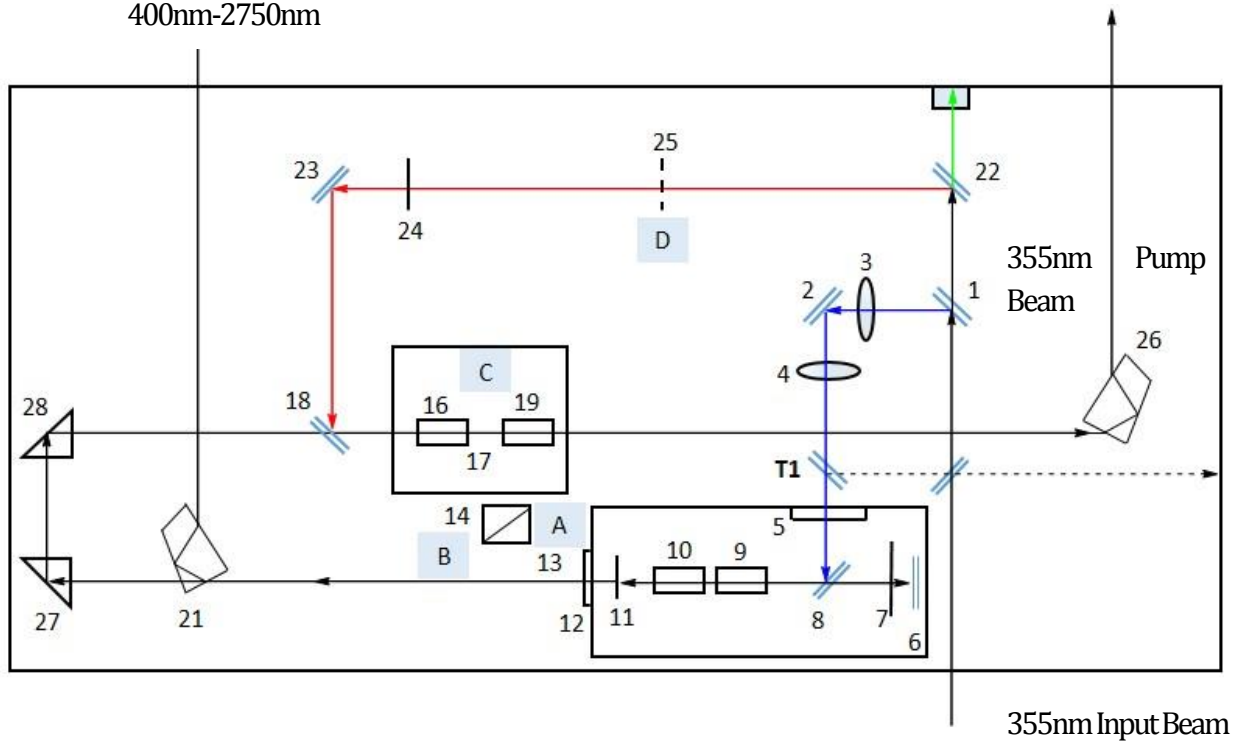


Figure 3.3.3. Functional layout of the Horizon optical parametric oscillator.

### 3.5 Installations

A birds-eye outlay of the installation is given below. Observe:

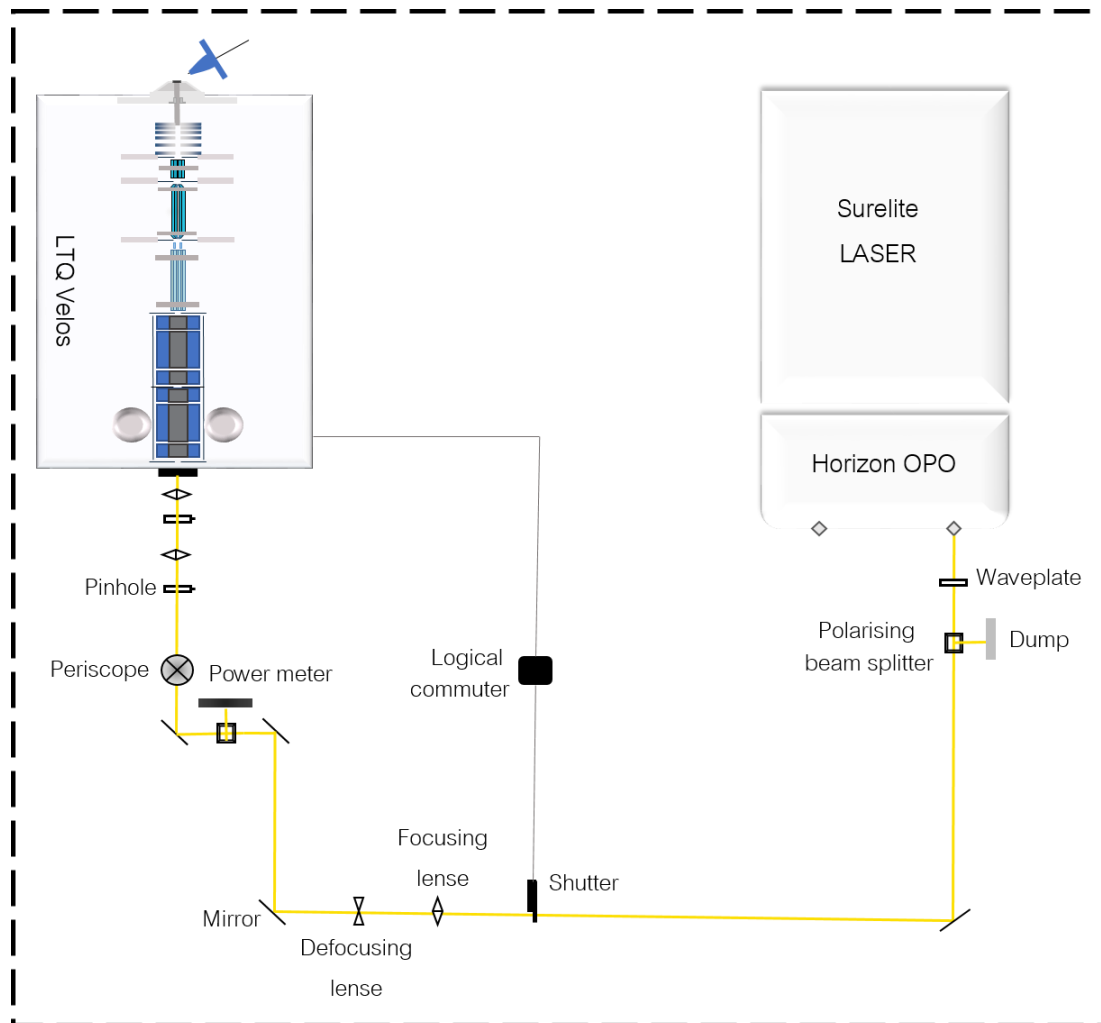


Figure 3.5.1. A bird's eye view on the arrangement of the LASER-MS appliance.

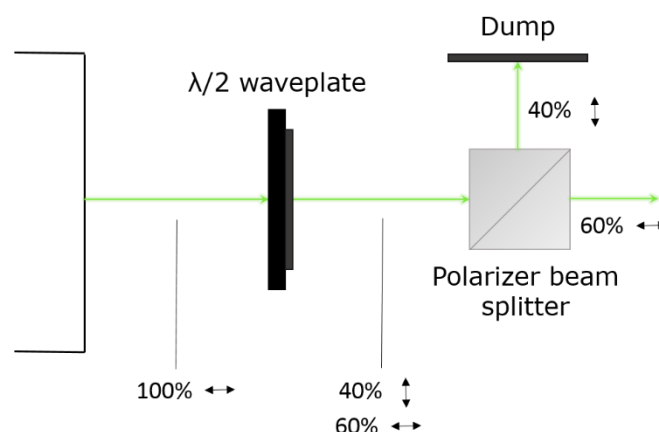


Figure 3.5.2. A brief outline on the setup used to modulate power of the produced coherent light.

### 3.5.1 LTQ Velos and LASER UV-Vis coupling set-up.

In a purposely built laboratory station is housed; a pair of optical benches (Newport), both the Panther EX OPO and a Horizon OPO, the LTQ Velos connected to its vacuum rotary pumps, gas lines and electrical power supply together with other peripherals. The Horizon OPO UV-Vis LASER sits on one of the tables leaving the other free to mount all the required optical pieces to orientate the beamline. The LASER wave is pinpointed to align with the central axis of the dual linear ion traps of the mass spectrometer. The core is accessed through a modification in the back panel of the instrument where a fused silica porthole (3mm thick, 2cm diameter) gives way to a 1-2mm diameter circular opening in the trapping electrodes cladding the free-floating ions. The laser wave is collimated by a series of pinholes, lenses and mirrors as to insure a maximum beam to ion bundle coverage. The ray is channeled into the trap by a 1000mm focal length convergent lens mounted on an optical rail. The irradiation is repeated at a rate of 10Hz with pulse widths of 5ns. An electromechanical shutter is temporarily synced to an 'ion activation window' of the LTQ Velos *i.e.* a time laps spanning from the onset the light enters the trapping chamber and the moment it takes to activate the ion ensemble. This connected obturator module adjusts the triggering to work in perfect unison with the mass spectrometer. The shuttering of the plate is in the order of a 10ms and thus does not influence the practical experiments which are of higher time proportions ( $> 100\text{ms}$ ). The necessary irradiation time is then matched for ion photo-activation and can be expressed as n number of laser pulses. In this way, an activation window of 100ms would correspond to the right injection time for the channeling of one 10Hz laser pulse, Figure 3.5.3.

Finally, a polarizing beam splitter crosscuts the pathway of the laser beam as to deviate a fraction ( $\sim 10\%$ ) of light that is used to take real time power measurements of the photophysical experiments. These fine power adjustments are made possible downstream the laser path using a half-wave plate, placed ahead of the polarizing beam splitter. The polarizer relies on Malus's law that states:  $I = I_0 \cos^2 \theta$  [23]. It tells us that as one varies the  $\theta$  angle, the angle between the polarization of the polarizer and the laser's incident polarization telescope orientation, the intensity of the output wave of a given polarizability can be decreased or increased progressively, Figure 3.5.2.

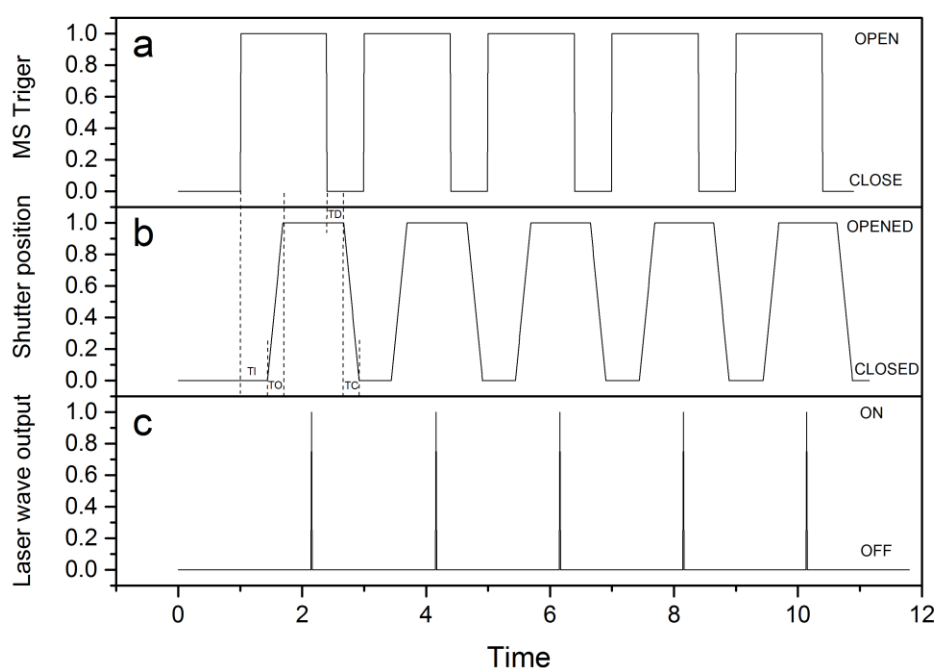


Figure 3.5.3. A panel illustrating the synchronisation between the triggering from the MS computer, the shutter mechanics, and the laser wave pulsing. (TI) transfer initialize (TO) transfer open (TD) transfer dwell (TC) transfer close.



### 3.5.3 LASER alignment

All of the photophysical methods developed within this thesis commend for a precise alignment of the LASER wave with the linear ion trap's cells. In retrospective there is not much to it, in steering the LASER ray. All that is needed is a business card, phosphor paper and pinholes in order to align the LASER beam exiting the Horizon OPO to the center of the silica opening of the MS. The final result can be diagnosed by injecting a 10 $\mu$ M solution of QSY chromophore that fragments at a known wavelength of 545nm and setting the LASER system to 545nm output reading. Fine tuning can be carried out by gently adjusting the knobs of the final mirrors of the periscope and aligning the beam onto a closed iris located at the end of the optical rail close to the built-in window. It is possible to sweep the position whereby the LASER hits in order to find an optimum in LASER alignment that translates to a maximum in QSY fragmentation signal of the parent peak. At the beginning of this thesis, Guidestar II LASER beam Steering correction system (Newport) was used. This package was employed to so-call bring unprecedented improvements in accuracy, reliability and ease of use. It was however flawed and had major problems in routinely acquiring the initial position on the LASER beam and following this straightforwardly between wavenumbers. The optional module proved inaccurate and fatiguing in the long run versus correcting the LASER path manually.

### 3.6 References :

1. Creighton TE: *The physical and chemical basis of molecular biology*. Helvetian press; 2010.
2. Wysocki VH, Resing KA, Zhang QF, Cheng GL: **Mass spectrometry of peptides and proteins**. *Methods* 2005, **35**:211-222.
3. Strupat K: **Molecular weight determination of peptides and proteins by ESI and MALDI**. In *Mass Spectrometry: Modified Proteins and Glycoconjugates. Volume 405*. Edited by Burlingame AL. San Diego: Elsevier Academic Press Inc; 2005: 1-36: *Methods in Enzymology*.
4. Kaltashov IA, Eyles SJ: *Mass spectrometry in biophysics*. Hoboken, New Jersey: Wiley; 2005.
5. John R. Dean AMJ, David Holmes, Rob Reed, Allan Jones, Jonathan Weyers: *Practical skills in chemistry*. 2<sup>nd</sup> edn: Prentice Hall; 2011.
6. Gross. JH: *Mass Spectrometry.*: Springer.; 2004.
7. Scientific TF: **LTQ Series**. In *Hardware Manual*; 2009.
8. Domon B, Aebersold R: **Review - Mass spectrometry and protein analysis**. *Science* 2006, **312**:212-217.
9. Smith RD, Loo JA, Edmonds CG, Barinaga CJ, Udseth HR: **New developments in biochemical mass-spectrometry - electrospray ionization**. *Analytical Chemistry* 1990, **62**:882-899.
10. Fenn JB, Mann M, Meng CK, Wong SF, Whitehouse CM: **Electrospray ionization-principles and practice**. *Mass Spectrometry Reviews* 1990, **9**:37-70.
11. Ikonomou MG, Blades AT, Kebarle P: **Electrospray ion spray - a comparison of mechanisms and performance**. *Analytical Chemistry* 1991, **63**:1989-1998.
12. Dole M, Mack LL, Hines RL: **Molecular beams of macroions**. *Journal of Chemical Physics* 1968, **49**:2240-&.
13. Iribarne JV, Thomson BA: **Evaporation of small ions from charged droplets**. *Journal of Chemical Physics* 1976, **64**:2287-2294.
14. Metwally H, McAllister RG, Popa V, Konermann L: **Mechanism of protein supercharging by sulfolane and m-nitrobenzyl alcohol: molecular dynamics simulations of the electrospray process**. *Analytical Chemistry* 2016, **88**:5345-5354.
15. Brodbelt JS: **Ion Activation Methods for Peptides and Proteins**. *Analytical Chemistry* 2016, **88**:30-51.
16. Second TP, Blethrow JD, Schwartz JC, Merrihew GE, MacCoss MJ, Swaney DL, Russell JD, Coon JJ, Zabrouskov V: **Dual-Pressure Linear Ion Trap Mass Spectrometer Improving the Analysis of Complex Protein Mixtures**. *Analytical Chemistry* 2009, **81**:7757-7765.
17. March RE: **Quadrupole ion traps**. *Mass Spectrometry Reviews* 2009, **28**:961-989.
18. Vernier MA: **Développement instrumental en spectrométrie de masse pour le diagnostic *in vitro* en microbiologie clinique. Développement instrumental en spectrométrie de masse pour le diagnostic *in vitro* en microbiologie clinique**. Thèse de l'université de Lyon, École doctorale de physique et d'astrophysique; 2014.
19. Hager JW: **A new linear ion trap mass spectrometer**. *Rapid Communications in Mass Spectrometry* 2002, **16**:512-526.
20. **Mass spectrometer specifications guide: Thermo Fisher Scientific's Thermo Scientific LTQ Velos**.
21. Continuum: **Horizon I and II OPO. Operation and Maintenance**. In *Manual*. pp. 67; 2012:67.
22. Continuum: **Operation and maintenance manual for surelite lasers.**, 2013.
23. Brunet C: **Photodetachment d'électron de polyanions: aspects fondamentaux et applications en spectrométrie de masse**. Thèse de l'université de Lyon, École doctorale de physique et d'astrophysique; 2012.



## Chapter 4 FRET.

Herein is discussed the current state of understanding of the different types of energy transfer, chiefly; Dexter, Forster and radiative coupling. In this section, definitions, differences and similarities and the mathematical treatment are covered where applicable with regards to the three aforementioned energy transfers. This chapter also discusses developments of FRET in solution and how it has been used to approach investigations in the gas phase. Afterwards, the innovation of the experimental work and data analysis in FRET is described. Information on how it has been taken to studying a section of i) the wild type 42-residue form of amyloid beta protein ii) a cyclodextrin system.

### 4.1 Types of energy transfer

#### 4.1.1 FÖSTER

Föster resonance energy transfer (FRET) is a photophysical phenomenon first observed empirically by Perrin at the beginning of the 20<sup>th</sup> century [1]. However, it was Theodor Föster who first postulated a theory describing the molecular interaction in the late 1940s [2-4]. Today the coined term is also known as fluorescence resonance energy transfer. FRET is a very important area of investigation as it is pertinent to many theoretical and experimental subjects from different research disciplines. It has its place in the fundamental life sciences on theoretical physics and chemistry, and furthermore, the applied sciences in physics, electronics, chemistry, medicine and biology [3]. Nowadays, it finds many use in contemporary science as it fits extremely well with the recent discoveries and investigations made in nanoscience and nanobiotechnology [3]. Recent representative highlights to this claim include the described nano-biosensors that are used to detect physiological relevant native protein substrate activity, the cleavage activity of several deubiquitinating enzymes in real time or the determination of the inhibitory efficiency of different enzymes [5].

An adequate definition of Foster or Fluorescence energy transfer is offered by Renato Zenobi [6]; "Fluorescence resonance energy transfer (FRET) is a distance-sensitive method that correlates changes in fluorescence intensity with changes in distance and orientation of specific spectroscopically active (donor, acceptor, quencher) moieties. The distance between fluorophores is defined as the distance between the centers of the donor and acceptor chromophores". Another excellent resumé is offered in the handbook, photochemistry and photobiology, ASP Edition, p.16 [7]. In other words, it is a radiation-less process whereby an energy donor (*d*) that gets electronically excited by photonic means and passes, transfers, its energy in a non-radiative manner by dipole-dipole interaction to the complementary energy acceptor (*a*) which consequently relaxes by fluorescence (see Figure 4.1.1).

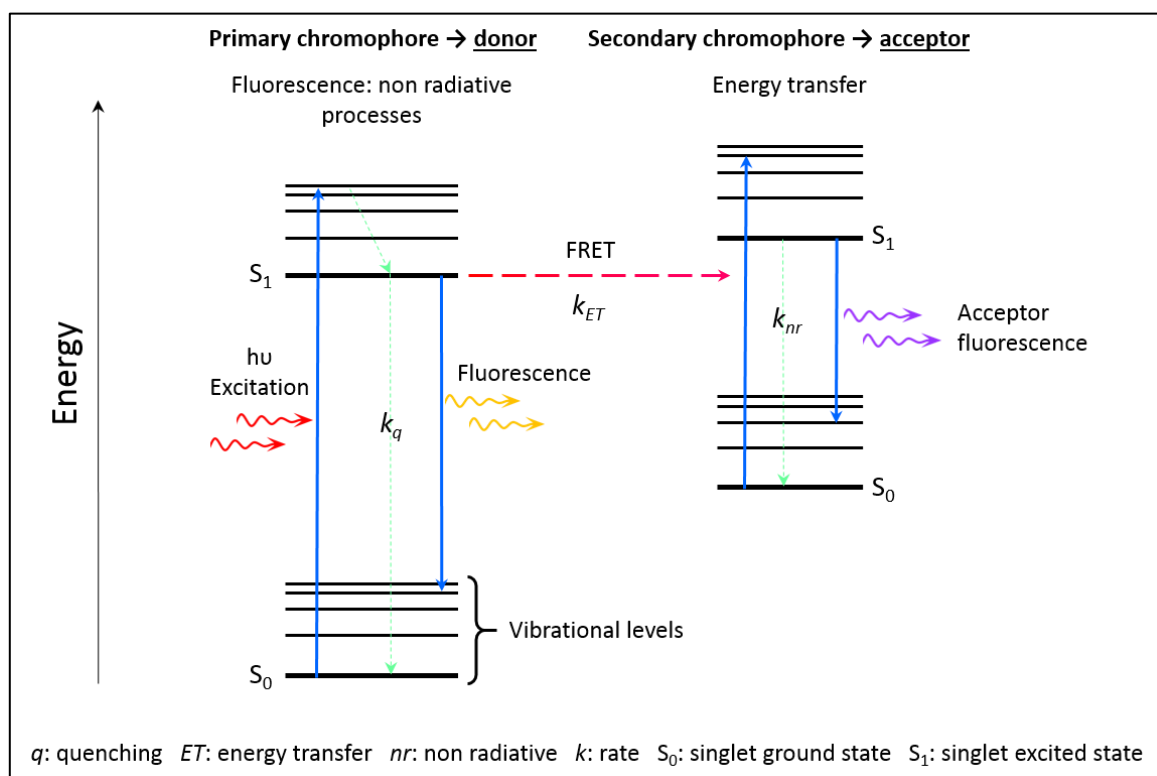


Figure 4.1.1. FRET described in a Jablonski diagram, adapted [8].

The energy acceptor ( $a$ ) must be able to absorb the light of the same spectral region to that of the emission of  $d$ : the excitation region of the donor must overlap with that of the acceptor, see Figure 4.1.2.

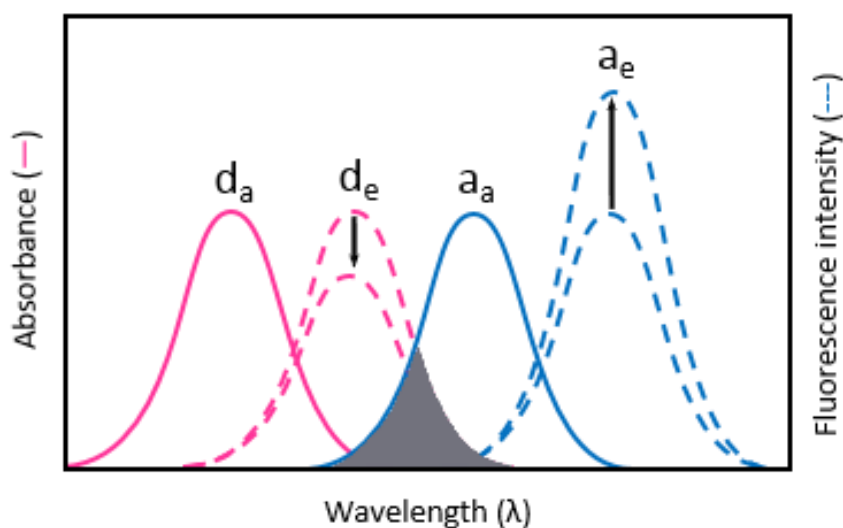


Figure 4.1.2. The spectra of a pair of fluorescent dyes suitable for fluorescence resonance energy transfer. The absorption spectra (full lines) of the donor ( $d_a$ ) and acceptor ( $a_a$ ) and the emission spectra (broken lines) of the donor ( $d_e$ ) and acceptor ( $a_e$ ) are depicted. The down arrow indicates the quenching of the donor emission induced by energy transfer and the up arrow highlights the enhanced emission of the acceptor.

Example of emission and excitation spectra for a chromophore is given in Figure 4.1.3 for support.

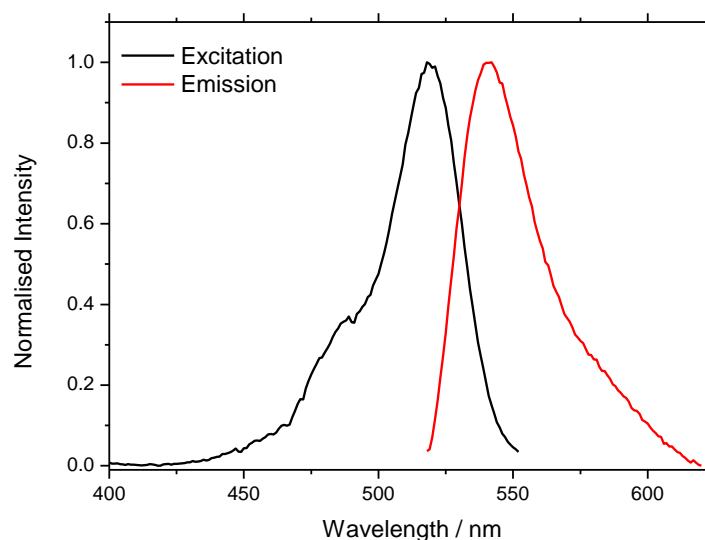


Figure 4.1.3. Spectral excitation-adsorption band and spectral emission band of Eosin Y in H<sub>2</sub>O at pH 2.53. Fluorecence monitored at 555nm, Fluoromax-4 spectrophotometer (Horiba).

This is what is referred as being the *resonance condition* (FRET= Föster Resonance Energy Transfer) [3]. It should also be checked that the chromophore FRET pair of choice can be coupled to the species of interest (*e.g.* bioconjugation to a protein). Another point to consider is whether the framework of interest will be studied on the single molecule level or together in concert as FRET acts either inter-or intramolecularly [3].

#### FRET the basic concept

The distance dependence of this energy transfer covers a distinctive range in the order of 10 to 100 nm. More accurately, the energy transfer efficiency between donor and acceptor molecules decreases according to the evolution of the sixth exponential of the distance separating the two FRET chromophores (see equ. 4.1.1.1). In sum it is a through-space interaction as opposed to Dexter energy transfer discussed below [9]. This main basic principle of FRET is typically conceptualised together with a Jablonski type diagram, Figure 4.1.1. It shows how the Coulombic mechanism, where an electronic transition from a higher to a lower energy level, in *d*, leads to an electronic transition from a lower to a higher energy level in *a* (with no electron exchange) for transitions that are in energetic resonance [3].

Föster ultimately brought about a mathematical relationship, a rate constant ( $k^{Föster}$ ) for this molecular interaction between the acceptor and the donor which tells us that;

$$4.1.1.1 \quad k^{Föster} = \frac{1}{\tau_D} \cdot \frac{9000(\ln 10)\kappa^2 QY_D J(\lambda)}{128\pi^5 N n^4} \cdot \frac{1}{R^6}$$

$k^{Föster}$  is the rate transfer constant       $\kappa$  is the dipole dipole orientation factor  
 $QY_D$  is the fluorescence quantum yield       $J(\lambda)$  is the Föster spectral overlap in  $M^{-1}cm^3$   
 $N$  is avogadro's number       $\tau_D$  is donor lifetime  
 $R$  is the centre to centre donor – acceptor distance in cm  
 $n$  is the refractive index of the intervening medium; the solution

Equation 4.1.1.2 describes the orientation factor  $\kappa$  between the transition dipole moments of the acceptor and donor chromophores.

$$4.1.1.2 \quad \kappa = \hat{\mu}_D \cdot \hat{\mu}_A - 3(\hat{\mu}_D \cdot \hat{r})(\hat{\mu}_A \cdot \hat{r}) = \cos \theta_{DA} - 3\cos \theta_D \cdot \cos \theta_A$$

The vectors and angles are depicted in the figure below.

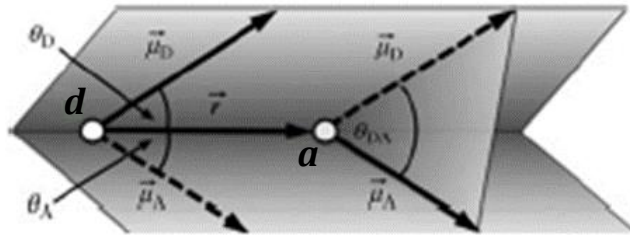


Figure 4.1.4. Angles describing the orientation of the dipoles used in the theoretical treatment of equation 4.1.1.2. Adapted from (Medintz I, Hildebrandt N: FRET - Foster resonance energy transfer: From theory to applications; 2013).

The so-called orientation factor kappa-squared ( $\kappa^2$ ) is taken on a case by case basis or more frequently considered in an average to the ensemble of objects in a given experiment. In a single molecule level only, time averaging is possible whereas in a multimolecular experiment average over time as well as a rolling average reflecting the response of the ensemble may be put forward. Taking the different angles between the transition dipole moments of  $d$  and  $a$  ( $\vec{u}_D$  and  $\vec{u}_A$ ) and the connection vector between  $d$  and  $a$  ( $\vec{r}$ ) manages the mathematics that solve the value for the orientation factor in equ. 4.1.1.2. Where  $\hat{u}_D$ ,  $\hat{u}_A$  and  $\hat{r}$  represent the unit vectors  $\vec{u}_D$ ,  $\vec{u}_A$  and  $\vec{r}$ , respectively, and  $\theta_{DA}$ ,  $\theta_D$  and  $\theta_A$  are the angles depicted in Figure 4.1.4.

In summary, average conditions rest on the idea that when all  $d$  and  $a$  can take any possible orientation during a said FRET time, the system is in dynamic averaging regime and  $\kappa^2$  can be considered to hold at  $2/3$ . This remains true if  $d$  and  $a$  are bound to polypeptides or proteins. If one of the chromophores has a fixed orientation, then  $\kappa^2$  can take values between  $1/3$  and  $4/3$ . When both are fixed, 'line to line', the case becomes more complicated: the full orientation factor range ( $0 < \kappa^2 < 4$ ) is weighed up [3].



### 4.1.2 Foster Radius

In many treaties discussing on FRET,  $R_0$  is often used. This term is commonly accepted as the Foster Radius. The term is defined as the distance at which the resonance energy transfer is 50% efficient (*i.e.*, 50% of excited donors are deactivated by FRET as it excites the acceptors). The  $R_0$  term, is dependent on the spectral properties of the donor and acceptor dyes and are calculated from transfer efficiencies [2], see Table 4.1.1.

For detailed values:

$$4.1.2.1 \quad R_0 = [8.8 \times 10^{23} \cdot \kappa^2 \cdot n^{-4} QY_D \cdot J(\lambda)]^{1/6} \text{\AA}$$

Here,	$\kappa^2 = \text{dipole orientation factor}$ ( $\kappa^2 = 2/3$ for randomly orientated donors and acceptors)
	$QY_D = \text{fluorescence quantum yield of the donor in the absence of the acceptor}$
	$n = \text{refractive index}$
	$J(\lambda) = \text{spectral overlap integral}$ $= \int \varepsilon_A(\lambda) \cdot F_D \cdot \lambda^4 d\lambda \text{ cm}^3 \text{ M}^{-1}$
And,	$\varepsilon_A = \text{extinction coefficient of acceptor}$
	$F_D = \text{fluorescence emission intensity of donor as a fraction of the total integrated intensity}$

Donor	Acceptor	$R_0$ (Å)
Fluorescein	Tetramethylrhodamine	55
IADENS	Fluorescein	46
EDANS	Dabcyl	33
Fluorescein	Fluorescein	44
BODIPY®FL	BODIPY®FL	57
Fluorescein	QSY®7 and QSY®9 dyes	61

Table 4.1.1. Typical values of  $R_0$  [10]. Values are calculated from spectroscopic data.

### 4.1.3 Dexter or Electron Exchange Energy Transfer

Aside from the FRET-like type of energy transfer mechanisms described herein, there are several other types of energy or charge transfer mechanisms. Among these there is the one that are considerably shorter to FRET ranges. In effect, there is the electron exchange mechanism (Dexter) which requires orbital overlap between donor and acceptor components, with exponentially decaying distance dependence ( $e^{-r}$  distance dependence) measured in the <1nm range [3, 9, 11]. The *sine qua non* condition of the electron exchange mechanism also implicates that exchange rate itself, depends on the spectral overlap of  $d$  and  $a$ .

In the case of overlapping orbitals of donor and acceptor grafted species, which require short  $d$ - $a$  interdistances, electron exchange between  $d$  and  $a$  can occur. This mechanism is different from the Coulombic interaction in FRET or the electron tunneling in charge transfer (Figure 4.1.5).

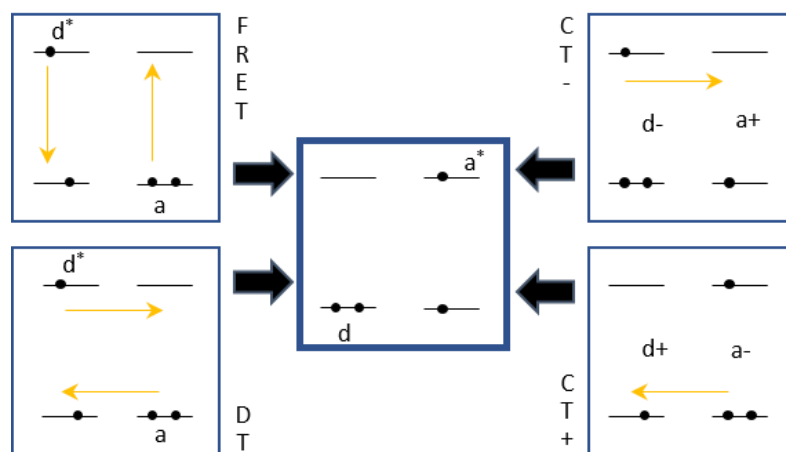


Figure 4.1.5. Functional mechanisms for generating a ground state donor and an excited acceptor ( $d+a^*$  as shown in the centre) by FRET (top left Coulombic coupling of  $d^*$  and  $a$ ), Dexter transfer (DT, bottom left: electron exchange between  $d^*$  and  $a^*$  and  $a$  and  $d$ ) or charge transfer (top right, CT-:  $d$  as electron donor, CT+:  $d$  as hole donor, bottom right)

The electron exchange rate is directly dependent to the extent of orbital overlap, which is seen to decrease exponentially with increasing  $d$ - $a$  distance. Electron exchange requires energetic resonance of  $d$  and  $a$  and therefore the exchange rate will also be dependent on the spectral overlap of  $d$  and  $a$  [3].

A theory for electron exchange-mediated energy transfer was developed by Dexter in 1953 [12]. The rate constant of electron exchange energy transfer (or Dexter transfer (DT)) is given by [3]:

$$4.1.3.1 \quad k_{DT} = K J_{DT} \exp\left(\frac{-2r}{l}\right)$$

$r$  is the distance between the two macrocycles  
 $K$  is an experimental constant

$J_{DT}$  is the integral overlap  
 $l$  is the average Bohr radius

Where  $K$  is a constant related to specific orbital interactions and  $J_{DT}$  is the spectral overlap integral. This spectral overlap is similar to the  $J$  in FRET with the important difference that both the fluorescence and the absorption spectrum are normalized. The corollary being that (in contrast to FRET) the spectral overlap integral is not dependent on the molar absorptivity (extinction coefficient). Here,  $r$  is the interdistance separation between  $d$  and  $a$  and  $l$  is the average Bohr radius ( $l = 4.8$  for porphyrin [11]). As the transfer rate of Dexter transfer decreases exponentially with  $r$ ,  $k_{DT}$  becomes negligibly small for  $d$ - $a$  distances in the range of 0.5 to 1 nm.

In contrast to charge transfer, the solvent plays a minor role (apart from establishing the collision of  $d$  and  $a$  via diffusion) for the transfer. As the constant  $K$  cannot be easily related to experimentally determinable quantities, it is difficult to perform a quantitative experimental characterization of Dexter transfer [3].

#### 4.1.4 Radiative coupling in atomic systems

Radiative coupling is another type of energy transfer phenomenon. It is a radiation-based process unlike FRET which is non-radiative. Compared to Foster energy transfer, it is a physical phenomenon where interferences lead an evolution to certain coherences and excitations, in consequence spontaneous emission is affected and a photon is emitted from a first atom (say atom  $A$ ) to a second accepting atom (say atom  $B$ ). It is a two-step process, a photon excites a ground state electron of atom  $A$ , and then the released photon is absorbed by the coupled atom of closely lying energy. It concerns neighbouring multilevel atom pair systems that have near degenerate states and are positioned at a distance where the two dipoles is less than that of the wavelength of radiation. The dipole-dipole coupling interaction between atoms leads to a population transfer from the first atom to the second. In other words, an energy transfer between both states take place (atom  $A$  and atom  $B$ ). The excitation of atom  $B$  to higher lying energy state can be triggered by single-photon transfer from  $A$  to  $B$ . However, the excitation of atom  $A$  to higher lying energy state occurs only via a relaxation of an excited atom  $B$  and the net transfer of two photons [13]. It is a formal process relevant to many physical topics such as quantum dots in the context of information processing [14], ZnO optoelectronic devices [15], plasmonics of nanoparticles [16] or the study of quantum wells and Bragg structures [17].

### 4.3 Conventional FRET — Applications.

Much on FRET has over arched on solution phase projects and it has transpired that FRET in the condensed phase spans a variety of application. These works are well documented and made available in the commercial handbook on molecular probes (eleventh edition) magasined by Invitrogen and life technology, the company. It seems valuable to present and expand on these application of FRET as an investigative tool.

#### 4.3.1 Selected applications of FRET in solution

##### Structure and conformation of proteins

A major usage of FRET has been in the probing and characterization of protein conformations. As early as 1993, by the means of monitoring the fluorescence intensity, Mardh and coworkers have been able to shed light on the different binding state pig kidney ATPase holds with  $\text{Na}^+$  and  $\text{K}^+$  ions and how it cycles through phosphorylation and dephosphorylation changes [18]. Futhermore, in another study, steady state measurements on donor-acceptor energy transfer between fluorescein elastase and rhodamine- $\alpha_1$ -protease inhibitor has allowed to observe fast formation of a complex to be observed, distinguished from a tight complex and a converted more dissociated inhibited complex [19]. Others describe a donor-acceptor based pair experiment that allowed the measurement of dissociation/unfolding rate constants of a protein, Arc repressor, under a set of denaturing concentrations and native microenvironments, Figure 4.3.1 [20]. Here the central insight is that energy transfer is used to monitor the formation of heterodimers made of the two proteins, of a donor and acceptor component.

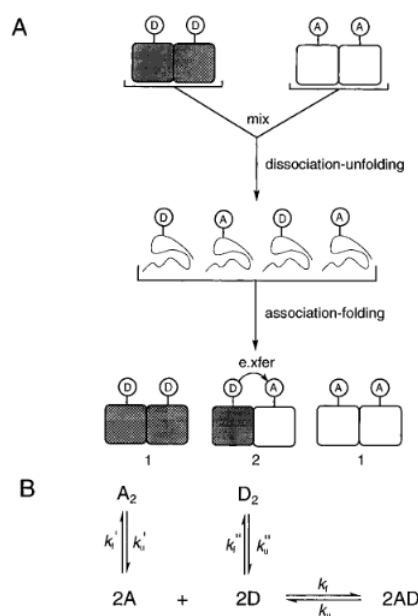


Figure 4.3.1. Illustration on the procedure for measuring unfolding rates by energy transfer. (A) Arc dimers, labelled with donors or acceptors, are combined, and the formation of heterodimers is monitored by energy transfer between the donor and acceptor. (B) Rate constants determining the equilibration between homo- and heterodimers following mixing. If bound to the fluorescent groups does not affect the kinetics of protein unfolding or refolding (i.e.,  $k=k'=k''$ ), then the global equilibrium dividing the native dimers and denatured monomers is not perturbed. The mixture approaches equilibrium with a rate constant corresponding to  $k_u$ , the unfolding rate of the heterodimer. Reprinted (adapted) with permission from (Jonsson T, Waldburger CD, Sauer RT: Non-linear free energy relationships in arc repressor unfolding imply the existence of unstable, native-like folding intermediates. *Biochemistry* 1996, 35:4795-4802). Copyright (2017) American Chemical Society.

Continuing in this theme, Tao *et al.* have applied the resonance transfer technique to delve deeper into the geometry of protein troponin and calque out how the cysteine residue of the protein coordinates in its complex system with or without the  $\text{Ca}^+$  regulatory ion [21]. Similarly, resonance energy transfer technique enabled to map out with considerable precision the inter-distance of the residues at a binding site giving an appreciation of the relationship of the key enzymatic subunit of the retinal cyclic GMP phosphodiesterase vis-a-vis the reactive subunit residue of transducing [22]. In the same context, Cheung's laboratory produced some results unveiling the inner reaction mechanics of actomyosin in hydrolysis of ATP. Their work suggests that a helical subsection, myosin subfragment move closer to the terminal end of actin whilst the second helical segment of the protein remains stationary in the weak binding state of actomyosin [23].

## Spatial distribution and assembly of protein complexes

A first highlight worthy of mentioning is the reported work of Remedios *et al.* that have applied the FRET method to scrutinize F-actin and determine distinguishable F-actin models and conformations, Figure 4.3.2 [24]. The major learning is that F-actin assembles itself around in a twist.

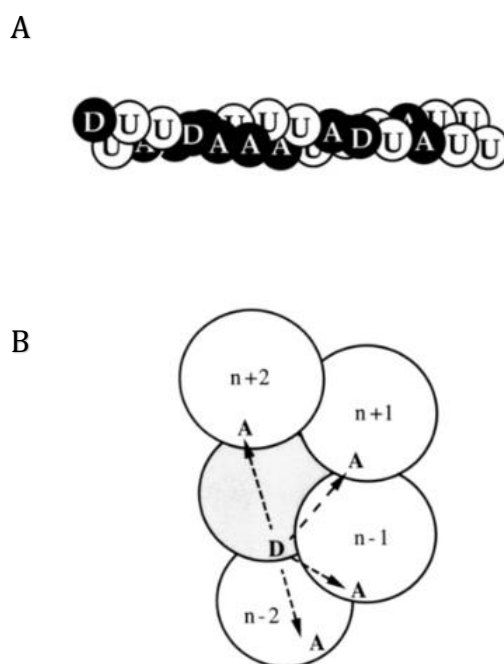


Figure 4.3.2. (a) Depiction of a randomly assembled actin filament (A, acceptor-labeled monomer; D, donor-labeled monomer; U, unlabelled monomer). (b) Putative distribution of acceptor-labeled monomers around a donor-labeled monomer. Reprinted (adapted) with permission from (Moens PDJ, Yee DJ, dos Remedios CG: Determination of the radial coordinate of cys-374 in f-actin using fluorescence resonance energy-transfer spectroscopy - effect of phalloidin on polymer assembly. *Biochemistry* 1994, 33:13102-13108). Copyright (2017) American Chemical Society.

There is also a literature record of using FRET to study proximity relationships between epidermal growth factor (EGF) molecules isolated from human epidermoid cells. It was found that if the microenvironment comprised divalent metal ions, activators of the EGF receptor/tyrosine kinase then a higher extent of FRET between EGF frameworks was observed [25]. As reported with this theme, FRET has been applied to render the localization of the haem moiety of cytochrome b5 in the membrane, describe aggregation states (bacteriorhodopsin), and clarify on interactions among red cell membrane proteins or rhodopsin-G-protein relationships. FRET has also been key in determining the orientation of cobra  $\alpha$ -toxin with respect to the nicotine acetylcholine receptor and the location of the retinal chromophore in the so-called purple membrane. The author goes further, on more assembly configurations that have been elucidated using FRET [26].

## Receptor ligand interaction

The current state of understanding on FRET has prompted research groups to utilize fluorescence polarization detection to assay for binding studies, notably G protein-coupled receptors (GPCR)-ligand binding assays. The technique has been developed and optimized so to replace conventional radioligand based assays. The principle relies on measuring the level of displacement of a fluorescently tagged peptide that binds to the receptor for the agonist framework, the drug candidate [27]. Their principal relies on auto-fluorescence and arguably does not work on FRET. The concerted efforts of Glossmann *et al.* have succeeded in measuring site binding densities between dihydropyridine (DHP) tagged with a chromophore, DMBODIPY-DHP and L-type  $\text{Ca}^{2+}$  channels. They found that specific binding increases the fluorescence yield of DMBODIPY-DHP and induced FRET to occur with the tryptophan residues of the  $\alpha_1$ -subunit of the L-type  $\text{Ca}^{2+}$  channels, review Figure 4.3.3 and Figure 4.3.4 for support [28].

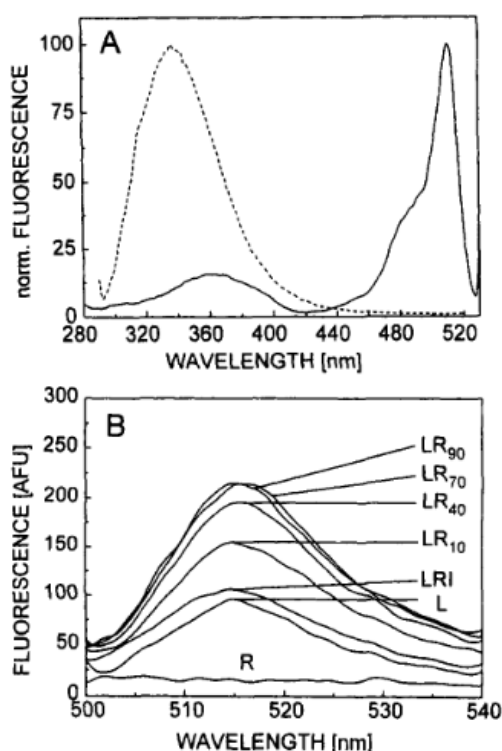


Figure 4.3.3. Fluorescence energy transfer between  $\text{Ca}^{2+}$  channel tryptophan residues and DMBODIPY-DHP. (A) Spectral overlap of protein emission profile and DMBODIPY-DHP excitation spectrum. (---) Emission spectrum of partially purified receptor in binding buffer, 285nm excitation wavelength. (—) Excitation spectrum of DMBODIPY-DHP. Arbitrary fluorescence was normalized. (B) Emission spectra of DMBODIPY-DHP in the absence and presence of receptor protein after excitation at 285nm. The acronyms; R, receptor alone in buffer, L ligand before addition of receptor protein; LR10, LR40, LR70, and LR90, recordings 10, 40, 70 and 90min after addition of or receptor protein. The LRI profile corresponds to a recording after dissociation of saturable DMBODIPY-DHP binding by (+)-isradipine (90min). Reprinted (adapted) with permission from (Berger W, Prinz H, Striessnig J, Kang HC, Haugland R, Glossmann H: Complex molecular mechanism for dihydropyridine binding to l-type  $\text{Ca}^{2+}$ -channels as revealed by fluorescence resonance energy-transfer. *Biochemistry* 1994, 33:11875-11883). Copyright (2017) American Chemical Society.

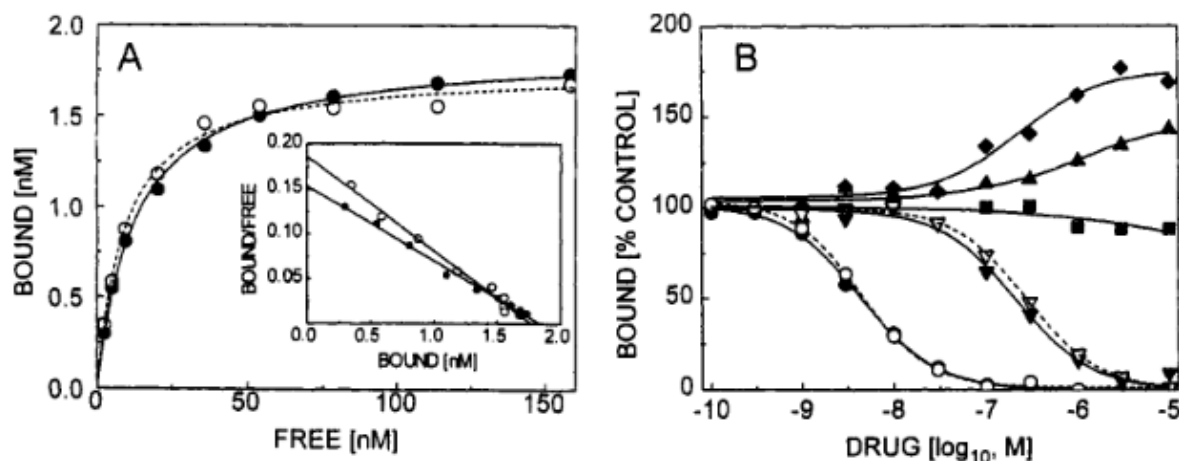


Figure 4.3.4. Equilibrium binding properties and pharmacological profile of DMBODIPY-DHP binding to L-type  $\text{Ca}^{2+}$  channels using FRET. (A) Saturation analysis: partially purified DHP receptor protein incubated for 60min with increasing concentrations of DMBODIPY-DHP in the absence (total binding) or presence (nonspecific binding) of  $1.5 \mu\text{M}$  (+)-isradipine (1ml final assay volume). Total ligand concentration was measured by excitation at 488nm. The FRET fluorescence was acquired by excitation of the samples at 285nm (emission measured at 517nm). The concentration of specifically bound DMBODIPY-DHP was determined in the same samples using the charcoal assay (open circles). The factor (1nM complex= 124 FRET fluorescence units,  $n=9$ ,  $r=0.98$ ) relating the two signals was calculated by linear regression analysis and used to convert FRET fluorescence into bound DMBODIPY-DHP concentration (filled circles). The binding parameters (drawn lines) obtained were as follows: charcoal assays,  $K_d=9.3 \text{ nM}$ ,  $B_{\text{max}}=18\text{nM}$  (100 pM/mg f protein); FRET,  $K_d=128\text{nM}$ ,  $B_{\text{max}}=1.9\text{nM}$ . Scatchard transformation (inset). (B) Modulation of DMBODIPY-DHP binding as determined by FRET. The DMBODIPY-DHP species was incubated with partially purified DHP receptor in the absence (control) or presence of nonfluorescent  $\text{Ca}^{2+}$  antagonists. Binding in the presence of drugs is expressed as a percent of control binding. The following binding parameters were obtained: (●) (+)-isradipine, (▼) (-)-isradipine, (▲) (+)-cis-diltiazem, (■) (-)-cis-diltiazem, (◆) (+)-tetrandrine. To illustrate the correlation of the FRET signal with the concentration of bound DMBODIPY-DHP, inhibition by the isradipine enantiomers was measured by charcoal assay in parallel (open symbols). (○) (+)-isradipine, (▽) (-)-isradipine. Reprinted (adapted) with permission from (Berger W, Prinz H, Striessnig J, Kang HC, Haugland R, Glossmann H: Complex molecular mechanism for dihydropyridine binding to l-type  $\text{Ca}^{2+}$ -channels as revealed by fluorescence resonance energy-transfer. *Biochemistry* 1994, 33:11875-11883). Copyright (2017) American Chemical Society.

The aim of being able to map information and structure appropriately labelled components is one that has been achieved again with FRET by a study spearheaded by Pecht. Their results show that they could measure in vivo the binding process between Florescein labeled, 2,4-dinitrophenyl (DNP)-specific monoclonal immunoglobulin (IgE) and it's biochemical angonist DNP-haptens. From their experiments and calculations they were also able to come up with binding constants, further supporting the FRET technique to probe ligand interactions [29].



Particular attention has also been paid to a three component FRET experiment that examines the efficiency of energy transfer between two fluorescently labeled  $\alpha$ -toxin inhibitors (N-fluorescein isothiocyanate lysine 23  $\alpha$ -toxin and monolabeled tetramethylrhodamine isothiocyanate  $\alpha$ -toxin) Torpedo acetylcholine receptor, AChR. Taylor's study interestingly demonstrates that the FRET efficiency is higher for membrane associated receptors compared to solubilized receptors, supporting the idea that intermolecular photomechanisms take place when chromophores are spaced closed to each other. This is as expected as with membrane associated layout, receptors are arranged in a tight array assembly. On the flipside in the fully solubilized form, intramolecular FRET is dominant and the measured efficiency is relatively lower, see Table 4.3.1 [30].

		Energy transfer parameters		
		Energy transfer efficiency	R	$R_{2/3}^a$
AChR			Å	Å
Membrane-associated		0.32 <sup>b</sup>	46-47	56
Solubilised		0.14 <sup>c</sup>	55-84	67
		Spectroscopic constants		
	$Q_D^d$	$J^e$	$K^2^f$	$R_0^g$
		$cm^6/mol$		Å
	0.34	$2.9 \times 10^{13}$	0.21-2.5	40.7-61.7
<sup>a</sup> Distance calculated by employing $K^2=2/3$ .				
<sup>b</sup> From an interpolation to zero FITC-toxin in the plot of the specific energy transfer in membrane-associated AChR as a function of donor occupancy.				
<sup>c</sup> From the best fit of the donor-occupancy dependence of apparent transfer efficiency to the two-equivalent-site model.				
<sup>d</sup> Quantum yield based on a value of 0.85 for fluorescein in 0.1N NaOH (24).				
<sup>e</sup> Calculated from equation 11.				
<sup>f</sup> Calculated from equations 12 and 13.				
<sup>g</sup> Calculated from Equation 10 using measured values for $K^2_{min}$ and $K^2_{max}$ and assuming a refractive index of 1.4.				

Table 4.3.1. Energy transfer parameters and spectroscopic constants for donor- N-fluorescein isothiocyanate lysine 23  $\alpha$ -toxin (FITC-toxin) and acceptor tetramethylrhodamine isothiocyanate  $\alpha$ -toxin (TRITC-toxin) on membrane-associated and solubilised AChR. Adapted with permission from (Johnson DA, Voet JG, Taylor P: Fluorescence energy-transfer between cobra alpha-toxin molecules bound to the acetylcholine-receptor. Journal of Biological Chemistry 1984, 259:5717-5725). Copyright (2017) American Chemical Society.

## Immunoassays

A method for carrying out immunoassays has been revisited, taking FRET in development. There is evidence that immunoassays can be performed by labelling a fluorescent donor to the antigen and labelling the corresponding antibodies with an acceptor. In this technique when the two components are anchored together the measurements of the fluorescence of the donor is quenched. This is as anticipated as the energy is transferred to the acceptor. In the negative case of the assay, both components do not bind and thus only measurement of the fluorescence of the donor is registered [31]. Other groups have followed, that have also taken care to register acceptor emission in addition to monitoring the quenching of the donor fluorescence. Interestingly, the efforts Morrison has looked to improve the technique by addressing the bias in acceptor emission. The photophysics at play are such that there is an emission from the acceptor due to the direct absorption of the excitation light intended for excitation of the donor fluorophore. This competes with the desired emission resulting from energy transfer. They could tackle this issue by selecting a judicious donor-acceptor pair where the fluorescence lifetime of the donor is greater than the fluorescence lifetime of the acceptor. In this way, in the presence of a long-lived donor, the acceptor fluorescence persists. In the absence of the donor the acceptor fluorescence would be very brief. In this experimental design one can thereby impart a temporal distinction among acceptor fluorescence resulting from energy transfer and acceptor fluorescence resulting from direct light absorption. With their time-resolved detections in their immunoassays they were then able to make sure to channel and process energy-transfer emission only [32].

## Probing interactions on single molecules

Weiss *et al.* have furnished ways to examine DNA as an individual framework and by same token set out to extend the observation of FRET down to a single pair of chromophores. Operating on the single molecular scale brings distinct advantages over more conventional experiments. First, it is validated that studying FRET on a single pair allows the observation of time-dependent phenomena *i.e.* protein and molecular motor conformational changes. Secondly, whilst there is uncertainty in the  $k^2$  parameter, the orientation factor in calculating distances in conventional FRET experiments, the knowledge of this factor can be measured in a single pair of dyes. It then entails that with single-pair FRET it is possible to detect dynamic events as the likes of relative motion between donor and acceptor species, something that cannot be done when observing the bulk that relies on signal averaging over many molecules. Finally, unlike with ensemble-FRET experiments, the problem of undesirably registering a response for single species complex (donor-only or acceptor-only) or other impurities is greatly lessened, Figure 4.3.5 [33]. The observation is that from 5 min on inspection (60<sup>th</sup> scan) and onwards the response in number of counts as a function of wavelength is overall constant and globally invariable (the maxima of peaks are relatively in the same place) and this is understood to be because of low noise from the donor or acceptor alone or optical response from impurities.

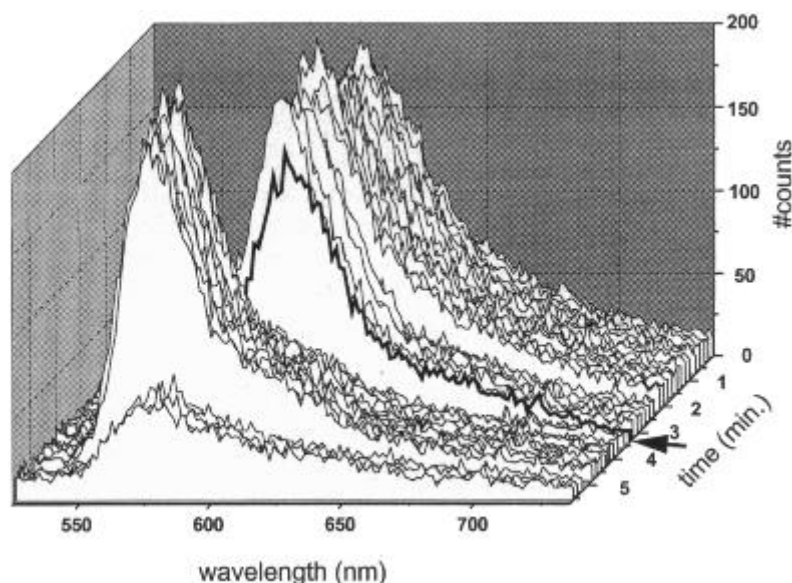


Figure 4.3.5. Time evolution of a doubly labelled DNA 20-mer molecule (Tetramethylrhodamineisothiocyanate- 20 nucleotides- texas red). On inspection, after 5min (60th scan) both donor and acceptor are bleached and a constant background remains. This background is due to autofluorescence from the near-field scanning optical microscopy and possibly an interference from fluorescence of distant molecules, the perturbation may occur due to reflected excitation light. Reprinted (adapted) with permission from (Ha T, Enderle T, Ogletree DF, Chemla DS, Selvin PR, Weiss S: Probing the interaction between two single molecules: Fluorescence resonance energy transfer between a single donor and a single acceptor. *Proceedings of the National Academy of Sciences of the United States of America* 1996, 93:6264-6268. Copyright (2017) National Academy of Sciences.

## Structure and conformation of nucleic acids

There has been a strong engagement in taking FRET to investigate the primary and secondary structure of single-stranded nucleic acids. The approach consists in covalently linking fluorescent dyes to oligonucleotides and pinning down where they complement with respect to the nucleic acid sequence. It is then possible to tease out the primary and secondary structure of DNA fragments and figure out the orientation of the various moieties and nucleoside units. Equally revealed are the structure of hairpin and the translocation of genes between two chromosomes [34]. Under the same banner of work, efforts have been made to sketch out the DNA's structure at its Holliday junction at low and high salt concentrations. Using FRET it was possible to determine that at low salt concentrations there is a more pronounced acceptor fluorescence suggesting that the four DNA arms hold a square, extended and unstacked conformation. In the presence of magnesium ions, FRET efficiency from anisotropy data tells us that the DNA junction features a folded X shape stacked arrangement [35]. Researchers in Japan have furthered the common understanding on DNA's role and behavior in setting a novel way on monitoring DNA denaturation. The purpose their study is to tether fluorescent groups onto complementary DNA strands during target-specific amplification by polymerase chain reaction (PCR) and then subsequently characterize any denaturation by FRET. The rational in including the donor-acceptor dyes during PCR is to obtain DNA strands with multiple FRET pairs at different locations

leading to a higher FRET change upon denaturation. Through this study they were able to measure denaturation initiated by alkali or heat change, Figure 4.3.6 [36].

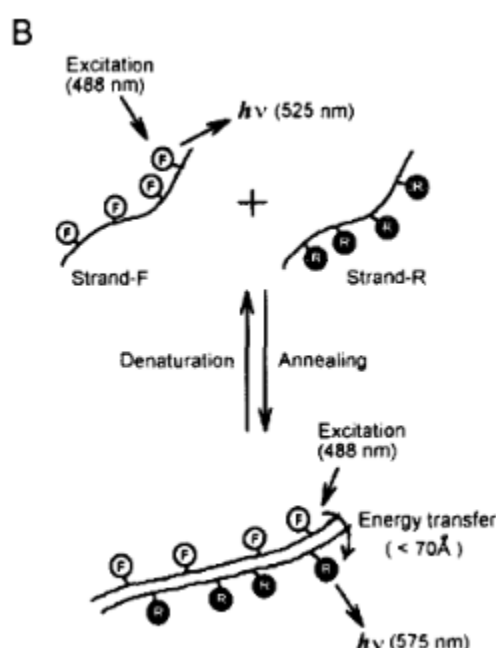


Figure 4.3.6. FRET in the context of DNA hybridisation. The fragments are the product of a polymerase chain reaction (PCR) step and after annealing FRET is taken between energy donors (F) and energy acceptors (R). Donors are fluorescein and acceptors are rhodamine. Reprinted (adapted) with license agreement from (Hiyoshi M, Hosoi S: Assay of dna denaturation by polymerase chain reaction-driven fluorescent label incorporation and fluorescence resonance energy-transfer. *Analytical Biochemistry* 1994, 221:306-311). Copyright (2007) Elsevier.

Langowski *et al.* have gone further in analyzing and characterizing DNA and have particularly focused on quantifying the curvature of DNA and how blocks of repeating adenine residues induce the DNA strand to take a permanent curvature on the helix axis. By measuring the end distances of a DNA fragment free in solution using FRET they were able to estimate the curvature given that average dye to dye distance is smaller than in extended DNA fragments. Their specimen of study has been a 31 long base pair DNA molecule, short enough to study with FRET, accommodating three A<sub>6</sub> tracts (adenine tracts) that subject the fragment to coil. Worth mentioning from their report is that the rate of curvature is very responsive to increasing NaCl salt concentration, up to 23° to 41° along a 10 to 500mM salt gradient [37]. Other researchers have devised an experiment to determine the arrangement and relationship a DNA template-primer has with a protein: the Klenow fragment of *Escherichia coli* DNA polymerase. By employing FRET some clear insights have been made in that the single stranded portion of DNA template-primer bundles into a helical framework when bound to the Klenow fragment. This finding is of special interest as the Klenow fragment has a direct relevance with more complex polymerases and proxies as a prototype [38].

## Real time PCR assays and SNP detection

Others have employed FRET to find more amenable path routes to run homogeneous assays (PCR systems) for nucleic acid sequence detection. First, in reviewing a report by Little *et al.* one can appreciate that major disadvantages of PCR have been side-stepped by the development of self-probing amplicons, or the Scorpion technique that rely on the signaling of the energy transfer between a fluorophore and proximal quencher molecule whereby changes of quenching are also detected. Real term benefits in kinetics, thermodynamics and probe reliability are claimed [39]. In further studying the mode of action and evaluating the Scorpion PCR mechanism the dual label design was ameliorated by including a FRET donor dye, fluorescein (FAM) to interact with the carboxy X-rhodamine (ROX) acceptor dye of the Scorpion probe. This represented a marked improvement on the system. In effect, on Scorpion probe ligating to the biomolecular target the FRET pair come in close spatial proximity and it is then possible to excite the donor chromophore to measure FRET emission from the acceptor dye. This specific increase in fluorescence is willingly made to be detected through a different channel than that for the fluorescence of the acceptor as used in earlier Scorpion probing systems. As such it renders the FRET hybridized Scorpion a more versatile and superior product [40]. Another dual labeled based PCR method that has been popular is that driven by the TaqMan probe [41]. This assay design has allowed the democratization of real time quantitative PCR. In this design, FAM (*i.e.*, 6 carboxyfluorescein) serves as the donor reporter. The suiting acceptor is TAMRA (*i.e.*, 6-carboxy-tetramethyl-rhodamine). On excision of the probe, the reporter chromophore emission is no longer passed efficiently to the quenching dye, consequently in an increase of the reporter chromophore emission spectra [42]. This theme of work, still with the incorporation energy transfer grafted primers in the amplification product, made more advances on other end use detections [43]. The concerted efforts of Kramer *et al.* reached proficiency in taken several molecular beacon probes to report the presence of nucleic acids in solution.

The principal of operation, Figure 4.3.7.

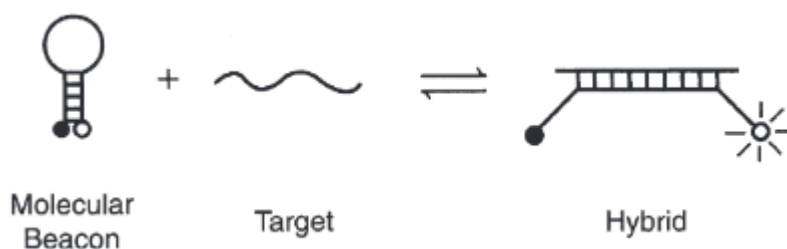


Figure 4.3.7. Operation of the molecular beacons. In the hairpin conformation (left) fluorophore is close to the quencher (DABCYL). After interaction with a target (an oligonucleotide), hybridisation engenders the rigid double helix to form. In doing so the quencher is separated from the fluorophore and fluorescence is restored (right).

Overview, Figure 4.3.8.

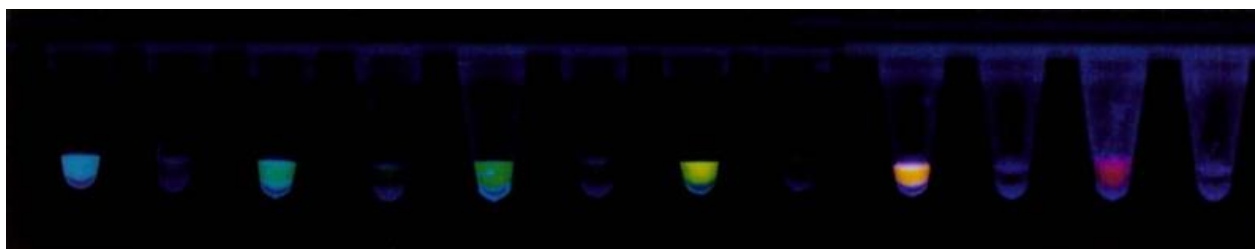


Figure 4.3.8. Chemiluminescence induced by differently coloured molecular beacons to the addition of a target. The fluorophore of the molecular beacons contained (left to right) are: coumarin (blue), EDANS (blue-green), fluorescein (green), Lucifer yellow, tetramethylrhodamine (orange), and Texas red. Complementary single stranded target oligonucleotides were treated the left tube of each pair. The Eppendorf tubes were illuminated with a broad-wavelength ultraviolet lamp.

Later efforts looked to take the molecular probes or beacons and design them with a unique fluorophore to distinguish different single nucleotide polymorph (SNP) oligonucleotide targets. Each molecular beacon was synthesized with the complementing nucleotide of this SNP so to only hybridize with one of the oligonucleotide targets specifically. Therefore it was demonstrated that color specific molecular beacons in the same solution can discriminate a given set of alleles that differ from one another by as little as a single nucleotide. The downstream application of this is to of course detect multiple targets in the same sample which had until yet been largely unrealized [44]. This research effort is supported by the documented works of Hamer *et.al* who also exploit FRET with donor-acceptor labeled primers to tackle SNP genotyping. However, here as opposed to with Kramer's report, they use a universal reporting reagent for each polymorphism [45].

## Detection of nucleic acid hybridization

There has been a longstanding interest in detecting hybridization of nucleic acids. This demand has been addressed by exploiting double-labeled oligomeric strands. In this setup researchers have taken a 16-base oligodeoxyribonucleotide labeled at the 3'-end with fluorescein and at the 5'-end with x-rhodamine, Figure 4.3.9.

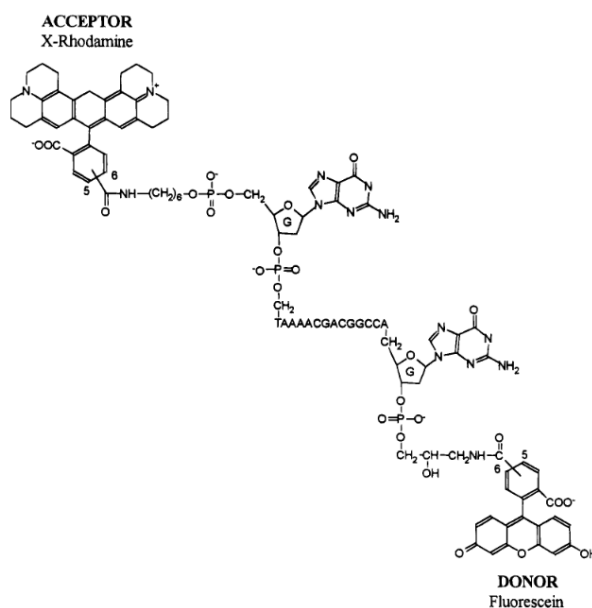


Figure 4.3.9. Double labelled probe: 16-base oligodeoxyribonucleotide with x-rhodamine bound to the 5'-end and fluorescein bound to the 3'-end. The fluorescein and x-rhodamine serve as a donor-acceptor FRET pair. The strong distance dependency on efficiency of transfer remains, flexibility of the polymer also. Reprinted (adapted) with permission from (Parkhurst KM, Parkhurst LJ: Kinetic-studies by fluorescence resonance energy-transfer employing a double-labeled oligonucleotide - hybridization to the oligonucleotide complement and to single-stranded-dna. *Biochemistry* 1995, 34:285-292.). Copyright (2017) American Chemical Society.

The probe was shown to signal hybridization in solution and measure the critical kinetics of duplex formation in its matching oligomer and its target sequence in M13mp18(+) phage DNA. The conceptual model for this study is that the single-stranded oligomer in solution alone would hold a random coil arrangement, one with the ends of the coil, on average coming short enough to allow efficient energy transfer. In return, when the 16-mer hybridizes to its complement the probe is locked into position and stretched out resulting in a large separation between chromophores and a low efficiency of transfer [46]. A report looks into the formation of oligonucleotides hybridizing, complementing (with its respective antisense). Fluorescence energy transfer has been used to study this intracellular line of work. An emphasis is put on that it takes places in oocytes. It is concluded, that injected oligonucleotides exogenous to the target cell engenders action on the nucleus species and others in the cytoplasm of the said cell in scope [47]. With the aim of detecting mutations and carrying high throughput screening, template directed dye terminator incorporation (TDI) assays have been developed. Oligonucleotide TDI primers are defined in their materials and methods section, they consist of CF508p species [48].

### Primer extension assays for detecting mutations

The employment of energy transfer primers conferred to forensic use is featured singularly, as a study by Glazer *et al.* It resiliates down to energy transfer acting as the key principal to genetic typing of STRs, DNA sequencing and DNA in situ hybridization. They unexpectedly function to hasten their value as used per say in their publication [49].

### Automated DNA sequencing

This section reviews the written information on a report focusing on ultra-high speed DNA sequencing by capillary electrophoresis chips (*e.g.* that is related to the electropherogram). Tangible to this thesis goal is that the study relies on the primaries or fundamentals on elemental energy transfer. Also, they employ dye labeled primers that are purposed to energy transfer – experimental section [50]. Second paper – the same author emphasizes that rhodamine is attached to a thymidine residue that is itself appended to and part of the primer sequence. All this, for fluorescence energy transfer dye-labeled primers for DNA sequencing and analysis. A hypothetical analogy would be if the users in question aim to taint fibrous slick multi-chrome plumage [51].

### Distribution and transport of lipids

Among others, FRET has been implemented to measure the migration of lipids within or between cellular corpuscles. In this theme Barrantes *et al.* have spearheaded a study looking at the preferential distribution of the fluorescent phospholipid probes in the exofacial leaflet of acetylcholine receptor rich membranes pertaining from torpedo marmorata, Figure 4.3.10. [52].

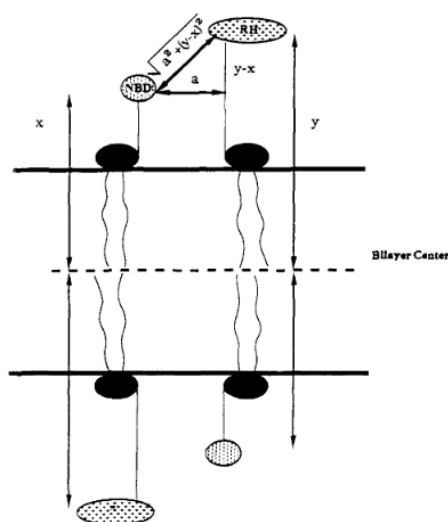


Figure 4.3.10. Illustrative diagram of model used to fit the FRET data. Donor NBD groups are assumed to be equally distributed between the two leaflets at a distance  $x$  from the bilayer center. It is assumed that within the plane of the membrane there is a distance ( $a$ ) of closest approach and that across the bilayer an RH group in one leaflet can directly position itself below an NBD group in the opposite leaflet. Thus, the distance of closest approach for cis transfer is  $[a^2 + (y-x)^2]^{1/2}$  and for transfer is  $(x+y)$ . Reprinted (adapted) with permission from (Wolf DE, Winiski AP, Ting AE, Bocian KM, Pagano RE: Determination of the transbilayer distribution of fluorescent lipid analogs by nonradiative fluorescence resonance energy-transfer. *Biochemistry* 1992, 31:2865-2873.). Copyright (2017) American Chemical Society.



Fluorescently labeled lipids have been used to model large unilamellar vesicle. Including a combination of donor-labeled and acceptor-label lipids in the vesicle body it is possible to measure the contributions of energy transfer between NBD and rhodamine dyes when their tethered component the lipid is arranged in either the same (cis) or opposite (trans) leaflet of the vesicle [53]. The kinetics of lipid transfer has also been investigated. As such, an assay has been developed that allows to determine the activity of protein mediated transfer of lipids between vesicles. The technique features major advantages in use over earlier methods: radiochemistry, electron spin or resonance based analytical techniques. Compared and contrasted, the FRET assay is faster, more flexible in the choice of composition and more straightforward in use. The resonance energy transfer regime that rides the experiment is that between the 7-nitro-2, 1, 3-benzoxadiazol-4-yl (NBD) grafted to acyl chain lipids; donor and synthesized N-(lissamine rhodamine B sulfonyl) dioleoylphosphatidylethanolamine; the acceptor. When both donor and acceptor pair are compartmentalized in a same vesicle, FRET occurs, and fluorescence is quenched. When free vesicles are added, the lipids typified with NBD migrate to the empty vesicle space. In consequence the donor and acceptor pairs are no longer within minimum distance for FRET and an increase in fluorescence is observed as the system is no longer quenched. The second part of this study reports the extension of this transfer on addition of bovine liver phosphatidylcholine-specific transfer protein (PC-TP) and nonspecific lipid transfer protein (nsL-TP). They also provide an explanation on the way both catalyst work. The first functions as a carrier whilst the other favors the unbinding of the NBD chromophore from its lipid monomer vesicle dissociation and association [54].

## Membrane fusion assays

On membrane fusion, a research group utilize the NBD and rhodamine phosphatidylethanolamine derivative based assay discussed above to quantify the evolution of lipid mixing when brought together with target vesicle and liposomes and their fusion by monitoring the increase of NBD donor fluorescence [55]. In a similar theme of research, fluorescein and rhodamine probes each incorporated in a population of cells from B16 mouse melanoma cell line were used to investigate the kinetics of cell fusion biology, review one of the results, Figure 4.3.11.

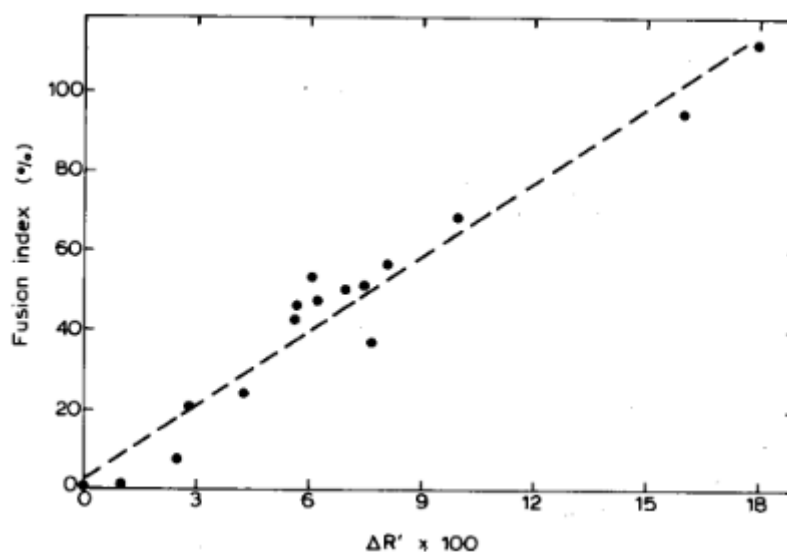


Figure 4.3.11. Linear correlation between fusion index and  $\Delta R'$ . Fusion index is an empirical estimate.  $\Delta R'$  is a parameter of resonance energy transfer refer to publication XX. The correlation coefficient is  $r=0.974$ . Rprinted (adapted) with license agreement from (Par-tearroyo MA, Cabezon E, Nieva JL, Alonso A, Goni FM: Real-time measurements of chemically-induced membrane-fusion in cell monolayers, using a resonance energy-transfer method. *Biochimica Et Biophysica Acta-Biomembranes* 1994, 1189:175-180). Copyright (2017) Elsevier.

The FRET technique allowed as anticipated to quantify the rate and the magnitude of cell fusion engendered by the addition of poly(ethylene glycol)s (PEG), a fusogen. This study then went on evaluating how this fusion rate evolved in time, the cell membrane fusion rate in relation to other fusion enhancers (surfactants) was also addressed [56]. Another tried vesicle-vesicle assay is documented, based on N-(7-nitro-2,1,3-benzoxadiazol-4-yl) as the donor and rhodamine as the corresponding acceptor. The fluorophore then couple to phosphatidylethanolamine and then bundle into place to the lipid vesicle bilayer. On interaction with and fusion with an undiluted population of phosphatidylserine vesicles, the membranes reshapes to accommodate the other. It turns out that this distortion results in the probes furthering apart and subsequently the empirically measured efficiency of resonance energy transfer reduces. This method allows to build on the kinetics and evolution of the fusion process, and particularly to this study, fusion and uptake of vesicles by cultured fibroblasts. The results of their assays revealed that vesicle transfer to the cells intact as whole vesicle [57].

## Membrane potential sensing

Cellular electrical activity is of great importance to many physiological processes. In the interest of better understanding this process a group of researchers have developed a way to combine FRET to determine depolarization for a collection of cell types: fibroblasts, astrocytoma, cardiac myocytes and B104 neuroblastoma cells. Using thiobiturate-trimethineoxonol based donors coupled to agglutinin together with fluorescein stapled lectin as the associated acceptor it emerged that it was possible to measure the voltage bias from the change of energy resonance transfer efficiency. The stepwise process of this method is as follows: i) at resting negative potential the permeable oxonols donor specimens concentrate at the extracellular plane of the plasma membrane, in close spatial arrangement with the extracellular acceptor, emission from the acceptor can be recorded ii) When the membrane potential is switched to a positive bias, the anionic oxonols displace to the intracellular layer of the membrane, donor-acceptor inter-distance is increased and energy transfer is reduced, Figure 4.3.12. It transpired that the oxonols translocate in  $\sim 3\text{ms}$  or less in response to a change in the electrical field across the membrane and are sensitive down to physiologically relevant potentials. A recording of their study among others claims a 19% decrease in FRET efficiency for a 120mV depolarization for example. In summary, the developed principle described herein is an effective way to transduce a charge displacement signal into an optical signal and shows promise for monitoring many biological applications [58].

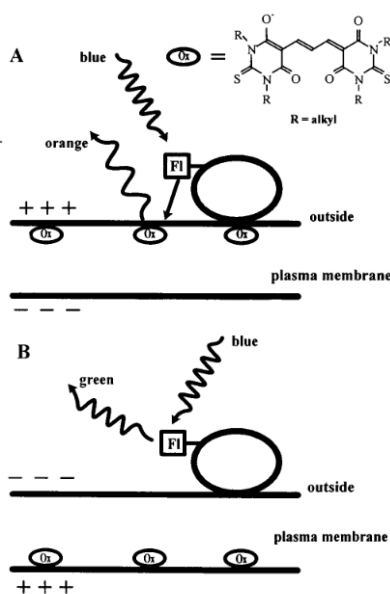


Figure 4.3.12. Voltage sensitive FRET mechanism. At a resting negative membrane potential (A) the permeable oxonols have a high concentration at the extracellular surface of the plasma membrane and energy transfer from the extracellularly bound fluorescein-labeled lectin. FRET is represented as the straight arrow from lectin to oxonol. At a positive membrane potential (B) the anions embedded along the intracellular surface of the membrane and energy transfer is greatly reduced because of the increased mean distance from the donors on the extracellular surface. Oxonols chemical structure are shown in the top right corner. Reprinted (adapted) with license agreement from Gonzalez JE, Tsien RY: Voltage sensing by fluorescence resonance energy-transfer in single cells. *Biophysical Journal* 1995, 69:1272-1280. Copyright (2017) Elsevier.

## Fluorogenic protease substrates

A new-found application of donor-acceptor FRET pairs has been in the development of more versatile and multipurpose assay for protease enzymatic activity. Similar to aforementioned techniques, the fluorophore and quencher groups lie in the same molecule, in this context they position along the peptide. On substrate cleavage an increase in fluorescence is detected as a result to the peptide breaking apart and monitored continuously by fluorescence spectroscopy means. In the contrary case, when the substrate is docked in its binding pocket, the peptide is in a tight arrangement such that the resonance energy transfer is quenched by the acceptor. Demonstrating this principle in a designed study on the enzymatic activity of Cathepsin D protease, a set of fluorogenic substrate were synthesized. These were all functionalized with EDANS-DABCYL as donor-acceptor FRET pairs, respectively. The advantage of this method as an assay of enzymatic activity is that the method does not rely on esterase or amidase evaluation. Thus, it is possible to study enzymes that do not operate such chemistries: aspartic proteinases of the pepsin family such as Cathepsin D [59]. Relying on the same principle, constructed Trypsin mutants, named K60D and K60E have had their enzymatic activity studied by the same technique with three DABCYL and EDANS fluorogenic peptide substrates (two heptapeptide and an octopeptide). Their study shows that their muted proteases catalyse the cleavage of dibasic residues in this case Arg-Arg binding by one order of magnitude compared to conventional trypsin and that residue 60 is major influencer of the catalyst's site propensity for a given substrate [60]. A different Foster energy donor-acceptor pair is used in a study that looks at human renin and fibroblast collagenase. In this system fluorogenic peptides are labeled with Lucifer Yellow CH (donor, LY) and 5-carboxytetramethylrhodamine (acceptor, CTMR). To be more precise, LY-IHPFHLVIHTK-CTMR the human renin substrate and LY-GPLGLRAK-CTMR the collagenase substrate was prepared. The designed substrates are then measured continuously against human renin and fibroblast proteinases in the same fashion as above-mentioned studies. The results of the study lended further support on Human renin to selectively hydrolyse the peptide bond between Leucine and Valine. Collagenase through this study was shown to cleave the peptidic covalent bond between Glycine and Leucine [61]. FRET enzyme activity based assay has also been the topic of a research effort to identify and detail a human immunodeficiency protease (HIV-1 PR), this study returns on DABCYL as a quencher and EDANS as the donor. Substrate hydrolysis was measured as an indicator of enzyme activity and resulted in the detection of a fluorescence increase by about 34 and 40 fold, a result of specific Tyr-Pro bond cleavage, Figure 4.3.13. [62].

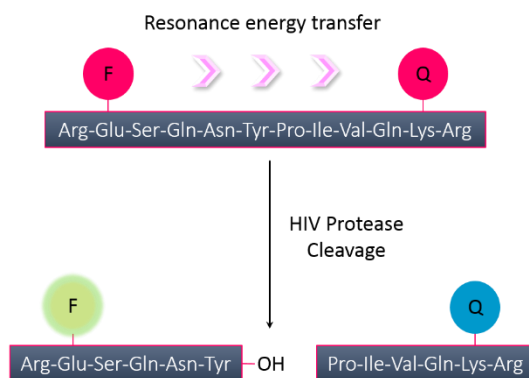


Figure 4.3.13. Quenching of the EDANS fluorophore (F) through distance-dependent resonance energy transfer to the dabcyL quencher (Q) that is terminated on cleavage of the peptide.

## Indicators for cyclic AMP and Zinc

The availability of sensitive and specific FRET pairs has opened new horizons in visualizing more on intracellular biochemistry of single living cells and the dynamics of its ion traffic. By combining the FRET technique to cyclic adenosine monophosphate (cAMP) dependent kinase in which the catalytic and regulatory subunits are labeled with a resonance energy transfer donor: fluorescein, and acceptor: rhodamine, one can obtain a method to analyze the intracellular biochemistry of cAMP. The catalytic subunit is tagged covalently with fluorescein isothiocyanate and the regulatory unit with tetramethylrhodamine isothiocyanate. The doubly labeled protein in its own displays detectable emission of the rhodamine acceptor via energy transfer of the fluorescein. On interaction with cyclic adenosine monophosphate, the catalytic protein subunits dissociate and subsequently the donor-acceptor pairs roam free and do not energy transfer. Direct emission of the fluorescein is then the major detectable reception and is associated with a lesser detection of the auto-fluorescence of the rhodamine in isolation. The holo-enzyme design, is suggested by the author to serve in further applications to monitor cyclic GMP, scrutinizing interactions between calmodulin and its target enzyme or between components of transcription-regulating complexes [63]. The FRET technique has also proven opportune in addressing previous difficulties in measuring zinc levels in a biochemistry context. As a reminder, zinc is important in DNA binding components, mitosis, and suppressing apoptosis in cells. By exploiting the zinc finger consensus peptide (CP) and altering it to include fluorescein to have a donor and lissamine to have an acceptor, it has been possible to image zinc binding levels, Figure 4.3.14.

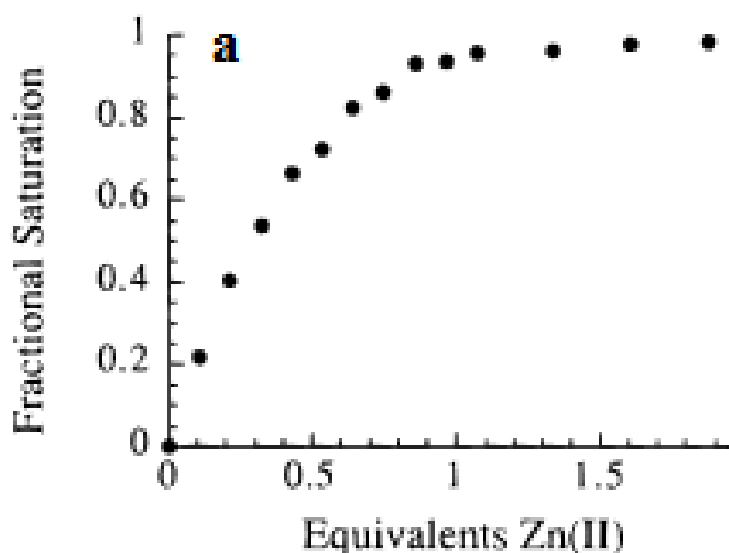


Figure 4.3.14. Fractional saturation of Zn (CP-L-F) as a function of Zn (II) added. Reprinted (adapted) with permission from (odwin HA, Berg JM: A fluorescent zinc probe based on metal-induced peptide folding. *Journal of the American Chemical Society* 1996, 118:6514-6515). Copyright (2017) American Chemical Society.

The fundamental principle is the same, the peptide is in an extended conformation and the dyes are distant from each other, consequently the intramolecular energy transfer is small. As the Zn (II) ions come to influence the peptide, this one changes conformation to accommodate it. In doing so, the fluorophores come in closer spatial proximity and an increase in the amount of intramolecular energy transfer is observed. This devised fluorogenic CP probe is praised as excellent candidate for in vivo studies. The rationale being that the emissive energy transfer is not obscured by native cellular components [64].

## 4.4 Gas phase mass spectrometry & action FRET

### 4.4.1 Gas phase mass spectrometry

Gaseous studies of ions and small molecules in the reaction chamber of the mass spectrometer is a mature and established technique that has spurred the gas phase handling and characterization of proteins and their biological structural arrangement [65]. As it stands today mass spectrometry (MS) is the method of choice in a variety of protein identification, sequencing and other biochemical studies such as antigen-antibody binding studies for identifying ligands to orphan receptors. The accomplishment of bringing large biomolecules such as proteins out of its typical solution or condensed environment into the gas phase intact was celebrated with a Nobel prize in 2002 [66]. Meaningful mass spectrometry methods with their own unique merits are available to examine molecules in the gas phase [6], which include:

1. Blackbody infrared radiative dissociation, whereby ions dissociate through energy exchange with the surroundings by absorption and emission of infrared photons.
2. Collision induced dissociation.
3. Hydrogen deuterium exchange.
4. Covalent and non-covalent tagging of biomolecules on accessible site-specific moieties.
5. Ion-mobility spectrometry where determined cross sections are measured and compared with theoretical ones.
6. Optical spectroscopy.

However pitfalls and shortcomings prevail with each approach and what is trending is the development of gas phase studies that can tackle larger biological structural systems that yield as much conformational information as what has been done in the condensed phase; inspection of conformational change in DNA hairpins [67-69], small peptides e.g. Trp-cage and alpha helices for example [70, 71]. Recent efforts on gas phase studies, and in bringing proteins to gas isolation, are included in a survey brought together by McLafferty *et al.* that lends particular attention on desolvation of biomolecules and their evolution to stable gas phase structure. The centerpiece of their work revolves around a stepwise description on the mechanism of transfer from solution to the gas phase, Figure 4.4.1.

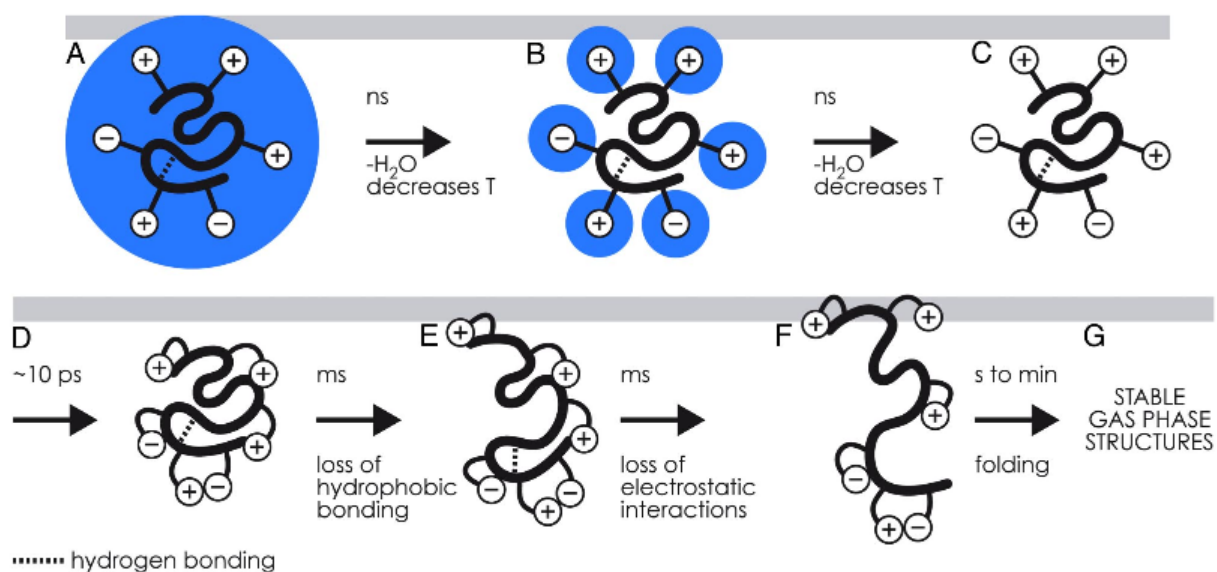


Figure 4.4.1. The mechanism of evolution in prior to ESI of the structure of a globular protein (e.g. cytochrome c, ubiquitin). (A) the native protein surrounded with a layer of H<sub>2</sub>O, supplanted by nanosecond H<sub>2</sub>O loss and simultaneous cooling. (B) Native protein with peripheral ionic functionalities hydrated and cool and lose H<sub>2</sub>O. (C) Dry protein undergoes  $\pm 10$ -ps collapse of its exterior ionic functionalities. (D-G) The exterior-collapse "near-native" protein undergoes thermal re-equilibration (D), millisecond loss of hydrophobic bonding (E), and millisecond loss of electrostatic interactions (F); the unfurled species form new noncovalent bonds in seconds to more stable gaseous ion arrangements (G); these stabilise to energy minima conformers in minutes. Copyright (2008) National Academy of Sciences.

This work was very important and provided much understanding for the research carried out in the group on building the proof of principle of action-FRET to elucidate the molecular conformation of a group of small alanine based peptides of differing chain length using a QSY7 and Rhodamine 575 pair of chromophores [72].

Works in the field continue to evolve apace bringing to light resonance energy mechanisms to further probe the structural details of proteins in the gas phase [73]. Julian *et al.* demonstrate through excitation energy transfer (EET) the interplay between the amount of fragmentation of the disulfide bond and the distance that separates the chromophore-disulfide bridge, offering valuable information on the polypeptide's conformation [74]. Jockusch *et al.* have also spearheaded a seminal gas-phase FRET investigation [75] whereby a series of 8, 14 and 20 proline repeat peptides have been measured as a function of charge state. In addition to this they have also looked at the structure of the fluorescently-labeled mutant variant of the protein GB1. They demonstrate that steady-state fluorescence emission spectra and time-resolved donor fluorescence measurements are a function of the number of charges melded to the gaseous protein [76, 77]. This thesis builds on the exploitation of resonance energy transfer, more specifically, Förster resonance energy transfer to bring about a 'molecular ruler' compatible with large ion trapped protein assemblies, an attractive addition to the analytical toolbox in studying biological macromolecules. Gas phase studies have not thus far been solely limited to proteins and polypeptides. Allison S. Danell and Joel H. Parks have applied the measurement of fluorescence resonance energy transfer to trapped oligonucleotide duplexes biopolymers to study their conformational dynamics [78]. The elegant work looks at the intermediate states immediately pre-

ceding dissociation of the double stranded oligonucleotide ions, effectively following the unfolding or unravelling of the noncovalent complex in the gas phase by measuring the increase in fluorescence associated to an expansion in the inter-distance of FRET donor and acceptor moieties. A following generation of work on FRET in the gas phase is reported by Renato Zenobi [77]. Another coverage of the same author provides information on evidence of fluorescence resonance energy transfer in gas-phase ions, again using mass spectrometry [6]. Of course, later works carried through this thesis, discussed in this manuscript, also testify of the possibility that the MS conciliated to a laser source, can produce results on gas phase biomolecules.

#### 4.4.2 Action spectroscopy

Action spectroscopy is one of the modalities by which the optical characteristics of ions can be assessed in the gas phase. It corresponds to the measurement of the fragmentation induced by the absorption of photons and sometimes results from ion-molecule reaction after photon absorption (*viz.* photodissociation or photodetachment). It is different to the measurement of multiple photons absorbed or emitted as is usually done by absorption or fluorescence emission spectroscopy [73, 79, 80].

Action spectroscopy is a standalone MS spectroscopy approach. It is important to reiterate that it measures the influence of photons on ions trapped in a mass spectrometer, by registering shifts in  $m/z$  resulting from the degree of fragmentation of an ion versus excitation wavelength. For further information this operation of measurement is well documented by chemical spectroscopists [73, 79-81]. Action spectroscopy is also commonly found under the denomination of photodissociation action spectroscopy, in this way it is emphasized that focus is applied in considering photodissociation alone, exclusively of other end fates such as fluorescence, electron detachment or photoisomerization, this is well described by Wellman and Jockusch [82].

This spectroscopic method of action spectroscopy that date's back to the 1970s [80] also has drawbacks. Since it is an indirect procedure of observation, an action spectrum may differ from a direct measurement of an adsorption or emission spectrum [79, 82]. Many situations arise when photon absorption is not registered by any photochemical stimulus [80]. Conversely, any signal that does arise, is due to photon absorption, this means zero background in the produced spectra [80]. Other advantages of action spectroscopy are that the technique exploits the benefits offered by mass spectrometers to detect ions conveniently, sensitively and precisely [73, 79]. Secondly, it is also possible to couple action spectroscopy to energy transfer. The energy transfer process is used to determine distant constraints between two or more atoms in the molecule, as commonly implemented with FRET experiments in the condensed phase [79]. This is effectively valid, on the precondition that energy transfer from a donor and acceptor provides unique fragmentation post energy transfer from the donor to the acceptor [79].

#### 4.4.3 Action FRET

Traditionally FRET data resulted in the careful measurement of the fluorescence decay by either photon-counting or phase modulation method [2]. There is an interest to observe confor-



mational changes in biomolecules in gas phase isolation and this has taken the recent development of action-FRET. In this way, it is possible to study the intrinsic properties of species in isolation, in the gas phase. Without environmental condition effects that would have found to carry implications if the system were in a solution phase (*e.g.* cytosol, a sheath fluid or a serum).

Solvent selection and consideration to the empirical observations were a constraint in determining Föster distances. The recent developments have made it so, as a mass spectrometer opens the possibility to transpose a trapped molecular system in gas isolation. Another main attraction is that all is set up to duty a measurement of the specific fragmentation of the Foster acceptor, completely circumventing the need to measure a fluorescence response. Such process has recently come in general agreement to be termed ‘action FRET’.

## 4.5 Experimental and data analysis techniques

Discussion of the experimental methods employed in the work presented in this thesis will begin with consideration of the various experimental techniques utilized in this undertaking. These are MS and the work up of the data to give action-FRET values and a determination of its efficiency.

### 4.5.1 Inspection of the MS spectrum

The MS was used in the first instance of our experimental methodology to identify i) that the targeted final product was synthesized and could be detected in sufficient amounts to experiment on ii) which charge states our targeted compound was being detected by the MS. In order to read the mass spectrum effectively tables of predicted  $m/z$  charged species (in the positive or negative mode) were prepared. In this way one could easily assign the spectral intensities and match a given  $m/z$  ratio with a predicted  $m/z$  value in the table that corresponds to the molecular weight of a target compound or framework at a given charge state. An example of tabulated  $m/z$  and exact mass (monoisotopic mass) values is given below, Table 4.5.1. In this example, on inspecting the  $m/z$  values of the two major intensities of the spectrum and referring back to the table, it is clear that QSY7-amino-  $\beta$ -cyclodextrin and  $\beta$ -cyclodextrin (different to amino- $\beta$ -cyclodextrin,  $m/z$  1133.39) are sampled by the MS instrument, Figure 4.5.1. To further support our reasoning in resolving a peak in the MS spectrum, two chemistry drawing packages (suites) were used: Chemdraw and MarvinSketch. The method here consists in drawing out the predicted structure of a starting material or product and to then instruct the software package to analyze it and give a calculated exact mass, molecular weight or chemical formula.

species	Exact mass	1+	2+	3+	4+	5+
$\beta$ -cyclodextrin	1134.37	1135.37	568.19	379.12	284.59	227.87
[QSY-amino- $\beta$ -CyD]	1773.61	n/a	887.81	592.20	444.40	355.72

Table 4.5.1. Catalogue of expected  $m/z$  values and calculated exact mass of species of interest.

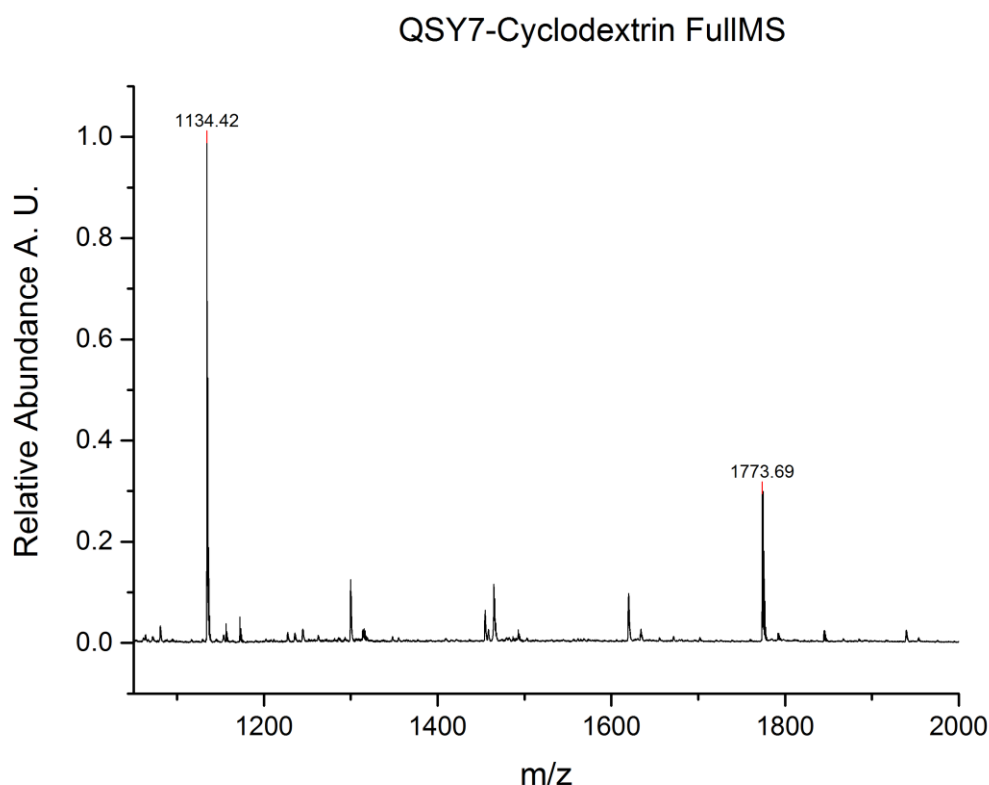


Figure 4.5.1. Spectrum: QSY7-amino-  $\beta$ -cyclodextrin FullMS.  $\text{NH}_2$ - $\beta$ -cyclodextrin:  $m/z$  1134.42.  $[\text{QSY-amino-}\beta\text{-CyD}]^+$ :  $m/z$  1773.69.

#### 4.5.2 Measuring fragmentation

The way the Xcalibur suit is used to churn out meaningful data is of central interest to those of the MS analytical community. In short, from the  $m/z$  spectrum, intensities of ions of particular interest are extricated and compared to the intensity of the associated total ion count (TIC). These selected skates or peaks are in fact intensities of daughter fragments from the parent ionic species, and are most typically associated to the chromophore component of a tagged species, in the context of the research discussed in this thesis.

Similarly, and popularly used by others, what is known as the fragmentation yield is used. In essence it formulates the following:

$$4.5.2.1 \quad \frac{\text{Parent+Daughter}}{\text{Intensity of the TIC}} / (\lambda \times P)^n$$

Where, Parent= intensity of the  $m/z$  signal of the parent and Daughter= intensity of the  $m/z$  of the daughter fragments.  $P$  symbolizes power,  $\lambda$  corresponds to the wavelength and  $n$  is the number of photons.

Later on in the next sections, it can be seen that the raw data that is made to go through this particular treatment is typically the intensity of specific chromophore fragments. Also more can be appreciated on how the fragmentation yield is key in the calculation of FRET efficiencies.

### 4.5.3 On building FRET frameworks.

Action-FRET is dependent on the observation of photofragments specific to the acceptor chromophore by excitation of the donor chromophore (in direct analogy to fluorescence based techniques where the fluorescence of the acceptor chromophore, when exciting the donor chromophore is used as a reporter of the FRET efficiency). This dynamic process is a two-component dependent process, where two chromophores, must reach a certain spatial proximity and come to interact electronically. This means that a pair of compatible chromophores has to be selected. The state of development and in combination, our understanding of conventional FRET, lead us to opt for QSY7 as the acceptor candidate as it fragments efficiently (best of its class). Sure to build on a solid basis, we first took time to demonstrate and confirm that laser induced dissociation (LID) engenders a breakdown of photofragments. Therefore, leaving a specific signature footprint in the MS spectrum of QSY7. Be it for the acceptor alone or covalently bound and purposely used as a tag of a species of interest. On the fundamental level, it was reported that the photofragments which are specific (*i.e.* they do not appear upon CID, they are specifically associated to LID) to the acceptor electronic excitation are principally  $m/z$  360 and 465 and in lesser abundance  $m/z$  531, see Figure 4.5.2. The specifics of the breakdown are shown in Figure 4.5.3.

The specific breakdown by LID:

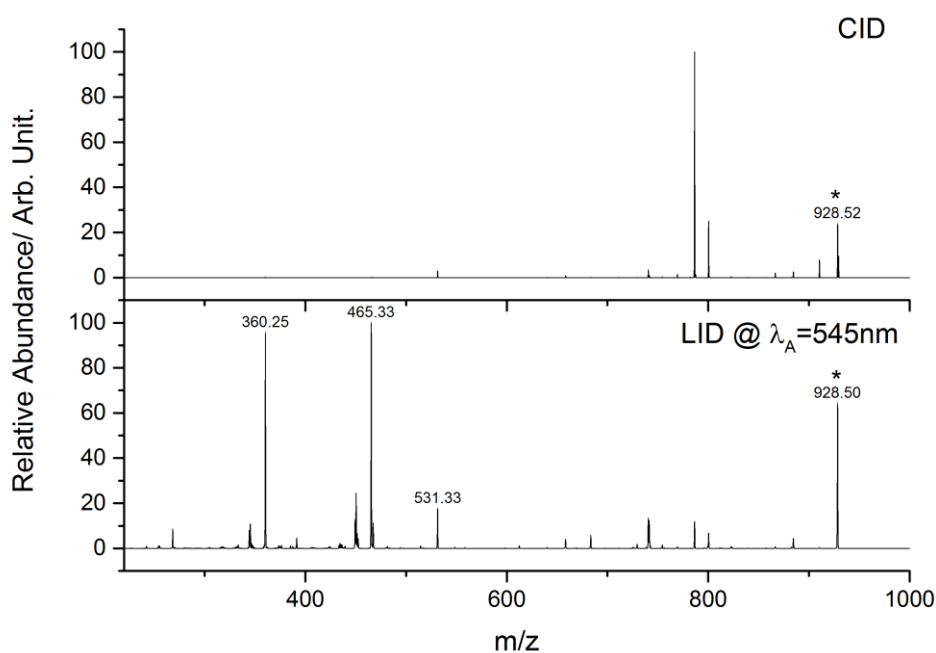


Figure 4.5.2. QSY7-AAK<sup>+</sup> QSY7-CID (normalised collision energy of 27) and LID at 545 nm (one photon process).

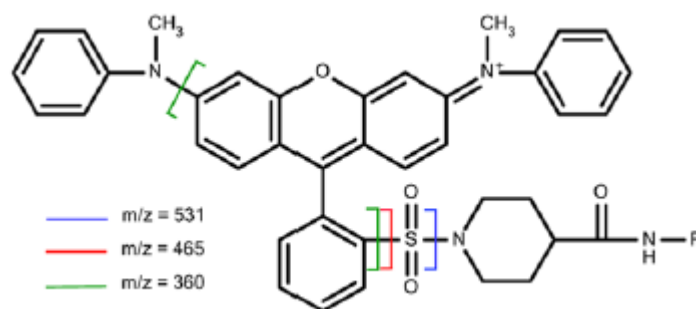


Figure 4.5.3. Breakdown sites of the acceptor chromophore QSY.

It was also noted that this intensity of photofragmentation reaches a maximum at a laser wave excitation of 545nm, irrespective of the power of the light source. This was well received as 545nm corresponds to the acceptor absorption maxima of QSY7. It is noteworthy that the optical spectra for the QSY7 bound to the tripeptide (AAK), Figure 4.5.4, is comparably very similar to the spectrum of QSY7 alone in solution which is available in the online spectral viewer ('spectraviewer' available at: <https://www.thermofisher.com/uk/en/home/life-science/cell-analysis/labeling-chemistry/fluorescence-spectraviewer.html>). There is also a match in comparing it to the spectrum of QSY9 alone in solution, Figure 4.5.5.

Chromophore spectra:

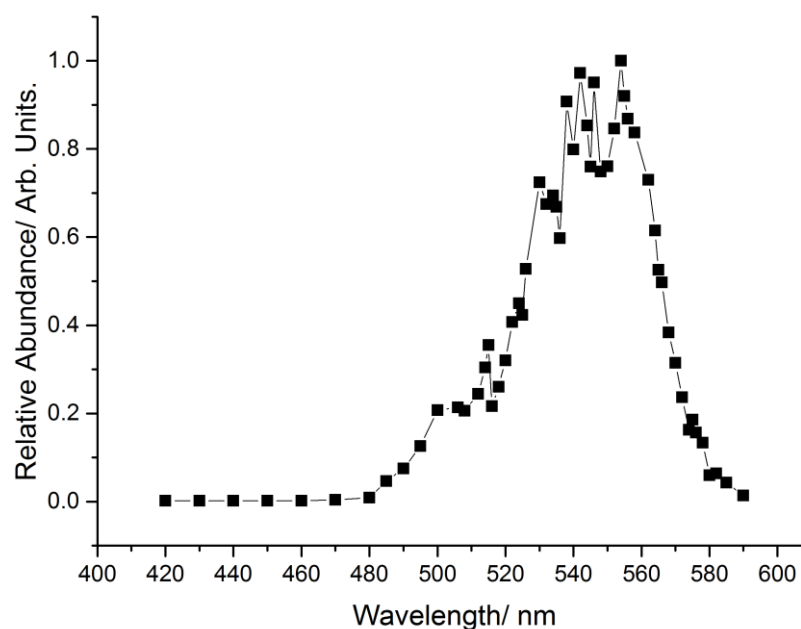


Figure 4.5.4. Acceptor, QSY7-AAK<sup>+</sup> optical action spectrum.

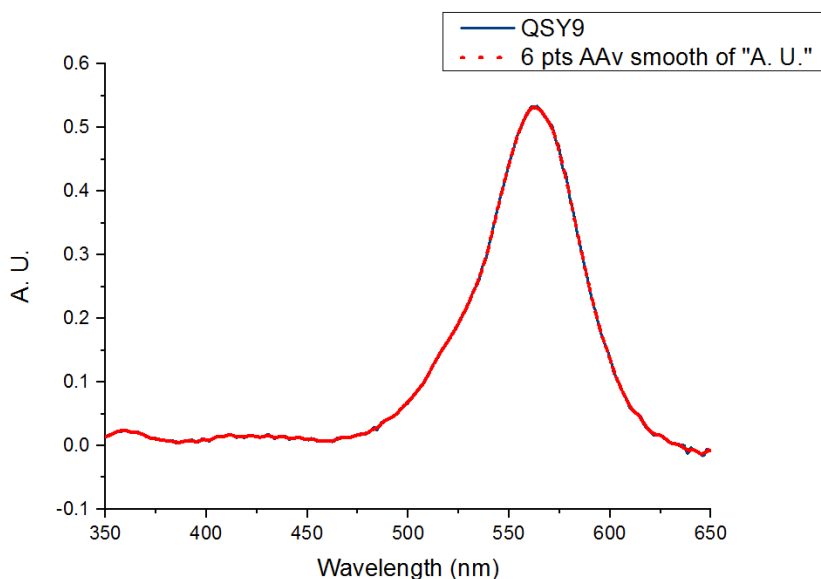


Figure 4.5.5. QSY9 solution absorption spectrum.

Now, onto the second part of a FRET framework, the donor component. The associated donor chromophore must be chosen carefully to fulfill two fundamental conditions. One that it emits close the 545nm wavelength so to excite and fragment the acceptor chromophore. In other words, the fluorescence emission of spectrum of the donor must overlap with that of the absorption spectrum of the acceptor (as mentioned previously). Two, that the donor chromophore holds an absorption band different to that of the acceptor thus to avoid its direct excitation. With this criteria in hand it was agreed that rhodamine was the best suiter to work with QSY [83], *cf.* Figure 4.5.6 and Figure 4.5.4.

Chromophore spectra:

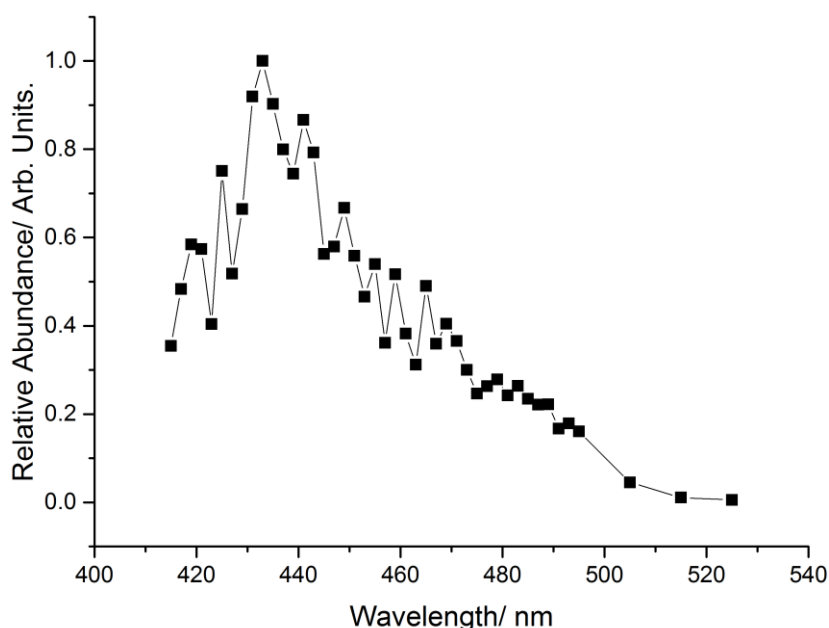


Figure 4.5.6. Donnor, Rh6G-AAK<sup>+</sup> optical action spectrum.

It should be said that, upon laser irradiation the Rh6G excites and fluoresces so, that no fragmentation is sighted (Figure 4.5.6). There is an established understanding that QSY7 is a quencher, laser irradiation harmonises with the chromophore and internal conversion jostles in. The internal conversion in turn leads to fragmentation (Figure 4.5.4).

Rhodamine 6G, had from the gas phase data made available in the literature the best absorption band and fluorescence profile that could match with the absorption maxima of QSY7. As the results of the research work carried in this lab can testify, rhodamine6G and QSY derivatives proved to perform well empirically in gas isolation with a range of peptides and biomolecules. In effect, as the third system can testify the band at 500nm is recovered as observable because the first luminescent is quenched with another Rh6G luminescent inducing fragmentation to go. Later it transpired that with laser irradiation at 505nm (the donor absorption maximum, rhodamine6G *cf.* Figure 4.5.7) would consistently result in fluorescence resonance energy transfer and yield an observation of the acceptor specific fragmentation of QSY. In addition, Figure 4.5.8, shows the action spectrum of mass selected (Rh6G-AAK-QSY7)<sup>2+</sup>. It is discussable on the standpoint of interpretation that excitation of donor leads to the fluorescence of rhodamine, and results in FRET and the fragmentation of QSY7 (observable from the coordinate points between 530nm and 580nm abscissa values). The second observable band between 530nm and 580nm is a result of direct excitation and fragmentation of the QSY7 acceptor.

Further spectra:

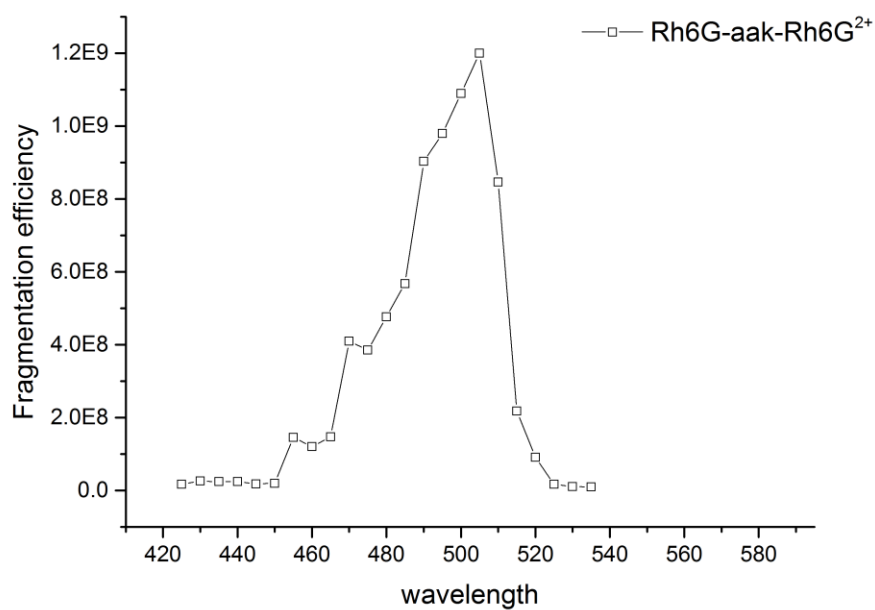


Figure 4.5.7.  $(\text{Rh6G-AAK-Rh6G})^{2+}$  optical action spectrum.

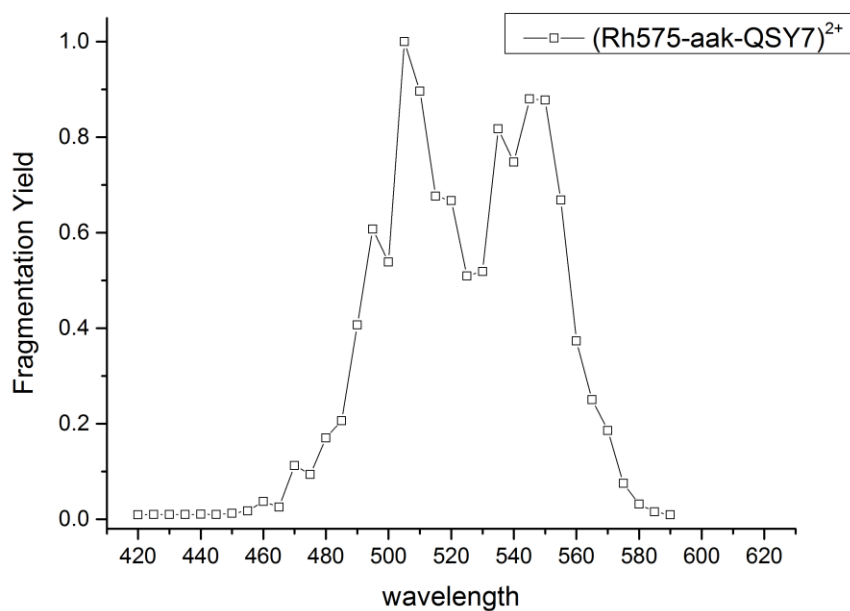


Figure 4.5.8.  $(\text{Rh6G-AAK-QSY7})^{2+}$  optical action spectrum

#### 4.5.4 Extracting FRET data

One of the remits of the efforts made was to formalize the methodology for obtaining FRET efficiencies by action-FRET in a coherent method which can be easily reproduced. A manner to treat this report of acceptor specific fragmentation (a fragmentation yield, see above), the signature footprint. To this end, the Xcalibur MS software that comes with the LTQ Velos makes it possible to extract the spectral intensities of ions of interest to calculate FRET efficiency. First the acceptor specific fragmentation yield ( $A$ ) is defined as the relative intensities of both the  $m/z$  360 and  $m/z$  465 peaks summed together (intensity of acceptor specific fragmentation, ( $B$ )) compared to the total ion count ( $TIC$ ) of the chromatogram, normalized to wavelength, power and number of photons; ( $\phi$ ), i.e:  $A=(B/TIC)/\phi$ . Phi in the context of the treatment of FRET data, ( $\phi$ ), encompasses the following:  $(\lambda \times P)^n$  where  $\lambda$  is the wavelength  $P$  the power of the laser (proportional to the number of photons in one laser pulse) and  $n$  the number of photons interacting (one in the experiments described herein). Nota bene: the  $m/z$  531 signal is used cautiously as it is considered too weak and stochastic signal and is seen also in CID.

#### 4.5.5 FRET efficiency determination

The FRET efficiency determination proceeds as described here. Measurements at 545 nm and 505 nm (LID spectra) are repeated 5 times consecutively, with each mass spectrum averaged over a period of two minutes. These spectra are treated to give  $A$  values: one set for 505nm irradiation and another for 545nm irradiation. The FRET efficiency is then calculated: the acceptor specific fragmentation yield at 505 nm is normalized to the value at 545 nm, i.e.  $(A^{(505\text{ nm})})/(A^{(545\text{ nm})})$ . This procedure is performed for every pair of measurements, yielding a total of five values of the FRET efficiency. The final FRET efficiency for the data set is then taken as the mean of these 25 values, and their standard deviation as the error. Finally, a correction factor of -0.25 is applied to the average FRET efficiency to take into account the non-zero absorption of the acceptor at 505 nm. The final result of the work-up generate FRET efficiency values that lie between 1 and 0 [84].

Alternatively, instead of recording a total of 10 LID spectra, five for each wavelength, it came at a moment on the doctoral undertaking to detract from this work methodology and move to an operating procedure based on a scan or sweep of all the spectral region of both donor and acceptor chromophores. Typically, this meant running a 120-130nm wide scan, rhodamine575 and QSY7 tagged species were swept from 465nm to 600nm for example. Similar to the earlier tested method, the  $B$  was extracted and reported over the extracted intensity of the total ion count or chromatogram (ITIC) and formulated with the normalization parameter ( $\phi$ ) to give an appraisal of  $A$ . The series of  $A$  data is the plotted against the wavelength range of the scan (see chapter 6). Treated correctly, this produces a two-humped relationship, the first hump reaches a top-line figure at 505 and another at 545nm along the abscissa. For a 505nm excitation, this is as a result of the absorption of the donor chromophore and the other band due to a 545nm excitation validates the more direct breakdown of the acceptor, QSY7.



The profile of the graph is then fitted with two Gaussians. Finally, the maxima or height of each Gaussian is given as a quotient of the FRET efficiency the height of the 505nm peak as the numerator and height of the 545nm peak *i.e.*  $(A^{(505\text{ nm})})/(A^{(545\text{ nm})})$ . Carrying out the division, the final result of the work-up generate FRET efficiency values that lie between 1 and 0. The attractive point of this procedure is that it can simultaneously record the power as it records the MS spectrum and its evolution along the sweep. This technique has the benefit to take many MS spectra and is different to taking LID MS spectra through multiple computer manipulations. This technique also represents a large improvement over the earlier operating procedure as one can be assured on inspection of the generated fragmentation yield graph to select the real-terms wavelength that induces maximum specific footprint fragmentation of a covalently bound acceptor species rather than blindly relying on the theoretical electronic excitation wavelength maximum.

#### 4.6 Studying amyloid-beta (12-28) alloforms using action-FRET

A major motivation of this thesis has been to introduce the new ‘frontier’ technique of action-FRET to elucidate fully or only partially answered questions in molecular biology on platelet (or plaque) formation in Alzheimer’s disease commonly observed in the brain tissue of patients suffering from the disorder. The amyloid beta protein ( $A\beta$ ) and its succession in the mechanism in fibrillar assembly and importance to plaque formation has been significantly studied over the past few years [85-95]. Research assessing the amyloid beta species with FRET has been addressed (Tryptophan-Thioflavin T donor-acceptor working pair), however not in connection to the herein MS developed method [96]. Research hinged on the study of the amyloid protein to ESI was examined by nationally resourced research investigators [97]. This led us to carry a major research investigation, this time on amyloid beta protein 12-28 cuts of the wild type and on one of its alloform which was well placed for action-FRET in combination of other techniques to build further understanding on the subject. The constituting alloform in question is a replacement of amino acid, phenylalanine for a proline (F19P). This version is of special interest as it was found absent to furl and influence aggregate development. The 12-28 fragment of the  $A\beta$  protein ( $A\beta_{12-28}$ ) on the other hand has attracted attention as it is the acting neurotoxic fraction of the  $A\beta$  protein that lends it its readiness to fold into a fibrillar motif. It is the acting component (L17 to A21), the ‘hydrophobic core’ nascent to the formation of large aggregates and fibrils in the full  $A\beta$  protein.

A second feature of this experiment is to describe both miniproteins in gas isolation. In this setting one can gain access on the conformational changes engendered by the protonation along the protein and effectively focus on the study of a species of particular charge state. Relevant structural characterization on the global structure and conformational changes was given by IMS. Action-FRET was used to draw measurements on the separation of two singular regions of a protein by solving FRET efficiencies. In a third part, molecular dynamics simulation (MD) have been geared towards producing frames or images of the aggregation of amyloid- $\beta$ . Lastly, comparison of FRET efficiency and collision cross sections (CCS) were established for the charge states of the two alloforms so to identify the dominant structural families for the charge state of each alloform. From this standpoint, the study progressed to gain insight on how the acting component comes together in triggering aggregation behavior and how protonation of the monomer follows throughout.

## Method

### Peptides and chromophores

Carboxyrhodamine 575 C<sub>5</sub>-maleimide (Setareh Biotech) (R575) and QSY7 C<sub>5</sub>-maleimide (Life Technologies) (QSY7) structures depicted, Table 2.2.1, chapter 2, were used as donor and acceptor chromophores for action-FRET measurements respectively. Their unique properties and characteristics were described in the gas phase, R575 absorbing at 505nm and QSY7 absorbing at 545nm. The target peptides were made sure to include cysteine residues so as to allow the functionalization with the chromophores (see above). Wild type A $\beta$ <sub>12-28</sub> with capped termini on the flanking cysteines residues (Ace-C-V<sup>12</sup>HHQKLVF<sup>19</sup>FAEDVGSNK<sup>28</sup>-C-NH<sub>2</sub>) and the F19P alloform (Ace-C-V<sup>12</sup>HHQKLVP<sup>19</sup>FAEDVGSNK<sup>28</sup>-C-NH<sub>2</sub>) were purchased from GeneCust (Luxembourg). Both were dissolved in a 1:1 mixture of H<sub>2</sub>O: acetonitrile made up to ~500 $\mu$ M concentration. Stock solutions were prepared for every dye in DMSO (~10mM). The peptide solutions were then treated with both dyes (10 $\mu$ l each). The mixture was left to run until completion for one hour at room temperature. A further dilution was conducted carrying the mixture down to ~50 $\mu$ M so to electrospray the solution. A second aliquot was put aside in order to prepare an electrospray solution with 0.1% acetic acid thereby outsourcing the 6+ charge state.

The details on how measurements and work up have been made with IMS and replica exchange molecular dynamics (REMD) are discussed in a chemical science article [98]. Without going into the details, IMS measurements were executed on a custom-built ion mobility spectrometer. This one is composed of a 1 m long drift tube connected one side to an electrospray source and on the other a time of flight mass spectrometer. Drift tube helium pressure is 15 Torr and temperature is kept at 300 K. Ions are introduced to the drift tube by an hourglass funnel ion trap. The time of flight measures both the mass to charge ratio of species and drift time out of the tube. Ion mobilities and collision cross section (CCS) are then subsequently calculated from the ion arrival time distribution as a function of the inverse drift voltage [98]. In terms of computation, REMD offers an efficient conformational sampling method to understand the events involved in protein folding [99-101]. It rests on a standard molecular dynamics simulation and allows systems of similar potential energies to sample conformations at different temperatures

[102]. In this way energy barriers on the potential energy surface might be overcome, allowing for the exploration of new conformational space. Gromacs 4.6.5 was used for the structural sampling of the wild type and F19P mutant simulations [98]. The FRET efficiency distribution is calculated from the chromophore distance and orientation distributions and ensemble average value from REMD. The distance distribution in question, that between the optically active units of the chromophores is calculated by evaluation of the geometrical centre of atoms in the xanthene moiety and side chains covalently bound by the nitrogen atom [103].

## Results and discussion

Four different charge states are observed after electro-spraying solutions containing doubly grafted A $\beta$ ; 3+,4+,5+, and 6+ corresponding to there being 1,2,3 or 4 protons embedded along the peptide the remaining two positive charges are to be accounted for the chromophores bearing each a positive charge. The 4+ and 5+ charge states were found to be the most predominant species. This is in striking accord with previous gas phase measurements of A $\beta$ <sub>12-28</sub> where mainly 2+ and 3+ species were identified [104]. This leverages strong support that the presence of the charged chromophore does not greatly perturb the charge state distribution of the untagged macrospecies. Action-FRET and IMS measurements afforded to collect the necessary CCS and FRET efficiencies for each charge state of the two doubly grafted A $\beta$ <sub>12-28</sub> alloforms and are plotted together in Figure 4.6.1. Just below a table compiling the FRET efficiencies and cross sections for wild type (left) and F19P (right) alloforms is made available to check out and arrive to a balance conclusion. It was not possible to obtain an experimental CCS value for the 3+ charge state since the ion count was extremely low in all electrospray trials. Thereby a calculated CCS value is plotted for both alloforms in countermeasure. On inspection one can appreciate that there are strong similitudes between the experimental and theoretical data points most especially with the 4+ and 5+ charge states of both alloforms. Critically it is important to comprehend that for the 3+ FRET efficiencies, the calculated chromophore interdistance is commonly found below 15 Å. From this, it is impossible to disconnect from a Dexter energy transfer or a breakdown in the Förster principle. From Figure 4.6.2 it is also clear on interpretation that changes in the peptide structure are induced as protonation increases. There is a large change in the FRET efficiency as the 3+ charge state moves up to the 4+ charge state. Likewise, a reasonable change in the calculated CCS is also observed, and although there is no experimental data for the 3+ charge state, the discernable similarities between theory and experiment for the other data points backs up the argument for real term increase. This observation leads to the understanding that there is a large shift in the secondary structure in the two charge states. Conversely, only a small change in the CCS is observed for the 4+ and 5+ charge states suggesting that the overall spatial arrangement of the peptide prevails the same. All the same, there is a larger relative decrease in the FRET efficiency between these two charge states (4+ and 5+). In the context of structural analysis this means a total increase in the extension of the peptide. The information gleaned for the change in FRET efficiency from the 4+ to the 5+ associated with the F19P alloform is encompassed in the error bars for the 4+ FRET efficiency. This is indicative of a greater flexibility for the relative position of the chromophores. Lastly, there is a further large change in the CCS when comparing the 5+ and 6+ charge states, and a minor

cut-back in the FRET efficiency. This points out a further evolution in the global framework with nevertheless the overall proximity of the chromophores left unaltered. It is important to mention that as FRET efficiency of 0 is approached, a relatively small shift in FRET efficiency may correspond to a large change in the chromophore interdistance. A highlight of this concerted work are the depictions representing the structures for the charge states of each alloforms, Figure 4.6.2, confirming the discussion of the above passage, the interpretation of the observations made.

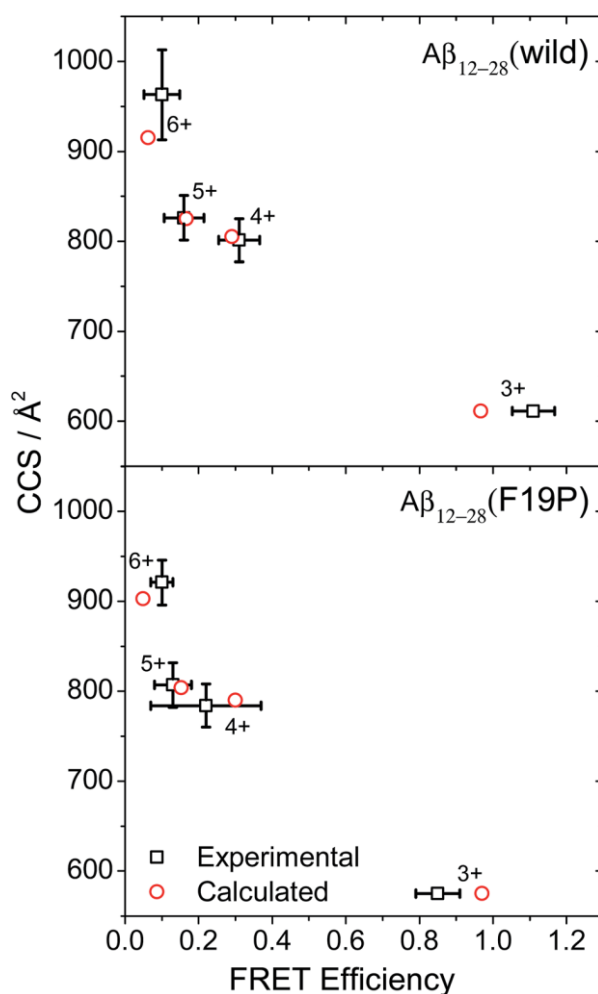


Figure 4.6.1. CCS plotted against FRET efficiency for the four charge states of the WT (top) and F19P (bottom) alloforms of A $\beta_{12-28}$ . The black hollow squares depict empirical data points whilst the red circles ascribe the average values of the conformational ensemble worked out by REMD.

Charge	Wild type				F19P			
	Exp. FRET efficiency	Calc. FRET efficiency	Exp. CCS	Calc. CCS	Exp. FRET efficiency	Calc. FRET efficiency	Exp. CCS	Calc. CCS
3+	1.11 $\pm$ 0.06	0.97	n/a	611	0.85 $\pm$ 0.06	0.97	n/a	575
4+	0.31 $\pm$ 0.06	0.29	801 $\pm$ 24	805	0.22 $\pm$ 0.15	0.30	784 $\pm$ 24	790
5+	0.16 $\pm$ 0.05	0.17	826 $\pm$ 25	825	0.13 $\pm$ 0.05	0.15	807 $\pm$ 25	804
6+	0.10 $\pm$ 0.05	0.063	963 $\pm$ 50	915	0.10 $\pm$ 0.03	0.049	921 $\pm$ 25	903

Table 4.6.1. Summary compiling the measured and calculated collision cross sections and action FRET data.

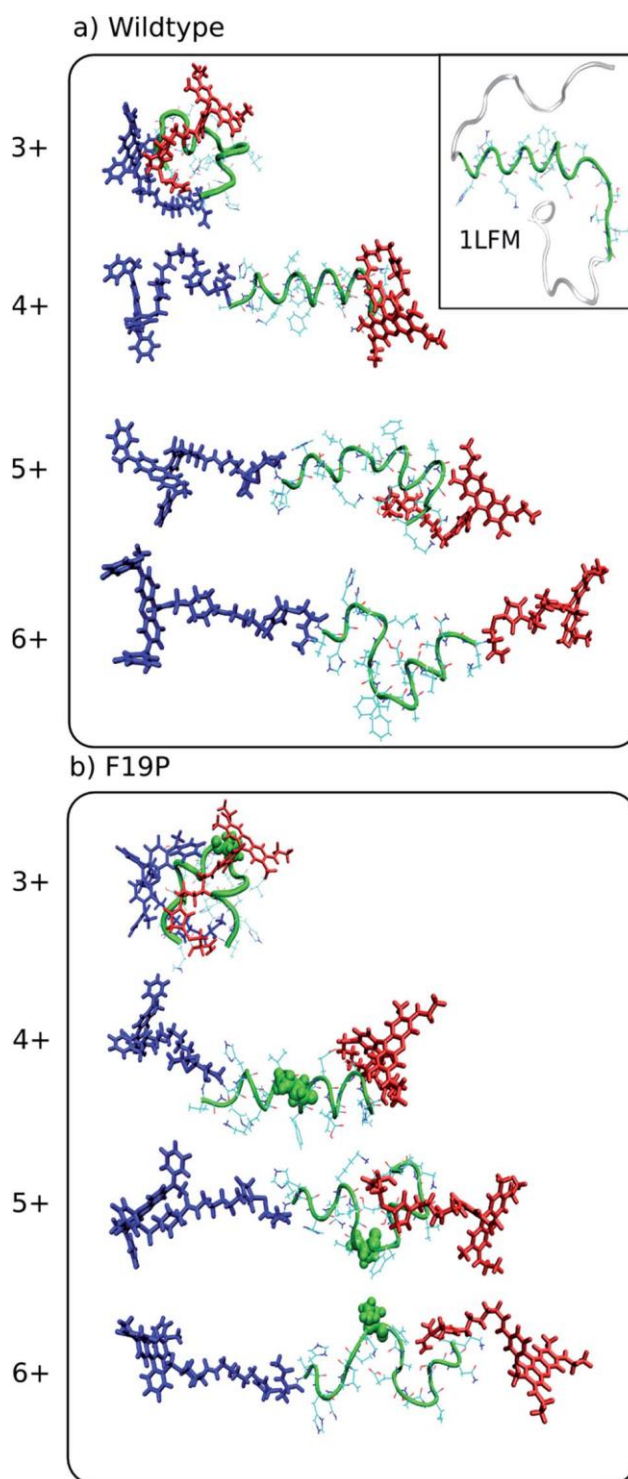


Figure 4.6.2. Conformations simulated at 292K associated to the structures of increasing charge states of; top, the wild and bottom, the F19P alloforms of  $A\beta_{12-28}$ . Here, the donor chromophore (covalently bound to the N-terminal residue) is shown in red whilst the acceptor chromophore is in blue and green colours the peptide backbone. The same trend in secondary structure as a function of charge state are observed for both of the possible doubly-grafted species of both alloforms, showing that the grafting location of the chromophore has only minor influence on the peptide's structure.

Inset 1LFM is a NMR structure of  $A\beta_{12-28}$ .

In addition, calculations on the changes in the dihedral angles of the peptide backbone are taken to be compared and contrasted with the depicted representative structures. These are reported in a form of a Ramachandran plot.

Ramachandran plots are contour plots of potential energy coordinating torsional angles  $\Psi$  versus  $\phi$  which were determined by the physicist in honour, G.N. Ramachandran. The fundamental approach starts with modeling small peptides. These are used to systematically vary  $\Psi$  and  $\phi$  with the purpose of debarking on stable conformations. The given symbols  $\Psi$  and  $\phi$  in particular combination ascribe a given conformation. These are examined and only values of  $\Psi$  and  $\phi$  for which no close contacts between atoms are produced are taken in as 'permitted' and finally go through to be represented in the two dimensional map, the Ramachandran plot [105].

It is important to take into account an actual plot, here that of a poly-alanine, Figure 4.6.3:

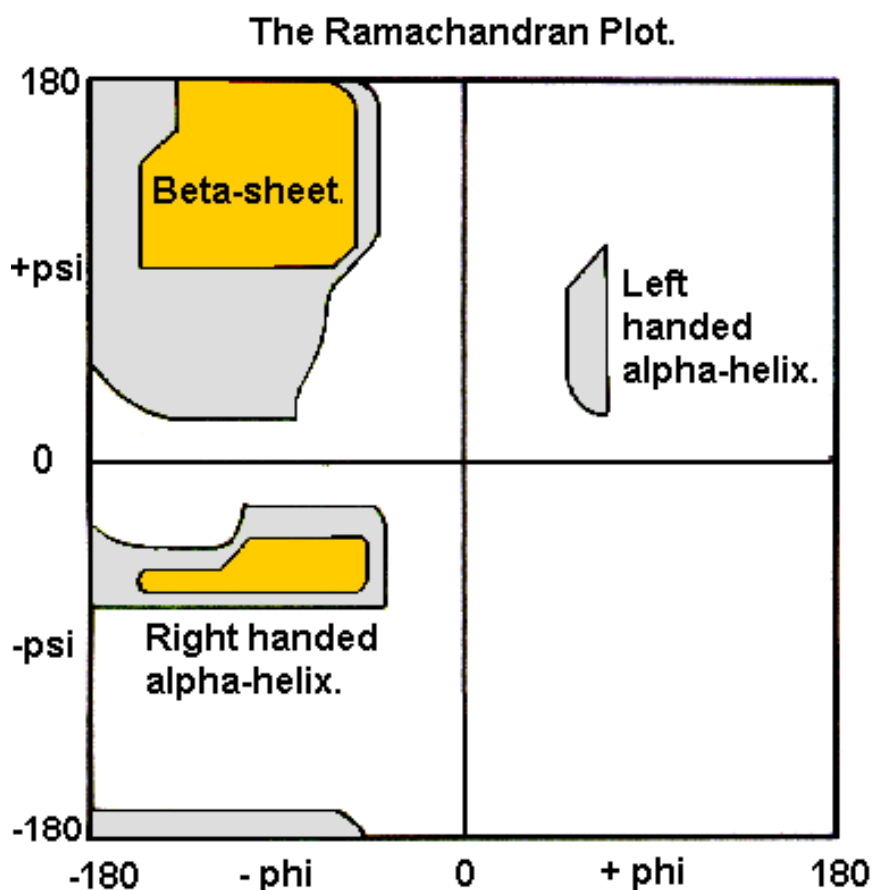


Figure 4.6.3. The Ramachandran plot for poly alanine.

The white spaces cover conformations where atoms of the oligopeptide come closer than the sum of their van der Waals sphere. These regions are sterically forbidden for all amino acids bared for the glycine residue which is singularly different as it has no side chain. The tuscan yellow region correspond to where the molecules take a fold where there is no steric hindrance, *i.e.* where  $\alpha$ -helical (right handed) and beta-sheet character is found. The gray space denominates the allowed regions of interaction with a selection of shorter van der Waals radii in calculations. The atoms are allowed to come closer together. Subregion of slightly unfavored left-handed  $\alpha$ -helical character can then be made out (second quadrant of the two-dimensional map).

Below is included the plot for the amino acids making up the hydrophobic segment: for the C-terminal donor chromophore Figure 4.6.4 and its homologue, the Ramachandran plot for the N-terminal donor chromophore, Figure 4.6.5. From these figures it can be confirmed that the protein architectures from 3+ to 6+ are conformationally different. On the standpoint of interpretation, the keypoint is to integrate that differences in the Ramachandran plots are present for 5+ and 6+ charged species of the amyloid fibril data (black squares). The black square data-points for the for 3+ and 4+ charged species globaly converge in the same way, Figure 4.6.4 and Figure 4.6.5.

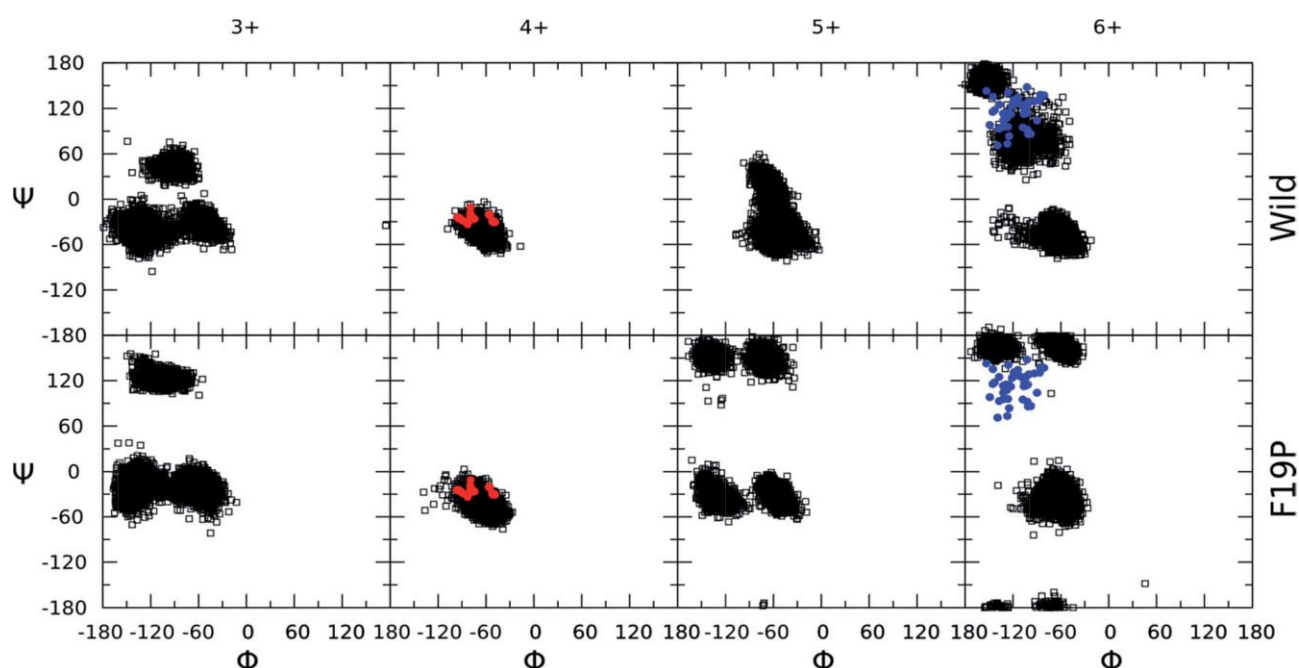


Figure 4.6.4. Ramachandran plots ascribed to the hydrophobic core region (residues 17-21) of the different charge states of the wild (top) and F19P (bottom) alloforms of A $\beta$ 12-28 (donor chromophore bound to the C-terminal residue). Black squares correspond to the 5 dihedral angle ( $\phi$ ,  $\Psi$ ) pairs of residues 17-21 for all the structures computed at 292K. Red dots indicate the corresponding average dihedral angles of the partially folded solution structure from the pdb file 1LFM. Blue dots indicate the dihedral angles of the A-chains in the pdb file 2BEG.

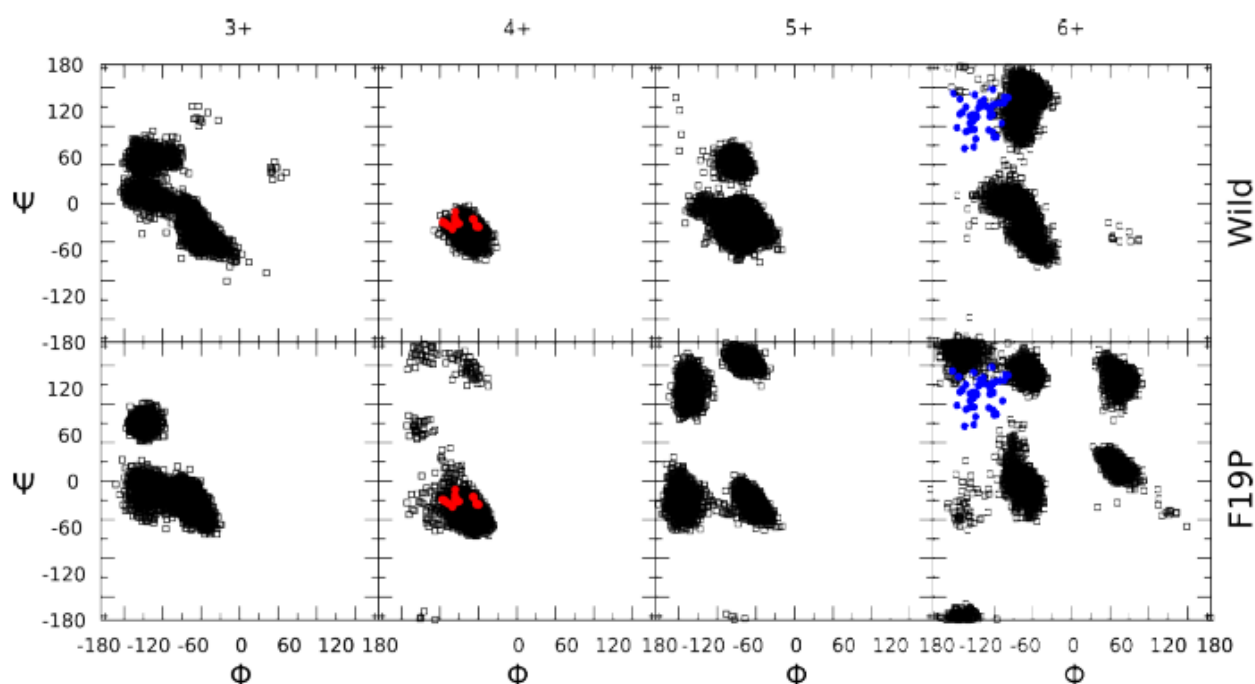


Figure 4.6.5. Ramachandran plots ascribed to the hydrophobic core region (residues 17-21) of the different charge states of the wild (top) and F19P (bottom) alloforms of  $A\beta_{12-28}$  (donor chromophore bound to the N-terminal residue). Black squares correspond to the 5 dihedral angle ( $\phi$ ,  $\Psi$ ) pairs of residues 17-21 for all the structures computed at 292K. Red dots indicate the corresponding dihedral angles of the partially folded solution structure from the pdb file 1LFM. Blue dots indicate the dihedral angles of the A-chains in the pdb file 2BEG.

A fundamental hurdle that needed to be overcome in this study on doubly grafted  $A\beta$  was to demystify whether the anchoring of the chromophores perturbs or not the secondary structure of the peptide as compared to the un-grafted polymer. The study came to the balanced conclusion that (for a said alloform of said charge state) by virtue of their long  $C_5$  linker chain, the chromophores are very flexible. Opposedly, the peptide is more characteristically rigid and has a small propensity to change and favors a low energy structure. These structural trends also characterise the series of charge states of both the N- and C- terminally grafted QSY7. The C-terminally grafted F19P species however present a greater likeliness to take on a random coil like twist. This is certainly due to the secondary amine nature of the amino acid that is proline. From this, the structural influence of the chromophores reduces to the existence of two positive charges at the N- and C-terminus. A major point has been the observation of secondary structure change for the doubly grafted species that unilaterally agrees with observations in other reports on the gas phase study on the structure of doubly and triply protonated  $A\beta_{12-28}$ . Specifically reporting a transition existing between the globular and helical conformation when a third proton moves 2+ charge state to 3+. This transition reemerges as can be interpreted from Figure 4.6.2, although at a different protonational charge state (*i.e.* the 3+ and 4+ charge states). Thereby it is suggestive that although similar structural trends are observed in these two systems, for frameworks (peptides linked to chromophores) at lower protonation states, the presence of the N- and C-terminal charges by the chromophores engender the system in a coil like assembly to transition to a helical arrangement.



Another point of order has been to recognize any physiological similarities between two different amyloid beta proteins: one related to solution phase structure of the A $\beta$ <sub>1-42</sub> and the other that of the doubly grafted A $\beta$ <sub>12-28</sub> in gas isolation. The visualization of the NMR structure of A $\beta$ <sub>1-42</sub> is included as an inset in Figure 4.6.2. The 12-28 region is conveniently emphasised in green. One can see that there is an evident helical motif for the 12-28 region, which is also observed for the 4+ charge state in both wild and F19P alloforms. The transpiring fact of the 4+ charge state holding a similar fold to the one in solution is most likely due to there being the same on the peptide in both cases (solution and gas): doubly charged peptide in the case of doubly grafted A $\beta$ <sub>12-28</sub> and the property of the 12-28 segment to have 4 basic and 2 acidic amino acids amounting to a net charge of 2+ (solution). Exploring this similarity further, the backbone dihedral angles in the hydrophobic segment of A $\beta$ <sub>1-42</sub> are overlaid as red dots on 4+ Ramachandran plots of Figure 4.6.4 and Figure 4.6.5. An almost total agreement is with the backbone conformation in the two systems providing striking evidence for the mimicking of native secondary structure in the doubly grafted species. The presence of the N- and C-terminal chromophores draw a structural similarity for both 12-28 segments and it is thought to be by the chromophore's presence that 'space fills' and substitutes the missing N- and C-terminal peptidic trunks of the protein.

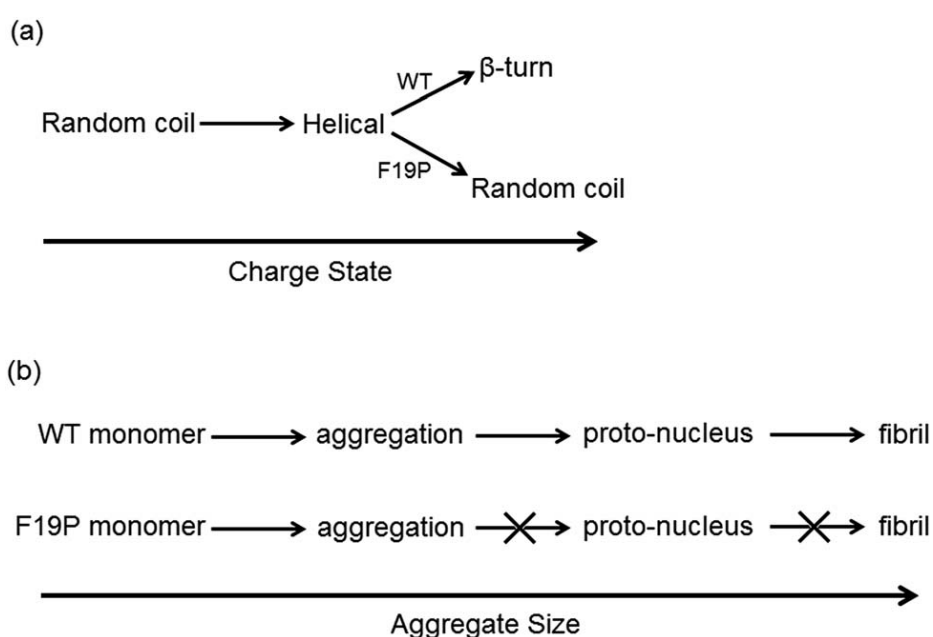
Compellingly, the hydrophobic segment presents two alternative backbone configurations in the 3+ species which are completely absent from the solution phase structure. It was found that the 3+ charge state presents globular random-coil type structure in both alloforms. The large change in the structural motif: a globular onset developed to a random coil and finally an alpha-helical motif is as predicted from the change in FRET efficiencies shown in Figure 4.6.1. In the 4+ charge state of the wild type alloform, lysine residues K16 and K28 carry a positive charge that account for a certain Coulomb repulsion that has the effect of triggering unfurling of the alloform. The F19P also displays some conformational memetics with the wild alloform for the 3+ and 4+ charge states and is backed up by comparison with the dihedral angle data of the hydrophobic core, Figure 4.6.4. In either case there is a change in structure from globular random coil of the 3+ charge state to the drawn out helical form of the 4+ charge state.

Focusing now on the 5+ charge state, the additional proton is accommodated on the histidine residue, H13 or H14 since the N-terminus is acylated. It is found that, for both possible grafted species it is thermodynamically favorable for the third proton to be bonded on the H14 residue. This may be due to the fact that the K16 and H14 are located on opposite sides of one of the helical turns, allowing the charges to maintain a maximum separation whilst holding the favoured helical motif.

The promotion so to speak from the 4+ charge state to the 5+ charge state results in an overall elongation of both systems as supported by the decrease in FRET-efficiency and the small increase in CCS. There is a clear demarcation in the helical motifs in both alloforms, especially in the hydrophobic core region, Figure 4.6.2. Figure 4.6.4 demonstrates a clear demarcation from the "all-alpha" configuration of the 4+ charge state in both alloforms, but the nature of this deviation is noteworthy different. In the wild type alloform the demarcation leads to loss of the helical arrangement and does not go as far as full fraying of the species. The change is more

acute with F19P. The F19P alloform dynamics transition the structure to a more complete unfolding of the helical bundle resulting in a significant random-coil character in the dihedral angle plot, Figure 4.6.4 and Figure 4.6.5. The underlining agreement here is that the helical stabilizing interaction cannot compensate for the charge induced structural stress of the F19P alloform, which can be interpreted as a weakening of the stability of the helix as compared to the wild type. The fourth proton added to the H13 residue came to give the maximally charged, 6+ species. Both alloforms are withdrawn of all helical character in the N-terminal region at this charge state. Although similar tendencies are revealed for both alloforms in the context of their conformational evolution, there is a pronounced difference in the structural motifs located at the hydrophobic core region. For the F19P alloform, the dissimilarity between the 5+ and 6+ charge state looms to the greater loss in helical character and a concurrent increment in random coil curl. The wild type alloform was equally found to collapse its helical structure, but in consequence a significant  $\beta$  character emerged.

There is a frank connexion that large aggregates of A $\beta$  are assembled as  $\beta$ -sheets and it has been proposed that the conformational change from helical to  $\beta$ -like structures in the monomer are key in triggering the aggregation process. The dihedral angles for the hydrophobic core region of the Alzheimer's amyloid fibril (pdb structure 2BEG) are included in Figure 4.6.4. and Figure 4.6.5 for the 6+ charge states of the two alloforms as blue circles. The wild type alloform possesses the same range of dihedral angles as those from the Alzheimer fibrils. Suggesting that a fibril-like conformation describes the wild type. Conversely, there is no evidence of population of fibril-like monomer structures in the F19P alloform, *i.e.* there is no overlay with the black squares and the blue points. The deployal of each structure as charge increases is summarized figuratively below, scheme (6):



(6)

The two-acting species on the study: F19P and wild type alloforms of A $\beta$  protein have been examined in the gas phase previously by Bernstein *et al.* The survey concludes that although both alloforms form small aggregates, it is only the wild-type in which further oligomerization carries through to large fibril-like molecular edifices [90]. This finding set their consensus that there is a key protonucleus formation central to the nascence of fibrils which are formed in the observed aggregates of the wild type but not the F19P alloform. Details on the exact nature of this proto nucleus have not been demystified. A prospective model for understanding fibril self assembly rests on that there being a dimension factor with the first aggregates that start of as random coils and bundle into  $\beta$  conformational structures providing favorable geometry for nucleation to occur. This event cascades into further oligomerization. Bleiholder *et al.* found evidence for the existence of paranuclei that are of great significance to the aggregation step of fibril forming proteins [106]. However, they did not observe this with peptide sequences which go on to form isotropic aggregates.

All this information at hand allows us to ascertain a tentative hypothesis for the difference in aggregation behavior of the hydrophobic core in the monomer discussed above and summarized in scheme (6). Here it can be drawn up that the structural transition from the mostly helical 4+ species and the 5+ charged species to the more  $\beta$ -turn-like structure of the 6+ for the wild type alloform indicates that a structural transition similar to that suggested and that depicted in scheme (6), checking through proto-nucleus precursor formation and yielding fibril molecular structures is at play (scheme (6), (b)). Contrarywise, this transition is not observed in the F19P alloform. The evolution of events is different. With the F19P alloform no proto-nucleus forms and incidentally the self aggregation process into extended fibril-like structures does not occur.

## Summary

This study that conciliates IMS and REMD simulations as well as the action-FRET technique is useful as it gleans information that either technique alone cannot access, it ameliorates prediction of structural change. The consensus has been that amyloid beta fragment peptides is influenced by its charge state, repercussions are on its structure that transition between random coil and helical form when going from singly to doubly protonated (3+ and 4+ species). Addition of a third proton on the peptide was found to destabilize the helix in the wild type alloform and engender partial unfolding of the F19P alloform. Proton number four to the peptide placed to the peptide, pieces the maximally 6+ charged species and causes unfolding of the helix in both alloforms. The REMD has provided much valuable insight. The measurement of the dihedral angles of the peptide backbone in the hydrophobic core region of both alloforms, demonstrated that although the two constructs do exhibit similar behavior as a function of charge state, there are noteworthy demarcations in the structural motifs of the hydrophobic core. Comparison to the dihedral angles of the solution phase structure of both monomer and fibrillar A $\beta$ <sub>1-42</sub> put forward for understanding that the helical to the  $\beta$ -turn conformational transition step takes place during aggregation and only occurs in the wild type alloform, whilst the F19P alloform presents a random coil structure. Thereby it was postulated that the tendency of the F19P alloform to undergo a helical random coil conformational transition prevents formation of the fibrillary proto nucleus and thus the F19P alloform does not down stream to fibrillary aggregates. The importance of such a transition in A $\beta$  peptides potentially provides a glimpse into the aggregation propensity of other A $\beta$  mutants. *In fine*, the connection that exists between helix stability of the hydrophobic core and the propensity for aggregation may provide crucial to drug and medication development programs.

## 4.7 Action-FRET in application. Second study.

The opportunity has risen to elaborate and test an experiment with action-FRET on supramolecular species. This work was performed as there was an interest of the group and collaborators from the mass spectrometry research group of Mons, Belgium and because a many of the molecular frameworks were made available synthetically by the latter, this feasibility of the study was also taken forward as there is an interest in studying complexes in the gas phase. It has also been claimed that cyclodextrins interaction on amyloid beta protein inhibits aggregation [107] and this has motivated the herein study of amyloid beta species with  $\beta$ -cyclodextrin complex. This section here will store the details of how the application of action-FRET was brought about to probe the system. This is important to modern day living and society because supramolecular complexes are the heart components in an array of targets ranging from metal ion sensing to refining peptides properties [107]. Another addition is the appreciation the gas phase offers for the study of species with great stoichiometric control and size selection. The constituting acting reagents are i) tagged  $\beta$ -cyclodextrin (CyD) receptor and ii) donor chromophore tagged amyloid beta peptide segment. Figure 4.7.1. The beta, in  $\beta$ -cyclodextrin is a denomination related to the size of the cyclodextrin, it is because it is based on specifically seven  $C_6H_{10}O_5$  repeats.

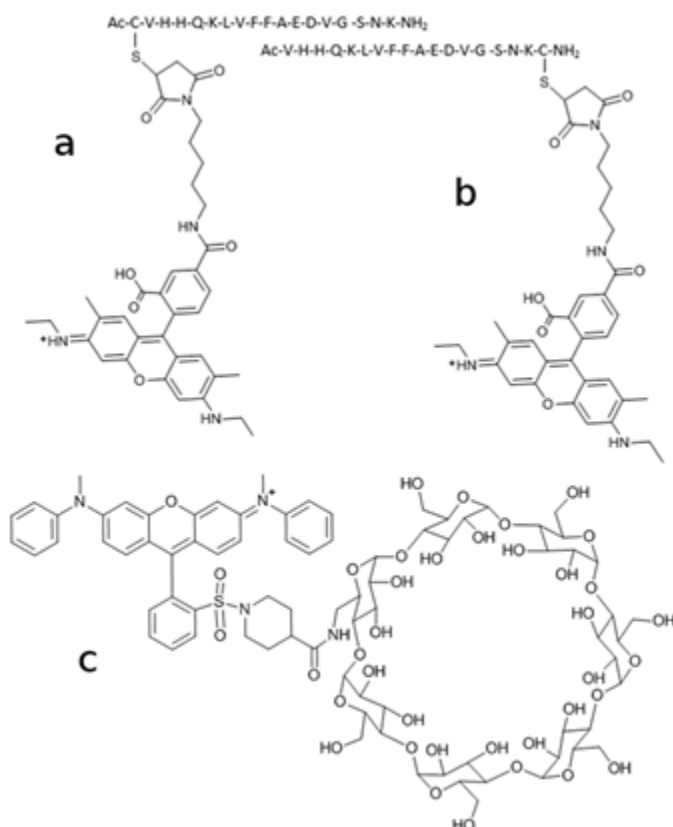


Figure 4.7.1. Selected host-guest partners for experimentation: (a)  $A\beta_{12-28}$  wild sequence with covalent attachment of Rhodamine (at the N-terminus, capped peptide) (b)  $A\beta_{12-28}$  wild sequence with covalent attachment of Rhodamine donor (at the C-terminus) and (c) amino- $\beta$ -CyD macrocyclic receptor with covalent attachment of QSY7 acceptor to the amino group.

## Method

The amino- $\beta$ -CyD-QSY7 receptor production is based and calqued from previously discussion peptide tagging methodology. The synthetic constitution was taken care to proceed at room temperature for a long time until the next day by stirring an equimolar mixture of conventioned beta Cyclodextrin ( $\beta$ -CyD-NH<sub>2</sub>) with succinimidyl ester QSY7. Succinimidyl QSY 7 (Invitrogen) was desolidified as fallen in the liquid media (DMSO, 500 $\mu$ l) to reach a final concentration of 10mM. A 10mM solution of amino- $\beta$ -cyclodextrin (amino- $\beta$ -CyD, TCI Europe) was prepared in water. Note: 100 $\mu$ l of the QSY7 solution was mixed with 100 $\mu$ l of amino- $\beta$ -CyD in a vial. This vial was sealed closed, aluminium covered in fact so to keep its contents away from a UV-visible light interference. It is noteworthy to mention that the made-up mixture preparations were kept equimolar. Assention for reaction work up was taken on the next day, at room temperature. An aliquot of the solution was poured in water:methanol (amino- $\beta$ -CyD-QSY7 solution (10 $\mu$ l) was diluted in H<sub>2</sub>O:MeOH 1:1 (5ml)) and analysed by ESI-MS (Waters Synapt G2-Si HDMS-UMONS). The detection of peaks at  $m/z$  887.81,  $m/z$  899.31 and  $m/z$  907.36 corresponds to doubly charged  $\beta$ -CyD-QSY7 with H<sup>+</sup>, Na<sup>+</sup> and K<sup>+</sup> respectively, quality assures the completion of the amino- $\beta$ -CyD-QSY7 receptor. This solution was employed formerly without any further purification, *ensuite*, ruled in action-FRET development. Donor-tagged A $\beta$ <sub>12-28</sub> oligopeptides were produced by mixing equimolar solutions of Rhodamine 575 C<sub>5</sub> maleimide with either N or C terminally cysteinated A $\beta$ <sub>12-28</sub> (CA $\beta$  and A $\beta$ C respectively) at a concentration of 30  $\mu$ M in 1:1 H<sub>2</sub>O:CH<sub>3</sub>CN solution by volume. The scientific manner the laser was used was scan based. Wavelengths from 600 to 465 nm were swept with 0.1 nm steps and a dwell time of 1s. Regarding ion confinement, trapping periods of 100 ms were effectuated and irradiation buffeting was taken by a single laser pulse from the laser resonator. Each point in the action spectrum is indiced in manner to speak to the number of microscans of the LTQ Velos: 9. This could approximately be debated to be near 1 mass spectrum recording per second. To normalize with regards to the laser power, a separate wavelength scan is performed immediately following acquisition of the action spectrum under the same parameters.

## Results and discussion

Electrospray ionization in the positive ion mode of an acceptor-tagged amino- $\beta$ -CyD ( $\text{H}_2\text{O}$ : MeOH; 1:1) solution fulfilled its expectation to give singly charged QSY7-amino- $\beta$ -CyD (QSY7- $\beta$ CyD) cations in high relative abundance in the mass spectrum at  $m/z$  1774. Inspect Figure 4.7.3. below. Prior to analysing the gaseous non-covalent approachement between this macro-cyclic receptor and the amyloid peptide and, in particular gaoling the complex ions to the action-FRET experiments, the pursuit consisted in probing whether the absorption properties of the QSY7 acceptor are uninfluencible by the covalent attachement to amino- $\beta$ -CyD or by the possible interaction of the chromophore with or within the hydrophobic cavity. As a related side shot, it was reported that the grafting of dyes to carbohydrates in a push-pull framework does favour several electronic excitations to take place, in turn considerably modifying the photoabsorption spectra. The action spectrum registered for singly charged QSY7- $\beta$ -CyD is shown in Figure 4.7.2.

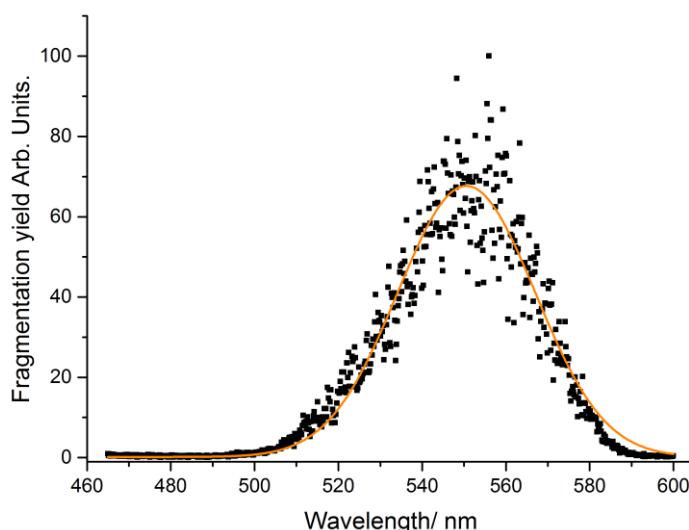


Figure 4.7.2. Action spectrum of mass selected [amino- $\beta$ -CyD-QSY] $^+$ . The fragmentation yield is determined using only the LID specific fragments ( $m/z$  360, 465 and 531) and is calculated as the ratio between the sum of the LID specific fragment intensities and the Total Ion Current – TIC – in the LID spectrum. The graph is fitted.

This spectrum is generated by monitoring the change of the abundances of QSY7-specific photo-fragment ions ( $m/z$  360 +  $m/z$  465 +  $m/z$  531) over their excitation wavelengths. For the singly charged species, the position of the absorption maximum is close to 550nm and the band-shape is very close to that previously recorded for isolated QSY7, which suggests a minimal influence of the amino- $\beta$ -CyD on the optical properties of the chromophore. This points to the fact the absorption properties of the acceptor chromophores are not greatly perturbed either by the covalent attachement to amino- $\beta$ -CyD or by interaction of the chromophore with or within the hydrophobic concavity. The technical object of collision induced dissociation (CID) experiments is held in Figure 4.7.3. (a).

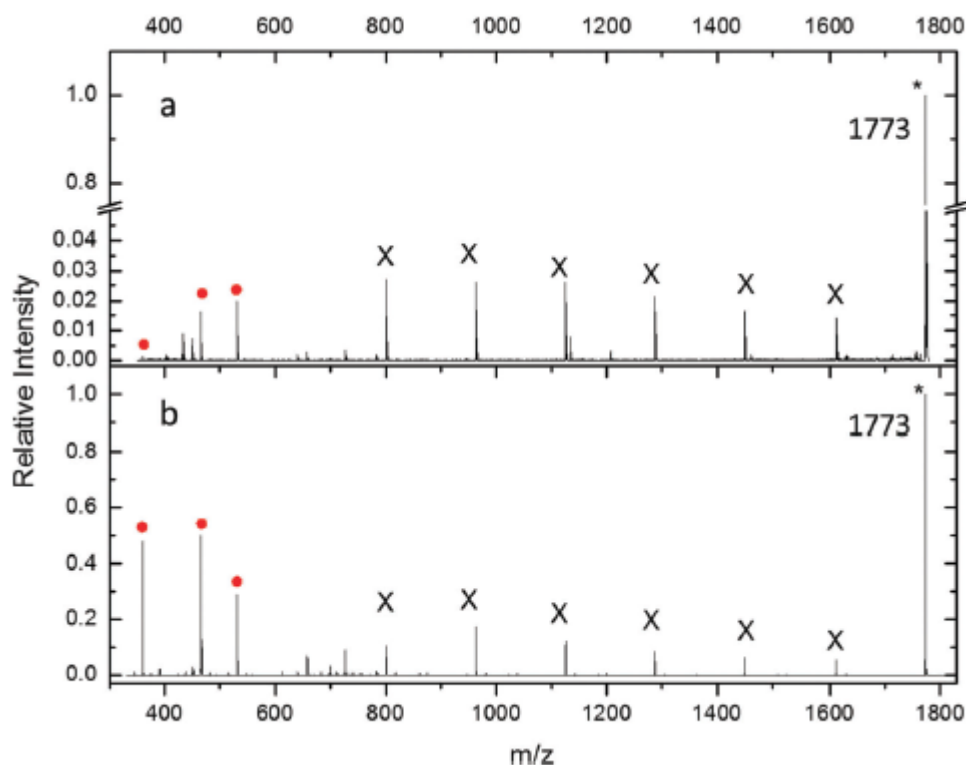


Figure 4.7.3. Gas phase fragmentation mass spectra of singly charged QSY7- $\beta$ -CyD ( $m/z$  1774): (a) CID (Normalized collision energy = 35, 100 ms activation time) and (b) LID at 545nm. (X) Glucopyranoside residues losses, red circles highlight photospecific chromophore fragmentation channels,  $m/z$  531,  $m/z$  465, and  $m/z$  360.

The dominant fragmentation reactions observed are specific to the cyclodextrin ring, *i.e.* dextrose unit losses (162 u) (tagged X in Figure 4.7.3.). Fragments associated with the decomposition of the QSY7 moiety are also noticed, crucially  $m/z$  531,  $m/z$  465, and  $m/z$  360. Focus on the laser induced dissociation (LID) mass spectrum Figure 4.7.3. (b) shows that, whilst the fragmentation pathways that resulted by irradiation at 545nm are appreciably comparable to those observed after CID excitation in Figure 4.7.3. (a), there is an impressive increase in the relative intensities of all the fragments as compared to CID. One could also woefully notice that the dominant fragmentation channels lead to the  $m/z$  360, 465 and 531 ions, and that the dextrose unit losses become lower. The fragmentation channel has reduced in intensity with this regard. This difference in the fragmentation pattern can be associated to slow rate heating in CID or electronic excitation in LID experiments of the parent ions. It is emphasised in this section that the losses of dextrose units are still observed, reflecting that some degree of vibrational energy distribution, formerly referring to (IVR), repercussions into fragmentation in this system. Compared to photofragmentation it is checked as rather meaningless. Having established that amino- $\beta$ -CyD-QSY7 conducts its propriety chemical characteristics suitably it was selected to fit as an acceptor for action-FRET, it thus is possible to vestigate FRET by measuring the relative intensity of these fragments as a function of wavelength for non-covalent interactions relevant to the Rh575-CA $\beta$  and A $\beta$ C-Rh575 donor peptides and the amino- $\beta$ -CyD-QSY7 reactive ensemble. From onset of electrospray of equimolar peptide-cyclodextrin methanolic solutions ( $10^{-5}$  M), binary complexes associating one peptide to one receptor were produced and observed as 3+ and 4+ dotated ions within the mass spectra at respectively  $m/z$  1499.61 (3+) and 1126.44



(4+). This is in agreement with previous ESI mass spectrometry analyses of the interaction between a 40 amino acid  $\beta$ -amyloid peptide ( $\beta$ 1-40) and  $\beta$ -cyclodextrin. The CID mass spectra for both charge states of both peptide-cyclodextrin complexes were recorded and are presented in

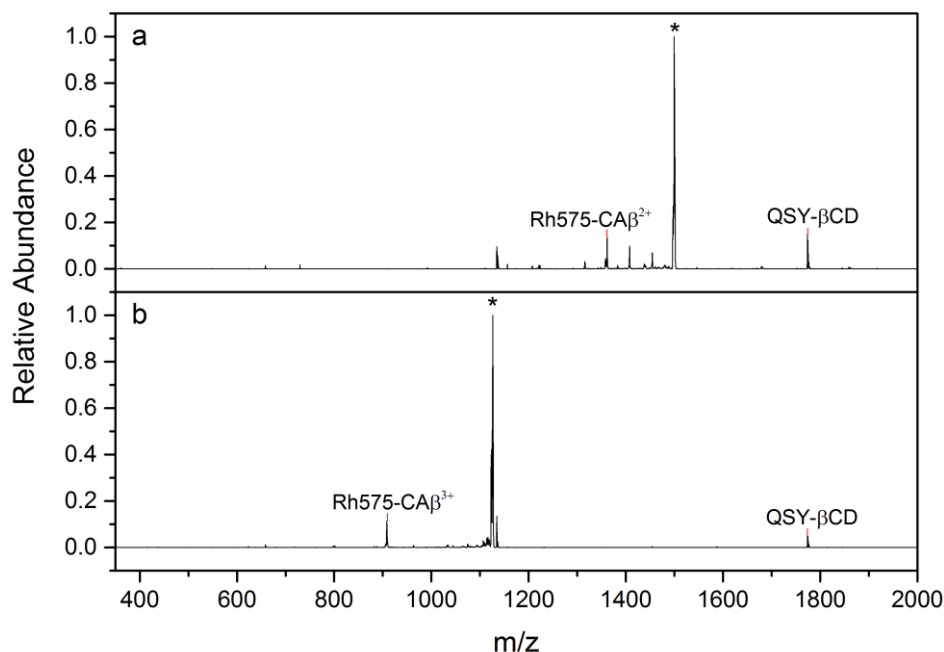


Figure 4.7.4. CID (normalised collision energy set at 15, 10) mass spectra of binary complexes containing Rh-CA $\beta$  and amino- $\beta$ -CD-QSY7 as the guest and the receptor, respectively. (a) [Rh-CA $\beta$ ][QSY- $\beta$ -CyD]<sup>3+</sup> ( $m/z$  1499.61 (\*)) and (b) [Rh-CA $\beta$ ][QSY- $\beta$ -CyD]<sup>4+</sup> ( $m/z$  1126.44(\*)).

The LTQ Velos at this stage was used for collisional activation, the adduct ions mostly dissociate by rupturing the non-covalent interactions leading to singly-charged amino- $\beta$ -CyD-QSY7 ions at  $m/z$  1773.62 and 2+ or 3+ Rh-CA $\beta$  (or A $\beta$ C-Rh) peptides at  $m/z$  1361.69 and 908.10, respectively. The observation is that charge separation processes confirms the non-covalent association between the peptides and the cyclodextrin receptor. From the standpoint of photofragmentation observation; QSY fragments did not register at the applied normalised collisional energy: 15, 10. Commandeering point two: an account has to be given that both chromophores bear a starting point from sparkle onset. It can be concluded that, the CID-generated 2+ and 3+ tagged peptides, the peptide backbones can be considered to be charge levelled up to mono- or either a di-protonated species, respectively. The LID mass spectra (545nm excitation) for both charge states of both peptide-cyclodextrin complexes were also recorded and presented in Figure 4.7.5.

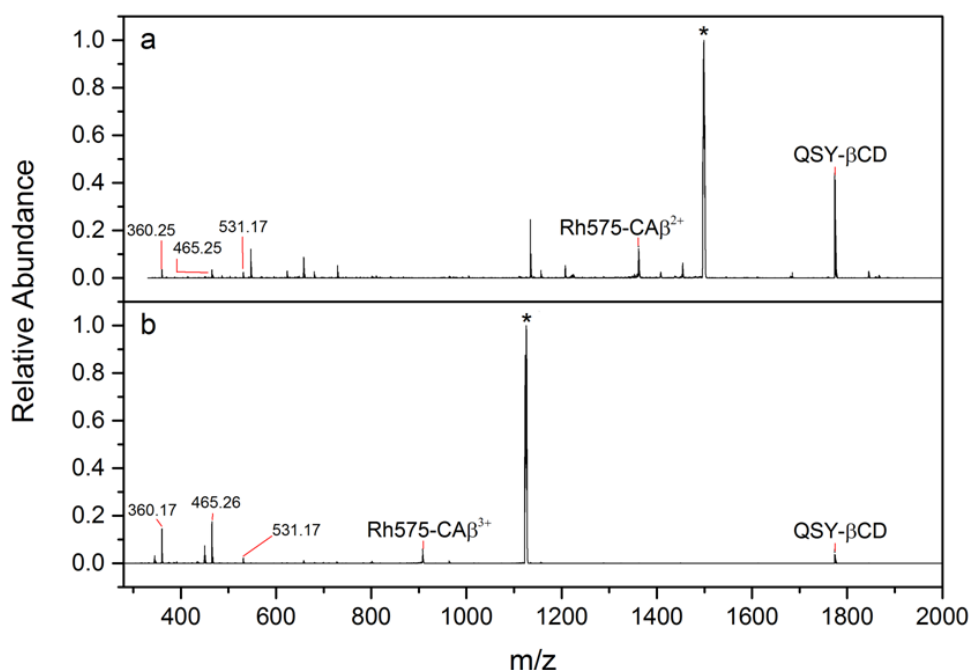


Figure 4.7.5. LID mass spectra (545nm excitation) of binary complexes containing Rh-CA $\beta$  and amino- $\beta$ -CyD-QSY7 as the guest and the receptor, respectively. (a) +3 ( $m/z$  1498.61 (\*)) and (b) +4 ( $m/z$  1126.44(\*)).

Fragment ions observed in LID and CID are different. While major ions in CID spectra correspond to the dissociation of the complex, fragment ions at  $m/z$  360, 465 and 531 are also observed in the spectra of LID, the heterologue. The keypoint on the comparison dividing the LID and CID mass spectra (Figure 4.7.4 and Figure 4.7.5) reveals that only under photo-excitation the complex ion dissociation yields the QSY7 specific (photo) fragment ions at  $m/z$  360, 465 and 531. At this stage it is important to take in that the Rh575-peptide in the gas phase is not prone to any fragmentation by optical excitation at 505nm due to the high fluorescence statistical, see Figure 4.7.6 and Figure 4.7.7.

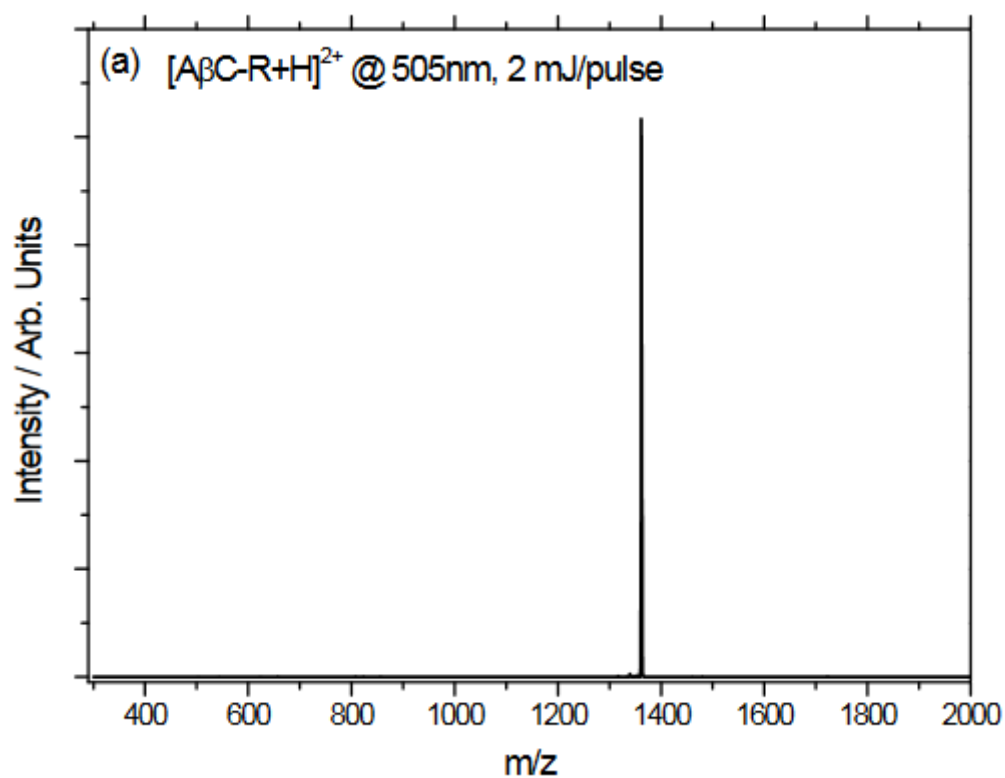


Figure 4.7.6. LID (505nm) of mass selected  $[\text{A}\beta\text{C-Rh575+H}]^{2+}$  ions irradiated with a single laser pulse (2mJ).

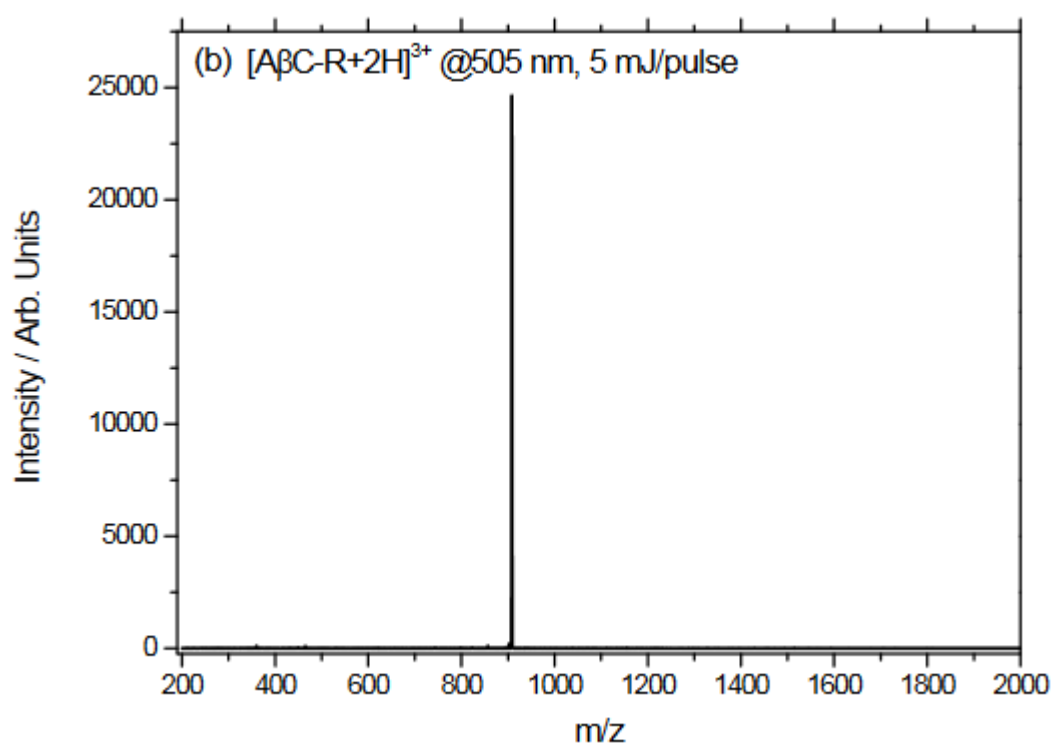


Figure 4.7.7. LID (505nm) mass spectrum of mass selected  $[\text{A}\beta\text{C-Rh575+H}]^{3+}$  ions irradiated with single laser pulse (5mJ).

It then becomes clear to conclude that, when irradiating at Rh575 excitation wavelength (505nm), FRET towards QSY7 leads to the photospecific fragment end products ( $m/z$  360, 465 and 531). Incidentally, the action-spectra for both charge states and both donor tagged peptide-cyclodextrin complexes were set down and are presented in Figure 4.7.8. In this way only the specific photofragmentation of the acceptor chromophore is monitored.

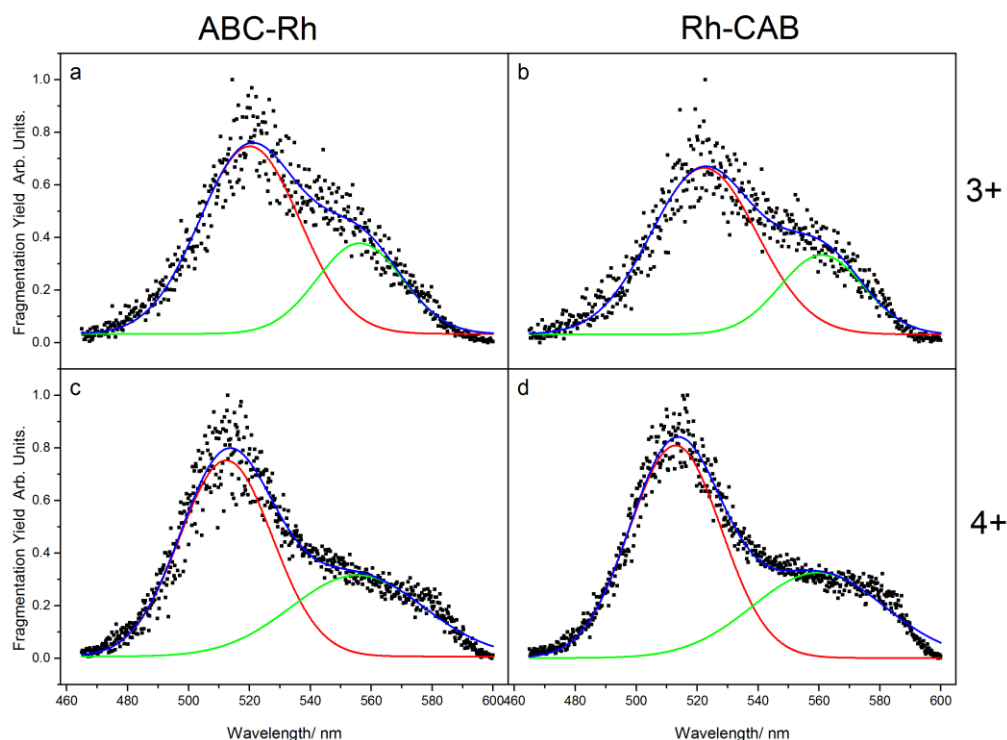


Figure 4.7.8. Action spectra of 3+ (a and b) and 4+ (c and d) binary complexes associating A $\beta$ C-Rh (a and c) Rh-Ca $\beta$  (b and d) and amino- $\beta$ -CyD-QSY7 as the guest and the receptor, respectively. The fragmentation yield is determined using only the LID specific fragments ( $m/z$  360, 465 and 531) and is calculated as the ratio relating the sum of the LID specific fragment intensities and the Total Ion current or TIC in the LID spectrum.

It can be drawn out that both charge states of both peptides, the action spectra are bi-modal. In real terms, the observation of QSY7 specific fragment ions can be made. The band located at 545nm (green fit) ascribes the direct absorption and fragmentation of the QSY7 acceptor. The manifestation of the band centered at 505nm is very well received as this band corresponds to the absorption of the donor chromophore Rh575. In spite of this, before claiming that the observation in our action-spectra of this 505nm band confirms the occurrence of the FRET process exercising over Rh575 and QSY7, it was crucial to first consider the measurements carefully and stay prudent that no other major process can inflict the observation of QSY7 fragmentation. At this stage it was considered if the two processes compete with other relaxation pathways such as fast photofragmentation or internal vibrational redistribution (IVR) that may contribute to the occurrence of QSY7 specific fragment ions. It was realized that the 505nm band is clearly the result of the absorption of the donor chromophore and that IVR is very unlikely to redistribute enough energy from the peptide to the cyclodextrin in enough quantity to induce

the acceptor chromophore to fragment without causing dissociation of the complex. This insight is confirmed by CID spectra, see Figure 4.7.4. Moreover, on inspection of the LID efficiencies (branching ratios) of the direct disassembly of the complex in Figure 4.7.9. and Figure 4.7.10. It can be observed that the dissociation of the complex presents the highest efficiency below 490nm, a region which is related to where an increased internal conversion or multiphoton absorption of Rh575 exists (the acceptor chromophore has no oscillator strength at these wavelengths). This strongly suggests that internal conversion of the donor chromophore leads to direct dissociation of the complex and thus, it is feasible to assign the band at 510nm in Figure 4.7.9 to the FRET between the donor (Rh) and the acceptor (QSY7).

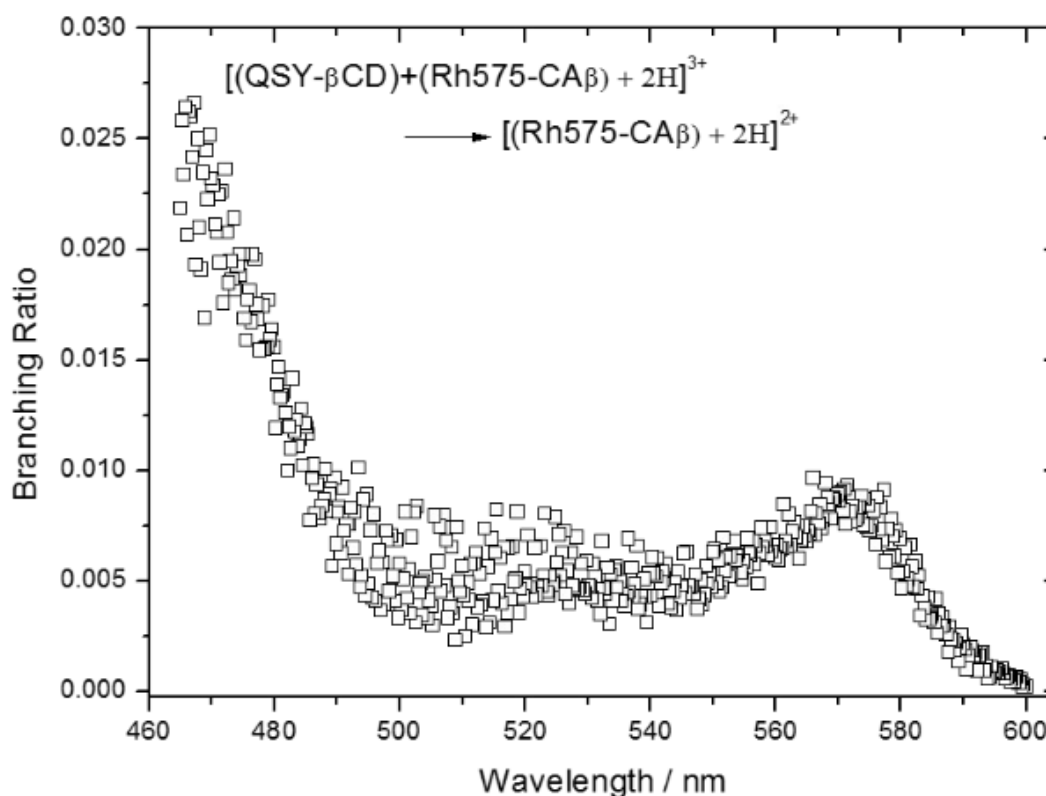


Figure 4.7.9. Branching ratio for the fragmentation  $[(\text{QSY})\text{-}\beta\text{CD})+(\text{Rh575-CA}\beta)+2\text{H}]^{3+} \rightarrow [\text{Rh575-CA}\beta+2\text{H}]^{2+}$ . The branching ratio consists of the ratio between the fragment intensity and the parent intensity in the LID spectrum.

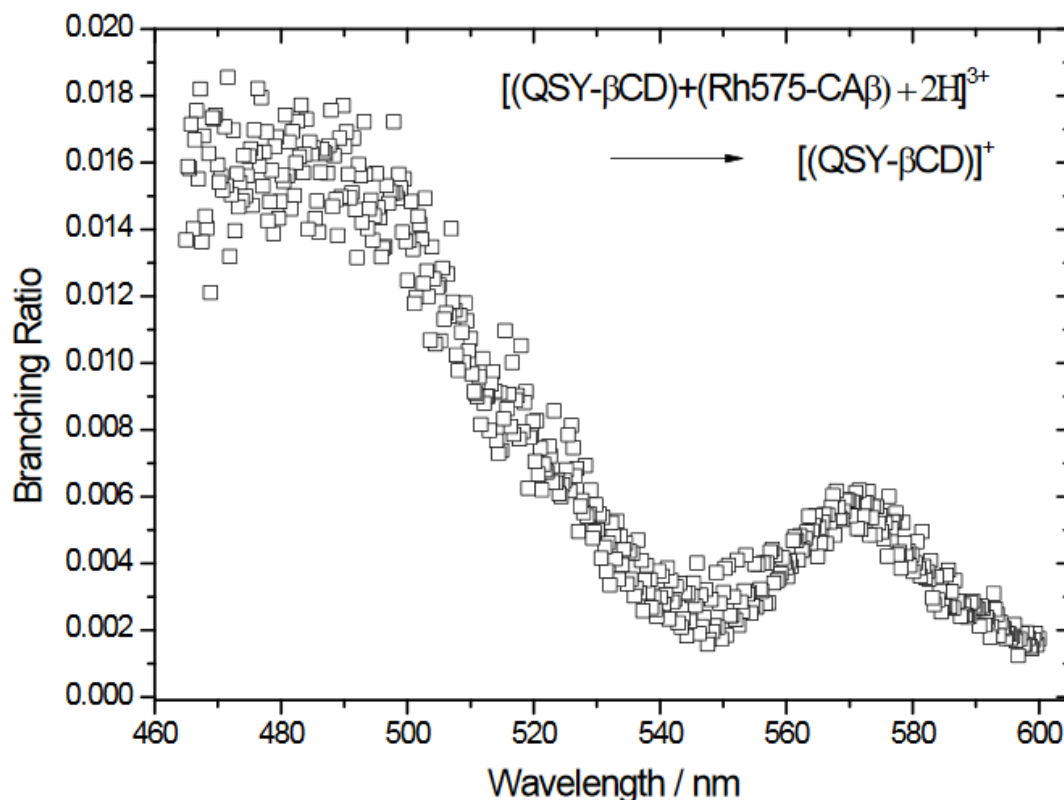


Figure 4.7.10. Branching ratio for the fragmentation  $[(\text{QSY}-\beta\text{CD})+(\text{Rh575}-\text{CA}\beta)+2\text{H}]^{3+} \rightarrow [\text{QSY}-\beta\text{CD}]^+$ . The branching ratio consists of the ratio between the fragment intensity and the parent intensity in the LID spectrum.

From the literature material, particularly on a previous study on the binding of the 12-28 fragment of amyloid beta ( $\text{A}\beta$ ) to cyclodextrin (CD), it was found that the Val18, Phe19 and Phe20 residues are involved in the specific binding within the hydrophobic pocket of the cyclodextrin receptor. That the so called hydrophobic cavity is responsible for the specific binding is consistent with the observation of the inhibition of aggregation by Cyclodextrin, since conformational changes in this hydrophobic region of the peptide are proposed to be at the origin of the fibril formation. This present undertaking must be taken on the perspective that it is a proof of concept report on the applicability of action-FRET for probing the gas phase structure of non-covalent host-guest chemistries. Great many more conclusions are made however from these results. First of all, given for 3+ and 4+ charge species for the binary complexes, it turns out that only one and two protons are embedded along the peptide as both chromophores bear a single positive charge from this it can be anticipated that the peptide adopts a random coil geometry. As it stands, it then comes around that both chromophores coordinate together with a small interdistance separation. This is empirically supported by the significantly large and similar FRET efficiencies produced and observed in Figure 4.7.8. In effect by comparing the intensity ratio between the FRET band (505nm – absorption of the Rh575 donor – red fit) and the acceptor absorbance band (545nm – absorption of the QSY7 acceptor – green fit). The insight that can be gained is that the influence of the different grafting locations (N- vs. C-terminus) is small and this is as expected as there are minimal changes in the relative (absolute) intensities of the two bands. This finding leads to the belief that there is no preferred orientation of the peptide

upon binding to the cyclodextrin, or alternatively, if the interaction is with the central hydrophobic region of the peptide, that the terminal regions of the peptide are unable to unfurl a sufficient distance to reduce the FRET efficiency. Further investigations are necessary such as ion mobility experiments and theoretical treatment. All in all, the emerging picture is that action-FRET experiments provide a valuable addition to the techniques and “tools” made available for studying non-covalent complexes in gas confinement.

## Summary

This application of action-FRET to  $\beta$ -cyclodextrin inclusion complexes has shown that measurements on non-covalent complexes with one side chromophore tagged amino- $\beta$ -cyclodextrin and the other tagged amyloid-beta fragment peptides can reveal valuable insights on their conformation and molecular complex assembly. The key elements are that with a rhodamine 575 donor and a QSY7 FRET acceptor: respectively covalently attached to the guest peptide ( $A\beta_{12-28}$ ) (the donor) and secondly the macrocyclic host (amino- $\beta$ -cyclodextrin) (the acceptor). On collision-induced dissociations (CID), the complex ions mainly dissociate by loosing off from their weak non-covalent interactions. Interestingly, upon laser-induced dissociation (LID) at the donor wavelength (505 nm), specific photofragments of the QSY7 acceptor are detected validating the occurrence of the FRET regime related to the donor and the acceptor. They are understood to be close to each other in the complex ions architecture. Such an experiment opens future prospective avenues of research not only for studying interactions between peptides and synthetic receptors, but also interactions between proteins and chaperones. In a broader scope, this technique could one day also offer benefits in probing non-biological partners involved in any field of supramolecular chemistry, provided the action-FRET reported chromophores can be chemically appended onto the relevant supramolecular edifices.

## 4.8 References :

1. Clegg RM: *The history of FRET*. Springer; 2006.
2. Wu PG, Brand L: **Resonance energy-transfer - methods and applications**. *Analytical Biochemistry* 1994, **218**:1-13.
3. Medintz I, Hildebrandt N: *FRET - Foster resonance energy transfer: From theory to applications*; 2013.
4. Forster T: **Energiewanderung und fluoreszenz**. *Naturwissenschaften* 1946, **33**:166-175.
5. Hotzer B, Medintz IL, Hildebrandt N: **Fluorescence in Nanobiotechnology: Sophisticated Fluorophores for Novel Applications**. *Small* 2012, **8**:2297-2326.
6. Dashtiev M, Azov V, Frankevich V, Scharfenberg L, Zenobi R: **Clear evidence of fluorescence resonance energy transfer in gas-phase ions**. *Journal of the American Society for Mass Spectrometry* 2005, **16**:1481-1487.
7. Wagner BD: **Fluorescence studies of supramolecular host-guest inclusion complexes**. In *Handbook of photochemistry and photobiology. Volume 3*. Edited by Nalwa HS: American scientific publishers.; 2003
8. Turconi S, Bingham RP, Haupts U, Pope AJ: **Developments in fluorescence lifetime-based analysis for ultra-HTS**. *Drug Discovery Today* 2001, **6**:S27-S39.
9. Lazarides T, Sykes D, Faulkner S, Barbieri A, Ward MD: **On the Mechanism of d-f Energy Transfer in Ru-II/Ln(III) and Os-II/Ln(III) Dyads: Dexter-Type Energy Transfer Over a Distance of 20 angstrom**. *Chemistry-a European Journal* 2008, **14**:9389-9399.
10. Anon.: *The molecular probes handbook. A guide to fluorescent probes and labeling technologies*. 11th edn; 2010.
11. Faure S, Stern C, Guillard R, Harvey PD: **Role of the spacer in the singlet-singlet energy transfer mechanism (Forster vs Dexter) in cofacial bisporphyrins**. *Journal of the American Chemical Society* 2004, **126**:1253-1261.
12. Dexter DL: **A theory of sensitized luminescence in solids**. *Journal of Chemical Physics* 1953, **21**:836-850.
13. Agarwal GS, Patnaik AK: **Vacuum-induced coherences in radiatively coupled multilevel systems**. *Physical Review A* 2001, **63**:8.
14. Minkov M, Savona V: **Radiative coupling of quantum dots in photonic crystal structures**. *Physical Review B* 2013, **87**:16.
15. Kinoshita T, Ishihara H: **Radiative coupling of A and B excitons in ZnO**. *Physical Review B* 2016, **94**:9.
16. D'Agostino S, Della Sala F, Andreani LC: **Radiative coupling of high-order plasmonic modes with far-field**. *Photonics and Nanostructures-Fundamentals and Applications* 2013, **11**:335-344.
17. Ammerlahn D, Kuhl J, Grote B, Koch SW, Khitrova G, Gibbs H, Hey R, Ploog KH: **Radiative coupling in single quantum wells and Bragg structures**. *Physica Status Solidi B-Basic Research* 2000, **221**:101-106.
18. Taniguchi K, Mardh S: **Reversible changes in the fluorescence energy-transfer accompanying formation of reaction intermediates in probe-labeled (Na<sup>+</sup>,K<sup>+</sup>)-ATPASE**. *Journal of Biological Chemistry* 1993, **268**:15588-15594.
19. Mellet P, Boudier C, Mely Y, Bieth JG: **Stopped flow fluorescence energy transfer measurement of the rate constants describing the reversible formation and the irreversible rearrangement of the elastase-alpha(1)-proteinase inhibitor complex**. *Journal of Biological Chemistry* 1998, **273**:9119-9123.
20. Jonsson T, Waldburger CD, Sauer RT: **Nonlinear free energy relationships in arc repressor unfolding imply the existence of unstable, native-like folding intermediates**. *Biochemistry* 1996, **35**:4795-4802.
21. Luo Y, Wu JL, Gergely J, Tao T: **Localization of Cys(133) of rabbit skeletal troponin-I with respect to troponin-C by resonance energy transfer**. *Biophysical Journal* 1998, **74**:3111-3119.
22. Erickson JW, Mittal R, Cerione RA: **Use of resonance energy -transfer to determine the proximity of the guanine-nucleotide-binding site of transducin relative to a conformationally-sensitive site on the gamma-subunit of the cyclic-gmp phosphodiesterase**. *Biochemistry* 1995, **34**:8693-8700.
23. Xing J, Cheung HC: **Internal movement in myosin subfragment -1 detected by fluorescence resonance energy-transfer**. *Biochemistry* 1995, **34**:6475-6487.
24. Moens PDJ, Yee DJ, Dosremedios CG: **Determination of the radial coordinate of Cys-374 in F-Actin using fluorescence resonance energy-transfer spectroscopy - effect of phalloidin on polymer assembly**. *Biochemistry* 1994, **33**:13102-13108.
25. Carraway KL, Koland JG, Cerione RA: **Visualisation of epidermal growth-factor (EGF) receptor aggregation in plasma-membranes by fluorescence resonance energy-transfer - correlation of receptor activation with aggregation**. *Journal of Biological Chemistry* 1989, **264**:8699-8707.



26. Matyus L: **Fluorescence resonance energy-transfer measurements on cell-surfaces - a spectroscopic tool for determining protein interactions.** *Journal of Photochemistry and Photobiology B-Biology* 1992, **12**:323-337.
27. Gagne A, Banks P, Hurt SD: **Use of fluorescence polarization detection for the measurement of FluoPeptide (TM) binding to G protein-coupled receptors.** *Journal of Receptor and Signal Transduction Research* 2002, **22**:333-343.
28. Berger W, Prinz H, Striessnig J, Kang HC, Haugland R, Glossmann H: **Complex molecular mechanism for dihydropyridine binding to L-Type CA2+-channels as revealed by fluorescence resonance energy-transfer.** *Biochemistry* 1994, **33**:11875-11883.
29. Kubitscheck U, Kircheis M, Schweitzerstenner R, Dreybrodt W, Jovin TM, Pecht I: **Fluorescence resonance energy-transfer on single living cells - application to binding of monovalent haptens to cell-bound immunoglobulin-E.** *Biophysical Journal* 1991, **60**:307-318.
30. Johnson DA, Voet JG, Taylor P: **Fluorescence energy - transfer between cobra alpha - toxin molecules bound to the acetylcholine -receptor.** *Journal of Biological Chemistry* 1984, **259**:5717-5725.
31. Khanna PL, Ullman EF: **4',5'-Dimethoxy-6-Carboxyfluorescein - a novel dipole-dipole coupled fluorescence energy-transfer acceptor useful for fluorescence immunoassays.** *Analytical Biochemistry* 1980, **108**:156-161.
32. Morrison LE: **Time-resolved detection of energy-transfer - theory and application to immunoassays.** *Analytical Biochemistry* 1988, **174**:101-120.
33. Ha T, Enderle T, Ogletree DF, Chemla DS, Selvin PR, Weiss S: **Probing the interaction between two single molecules: Fluorescence resonance energy transfer between a single donor and a single acceptor.** *Proceedings of the National Academy of Sciences of the United States of America* 1996, **93**:6264-6268.
34. Mergny JL, Botorine AS, Garestier T, Belloc F, Rougee M, Bulychev NV, Koshkin AA, Bourson J, Lebedev AV, Valeur B, et al: **Fluorescence energy-transfer as a probe for nucleic-acid structures and sequences.** *Nucleic Acids Research* 1994, **22**:920-928.
35. Clegg RM, Murchie AIH, Lilley DMJ: **The solution structure of the 4-way DNA junction at low-salt conditions - a fluorescence resonance energy-transfer analysis.** *Biophysical Journal* 1994, **66**:99-109.
36. Hiyoshi M, Hosoi S: **Assay of DNA denaturation by polymerase chain reaction-driven fluorescent label incorporation and fluorescence resonance energy-transfer.** *Analytical Biochemistry* 1994, **221**:306-311.
37. Toth K, Sauermann V, Langowski J: **DNA curvature in solution measured by fluorescence resonance energy transfer.** *Biochemistry* 1998, **37**:8173-8179.
38. Furey WS, Joyce CM, Osborne MA, Klenerman D, Peliska JA, Balasubramanian S: **Use of fluorescence resonance energy transfer to investigate the conformation of DNA substrates bound to the Klenow fragment.** *Biochemistry* 1998, **37**:2979-2990.
39. Whitcombe D, Theaker J, Guy SP, Brown T, Little S: **Detection of PCR products using self-probing amplicons and fluorescence.** *Nature Biotechnology* 1999, **17**:804-807.
40. Thelwell N, Millington S, Solinas A, Booth J, Brown T: **Mode of action and application of Scorpion primers to mutation detection.** *Nucleic Acids Research* 2000, **28**:3752-3761.
41. Lee LG, Livak KJ, Mullah B, Graham RJ, Vinayak RS, Woudenberg TM: **Seven-color, homogeneous detection of six PCR products.** *Biotechniques* 1999, **27**:342-349.
42. Heid CA, Stevens J, Livak KJ, Williams PM: **Real time quantitative PCR.** *Genome Research* 1996, **6**:986-994.
43. Nazarenko IA, Bhatnagar SK, Hohman RJ: **A closed tube format for amplification and detection of DNA based on energy transfer.** *Nucleic Acids Research* 1997, **25**:2516-2521.
44. Tyagi S, Bratu DP, Kramer FR: **Multicolor molecular beacons for allele discrimination.** *Nature Biotechnology* 1998, **16**:49-53.
45. Myakishev MV, Khripin Y, Hu S, Hamer DH: **High-throughput SNP genotyping by allele-specific PCR with universal energy-transfer-labeled primers.** *Genome Research* 2001, **11**:163-169.
46. Parkhurst KM, Parkhurst LJ: **Kinetic-studies by fluorescence resonance energy-transfer employing a double-labeled oligonucleotide - hybridization to the oligonucleotide complement and to single-stranded-DNA.** *Biochemistry* 1995, **34**:285-292.
47. Sixou S, Szoka FC, Green GA, Giusti B, Zon G, Chin DJ: **Intracellular oligonucleotide hybridisation detected by fluorescence resonance energy-transfer (FRET).** *Nucleic Acids Research* 1994, **22**:662-668.
48. Chen XN, Zehnbauser B, Gnirke A, Kwok PY: **Fluorescence energy transfer detection as a homogeneous DNA diagnostic method.** *Proceedings of the National Academy of Sciences of the United States of America* 1997, **94**:10756-10761.

49. Hung SC, Mathies RA, Glazer AN: **Optimization of spectroscopic and electrophoretic properties of energy transfer primers.** *Analytical Biochemistry* 1997, **252**:78-88.
50. Woolley AT, Mathies RA: **Ultra-high-speed DNA-sequencing using capillary electrophoresis chips.** *Analytical Chemistry* 1995, **67**:3676-3680.
51. Ju JY, Ruan CC, Fuller CW, Glazer AN, Mathies RA: **Fluorescence energy-transfer dye-labeled primers for DNA-sequencing and analysis.** *Proceedings of the National Academy of Sciences of the United States of America* 1995, **92**:4347-4351.
52. Gutierrezmerino C, Deromanelli ICB, Pietrasanta LI, Barrantes FJ: **Preferential distribution of the fluorescent phospholipid probes NBD-phosphatidylcholine and rhodamine-phosphatidylethanolamine in the exofacial leaflet of acetylcholine receptor-rich membranes from *torpedo-marmorata*.** *Biochemistry* 1995, **34**:4846-4855.
53. Wolf DE, Winiski AP, Ting AE, Bocian KM, Pagano RE: **Determination of the transbilayer distribution of fluorescent lipid analogs by nonradiative fluorescence resonance energy-transfer.** *Biochemistry* 1992, **31**:2865-2873.
54. Nichols JW, Pagano RE: **Resonance energy-transfer assay of protein-mediated lipid transfer between vesicles.** *Journal of Biological Chemistry* 1983, **258**:5368-5371.
55. Pecheur EI, Martin I, Ruysschaert JM, Bienvenue A, Hoekstra D: **Membrane fusion induced by 11-mer anionic and cationic peptides: A structure-function study.** *Biochemistry* 1998, **37**:2361-2371.
56. Partearroyo MA, Cabezon E, Nieva JL, Alonso A, Goni FM: **Real-time measurements of chemically-induced membrane-fusion in cell monolayers, using a resonance energy-transfer method.** *Biochimica Et Biophysica Acta-Biomembranes* 1994, **1189**:175-180.
57. Struck DK, Hoekstra D, Pagano RE: **Use of resonance energy-transfer to monitor membrane-fusion.** *Biochemistry* 1981, **20**:4093-4099.
58. Gonzalez JE, Tsien RY: **Voltage sensing by fluorescence resonance energy-transfer in single cells.** *Biophysical Journal* 1995, **69**:1272-1280.
59. Gulnik SV, Suvorov LI, Majer P, Collins J, Kane BP, Johnson DG, Erickson JW: **Design of sensitive fluorogenic substrates for human cathepsin D.** *Febs Letters* 1997, **413**:379-384.
60. Kurth T, Grahn S, Thormann M, Ullmann D, Hofmann HJ, Jakubke HD, Hedstrom L: **Engineering the S1 ' subsite of trypsin: Design of a protease which cleaves between dibasic residues.** *Biochemistry* 1998, **37**:11434-11440.
61. Geoghegan KF, Emery MJ, Martin WH, McColl AS, Daumy GO: **Site-directed double fluorescent tagging of human renin and collagenase (MMP-1) substrate peptides using the periodate-oxidation of N-terminal serine - an apparently general strategy for provision of energy-transfer substrate for proteases.** *Bioconjugate Chemistry* 1993, **4**:537-544.
62. Matayoshi ED, Wang GT, Krafft GA, Erickson J: **Novel fluorogenic substrates for assaying retroviral proteases by resonance energy-transfer.** *Science* 1990, **247**:954-958.
63. Adams SR, Harootunian AT, Buechler YJ, Taylor SS, Tsien RY: **Fluorescence ratio imaging of cyclic-amp in single cells.** *Nature* 1991, **349**:694-697.
64. Godwin HA, Berg JM: **A fluorescent zinc probe based on metal-induced peptide folding.** *Journal of the American Chemical Society* 1996, **118**:6514-6515.
65. Benesch JLP, Robinson CV: **Biological chemistry dehydrated but unharmed.** *Nature* 2009, **462**:576-577.
66. Markides K: **Advanced information on the Nobel prize in chemistry 2002.** (Gräslund A ed.: Kungl.Vetenskapsakademien.The royal swedish academy of sciences.; 2002.
67. Wallace MI, Ying LM, Balasubramanian S, Klennerman D: **FRET fluctuation spectroscopy: Exploring the conformational dynamics of a DNA hairpin loop.** *Journal of Physical Chemistry B* 2000, **104**:11551-11555.
68. Bonnet G, Krichinsky O, Libchaber A: **Kinetics of conformational fluctuations in DNA hairpin-loops.** *Proceedings of the National Academy of Sciences of the United States of America* 1998, **95**:8602-8606.
69. Qiu LL, Pabit SA, Roitberg AE, Hagen SJ: **Smaller and faster: The 20-residue Trp-cage protein folds in 4  $\mu$  s.** *Journal of the American Chemical Society* 2002, **124**:12952-12953.
70. Snow CD, Zagrovic B, Pande VS: **The Trp cage: Folding kinetics and unfolded state topology via molecular dynamics simulations.** *Journal of the American Chemical Society* 2002, **124**:14548-14549.
71. Marqusee S, Robbins VH, Baldwin RL: **Unusually stable helix formation in short alanine-based peptides.** *Proceedings of the National Academy of Sciences of the United States of America* 1989, **86**:5286-5290.
72. Daly S, Poussigue F, Simon AL, MacAleese L, Bertorelle F, Chirot F, Antoine R, Dugourd P: **Action-FRET: Probing the Molecular Conformation of Mass-Selected Gas-Phase Peptides with Forster Resonance**

- Energy Transfer Detected by Acceptor-Specific Fragmentation.** *Analytical Chemistry* 2014, **86**:8798-8804.
73. Hendricks NG, Lareau NM, Stow SM, McLean JA, Julian RR: **Bond-Specific Dissociation Following Excitation Energy Transfer for Distance Constraint Determination in the Gas Phase.** *Journal of the American Chemical Society* 2014, **136**:13363-13370.
  74. Hendricks NG, Julian RR: **Two-step energy transfer enables use of phenylalanine in action-EET for distance constraint determination in gaseous biomolecules.** *Chemical Communications* 2015, **51**:12720-12723.
  75. Talbot FO, Rullo A, Yao H, Jockusch RA: **Fluorescence Resonance Energy Transfer in gaseous, mass-selected polyproline peptides.** *Journal of the American Chemical Society* 2010, **132**:16156-16164.
  76. Czar MF, Zosel F, Koenig I, Nettels D, Wunderlich B, Schuler B, Zarrine-Afsar A, Jockusch RA: **Gas-Phase FRET Efficiency Measurements To Probe the Conformation of Mass-Selected Proteins.** *Analytical Chemistry* 2015, **87**:7559-7565.
  77. Zenobi R: **Coming of Age: Gas-Phase Structural Information on Biomolecules by FRET.** *Analytical Chemistry* 2015, **87**:7497-7498.
  78. Danell AS, Parks JH: **FRET measurements of trapped oligonucleotide duplexes.** *International Journal of Mass Spectrometry* 2003, **229**:35-45.
  79. Hendricks NG, Julian RR: **Leveraging ultraviolet photodissociation and spectroscopy to investigate peptide and protein three-dimensional structure with mass spectrometry.** *Analyst* 2016, **141**:4534-4540.
  80. Baer T, Dunbar RC: **Ion Spectroscopy: Where Did It Come From; Where Is It Now; and Where Is It Going?** *Journal of the American Society for Mass Spectrometry* 2010, **21**:681-693.
  81. Wu GH, Norris C, Stewart H, Cox H, Stace AJ: **State-resolved UV photofragmentation spectrum of the metal dication complex Zn(pyridine)(4) (2+).** *Chemical Communications* 2008:4153-4155.
  82. Wellman SMJ, Jockusch RA: **Moving in on the Action: An Experimental Comparison of Fluorescence Excitation and Photodissociation Action Spectroscopy.** *Journal of Physical Chemistry A* 2015, **119**:6333-6338.
  83. Sagoo SK, Jockusch RA: **The fluorescence properties of cationic rhodamine B in the gas phase.** *Journal of Photochemistry and Photobiology a-Chemistry* 2011, **220**:173-178.
  84. Daly S, Knight G, Halim MA, Kulesza A, Choi CM, Chirot F, MacAleese L, Antoine R, Dugourd P: **Action-FRET of a Gaseous Protein.** *Journal of the American Society for Mass Spectrometry* 2017, **28**:38-49.
  85. Kelly JW: **The alternative conformations of amyloidogenic proteins and their multi-step assembly pathways.** *Current Opinion in Structural Biology* 1998, **8**:101-106.
  86. Giacobini E, Gold G: **Alzheimer disease therapy-moving from amyloid-beta to tau.** *Nature Reviews Neurology* 2013, **9**:677-686.
  87. Woods LA, Radford SE, Ashcroft AE: **Advances in ion mobility spectrometry-mass spectrometry reveal key insights into amyloid assembly.** *Biochimica Et Biophysica Acta-Proteins and Proteomics* 2013, **1834**:1257-1268.
  88. Hayne DJ, Lim S, Donnelly PS: **Metal complexes designed to bind to amyloid-beta for the diagnosis and treatment of Alzheimer's disease.** *Chemical Society reviews* 2014, **43**:6701-6715.
  89. Abbasowa L, Heegaard NHH: **A systematic review of amyloid-beta peptides as putative mediators of the association between affective disorders and Alzheimer's disease.** *Journal of Affective Disorders* 2014, **168**:167-183.
  90. Bernstein SL, Dupuis NF, Lazo ND, Wytenbach T, Condron MM, Bitan G, Teplow DB, Shea JE, Ruotolo BT, Robinson CV, Bowers MT: **Amyloid-beta protein oligomerization and the importance of tetramers and dodecamers in the aetiology of Alzheimer's disease.** *Nature Chemistry* 2009, **1**:326-331.
  91. Wytenbach T, Bowers MT: **Intermolecular interactions in biomolecular systems examined by mass spectrometry.** In *Annual Review of Physical Chemistry. Volume 58*. Palo Alto: Annual Reviews; 2007: 511-533: *Annual Review of Physical Chemistry*.
  92. Zganec M, Zerovnik E: **Amyloid fibrils compared to peptide nanotubes.** *Biochimica Et Biophysica Acta-General Subjects* 2014, **1840**:2944-2952.
  93. Quinn SD, Dalgarno PA, Cameron RT, Hedley GJ, Hacker C, Lucocq JM, Baillie GS, Samuel IDW, Penedo JC: **Real-time probing of beta-amyloid self-assembly and inhibition using fluorescence self-quenching between neighbouring dyes.** *Molecular Biosystems* 2014, **10**:34-44.
  94. Rochet JC, Lansbury PT: **Amyloid fibrillogenesis: themes and variations.** *Current Opinion in Structural Biology* 2000, **10**:60-68.
  95. Grasso G: **The use of mass spectrometry to study amyloid-beta peptides.** *Mass Spectrometry Reviews* 2011, **30**:347-365.

96. Giry M, Gorbenko G, Trusova V, Adachi E, Mizuguchi C, Nagao K, Kawashima H, Akaji K, Lund-Katz S, Phillips MC, Saito H: **Interaction of Thioflavin T with amyloid fibrils of apolipoprotein A-I N-terminal fragment: Resonance energy transfer study.** *Journal of Structural Biology* 2014, **185**:116-124.
97. Nagaveni V, Lakshmi VVS, Prabhakar S: **Sulforaphane interaction with amyloid beta 1-40 peptide studied by electrospray ionization mass spectrometry.** *Rapid Communications in Mass Spectrometry* 2014, **28**:2171-2180.
98. Daly S, Kulesza A, Poussigue F, Simon AL, Choi CM, Knight G, Chirot F, MacAleese L, Antoine R, Dugourd P: **Conformational changes in amyloid-beta (12-28) alloforms studied using action-FRET, IMS and molecular dynamics simulations.** *Chemical Science* 2015, **6**:5040-5047.
99. Jani V, Sonavane UB, Joshi R: **REMD and umbrella sampling simulations to probe the energy barrier of the folding pathways of engrailed homeodomain.** *Journal of Molecular Modeling* 2014, **20**:14.
100. Calvo F, Chirot F, Albrieux F, Lemoine J, Tsybin YO, Pernot P, Dugourd P: **Statistical Analysis of Ion Mobility Spectrometry. II. Adaptively Biased Methods and Shape Correlations.** *Journal of the American Society for Mass Spectrometry* 2012, **23**:1279-1288.
101. Yu TQ, Lu JF, Abrams CF, Vanden-Eijnden E: **Multiscale implementation of infinite-swap replica exchange molecular dynamics.** *Proceedings of the National Academy of Sciences of the United States of America* 2016, **113**:11744-11749.
102. Sugita Y, Okamoto Y: **Replica-exchange molecular dynamics method for protein folding.** *Chemical Physics Letters* 1999, **314**:141-151.
103. Daly S, Kulesza A, Poussigue F, Simon AL, Choi CM, Knight G, Chirot F, MacAleese L, Antoine R, Dugourd P: **Conformational changes in amyloid-beta (12-28) alloforms studied using action-FRET, IMS and molecular dynamics simulations (vol 6, pg 5040, 2015).** *Chemical Science* 2016, **7**:1609-1610.
104. Le TN, Pouilly JC, Lecomte F, Nieuwjaer N, Manil B, Desfrancois C, Chirot F, Lemoine J, Dugourd P, van der Rest G, Gregoire G: **Gas-Phase Structure of Amyloid-beta (12-28) Peptide Investigated by Infrared Spectroscopy, Electron Capture Dissociation and Ion Mobility Mass Spectrometry.** *Journal of the American Society for Mass Spectrometry* 2013, **24**:1937-1949.
105. Holtje H.D. SW, Rognan D., Folkers G.: *Molecular Modeling. Basic principles and applications.* 3<sup>rd</sup>. edn: Wiley-VCH.; 2007.
106. Bleiholder C, Dupuis NF, Wyttenbach T, Bowers MT: **Ion mobility-mass spectrometry reveals a conformational conversion from random assembly to b-sheet in amyloid fibril formation.** *Abstracts of Papers of the American Chemical Society* 2011, **242**:1.
107. Duez Q, Knight G, Daly S, De Winter J, Halin E, MacAleese L, Antoine R, Gerbaux P, Dugourd P: **Action-FRET of beta-cyclodextrin inclusion complexes.** *New Journal of Chemistry* 2017, **41**:1806-1812.



## Chapter 5 Ubiquitin.

With the purpose of answering biological questions, a protein of long standing interest was taken to elaborate an action-FRET experiment in the laboratory. The context of the study was to make a quantitative study on a synthetically modified ubiquitin protein through derivatisation with donor-acceptor chromophores, such as to work out the proximity relationships held by the different structural states of the protein in gas isolation. An elucidation of the FRET efficiencies even if only partial, provided a real asset in developing an idea of the global structural motif of the framework. This study provides the basis for a better understanding of the roles of solvent composition and protein conformation and looks to demonstrate the viability of the new physical method to probe gas-phase three-dimensional protein structure.

### 5.1 Ubiquitin's identity

Traditionally Ubiquitin designates a 76 long amino acid [1] globular protein (Figure 5.1.1), *stricto sensu*, it is the prototype of a family of proteins that differ discretely in peptide sequence but maintain a similar structure, the ubiquitin fold among others. It is specifically found only in eukaryotes and is absent in the biochemistry of prokaryotes [2]. There has been a deliberate interest in the biochemistry of this protein that has owed its popularity within the scientific community. In this way, there has been a general agreement that ubiquitin plays a host of important roles in protein degradation and thus the control of a myriad of processes including cell-cycle progression, signal transduction, transcriptional regulation, receptor down-regulation, and endocytosis [1]. Just as our understanding of ubiquitin and its key implication in the immune response, development and cell death has progressed so has our knowledge of pathologies such as malignant transformation [1].

Ubiquitin Homo Sapiens — an amino acid sequence:

MQIFVKTLTGKTITLEVEPSDTIENVKAKIQDKEGIPPDQQRLIFAGKQLEDGRTLSDYNIQKESTLHLVLRLLGG

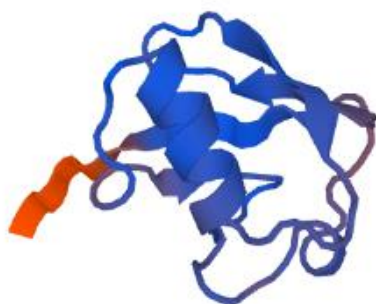


Figure 5.1.1. Seventy-six residue long ubiquitin (X-ray, 1.5Å, monomer state) adapted from ExPasy, the SIB Bioinformatics Resource Portal.

### 5.1.1 Function and mechanism

Briefly, the biochemical pathway of ubiquitin system, ubiquitin-mediated degradation, consists of various steps and intervention of associated molecular species and subunits. Their concerted participation ultimately leads to targeted ubiquitin-protein covalent ligation typically through the amino functionality of the target peptide and the modified terminal glycine of ubiquitin. More specifically, there are three types of common enzymes that partake in the selective covalent attachment of ubiquitin to the cellular protein [1]. They are categorized as E1, E2 and E3. E1s are activating enzymes allowing for the C-terminal Gly residue to activate and react to give a ubiquitin adenylate releasing  $\text{PP}_i$  thereby conjugating to a Cys residue of the E1 enzyme and forming a thiolester [1, 2]. Next the dedicated E2 enzyme to the newly formed Ubl-E1 substrate is recruited and the Ubl protein is transferred from the E1 cysteine residue to the E2 cysteine residue ('Ubl' refers to a ubiquitin-like modifier protein [2]). In doing so dictating a first echelon of biological course the given Ubl protein will take and target. This is a regulation tagging step, modulating the target protein selection [1]. For this reason, E2 enzymes are catalogued as carrier proteins. Finally depending on the intrinsic activity of the E2 enzyme and the anchored Ubl, a ubiquitin protein ligase, an E3, is anchored. E3s come in multiple families or E3 multiprotein complexes, they are uniquely different and range from several hundred to well over a thousand [1].

They evidently play a catalytic role in the enzymatic cascade reaction but are responsible for the final selectivity of the ubiquitin-protein ligation through exquisite cryptic recognition signals. Ubiquitin-mediated degradation terminates by digestion of the ubiquitin-protein conjugate ensemble by characteristic 20S and 26S proteasome complexes giving back the free ubiquitin and degraded peptides and amino acid blocks [1].

## 5.2 Ubiquitin in the gas phase

Ubiquitin's solvent free isolation, fold, and fragmentation has been investigated with an aim in shedding light onto any differences between protein unfolding in the gas phase and solution phase [3]. Studies have proceeded in taking a prepared solution of ubiquitin with the goal of preserving its native or at least a native-like conformation in the gas phase of the MS. Breuker *et al.* made up a solution of 2  $\mu\text{M}$  of ubiquitin in 79:20:1  $\text{H}_2\text{O}/\text{MeOH}/\text{AcOH}$  at pH 3, to which the author argues the protein holds its native form [4]. They especially inspect the 7+ ion of ubiquitin as the literature ascribes this as the most native ion of ubiquitin for the longest time scale. The take home message is that the Ubiquitin 7+ through Breuker's method of choice, electron capture dissociation (ECD), invariably unfolds as the analysis progresses. However, depending on the time scale varying degrees of fraying and 'resemblance levels' of native structures may be observed (see results and discussion). Works by Clemmer's team observed unfolding on a timescale of 0.1s with ESI. Conversely, studies by Wyttenbach and Bowers postulate that no unfolding occurs within 0.1s [4]. In contrast Segev *et al.* compute unfolding timescale to be 2ms. The same investigator partitions Ubiquitin into regions I to IV. These regions give a guideline to an order of stability  $\text{I} < \text{IV} < \text{II} < \text{III}$ . Region I (amino acids from 1 to 18) comprises  $\beta$ -strands 1

and 2. Region IV (residues 59-76) comprises  $\beta$ -strand 5. In the same line of logic, region II labels the sequence of amino acids 19 to 35 and region III amino acids 36 to 58 [4]. Another paper by McLafferty, provides a befitting illustration of the whole developmental pathway of ubiquitin desolvation and unfolding that ascribes his ionization method of choice, ESI [5]. A highlight in the works by HanBin Oh *et al.* is made that gathers the percept of Ubiquitins fixation in the tertiary domain to be 10+ to 13+ protein species. Ubiquitin has been recognized as a 'superhero' in cell biology, *dixit* Hanbin Oh *et al.* [6]. The article by Evan R. Williams, "Supercharging with m-nitrobenzyl Alcohol and propylene carbonate: Forming highly charged ions extended, near-linear conformations" also beautifully, illustrates and schemes out the supercharging of ubiquitin 7+ to 13+ and its continuation to 21+ [7]. Collaborative work by Skinner, Breuker and McLafferty develop a charge site mass analysis also based on ECD to provide intrinsic mechanistic information on the role of neighboring secondary structure regions and how they protonate on basic sites influencing hydrogen bonding to backbone carbonyls ultimately proving that a particular charge state of ubiquitin is not guaranteed to have a single conformation [8].

Whilst the preparation and ionization of ubiquitin has been studied, so has the conditioning gas in the trap used. Indeed, Rajabi brought about a sampling method for ubiquitin ion populations in a gas setting treated with microsecond D<sub>2</sub>O vapour pulses so to favor hydrogen deuterium exchanges. In this paper it is postulated that 7+ and 6+ charge state species of ubiquitin adopts a more compact conformation whilst 8+ and 9+ are more extended conformation-wise and that this is due to the coulombic repulsion and availability of protonation sites [9]. More evidence in Ubiquitin unfolding through an ESI-MS method is given by Segev *et al.* In this set of experiments ubiquitin is presented to hold its native structure and an unfolded structure commonly accepted as the *A state* [10], the structure involves an antiparallel  $\beta$ -sheet and a central  $\alpha$ -helix similar to the native state [3] portrayed in Figure 5.5.1 in this chapter. Again it is assumed that this elongated conformation is due to lack of solvation shell. The author further discusses the unfolding rate which progresses at increasing temperatures; 300K, 400K, 450K, 500K and 600K.

For ubiquitin 13+, two interesting intermediate states were found and a final near linear geometry was depicted with virtually no elongated structure. Arrhenius plot describing the rate constants from one transition to another are given [3]. Further conformational study of ubiquitin in the gas phase, especially focusing on ubiquitin 8+ is reported by Huilin Shi [11]. ESI-IMS is used to examine 20 different samples of ubiquitin with solution conditions from 100:0 to 5:95 water:methanol with a pH maintained at 2.0. Ubiquitin 8+ ion is chosen as it holds a constant percentage across all solution compositions. The IMS results indicate that at 100:0 water:methanol composition 2 major peaks suggesting 8+ populations are observed. An N, native compact geometry (collision cross section 1020 Å<sup>2</sup>) and an A state geometry (collision cross section 1650 Å<sup>2</sup> and 1680 Å<sup>2</sup>) ascribing a semi unraveled ubiquitin, as discussed by the author. As the proportion of methanol increases in the solution composition so does the intensity and sharpening of the A state feature distributions and U state distribution (Clemmer *et al.* [11]), collision cross sections 1650 Å<sup>2</sup> and 1680 Å<sup>2</sup> and 1160 Å<sup>2</sup> respectively. Similarly, the disappearance or annulation, of the peak at 1020 Å<sup>2</sup> as the methanol comprises more than 40% of the solution



infers the presence of any N state geometries of ubiquitin, see the second figure of the published article [11]. The dynamics of ubiquitin 7+ had also been investigated by Shi using the same IMS technique in order to measure collisional cross sections and tease out folding states of ubiquitin from four unique electrosprayed water:methanol acidic solutions [12]. Again, there is the general agreement that an increase in methanol composition in the solution means protein denaturation and greater A-state type populations. In this way, aqueous solutions are best at conserving a high compact N-state population at equilibrium with misfolded A-state intermediates [12]. This dependency on solvent agrees with the observations reported by Chait and co-workers and later Loo and co-workers, confirming that changes in solvent composition induce dramatic change on the charge state distribution of protein ions. In particular that shifting to a methanol solvent induces denaturation, the unfolded protein then can accommodate more charges as more basic sites become available [10, 13, 14]. The totality of the charge states of ubiquitin 5+ to 13+ in addition to 8+ having been studied in IMS is discussed in a paper by another member of the group David E. Clemmer, again it is evident that the species of interest can be categorized depending on their conformation: compact, unraveled or elongated [15]. As anticipated these results are consistent with measurements made by Huilin Shi [11]. Figure 5.5.2 is also available for review, it is interesting as a model of bovine ubiquitin erythrocyte mutant as it portrays the protein differently when it is modeled only by ribbon and other molecular fold.

### 5.3 Ubiquitin FRET in the condensed state

Up to date FRET studies on ubiquitin alone and in some form of liquid state including cellular, have not been made. However, there have been comparable FRET experiments with ubiquitin systems and conjugates. Quantitative studies of FRET looking at the SUMO (small ubiquitin like modifier) biochemical route has been reported by Ifor D.W. Samuel *et al.* In short a lasing at 400nm was applied to excite the first ensemble: CFP (cyan fluorescent protein) tethered to SUMO1 in order to record FRET emission at 530nm by the acceptor ensemble: Ubc-9 (ubiquitin carrier protein 9) linked to YFP (yellow fluorescent protein) in a well plate. This particular experiment then further discusses how no FRET is observed when the inhibiting agent RanBP2 competes, complexes with Ubc and antagonizes binding between the two aforementioned partners (CFP-SUMO1 and YFP-Ubc9) [16]. Cellular FRET on ubiquitin was achieved by designing genetically engineered, nonfluorescent 'dark' chromophore enhanced YFP that the authors nickname; Resonance Energy-Accepting Chromoprotein, REACH in short. This acceptor was utilized to couple with GFP (Green fluorescent protein) to give FRET between an ubiquitination substrate to which GFP is anchored and the REACH label that was covalently linked to ubiquitin in vivo [17].

## 5.5 Action-FRET on Ubiquitin in the gas phase

### 5.5.1 Method

Rhodamine 575 C5-maleimide (Setareh Biotech, Eugene, OR, USA) and QSY 7 C5-maleimide (Invitrogen, Carlsbad, CA, USA) were dissolved in DMSO (1 mg/100  $\mu$ L), and an equimolar (100  $\mu$ M) solution of both chromophores prepared in H<sub>2</sub>O. Bovine ubiquitin (Sigma Aldrich, St. Louis, MO, USA) was diluted in H<sub>2</sub>O, 1:1 H<sub>2</sub>O:CH<sub>3</sub>OH or CH<sub>3</sub>OH with 1% acetic acid by volume to a final concentration of 10  $\mu$ M; 10 mg of G35C L73C ubiquitin mutant (C-UBI-C, see Figure 5.5.4. (a)) was purchased (Genscript, Piscataway, NJ, USA) and dissolved in phosphate buffered saline solution for storage (1 mL, 0.37 mg/mL). Prior to grafting of the chromophores, each 1 mL aliquot was treated with an excess of TCEP (28 mM in H<sub>2</sub>O) to remove any disulphide bonding, and subsequently purified by HPLC (Agilent, Santa Clara, CA, USA) using a C4 column (Poroshell, 4.6  $\times$  150 mm, Analytical) employing a H<sub>2</sub>O 0.1% trifluoroacetic acid to CH<sub>3</sub>CN 0.1% trifluoroacetic acid gradient. The collected sample was blown with a jet of N<sub>2</sub> gas. The bulk of the CH<sub>3</sub>CN solvent removed the concentrated solution was rehydrated in 500  $\mu$ L H<sub>2</sub>O, and neutralized by dropwise addition of 1% NH<sub>4</sub>OH in H<sub>2</sub>O. To the purified, neutralized ubiquitin solution was added 110  $\mu$ L of the 100  $\mu$ M chromophore solution, and the resulting solution was rested for 24 h at room temperature to favor the tagging reaction to reach the right-hand side of the equilibrium. To meet MS electrospray conditions, the reaction mixtures were diluted to a concentration of 10  $\mu$ M in either H<sub>2</sub>O, 1:1 H<sub>2</sub>O:CH<sub>3</sub>OH or CH<sub>3</sub>OH with 1% acetic acid by volume.

Here in this experiment, each charge state was isolated and irradiated by one laser pulse of either 505 or 545 nm light, corresponding to the absorption maximum of the donor and the acceptor chromophore, respectively, (which undergo only minimal shifts upon covalent attachment). At each wavelength, the resulting mass spectrum following irradiation was averaged for a period of 2 min. The laser power was measured immediately preceding and following the accumulation of a mass spectrum for a period of 1 min, and the average of these two power readings was taken as the laser power for intervening mass spectrum. The relative intensity of the fragments specific to photo-excitation of the acceptor chromophore was determined for each mass spectrum and normalized to the laser fluence (power  $\times$  wavelength) [18]. The FRET efficiency was then determined by taking the normalized relative intensity at 505 nm and dividing it by the normalized relative intensity at 545 nm for each pair of measurements. The final value was taken as the average of these FRET efficiency values, whilst their standard deviation was taken as the error. A correction of -0.25 is applied to all the final FRET efficiency values to account for the non-zero fragmentation efficiency of QSY7 at 505 nm [18].

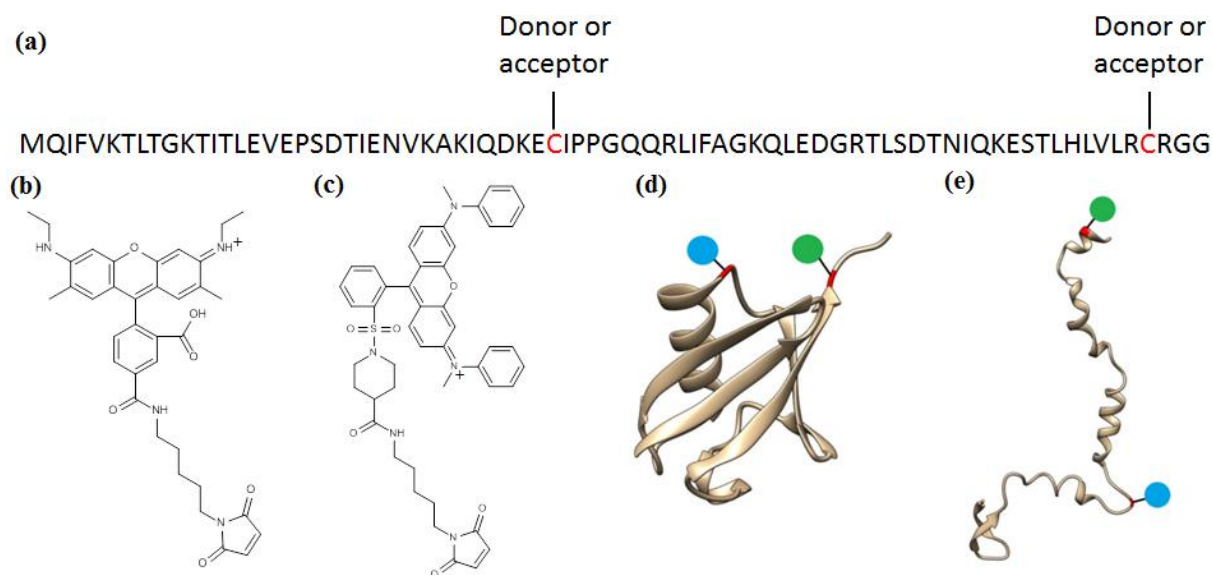


Figure 5.5.1. (a) Sequence of the double cysteine ubiquitin mutant with FRET probes. (b) The structure of the donor chromophore rhodamine 575-C5-maleimide. (c) The structure of the acceptor chromophore QSY7-C5-maleimide. (d) Secondary structure of the folded state of ubiquitin (pdb file 1UBQ) with chromophore position indicated by blue green circles. A representation of the secondary structure of the A-state of ubiquitin taken from a MD simulation (A. Kulesza), with chromophore positions indicated by blue and green circles.

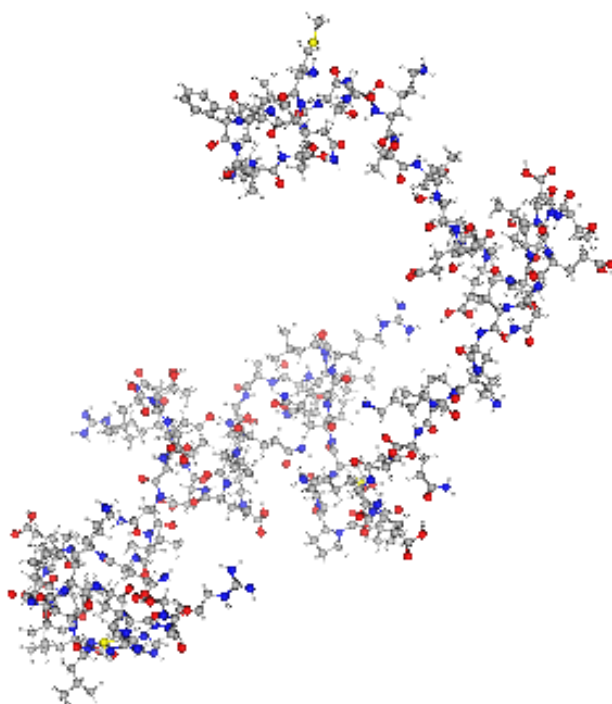


Figure 5.5.2. Bovine Ubiquitin erythrocyte mutant.

This experiment took on analysis of this system with ion mobility spectroscopy (IMS) measurements, an instrumental technique out of scope of this thesis and that will not be explained in this manuscript. In this regard, the crown jewel of the group, a custom-built ion mobility spectrometer with unique bespoke specifications, was used. What is important is that it permitted to further probe and sketch the protein in the gas environment. Here, ions were analyzed using 4 Torr helium as a buffer gas at room temperature and utilizing drift voltages between 250 and 500 V. Collision cross section values were determined by measuring ion arrival times as a function of the inverse voltage value across second drift tube, and all reported CCS values and profiles were obtained using helium.

Operatives carried through circular dichroism experiments on a ChiraScan qCD spectrometer (Applied Photophysics, Leatherhead, UK). Concentrations of approximately 100  $\mu$ M were used when obtaining circular dichroism spectra.

### 5.5.2 Results and discussion

In setting out to make FRET measurements on proteins in gas phase isolation, it is key that the grafting procedure is performed under mild conditions so to curtail the risk of disturbing the native protein fold in solution. A second point, on internal interactions, it is important to confirm that the architecture of the protein is likely to remain indifferent to cysteine point mutations necessary to later equip the FRET components. The colocalization of the mutation sites must also be picked so as to undergo a large change in spatial proximity on conformational change that is being probed. It is then understood that any conformational conversion in this setting would be a result of the native (N) ubiquitin unfolding to the A-state, a conformation consensually recognized as the dominant structure in acidified methanol solutions [18]. It is clear that on inspection of Figure 5.5.1, residues G35-Q40 and R72-G76 (as do the chromophores) distance themselves from their native state arrangement on conformational change. Whilst two site locations have been established for target mutation, one of these residues must be selected for cysteine mutation of each cut of the protein (an alternative-especially amenable at N- or C-termini-is to add a single cysteine amino-acid) [18]. Along the 35-40 region, two proline residues lend the characteristic turn to the protein between the helical and  $\beta$ -sheet secondary folds and are thus to be discarded as mutation sites. Correspondingly, residues with polar side chains play an integral part in shaping secondary structure and are unequally considered unsuitable candidates. In the 71-76 region, including the location of two arginine residues, tagging is not ideal as this section of the protein nearing the C-terminus, is very flexible. The rational funneled down to a sequence design where the best option was to mutate G35 for as first location of a cysteine introduction and L73 as the second mutation site, a relatively common procedure as the mutation occurs naturally [18].

As it has been mentioned above, cysteine mutation must not alter the native structure of the protein. This was confirmed by taking circular dichroism measurements on both the cysteine mutated ubiquitin (*viz.* C-UBI-C) and bovine ubiquitin. This exercise also served to verify that the chemistry of the tethering of chromophores does not cause loss of native structure. Noticeable differences are observable between the circular dichroism data for C-Ubi-C and wild-type

bovine ubiquitin in H<sub>2</sub>O and 1% acetic acid by volume, see Figure 5.5.3. Also included is a reference: the circular dichroic response of homo sapien ubiquitin in H<sub>2</sub>O, sketched out in red and used as a standard to compare to. It is important to remark that the figure features two y-axis on different scales. The reason being that C-UBI-C was HPLC processed and was analyzed at a lower concentration compared to bovine ubiquitin, that needed not to be processed by HPLC and was analysed from a 1mg/ 1ml sample. The circular dichroic response is concentration dependent, hence the use of the corresponding y-axis scales.

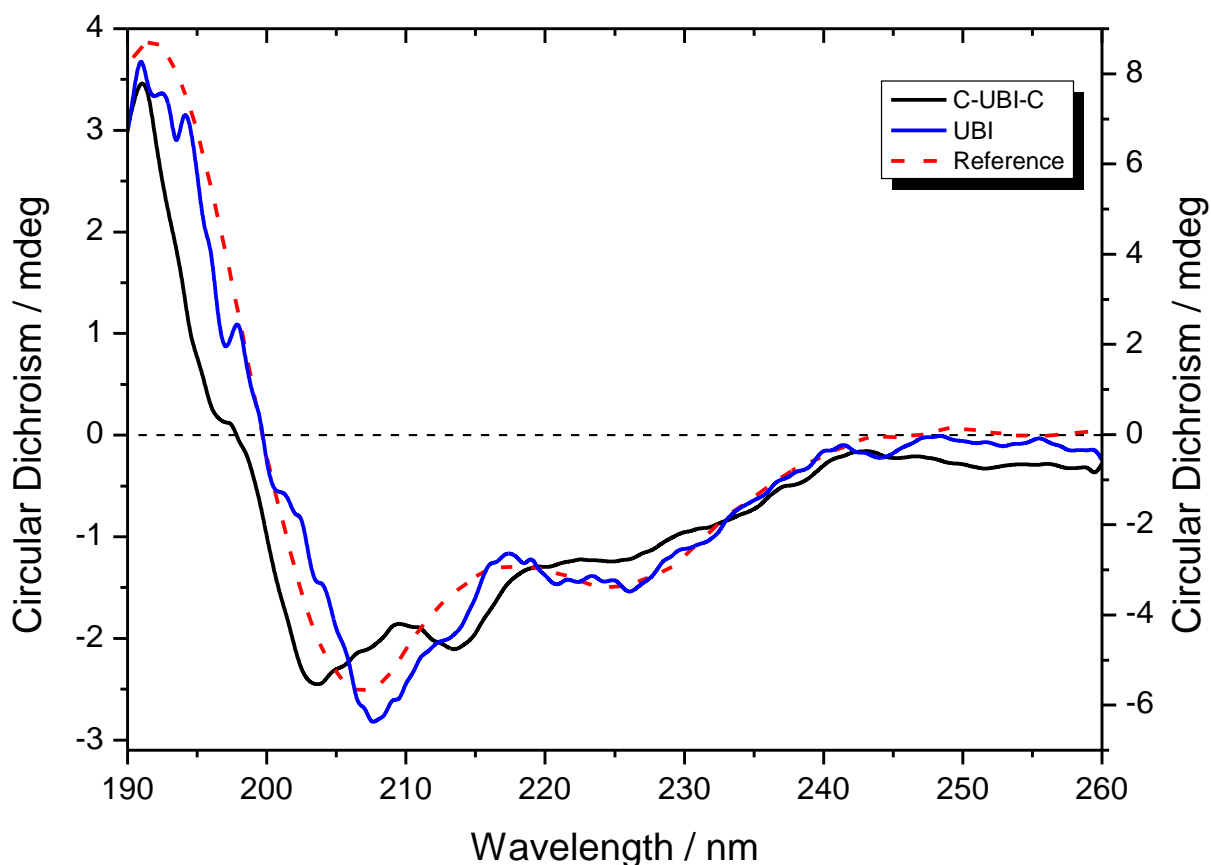


Figure 5.5.3. Circular dichroism signal for the G35 L73C ubiquitin mutant (solid black curves, left axis) and wild-type bovine ubiquitin (solid blue curves, right axis) in H<sub>2</sub>O with 1% acetic acid by volume. A reference spectrum taken from reference [19, 20] is shown as the dashed red curve.

The good news that this plot gives us is the approval that there is no prominent change in secondary structure either by two-point mutations or the work up of the analyte species (HPLC). This claim is put forward as both the mutated ubiquitin protein and doubly tagged C-UBI-C protein outline do not strongly disresemble the reference curve. The question on measuring the circular dichroic response on tagged ubiquitin however, was prohibitive as it came to light that by their nature, the chromophores absorb in the ultraviolet region and thus did not warrant a test to unveil any information on structural changes in solution. Nevertheless, this interest was addressed by exploring the tagged species in the gas medium and carrying FRET studies to tease out the structural shape of the protein and a corollary has been the opportunity to deduce what influence the chromophores may play on this one. Secondly, examining any charge state distribution changes as a function of electrospray ionization solute in conjunction with

observing the framework with ion mobility spectrometry, especially, to calculate collision cross sections contributed in setting a more detailed picture of the system.

These electrospray solutions consisted of bovine ubiquitin and doubly tagged C-UBI-C in i) H<sub>2</sub>O 1% acetic acid by volume (Figure 5.5.4, a) and c) respectively) ii) 1:1 H<sub>2</sub>O:CH<sub>3</sub>OH 1% acetic acid by volume (Figure 5.5.4, b) and d) respectively). On inspection it is clear that wild-type bovine ubiquitin takes a narrow profile of its charges states with 7+ being the most abundant species. This spectral pattern is consistent with the mass spectra on bovine ubiquitin in high aqueous solvent condition produced by others [14], and the distribution of charge states is in agreement with the claim of Chait and co-workers in that the mass spectra of this type exhibit ions with a wide distribution of charge states but keep a single dominant protonation state.

It is commonly accepted that the way species charge is in majority due to the ESI process. Those that sparkle out of the ionization device as compact native structures charge less compared to those molecules which have flayed open and denatured. For the most part, folded frameworks are less solvent accessible and therefore do not charge as much as the denatured molecules that are more solvent accessible and have a greater propensity to reach higher charge states [13]. Each signal for the charge state corresponding to doubly tagged ubiquitin is neighbored with a peak for the associated by-products of the grafting reaction of dyes seen in the 'triads' of the *m/z* spectrum. These are donor-donor (d-UBI-d), donor-acceptor (d-UBI-a), and acceptor-acceptor (a-UBI-a) labelled ubiquitin (green, red, and blue dots respectively). Charge state distribution for tagged ubiquitin in the more water based solution resembles closely to that seen in Figure 5.5.4 (a), for untagged ubiquitin, suggesting that the chromophores are not bearing a large denaturing effect on the protein framework. By its very nature, acceptor and donor each hold one charge. In consequence, when 7+ is preferential for d-UBI-a, it means that there are only five protons on ubiquitin, this is in contrast to untagged ubiquitin preferentially ionized to its 7+ charge state. In the methanol water mixture, Figure 5.5.4 (d), a wider panoply of charge states is produced. This phenomenon is paired with a shift in the liability of the ionization, tagged ubiquitin recessing a 10+ charge as opposed to 12+ seen for the unmodified ubiquitin. The resemblance between theses distributions lends to support that the tagging protocol do not greatly disturb the secondary structure in a way that completely unravels the protein. It has to be recognized however that the addition of an optical active pair of donor acceptor chromophores, that explains the shift in charge state distribution from the untagged protein, does implicate to make a concession on the degree of native character that can be kept.

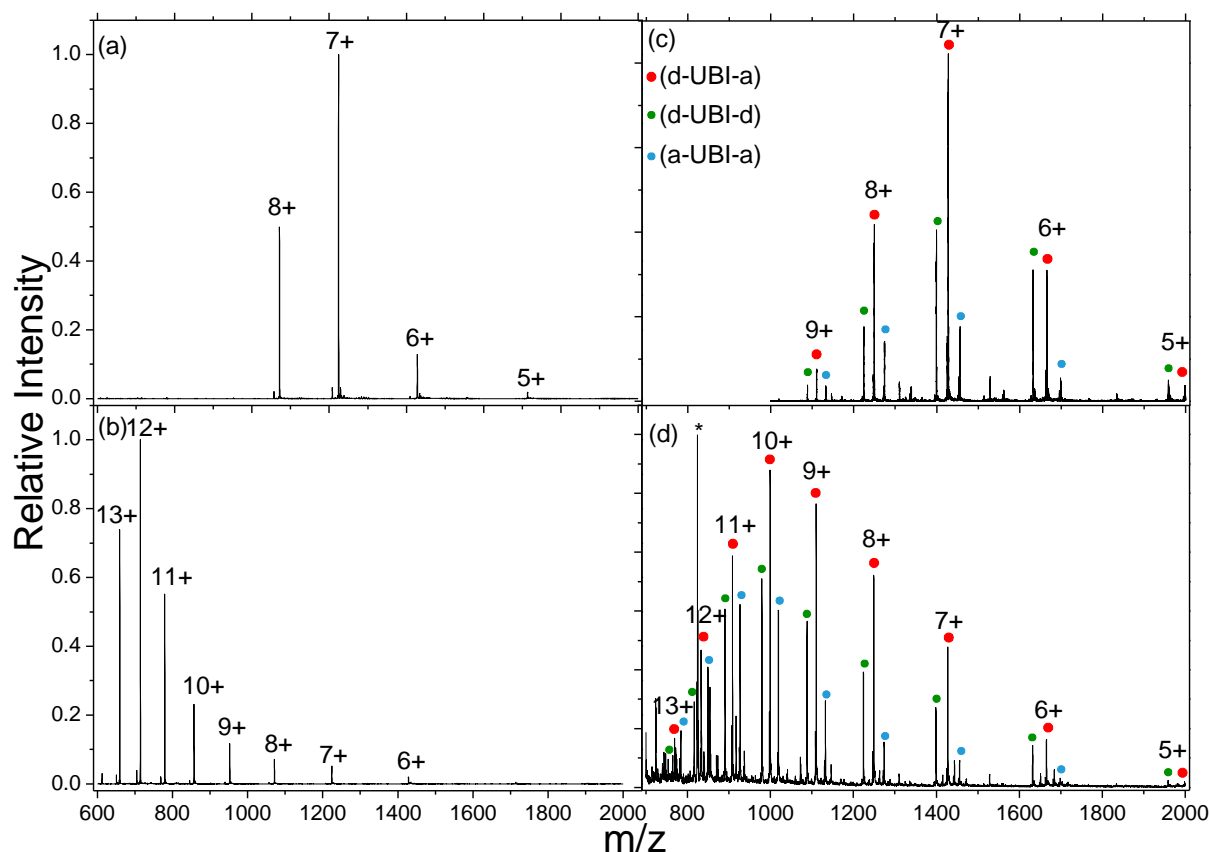


Figure 5.5.4. Mass spectrum following ESI of bovine ubiquitin and [d-UBI-a]<sup>2+</sup> cations in H<sub>2</sub>O (panels (a) and (c)) and 1:1 H<sub>2</sub>O:CH<sub>3</sub>OH (panels (b) and (d)), both with 1% acetic acid by volume. Red circles denote doubly-tagged species containing both a donor 'd' and acceptor 'a' chromophore. Smaller green and blue circles denote tagging with two d or a chromophores respectively. The asterisks in panel (d) denote peaks associated with unreacted acceptor chromophore, which is the cause of the congestion of peaks below *m/z* 900. The labels represent the total charge state of the system.

As previously mentioned above, IMS was used to further build a complete interpretation of proteins in gas isolation. In keeping with this goal, both tagged and untagged C-UBI-C were analyzed. The tagged framework for simplicity, in the interest of analyzing signal of sufficient spectral quality, consisted of ubiquitin only being labeled with the acceptor, giving a-UBI-a and this was used to compare with the untagged C-UBI-C framework. The ESI solution employed for this analysis was a 1:1 H<sub>2</sub>O:CH<sub>3</sub>OH 1% acetic acid mixture. The harvested results that the IMS produced were taken to draw and compare the collision cross section and the drift time distributions collected for C-UBI-C and a-UBI-a as a function of their charge state, Figure 5.5.5.

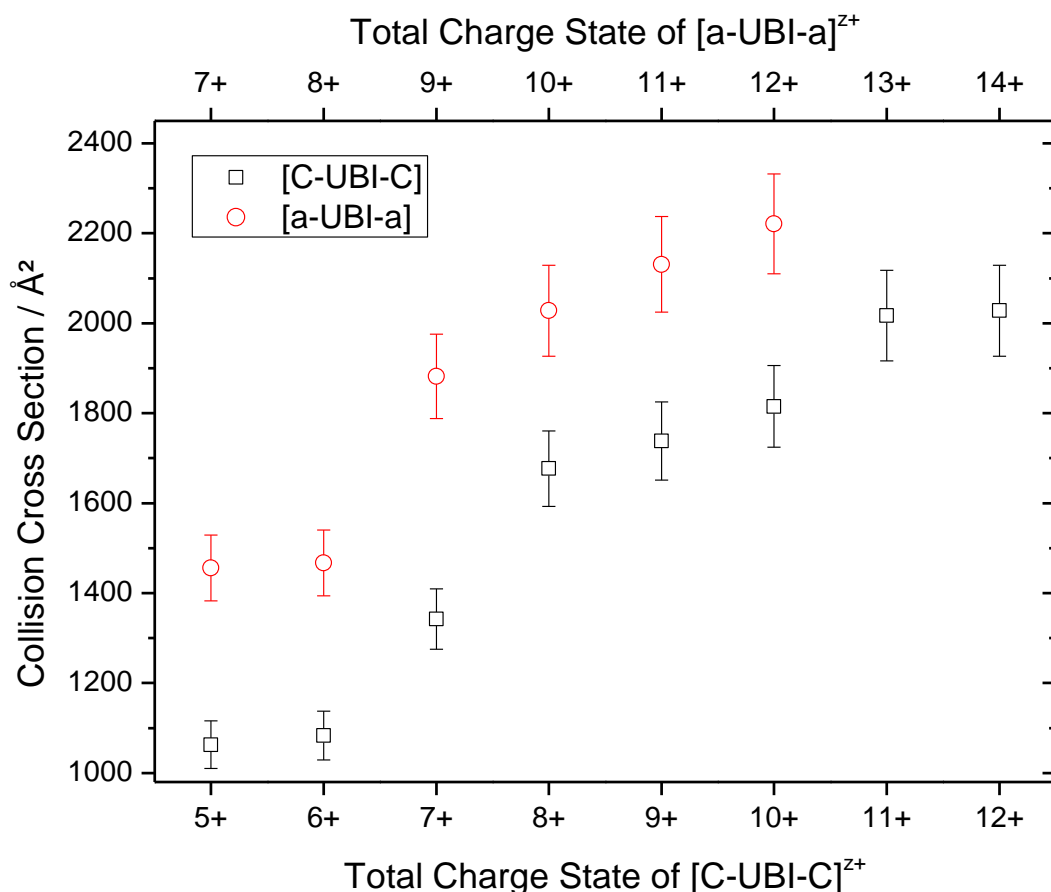


Figure 5.5.5. Collision cross section values (in He) of the highest peak for untagged C-UBI-C (black squares) and acceptor doubly tagged ubiquitin a-UBI-a (red circles) as a function of the charge state.

In summary, charge states from 5+ to 12+ were observed for C-UBI-C and 7+ to 12+ for a-UBI-a. From the CCS values, it is clear that barred a 2+ difference in the charge state for the tagged protein versus the untagged bovine ubiquitin mutant C-Ubi-C, both tagged and untagged frameworks overall trend similarly in their CCS evolution from increasing charge state species. The CCS slowly increase together consistently, with a noticeable difference in the magnitude of this increase observed from 6+ to 7+ charged species. Overall all CCS values are higher for tagged protein as they bear chromophores and thus are spatially larger frameworks with larger cross sections. It is possible to account for this 2+ shift in the charge state given that the chromophores recess two permanent positive charges meaning that charge state  $z$  of tagged ubiquitin, the protein alone, can be calculated:  $n = z - 2$  protons. This artefact of the experiment crucially points that system's protonation on to the species, goads it to unfold *i.e.* the protein framework.



Another major draw has been to plot the CCS profiles for tagged and untagged ubiquitin to further attest their resemblance, see Figure 5.5.6.

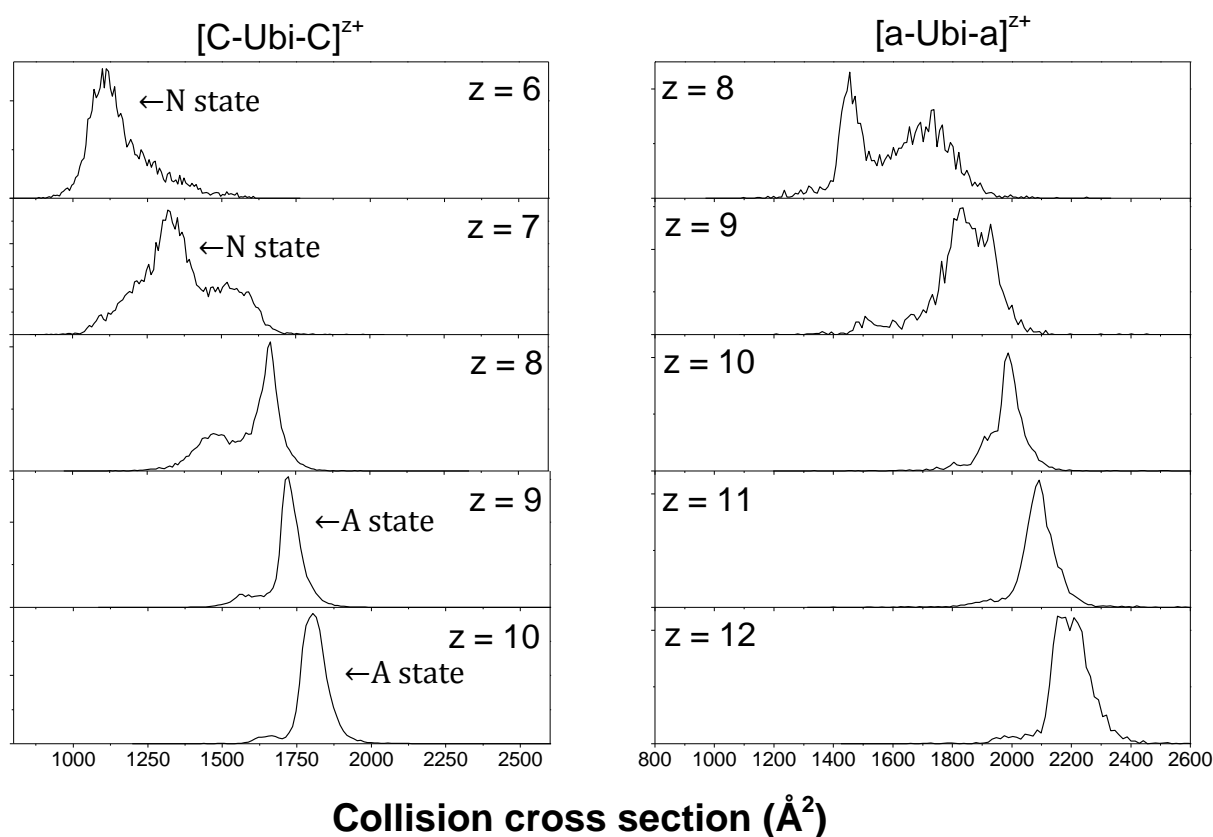


Figure 5.5.6. Collision cross section results (in He) for untagged mutant ubiquitin (left) and acceptor doubly tagged ubiquitin (right) where  $z$  is the total charge state of the system.

These findings show a dependency on charge state for CCS values of both untagged ubiquitin mutant and the doubly tagged ubiquitin. The observation is that on the left panel of results, a compact assembly ( $ca. 1000 \text{ Å}^2$  to  $ca. 1450 \text{ Å}^2$ ) from the produced CCS distributions agrees with the N state seen with lower charge states of untagged ubiquitin mutant (6+ and 7+). It is also observable that for higher charge states of untagged ubiquitin mutant (8+, 9+, 10+), the CCS are larger ( $ca. 1500 \text{ Å}^2$  to  $ca. 2000 \text{ Å}^2$ ) and more consistent to an A state conformation. The turning point between the N state and A state can be observed on the 8+ distribution on the graph. This difference and evolution in N state or A state likeness is also observed accordingly for the CCS results of the acceptor doubly tagged ubiquitin. Another of the most key observation is that a similar unfolding behavior can be seen when comparing the same protonation states of the protein. The noticeable difference is that between the tagged and untagged species there is an increased amount of extended arrangement for the tagged species. This is due to the number of charges recessed along the tagged protein that induce it to take an elongated conformation, this is not so an acute effect with the untagged species as it simply does not reach the same level of protonation. In short, the unfolding appears to depend on the propensity of the species to protonate, yet the inclusion of charged chromophores still influences the overall stability of the

protein structure, albeit at a much lesser magnitude. The observation is that the acceptors induce a difference in the CCS that is greater than zero. More precisely from inspection of the results in the above figure, one can notice a shift in the CCS of ca. 400 Å<sup>2</sup> between comparable untagged and tagged ubiquitin measurements (compare [C-Ubi-C]<sup>6+</sup>to [a-Ubi-a]<sup>8+</sup>; [C-Ubi-C]<sup>7+</sup>to [a-Ubi-a]<sup>9+</sup>; [C-Ubi-C]<sup>8+</sup>to [a-Ubi-a]<sup>10+</sup>; [C-Ubi-C]<sup>9+</sup>to [a-Ubi-a]<sup>11+</sup>; [C-Ubi-C]<sup>10+</sup>to [a-Ubi-a]<sup>12+</sup>).

## 5.6 On FRET efficiency determination: Ubiquitin framework

As indicated previously in the FRET efficiency determination section of this thesis, section 2.4. Action-FRET can be quantified by comparing the photofragmentation specific of the acceptor after excitation at i) 545nm and ii) 505nm. The purpose of this again, is to irradiate at the gas-phase absorption maxima of the rhodamine-QSY donor-acceptor pair used in this system. The LID spectra and photoactive response is given in the Figure 5.6.1 (a) below.

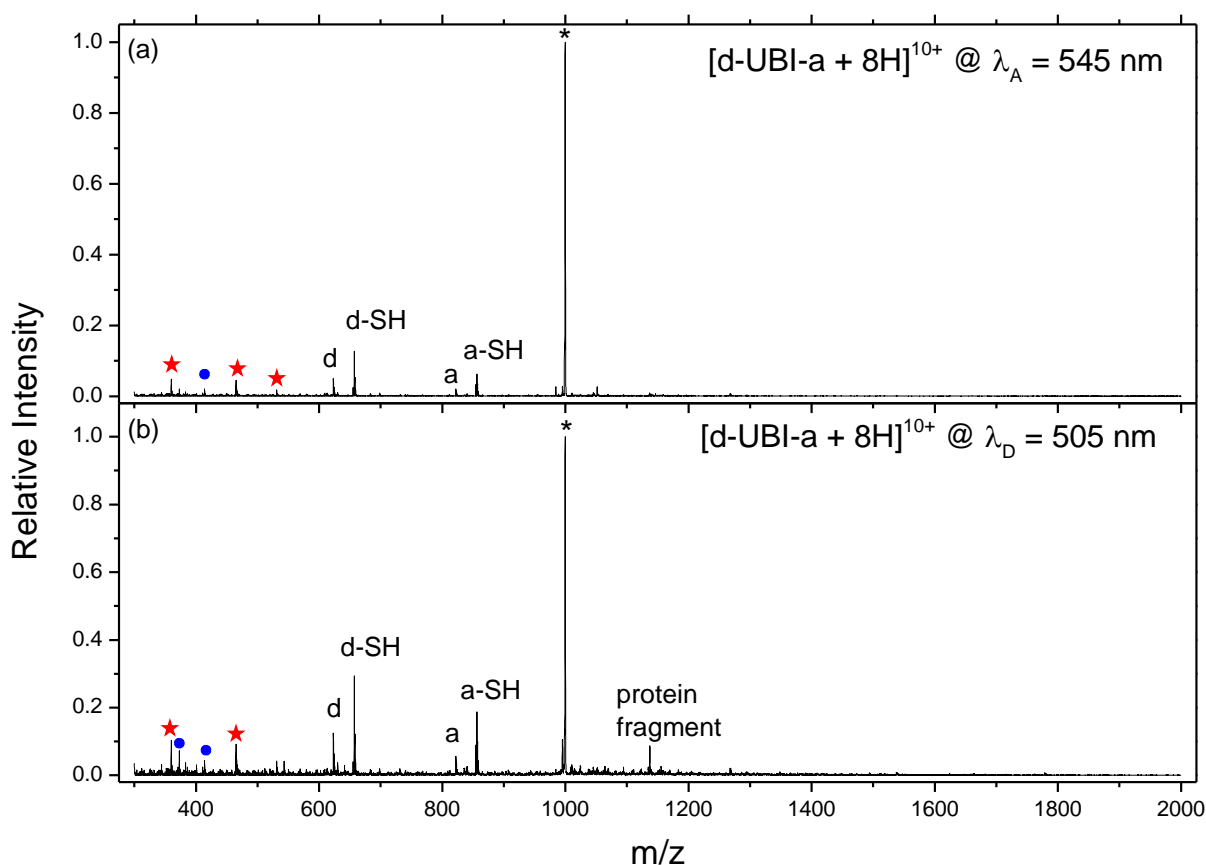


Figure 5.6.1. Mass spectra of mass-selected  $[d\text{-Ubi-a} + 8H]^{10+}$  ions – denoted by the asterisk – after irradiation at  $\lambda_A = 545$  nm (a) and  $\lambda_D = 505$  nm (b). The peaks denoted d/d-SH and a/a-SH correspond to breaking either of the side of the sulphur atom bond in the thioether linker. The red stars ascribe the acceptor chromophore specific photo-fragments. The blue circles denote fragments associated with the donor chromophore.

The photofragments unique to acceptor electronic excitation are  $m/z$  360 and 465 (denoted with red stars). Other fragments of interest include species  $m/z$  623 and 657 corresponding to donor and donor-SH respectively, see Figure 5.6.1, d and d-SH. Similarly, the peaks at  $m/z$  822 and 856 correspond to the acceptor (a) and the acceptor-SH (a-SH), see Figure 5.6.1. These

cleavages are common to the distinct thioether-chemistry afforded by the coupling reaction between the maleimide group and thiol functional group of the protein, these remain specially labile and break up by collision and laser induced dissociation. Other significant fragments include species giving about  $m/z$  414 and 373 (blue circles) and are associated to direct fragmentation of the donor. This goes against the expectation that all resonance energy relaxes down the FRET regime. This is important as the interest lies in the action spectroscopy response of the acceptor as a result of the FRET regime. It is apparent that in this experiment a dissociation of the donor cannot exclude to occur. Finally, a multiple charged species is registered at  $m/z$  1137 and this ascribes protein fragment with loss of chromophore. All assigned peaks are gathered in a table for review below.

$m/z$	Assignment
1110	Parent
1137	Protein fragment
1105	CO <sub>2</sub> loss
856	QSY7-SH
822	QSY7
657	R575-SH
623	R575
531	QSY7 internal fragment
465	QSY7 internal fragment
414	R575 internal fragment
360	QSY7 internal fragment

Table 5.6.1. Major fragment peaks observed in the LID mass spectrum of [d-UBI-a +8H]<sup>10+</sup> initiated by photon irradiation at either 545 nm or 505 nm.

The FRET efficiency is then calculated by weighing the specific photofragments  $m/z$  360 and 465 by the work through described earlier in this thesis. These results were processed to give a plot of FRET efficiency values per LID recording, Figure 5.6.2. Structural information from Figure 5.6.3 is also available for review, clarifying the distance distributions of chromophores for every charge state observable of doubly grafted Ubiquitin produced by the electrospray.

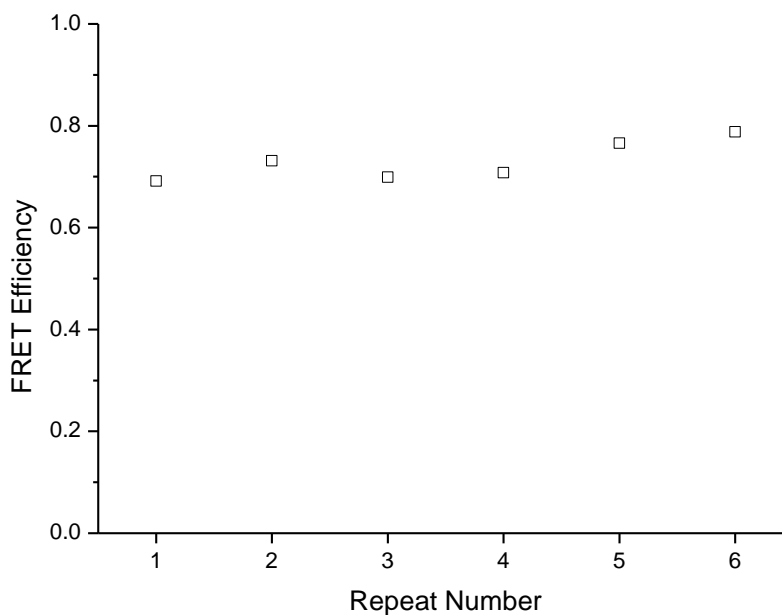


Figure 5.6.2. Experimental FRET efficiency for 6 data sets or measurements of mass selected  $[\alpha\text{-Ubi-d} + 8\text{H}]^{10+}$ . Repeats 1-5 were taken on the same day under identical conditions (including sample). Repeat number 6 was performed 6 days later as a single measurement from a different sample. Here we can nicely demonstrate that the FRET efficiencies are reproducible both within the same sample and experimental setup; and with different sample and laser realignment.

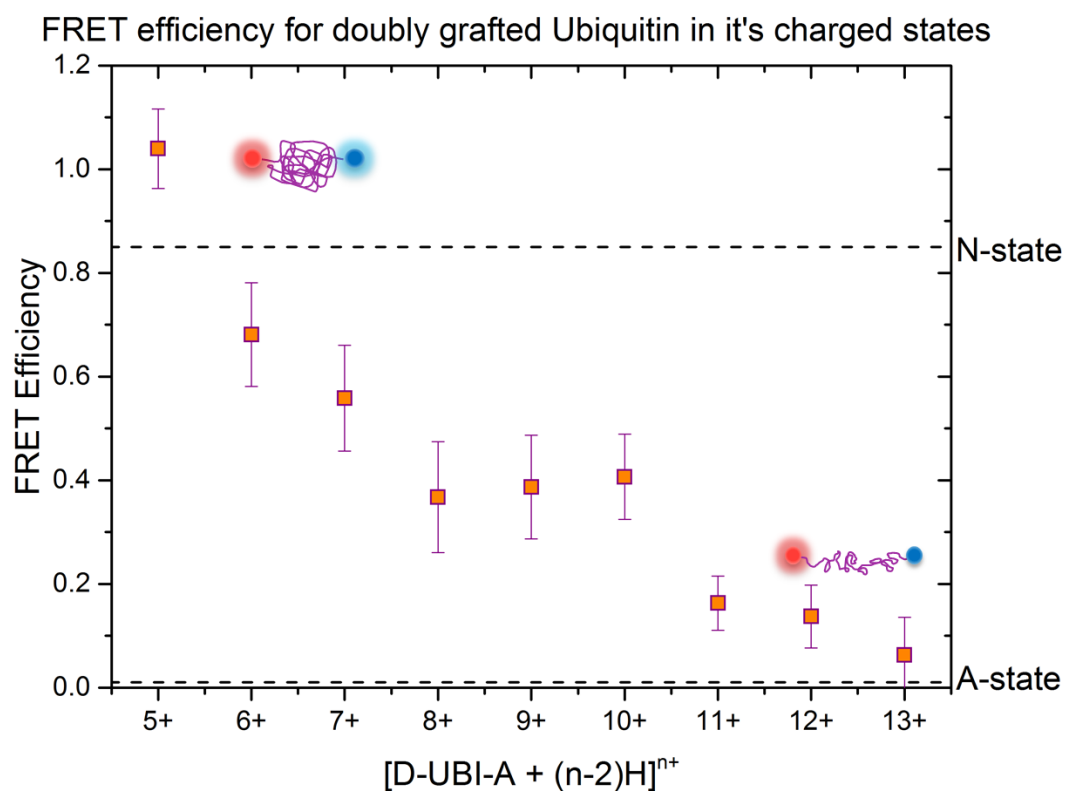


Figure 5.6.3. FRET efficiency as a function of charge state. The dashed lines indicate estimated FRET efficiencies for the native (N-state) and A-states of ubiquitin.

The highlight of this figure is that a conformational conversion can be made out for every macromolecule, from the 5+ charge state and following increasingly protonated doubly grafted ubiquitin proteins (6+, 7+, 8+, 9+, 10+, 11+, 12+ and 13+). The 5+ and 6+ charge states are more specifically N-state like (6+ charge state chromophore separation is in the order of 2.4nm to 4.4nm) whilst the 11+, 12+ and 13+ are more A-state like (13+ charge state chromophore separation is in the order of 8.7nm to 11.3nm) [18]. Bundled, low charge states are more atuned with the first model (†) whilst the high charged state hold an extended form as depicted in the second representation (‡), Figure 5.6.4. (results of 10ns gas phase molecular dynamics runs (A.Kulesza) [18]). This featuring characteristic of ubiquitin to fold into a tight or elongated conformation has compellingly been studied with simulations as well and elsewhere by Thirumalai *et al.* [21].

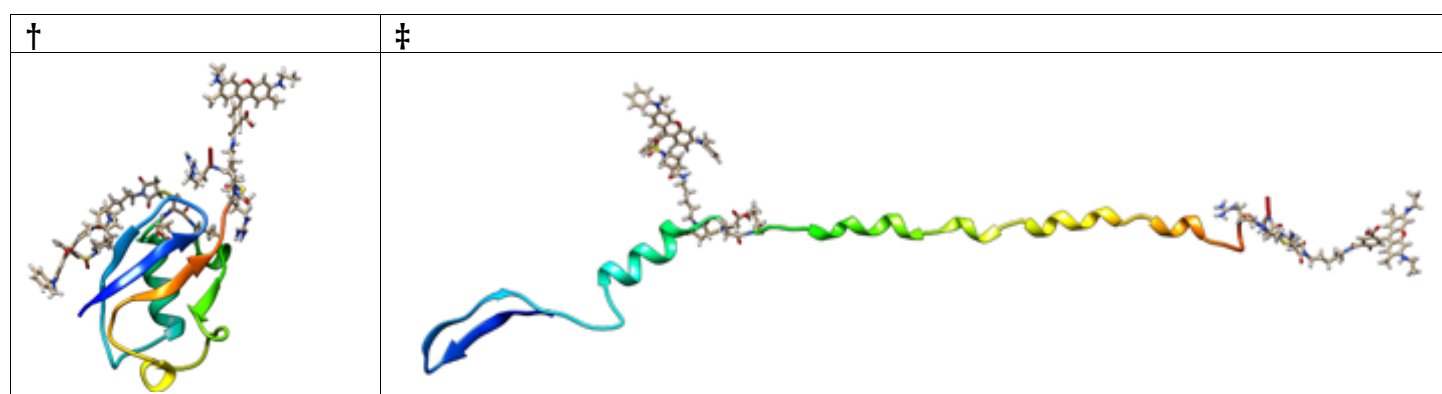


Figure 5.6.4. Representative folds of doubly grafted ubiquitin. Native like (†) and extended (‡) forms.

Compared to what has been done in respect to collision cross section results on tagged ubiquitin (Figure 5.5.6), there is an agreement on that there is a conversion in conformation between the proteins when their charge changes. It can also be deduced that ions with higher charges on, correspond to the more unfolded conformers whilst as these are ascribed with CCS values that a relatively big to the species. The proteins of lower charge state set-out to take a tighter fold and this is backed up by the fact they show CCS of lower value.

Intriguingly, this observation of ubiquitin's charge state distribution is also sighted very accordingly but not exactly as other results notably those produced by of Chait and Loo and co-workers [10, 13]. The view of conformation being dependent to charge state is noted, that a protein in tightly folded conformation will have a discounted number of charges on species versus proteins in their unfolded conformation [13].

In sum it can be put forward that both the produced FRET efficiency data appended to the herein developed action-FRET method is complementary to the technique and results produced by IMS. An appraisal of the FRET technique being complementary to other analytical methods is mentioned elsewhere [22]. It is worth mentioning, that a statement can be made that FRET efficiencies provide a more sensitive quantification of the interdistance and thus the global demarcation between tagged ubiquitin protein conformers.

## 5.7 References :

1. Hershko A, Ciechanover A: **The ubiquitin system.** *Annual Review of Biochemistry* 1998, **67**:425-479.
2. Pickart CM, Eddins MJ: **Ubiquitin: structures, functions, mechanisms.** *Biochimica Et Biophysica Acta-Molecular Cell Research* 2004, **1695**:55-72.
3. Segev E, Wyttenbach T, Bowers MT, Gerber RB: **Conformational evolution of ubiquitin ions in electrospray mass spectrometry: molecular dynamics simulations at gradually increasing temperatures.** *Physical Chemistry Chemical Physics* 2008, **10**:3077-3082.
4. Skinner OS, McLafferty FW, Breuker K: **How Ubiquitin Unfolds after Transfer into the Gas Phase.** *Journal of the American Society for Mass Spectrometry* 2012, **23**:1011-1014.
5. Breuker K, McLafferty FW: **Stepwise evolution of protein native structure with electrospray into the gas phase, 10(-12) to 10(2) S.** *Proceedings of the National Academy of Sciences of the United States of America* 2008, **105**:18145-18152.
6. Oh H, Breuker K, Sze SK, Ge Y, Carpenter BK, McLafferty FW: **Secondary and tertiary structures of gaseous protein ions characterized by electron capture dissociation mass spectrometry and photofragment spectroscopy.** *Proceedings of the National Academy of Sciences of the United States of America* 2002, **99**:15863-15868.
7. Going CC, Williams ER: **Supercharging with m-Nitrobenzyl Alcohol and Propylene Carbonate: Forming Highly Charged Ions with Extended, Near-Linear Conformations.** *Analytical Chemistry* 2015, **87**:3973-3980.
8. Skinner OS, Breuker K, McLafferty FW: **Charge Site Mass Spectra: Conformation-Sensitive Components of the Electron Capture Dissociation Spectrum of a Protein.** *Journal of the American Society for Mass Spectrometry* 2013, **24**:807-810.
9. Rajabi K: **Microsecond pulsed hydrogen/deuterium exchange of electrosprayed ubiquitin ions stored in a linear ion trap.** *Physical Chemistry Chemical Physics* 2015, **17**:3607-3616.
10. Chowdhury SK, Katta V, Chait BT: **Probing conformational-changes in proteins by mass-spectrometry.** *Journal of the American Chemical Society* 1990, **112**:9012-9013.
11. Shi HL, Pierson NA, Valentine SJ, Clemmer DE: **Conformation Types of Ubiquitin M+8H (8+) Ions from Water:Methanol Solutions: Evidence for the N and A States in Aqueous Solution.** *Journal of Physical Chemistry B* 2012, **116**:3344-3352.
12. Shi HL, Atlasevich N, Merenbloom SI, Clemmer DE: **Solution Dependence of the Collisional Activation of Ubiquitin M+7H (7+) Ions.** *Journal of the American Society for Mass Spectrometry* 2014, **25**:2000-2008.
13. Kaltashov IA, Eyles SJ: *Mass spectrometry in biophysics.* Hoboken, New Jersey: Wiley; 2005.
14. Loo JA, Loo RRO, Udseth HR, Edmonds CG, Smith RD: **Solvent-induced conformational-changes of polypeptides probed by electrospray-ionization mass-spectrometry.** *Rapid Communications in Mass Spectrometry* 1991, **5**:101-105.
15. Koeniger SL, Clemmer DE: **Resolution and structural transitions of elongated states of ubiquitin.** *Journal of the American Society for Mass Spectrometry* 2007, **18**:322-331.
16. Martin SF, Tatham MH, Hay RT, Samuel IDW: **Quantitative analysis of multi-protein interactions using FRET: Application to the SUMO pathway.** *Protein Science* 2008, **17**:777-784.
17. Ganesan S, Ameerbeg SM, Ng TTC, Vojnovic B, Wouters FS: **A dark yellow fluorescent protein (YFP)-based Resonance Energy-Accepting Chromoprotein (REACH) for Forster resonance energy transfer with GFP.** *Proceedings of the National Academy of Sciences of the United States of America* 2006, **103**:4089-4094.
18. Daly S, Knight G, Halim MA, Kulesza A, Choi CM, Chirof F, MacAleese L, Antoine R, Dugourd P: **Action-FRET of a Gaseous Protein.** *Journal of the American Society for Mass Spectrometry* 2017, **28**:38-49.
19. Weber PL, Brown SC, Mueller L: **Sequential H-1-NMR assignments and secondary structure identification of human ubiquitin.** *Biochemistry* 1987, **26**:7282-7290.
20. Lees JG, Miles AJ, Wien F, Wallace BA: **A reference database for circular dichroism spectroscopy covering fold and secondary structure space.** *Bioinformatics* 2006, **22**:1955-1962.
21. Reddy G, Thirumalai D: **Collapse Precedes Folding in Denaturant-Dependent Assembly of Ubiquitin.** *Journal of Physical Chemistry B* 2017, **121**:995-1009.
22. Aznauryan M, Delgado L, Soranno A, Nettels D, Huang JR, Labhardt AM, Grzesiek S, Schuler B: **Comprehensive structural and dynamical view of an unfolded protein from the combination of single-molecule FRET, NMR, and SAXS.** *Proceedings of the National Academy of Sciences of the United States of America* 2016, **113**:E5389-E5398.



## Chapter 6 Negative action FRET.

In this chapter, the concepts of action-FRET are taken and tested in the negative polarity mode of the mass spectrometer. This includes the experimental and spectroscopy developments made and a discussion of the photophysical observations made, manoeuvring two different sets of chromophore pairs. In effect, there is an increasing interest in study of biological molecules in the solvent-free, gas-phase medium using mass spectrometry techniques [1]. The main advantage being that it is possible to probe the intrinsic properties of a biomolecule free of any interference: average ensemble effects that would exist in solution measurements. The early use of Forster resonance energy transfer to study their conformation has proven particularly appealing and a well-attested accurate structural tool. Herein we give the first example of negative-mode action FRET using specific photofragmentation as a reporter of the distance between chromophores tethered to a range of polypeptides. The efficiency of working with negative voltages at the electrospray ionizer is studied as a function of charge state of the polypeptides. The observation of our results show that negative mode action FRET offers new spectral patterns unique to negative charged state species, critically enhancing the action FRET method as a structural tool for interrogating biomolecule conformational dynamics. The last section includes a conclusion on the novel undertaking and examinations made.

### 6.1 Honing into negative action-FRET. Introduction.

Previous methods in the positive mode have used QSY7 N-succinimidyl ester (Life technologies) as the acceptor and 5-carboxyrhodamine 575 N-succinimidyl ester (rh575) (Life technologies) as a donor chromophore [2-5]. Similarly, Talbot *et al.* also used Rh575 as a donor chromophore, both the fluorescence and excitation and emission spectra along with the photofragmentation mass spectra have been studied in detail. Zenobi and co-workers offer a detailed report on donor acceptor pairs suitable for gas phase FRET. Carboxyrhodamine 6G (cR6G)-ATTO590 hexamethylenediamine and carborhodamine 6G (cR6G)-Bodipy TR cadaverine [6]. In the workings aforementioned herein, we carry out measurements in the negative mode to evaluate the feasibility of using a chromophore as a FRET gas phase component. The donor chromophore, NBD-maleimide, absorbs at 440nm in the gas phase and serves with the acceptor chromophore 5-Maleimido-eosin.

#### 6.1.1 Mass Spectrometry and Optical Spectroscopy.

The experimental setup used to execute the experiments presented in this paper has been described in detail before. In short, a linear quadrupole ion trap mass spectrometer (LTQ Velos, Thermo Fisher Scientific, San Jose, CA) was used for ion preparation, ion selection and trapping, fragmentation (CID and photodissociation), and subsequently, final mass analysis. The back panel of the vacuum manifold was modified by drilling a hole and fitting a quartz window (30 mm diameter and 5 mm thickness). This window was positioned in front of the linear ion trap such as to allow the direct irradiation of trapped ionic species within the axis of the laser beam.



The light source used is a Horizon OPO pumped by the third harmonic (355nm) of a Surelite II Nd: YAG laser (Continuum, Santa Clara, CA). A repetition rate of 10 Hz and pulse widths of the order of 5 ns were used. The visible portion of the spectrum was used directly via the signal beam of the OPO (410-700nm), which is collimated and refocused with a long focal distance lense of 1000 mm. A mechanical shutter synchronized with the mass spectrometer, is used to stop the beam at discrete time intervals set in accordance with "the ion activation window" - a time laps starting after ion accumulation and concluding, short to, the mass analysis. A single laser pulse is effectively used for the irradiation of the trapped ions. When irradiating ions the normalized collision energy is kept at zero. In this experiment laser power is measured by placing the power meter in a way so that it crosscuts its path. The power is monitored using a power meter (Ophir-Spiricon GmbH, Ahrensburg, Germany). The value of the power used for normalization is taken via two manners. One - over the duration of a measurement that is to say, an internal scan of the laser beam from 540nm to 420nm, step 0.1, delay 1, number of scans 1. The effective power for all spectra presented here is kept at an average of 1.9 mW. Two - for 1 min before or after an LID mass spectrum acquisition. Measured power averaged 5.5mW in this way.

### 6.1.2 Experimental

Peptides and chromophores. An account on the rational in the choosing of peptides and chromophores is given in the following section. The acceptor chromophore is 5-Maleimido-eosin (Sigma-Aldrich), a quencher absorbing at 524nm in solution and known to fragment efficiently at 520nm and 530nm for the first and second of its respective charge states in the gas phase. The donor chromophore is 1-[2-benzoxadiazol-4-yl]amino]ethyl]2, 5dihydro-1H-pyrrole-2, 5-dione (NBD-maleimide). It is the product of the reaction NBD-Cl (0.092g) treated with ethylamine maleimide (0.091g) and triethylamine (0.010g) in acetonitrile (0.615g) at room temperature, it was observed that the reaction yielded better after 50°C heating for *ca.* 2 hours. Both chromophores in this experiment are designed to tether onto the thiol groups pertaining to the cysteine amino acids, and thus peptides containing two cysteine amino acids at the N and C termini were chosen, in this instance CAKAK, CAADAAEAA and CAADAAEAAC. The chromophores were grafted individually onto the peptides, the 5-maleimido-eosin (eosin) first followed by the NBD-maleimide. The reaction conditions were as followed: a stock solution of CAKAC was prepared in water (1.3mg/ 1ml, 2.6M). A 60µl aliquot of this stock solution was taken and treated with 30µl NH<sub>4</sub>OH (1 mM) and 20µl eosin (~0.015mM) in 390µl distilled H<sub>2</sub>O. To facilitate dilution, eosin was dissolved in DMSO prior to further work up (2mg/200µl). Then this mixture was treated with 30 µl NBD-maleimide (~0.01mM). It is important to note that it is highly improbable for the chromophore to tether to the carboxylic and amide moieties of the peptides as the thiol groups are more competitive and tend to prohibit further chromophore grafting. The other peptides were uniformly treated to give doubly grafted species.

### 6.1.3 Results and discussion

Several physicochemical events are involved in action-FRET: the resonant energy transfer itself, as well as the competing radiative and nonradiative relaxation mechanism of both acceptor and donor chromophore pair. In order to observe FRET in solution [7], the chromophores must have clearly resolved absorption bands and there must be significant overlap of the donor fluorescence spectrum and acceptor absorption spectrum also as understood from above sections of this manuscript and that this condition consistently carries to the gas phase.

Moreover, the resonant energy transfer must happen on a shorter time scale than the relaxation of the donor chromophore. Similar constraints exist for action-FRET in the gas phase, with the additional constraints that the acceptor chromophore must have a fragmentation pattern that is specific to laser induced dissociation (LID) and different from statistical fragmentation that occurs after heating (for example, by CID or IRMPD). Therefore, acceptor fragmentation must happen on a shorter time scale than fluorescence and the statistical redistribution of the energy over the entire molecule. Indeed, by analyzing EosinY-Cystein we confirm that LID and CID show distinctive fragmentation pathways both with their own corresponding major fragment ions, Figure 6.1.1. Note that photo-electron detachment is a unique fragmentation channel to LID and that this is not observable in the analogue CID fragmentation pathway. From the CID panel, our understanding is that from the parent,  $m/z$  285.09, EosinY-Cystein 3- dissociates to yield; EosinY 2-,  $C_{24}H_{11}Br_4NO_7S^{2-}$ ,  $m/z$  370.09; a reduced EosinY-Cystein 3-variant with a cleaved S-C bond,  $C_{24}H_{11}Br_4NO_7^{3-}$ ,  $m/z$  258.09 and Cystein 1-,  $C_3H_6NO_2S^-$ ,  $m/z$  120.17. Critically, from the LID panel it is evidenced that the parent,  $m/z$  286.67 ratio, EosinY-Cystein 3- photo-dissociates to give its electron detached species; EosinY-Cystein 2-,  $C_{27}H_{18}Br_4N_2O_9S^{2-}$ ,  $m/z$  430.09 and a close similar  $C_{26}H_{17}Br_4N_2O_7S^-$ ,  $m/z$  408.09. Attention should be brought to the difference in mass of the parent in this figure between the top and lower bottom panels. The difference is due to an effect of the isolation conditions and the lasing that has an influence on the isotopic distribution. This however remains a subject to debate.

Thus, in the doubly grafted species, by monitoring the photodetachment, we conclude that the observation of two absorption bands is due to FRET. It is also important to show the amenability of both donor and acceptors to work as a FRET pair. Figure 6.1.2 shows the action spectra for mass-selected (eosin 1- ), (eosin2-) and NBD-maleimide grafted to a cysteine amino acid (NBD-Cys).

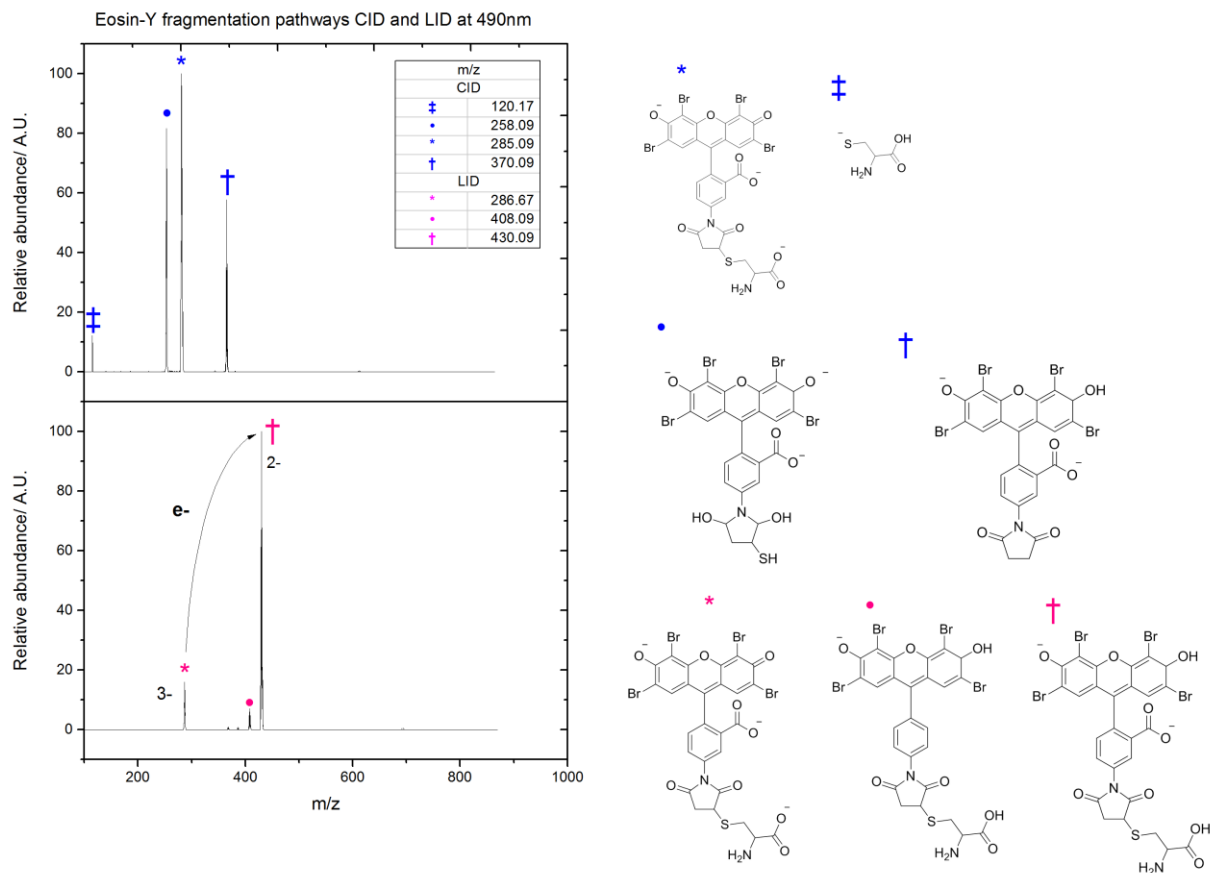


Figure 6.1.1. Eosin-Y cystein negative mode fragmentation pathways, CID (top) and LID (bottom) at 490nm.

As discussed previously, FRET depends on the overlap of the emission spectrum of donor chromophore and absorption spectrum of acceptor chromophore. From Figure 6.1.2 we can envision that both chromophore pairs fulfill this condition as the action spectrum effectively shows the absorption of the donor and acceptor. We can be confident that the emission Gaussian for the NBD-maleimide would be in an adequate region with respect to the measured absorption spectrum of EYM inspected in the spectrum of Figure 6.1.2.

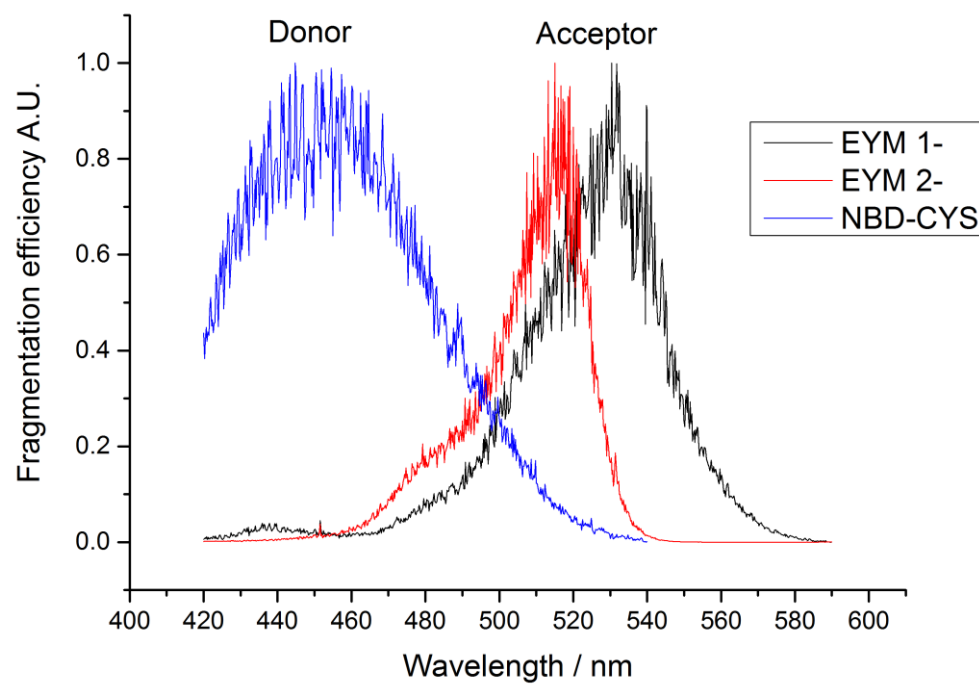


Figure 6.1.2. Action optical spectrum for EYM 1-, 2- and NBD-CYS.

The fragmentation efficiency of laser irradiation (irradiation on CAADAAEAA peptide) was then checked, the intensity of peptide ion fragments measured as a function of power showed a linear dependence suggesting that the fragmentation is a one photon process, see Figure 6.1.3.

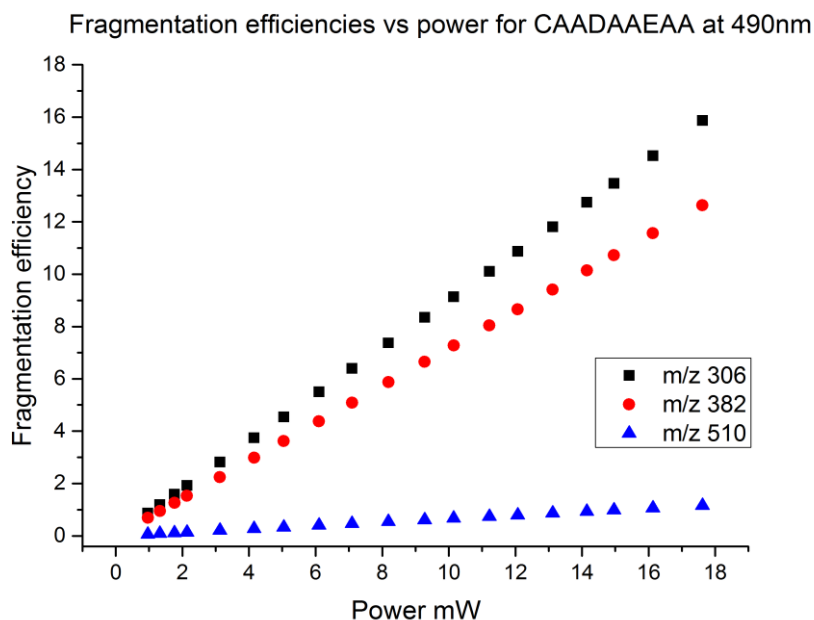


Figure 6.1.3. Linear dependence of the fragmentation of CAADAAEAA with power. A one photon process.

The suitability and amenability of the chromophore having been demonstrated, a fragmentation efficiency scan was acquired for the synthesized NBDmaleimide-CAKAC-Eosin Figure 6.1.4. Finally, EosY-CAADAAEAAC-NBDmal was synthesized and four of its negative charges states were isolated ( $m/z$  969,  $m/z$  645,  $m/z$  484 and  $m/z$  387). Mass spectra were acquired for these, five times for each charge state. The amount of electron loss was measured. The efficiency was taken as this amount of electron loss species and normalized, the values were plotted, Figure 6.1.5.

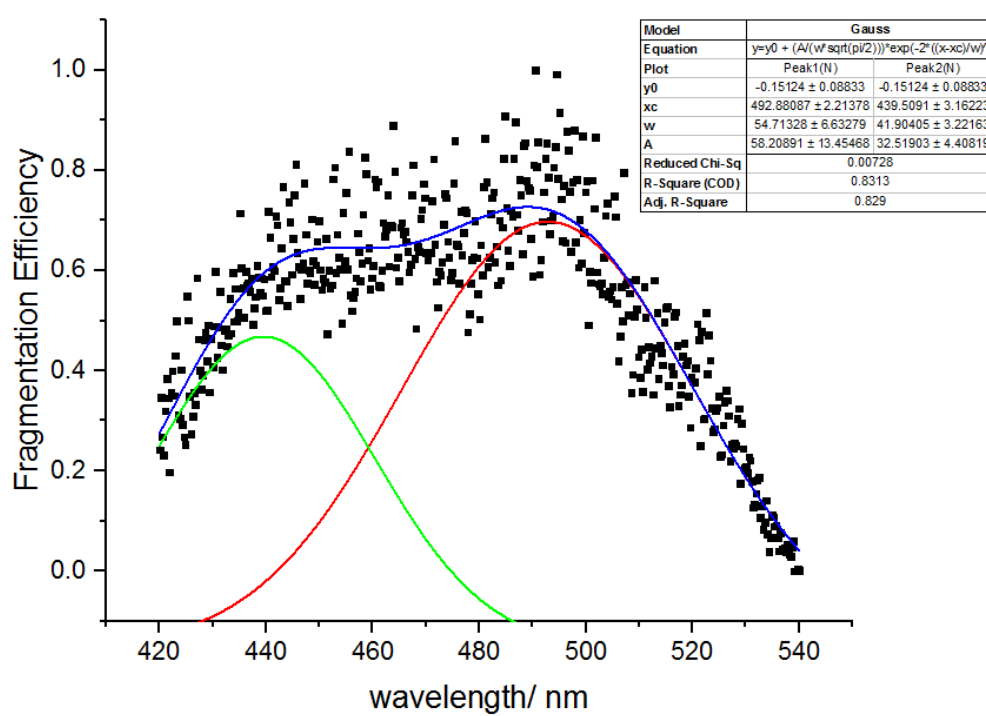


Figure 6.1.4. Action optical spectrum for NBDmaleimide-CAKAC-Eosin.

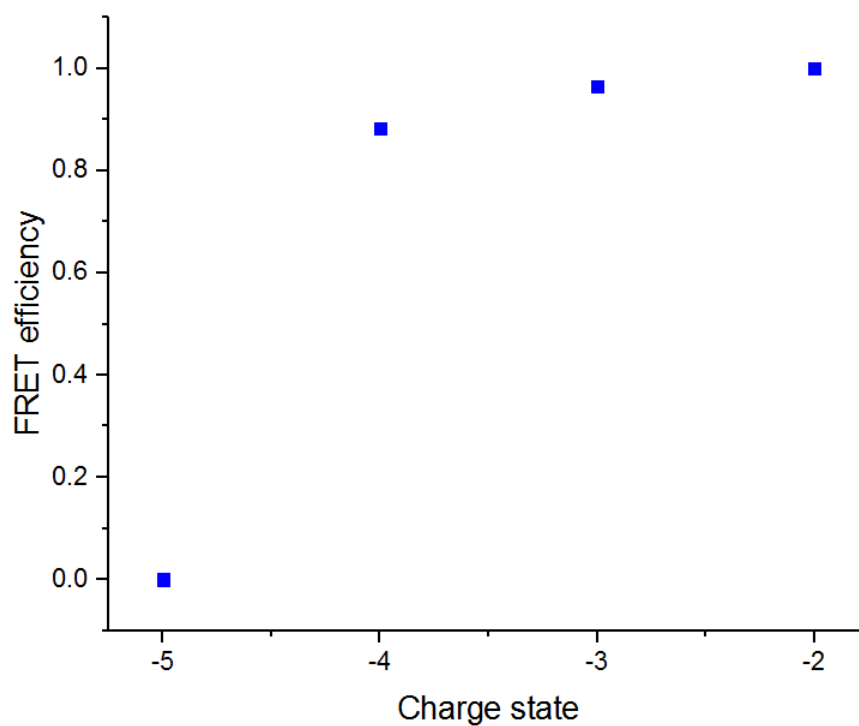


Figure 6.1.5. FRET efficiency against charge state of EosY-CAADAAEAAC-NBDmal.

#### 6.1.4 Conclusion

In this section a demonstrated feasibility of studying peptides through action-FRET in the negative mode of an LTQ velos has parthened. We first demonstrate that in the negative mode the fragmentation of EosinY-Cystein is different through LID or CID, as anticipated. The action-FRET methodology provides a significant advance in the study of the conformation and structure of gas-phase molecular ions. A clear and coherent methodology is presented on chromophore pairs for performing action-FRET in the negative regime on a peptide, which can provide a basis for future studies on other biomolecules that are of higher analytical interest in the negative mode and weakly responsive to the positive mode of a mass spectrometer's ESI. In doing so, bolstering the action-FRET approach to its full potential as both a positive and negative mode MS technique. Nevertheless, the method is difficult in that the signature fragments proved difficult to express rigorously, in sum the interest remained in establishing the negative mode technique with a QSY acceptor so to continue with a familiar integrity in signature fragmentation. Something that has been addressed and is discussed in the next sections of this chapter.

### 6.2 A case of action-FRET II in the negative mode.

Foster resonance energy transfer (FRET) has found numerous uses in structural biology, biochemistry, polymer science [8] and chemical biology for measuring proximity changes in the order of distances and dimensions pertinent to biological macromolecules and their mechanisms. To recapitulate, FRET is a non-radiative quantic transfer interaction between the excited state of a donor molecule and of an acceptor molecule. The ability to measure FRET is dependent on three conditions: i) that the donor-acceptor pair inter-distance be within range (10- to 100-Å) ii) that the absorption spectrum of the acceptor juxtaposes that of the fluorescence emission of the donor iii) that donor and acceptor transition dipole geometry must be approximately parallel. For action-FRET and its gas phase medium, disintegration must be the end fate of the acceptor chromophore so to breakdown to produce a recognizable and specific fragmentation pattern. These set of peaks are then the reporting signal of specific electronic excitation that is different from statistical fragmentation that occurs through heating (e.g. CID or IRMPD). The experiments, is devised so that the user goes on to raster laser-induced dissociation (LID) on the doubly stapled species. In this way, from triggering specific excitation (fragmentation) at each wavelength and profiling a bimodal action spectrum one can critically assess FRET. What we wish to do is to extend the earlier method of action-FRET in the positive mode [9] and transpose it to demonstrate that it works in the negative mode of the MS and that the negative action-FRET principle is possible. The results of these experiments provide evidence of negative mode reporters that are comparable to the profile of action spectra produced in the positive mode and used to evaluate FRET. It has therefore been fundamental to measure the yield of these specific photo fragments of negatively trapped species. It is also important to show that, just as in positive mode, the strength of the observed action-FRET depends on the distance between chromophores.

### 6.2.1 Materials and methods

For recordings of all spectra presented here, the average power at each wavelength is held between 30 and 32 mW.

### Chemicals

The modular molecular framework, *i.e.* QSY9-CA<sub>3</sub>DA<sub>3</sub>C-ATT0514, has been synthesized by weighing the oligopeptide (1mg) that was then made up to a 1mg/ ml solution (H<sub>2</sub>O). To this 50μl TCEP (1 μM) of the previous made up solution was used. The mixture in question had no business in needing neutralization by addition of a simple base compound. This made up solution was treated to covalent bonding with the respective dyes; using a solution of QSY9 (100μl, 100μl/1000μl H<sub>2</sub>O, ~0.01mM), using a solution of ATT0514 (40μl, 100μl/1000μl H<sub>2</sub>O, ~0.1mM). The research methodology for the other peptide constructs were tracked forward in a uniformly carried through manner.

### 6.2.2 Results and discussion

It has also been fundamental to confirm and complete a test on the optical properties of the chromophores individually without coupling to a peptide molecule. The essential information for QSY9 and ATT0514 was gathered in a Table 6.2.1 below.

Species	$\lambda_{\max}$		$\lambda_{\text{fl}}$
	Solution phase	Gas phase	Solution phase
QSY9	561	545	-
ATT0514	514	513 for bound caa	537

Table 6.2.1. Absorption maxima ( $\lambda_{\max}$ ) in the gas and solution phase and fluorescence maxima ( $\lambda_{\text{fl}}$ ) for QSY9 and ATT0514 where available.



Figure 6.2.1 depicts the donor (ATTO514) action spectrum and acceptor (QSY9) action spectrum, with a maximum at 546nm. Interestingly, the results show a very slight overlap, suggesting that both chromophore function as a FRET pair for negative mode in gas confinement.

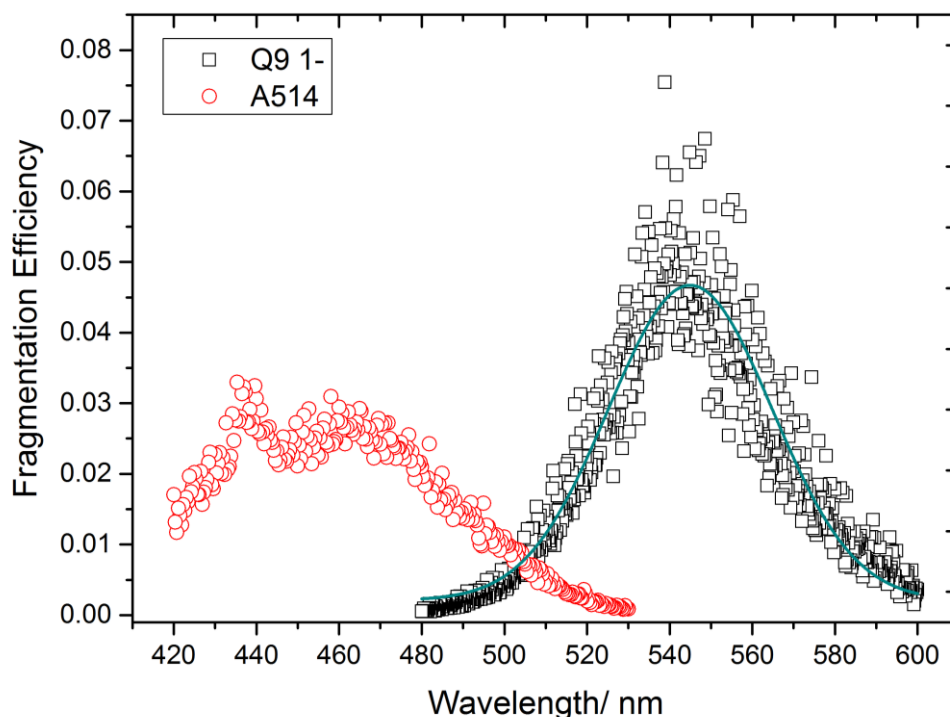


Figure 6.2.1. Optical action spectra of [ATTO514]<sup>-</sup> and [QSY9]<sup>-</sup>.

Figure 6.2.2 shows the action spectra of the chromophore this time tethered to a tripeptide. The species for mass selection are (ATTO514-CAA)<sup>-</sup> and (QSY9-CAA)<sup>-</sup> and are measured as total fragmentation yield. Figure 6.2.3 is available for comparison as to show that the absorption profile of the ATTO514 species (as in solution) stays globally the same irrespective of i) its phase (gas or liquid) ii) it being covalently bound to a tripeptide. It is also purposefully included so to confirm that its emissive profile overlaps with that of the absorption region of the acceptor, QSY9. Back on Figure 6.2.2, it is noteworthy to mention that the differences in the amplitudes of the fragmentation yield of the two chromophores is due to competition with other relaxation pathways. This is predominantly marked with the fragmentation profile of (ATTO514-CAA)<sup>-</sup> as this chromophore competes with fluorescence as the relaxation channel as opposed to total relaxation via fragmentation. On the flipside with, (QSY9-CAA)<sup>-</sup>, the dye component is QSY9, a quencher, fluorescence is not available instead fragmentation is favored. As expected, the action spectra profile is characteristic of efficient fragmentation and relaxation via the latter. Importantly, in conclusion of the action spectrum, ATTO514 and QSY9 satisfy the first condition required for FRET: that the absorption bands are clearly distinguished, with absorption maxima  $\lambda_D = 510\text{nm}$  and  $\lambda_A = 545\text{nm}$ , respectively.

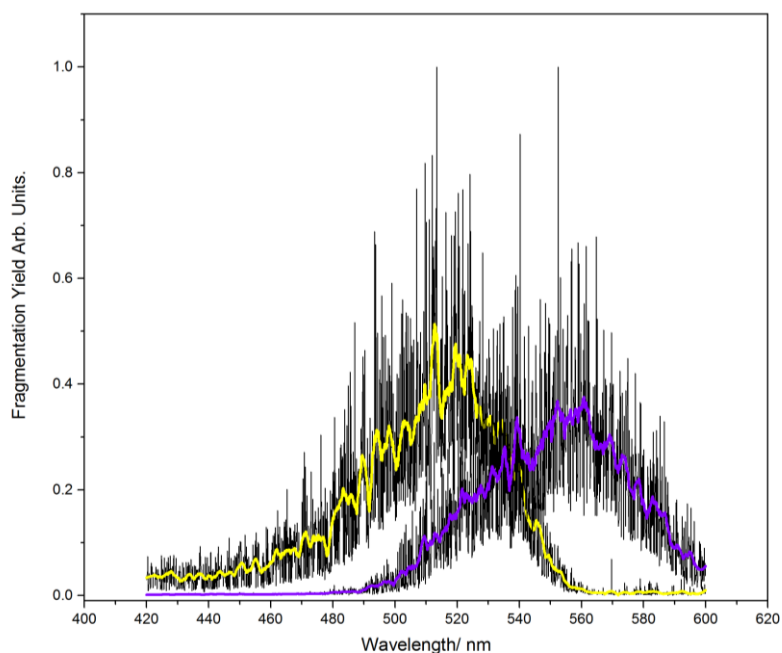


Figure 6.2.2. ATTO514-CAA (yellow curve) and QSY9-CAA (purple curve) normalized optical spectra.

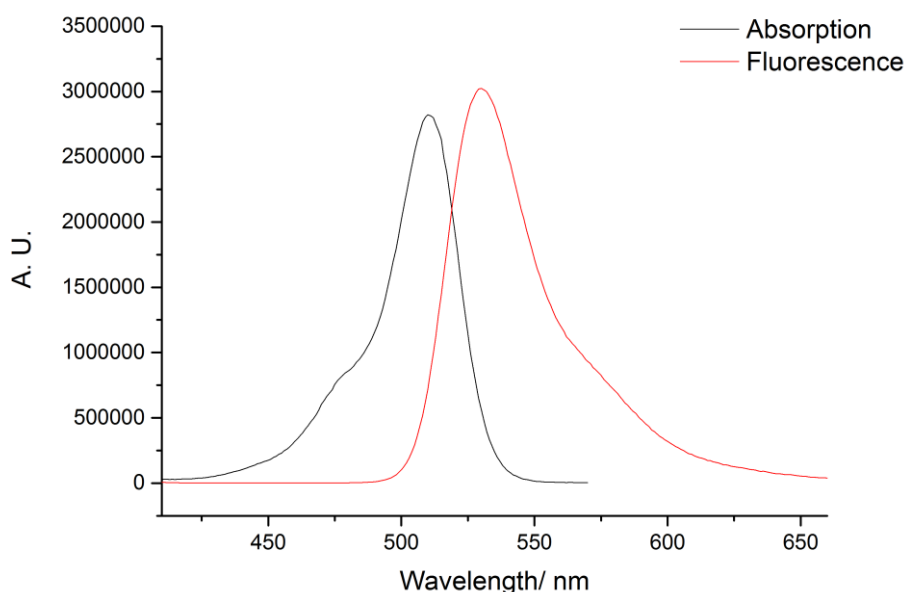


Figure 6.2.3. Excitation and emission spectrum for ATTO514 in solution.

On inspection, a dip or shoulder (*ca.* 475nm) in the fragmentation efficiency curve for ATTO514 can be observed. This is indicative that the chromophore alone has a stronger propensity to fluoresce, typical of fluorophores that exhibit high fluorescence quantum yields *cf.* experimental results [10]. Secondly the dip could be taken as an artefact of the measurement, as research in the laboratory has pointed out that action-spectra is not of most desirable quality for recovering the true absorption spectrum of fluorescent dyes *cf.* results and discussion to publication [11]. Some given understanding on this shoulder is understood, plausibly, it increments

proportionally to concentration [12]. Alternatively, it is due to a vibrational progression, this claim is supported with the observations reported for gas phase photophysics of another fluorescent and an assimilation of the literature. The converging understanding is that the shoulder's manifestation is due to a vibrational progression connected with the nature of the xan-thene ring system and has more exactly to do with the intrinsic property of the  $S_1 \leftarrow S_0$  transition of this one [13].

In a second part it has been important to consider how both chromophore work together, interrelated as a dimer and see how absorption and optical profile changed versus in isolation. These results are presented in Figure 6.2.4.

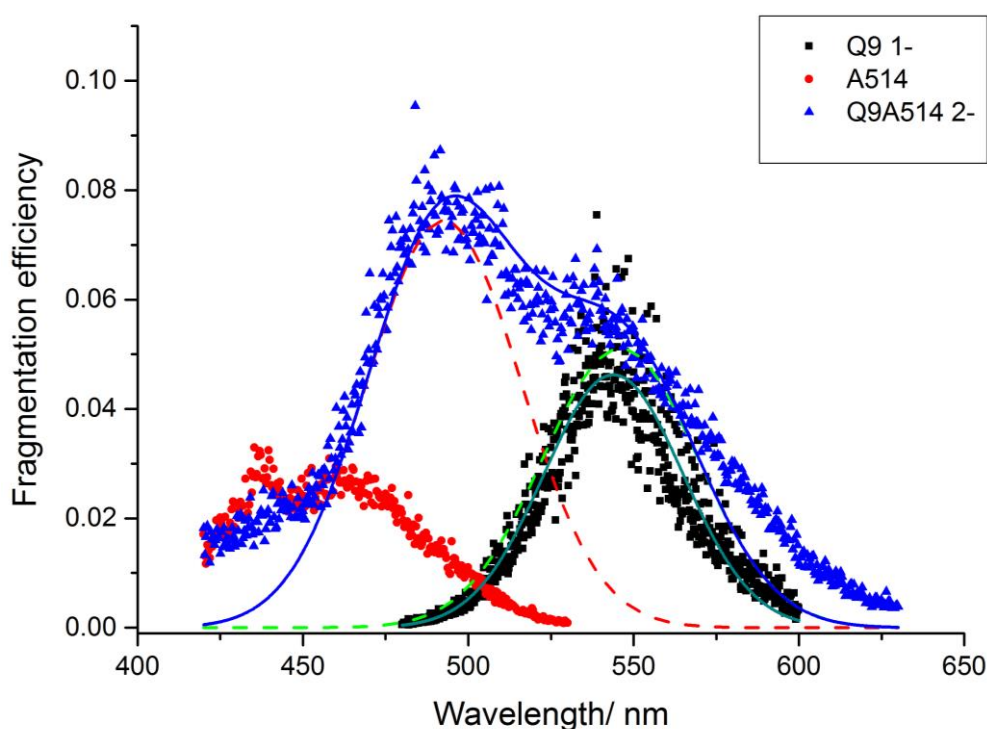


Figure 6.2.4. Optical absorption spectra of  $[\text{ATT0514}, \text{QSY9}]^{2-}$  dimer overlaid against optical absorption spectra of  $[\text{ATT0514}]^{-}$  and  $[\text{QSY9}]^{-}$ .

These results demonstrate that the ATT0514 chromophore rather than it characteristically fluorescing unreservedly as it is alone, switches to a relaxation regime of fragmentation when engaged to another species (in this instance as a dimer with QSY9). The more pronounced band (blue scatter points) with a maximum at 492nm is in effect the basis of ATT0514 relaxing the surplus energy (via IVR or FRET) by fragmentation (dissociation) of the [ATT0514,QSY9]<sup>2-</sup> dimer. The suite of the photophysical absorption pattern captures a second band, the response of QSY9 that remains systematically unperturbed (maximum 546nm) in its function as a quencher as can be seen by the overlap of a second band, 546nm and the optical spectra of QSY9 alone, 543nm (*cf.* Figure 6.2.4). In summary, these results have led to the useful understanding that i) A514 is fluorescent in the gas phase ii) absorption spectrum bands are well spaced and validate the principle that both chromophores can function as a FRET pair in the negative mode.

To test that the fragmentation observed for the acceptor chromophore is LID-specific so that one can discriminate the origin of the excitation, mass spectra was acquired. Figure 6.2.5 reveals that the mass spectra of mass-selected (QSY9-CAA)<sup>-</sup> following LID at  $\lambda_A = 545\text{nm}$  (top) and in a second part shows the CID mass spectra of (QSY9-CAA)<sup>-</sup> (bottom). On inspection it is clear that there lies a different pattern depending if heating or electronic excitation is featured. The fragment species in CID correspond to fragmentation of linking moiety of the peptide-chromophore framework. In the case of LID, the mass spectrum is typified by  $m/z$  980 fragments and  $m/z$  625 and other daughter fragments of the latter, which are associated to the scission of the S-C bond alone or/and cleavage at the sulfonamide connecting the xanthene group. The data also suggest a simultaneous cleavage of the sulphone side chain, see Figure 6.2.5 a) and b). The fragments can be referred to their structural composition in the Table 6.2.2 below, see Table 6.2.3 and review also Figure 6.2.6. These mentioned fragments are not observed at all or in the same proportionality as with LID, and their observation is hence a clear signature that QSY9 has been electronically promoted. It therefore entails that it is possible to follow FRET by measuring the relative intensity of these fragments as a function of wavelength for the doubly grafted peptides.

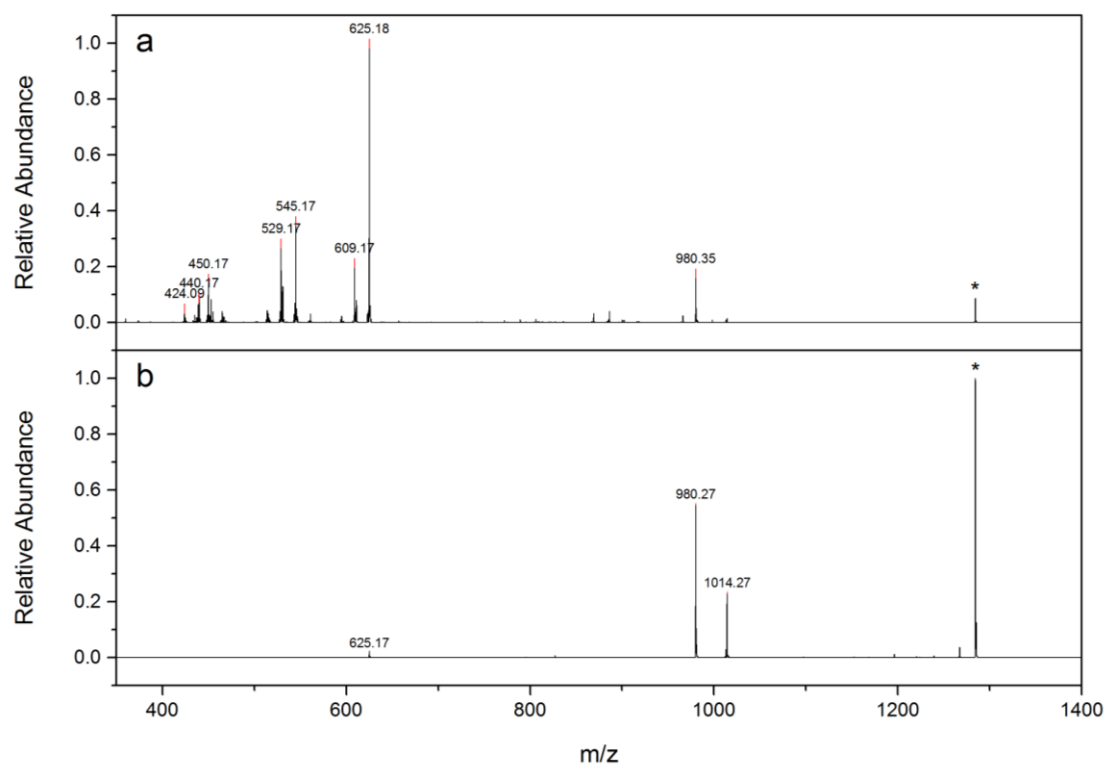


Figure 6.2.5. a)  $[QSY-CAA]^-$  LID 545nm  $m/z$ 1284 Power: 30mW b)  $[QSY-CAA]^-$  CID  $m/z$ 1284, (normalized collision energy 20).

$m/z$	Loss	Relative Intensity		Assignment
		CID	LID	
1284.5	0	1	0.087	Parent
1014.3	270.3	0.23	-	QSY9-SH and peptide breakoff
980.4	304.2	0.55	0.18	QSY9
625.2	659.4	0.018	1	C - S bond break from the chromophore
609.2	675.4	-	0.20	C-S break + side chain loss + reduction of $\text{SO}_3 \rightarrow \text{SO}_2$
545.2	739.4	-	0.36	C-S break + side chain loss
529.2	755.4	-	0.18	N-C break + heavy side chain loss and re-arrangement
450.2	834.4	-	0.16	C-S break + heavy side chain loss
440.2	844.4	-	0.073	C-S break + heavy side chain loss
424.1	860.4	-	0.031	C-S break + heavy side chain loss + reduction

Table 6.2.2. The fragmentation species.

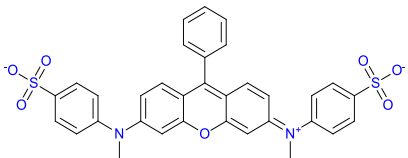
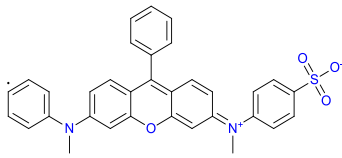
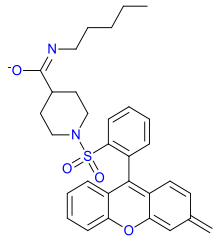
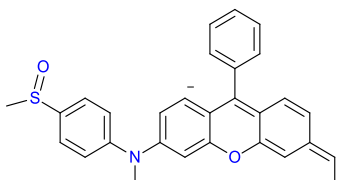
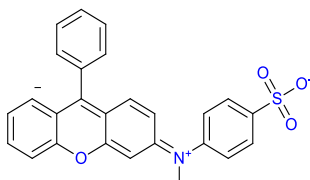
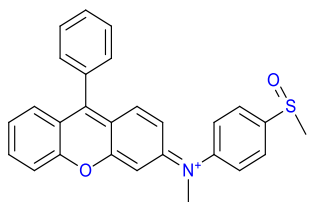
breakdown I	breakdown II	breakdown III
 <p>Exact Mass: 625.11</p>	 <p>Exact Mass: 545.15</p>	 <p>Chemical Formula: <math>\text{C}_{31}\text{H}_{33}\text{N}_2\text{O}_4\text{S}^-</math> Exact Mass: 529.22</p>
breakdown IV	breakdown V	breakdown VI
 <p>Exact Mass: 451.16</p>	 <p>Exact Mass: 441.10</p>	 <p>Exact Mass: 424.14</p>

Table 6.2.3. The structures of the breakdown species.

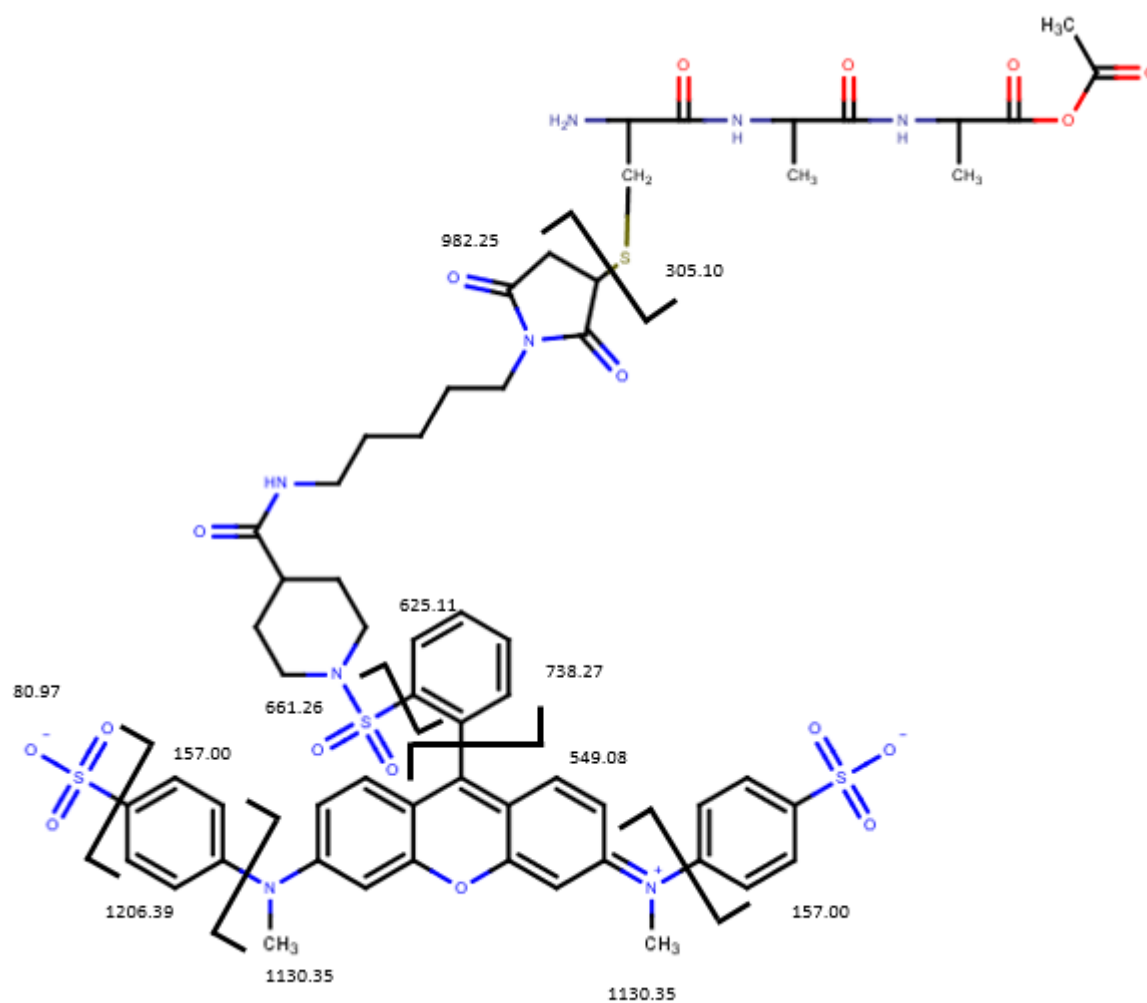


Figure 6.2.6. Bond breaking sites of QSY9 molecule.

It is also noteworthy to test whether the specific photofragment ( $m/z$  625) detaches at the same wavelengths to where the QSY-CAA<sup>-</sup> parent absorbs and fragments. This is verified together in Figure 6.2.7 and from inspection suggests that specific photofragmentation ( $m/z$  625 detachment) is proportional to absorption from the QSY-CAA<sup>-</sup> parent.

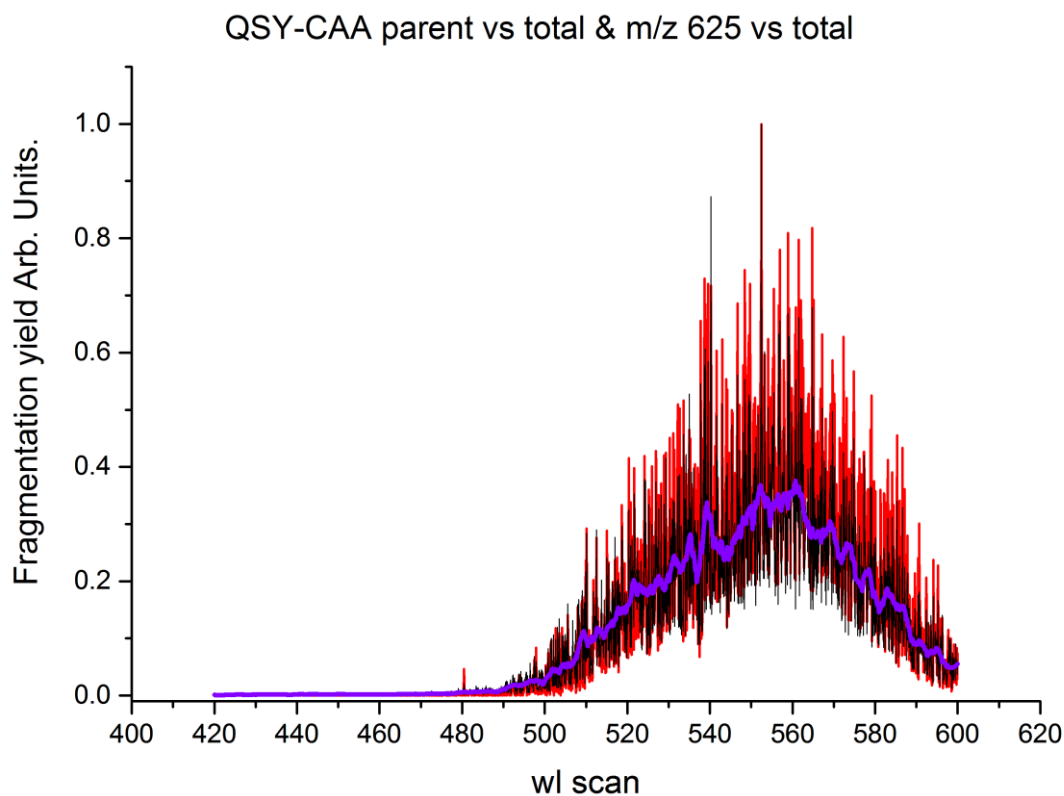


Figure 6.2.7. Comparing the [QSY-CAA]<sup>-</sup> spectra:  $m/z$  625 (red), parent signal (black) smoothed parent signal (purple curve).



From the following study of the  $[\text{ATTO514}, \text{QSY9}]^{2-}$  species it was observed that at unique wavelengths atuned with the excitation and absorption region of the QSY9 quencher, photospecific fragment of QSY9 emerged (magenta triangles). This manifestation can be observed in the experimental results presented in Figure 6.2.8. (magenta triangles). The distinct fragmentation study also confirms as expected that there is no response that could be associated to ATTO514 fragmentation.

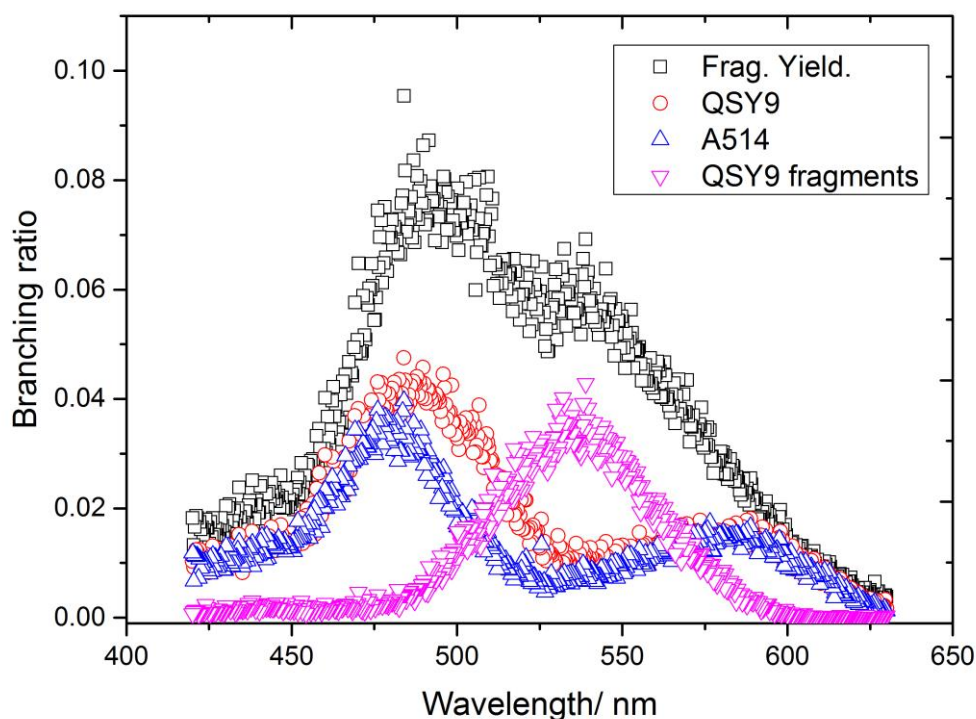


Figure 6.2.8. Branching ratio of the fragmentation efficiency associated with  $[\text{ATTO514}, \text{QSY9}]^{2-}$ , QSY9 (red circles), ATTO514 (blue triangles) and QSY9 photospecific fragments (magenta triangles).

Figure 6.2.9 shows the result of the action spectrum for mass selected (ATTO514-CAC-QSY9)-, conferred only by the  $m/z$  625 LID-specific acceptor fragment noted above. This figure is also arranged with the recording, in the lower panels, of the LID triggered loss of the chromophores and related fragments that are products to heating (*i.e.*  $m/z$  980, and 874). Figure 6.2.10 and Figure 6.2.11 shows the result of the action spectrum for mass selected (ATTO514-  $\text{CA}_3\text{DA}_3\text{C}$  -  $\text{QSY9}$ )<sup>2-</sup> and (ATTO514-  $\text{CA}_3\text{DA}_3\text{C}$  -  $\text{QSY9}$ )<sup>3-</sup>. If there were no energy transfer, the same action spectrum as the one for QSY9 would be expected. Inkeeping with the hypothesis, there are clearly two bands present in the spectrum: one at 545nm emerging in response to the absorption of the acceptor chromophore, and one at 505nm matching with the absorbing region of the donor chromophore. Observation of the donor chromophore absorption band via measurement of fragments specific to electronic excitation of the acceptor chromophore serves in supporting that electronic energy transfer has come about. Furthermore, it is clear that when looking at the fragments that are other than  $m/z$  625 (*i.e.*  $m/z$  980, 874), their profile and positioning is the same as for the respective action spectra revealed in Figure 6.2.8. This confirms that the  $m/z$  980 and  $m/z$  874 species are a result of IVR heating relaxation.

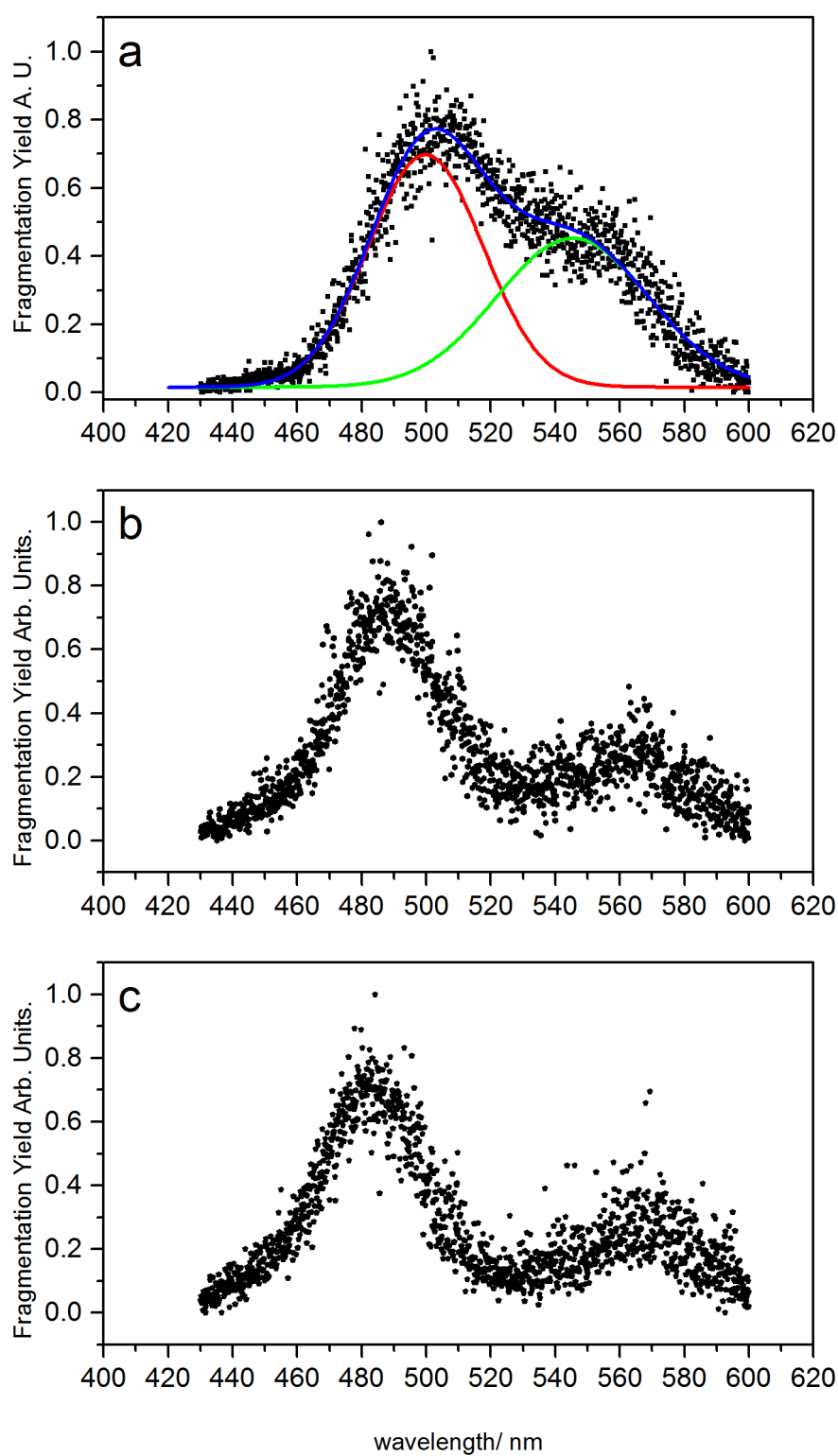


Figure 6.2.9. a) d-CAC-a ( $2^-$ ) normalized optical spectra reserved to the  $m/z$  625 specific photofragment b) loss of QSY9  $m/z$  980 c) loss of ATT0514  $m/z$  874.

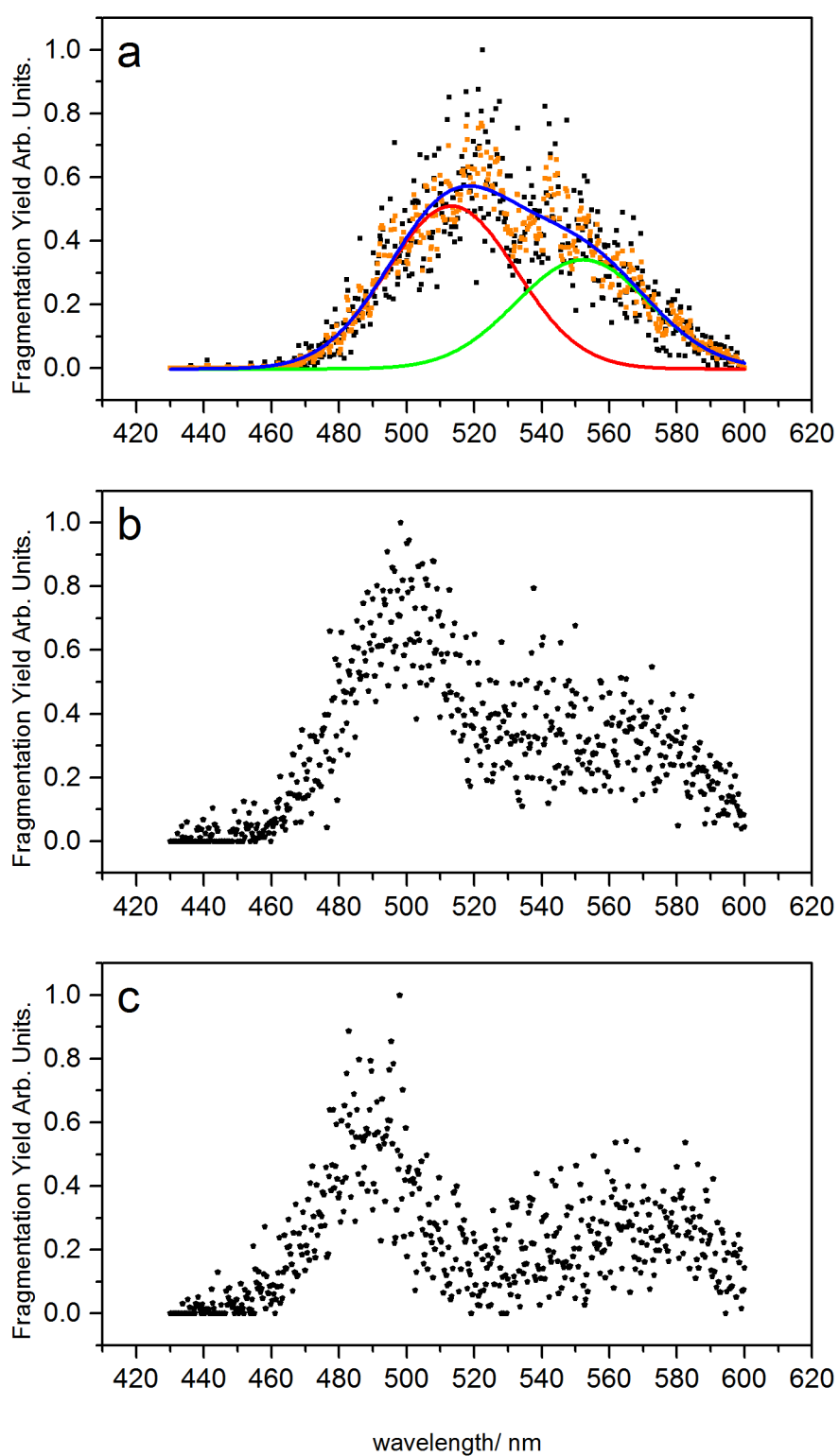


Figure 6.2.10. a) d-CA3DA3C-a (2-) normalized optical spectra reserved to the  $m/z$  625 specific photofragment (black), three point averaging (orange), b) loss of QSY9  $m/z$  980 c) loss of ATT0514  $m/z$  874.

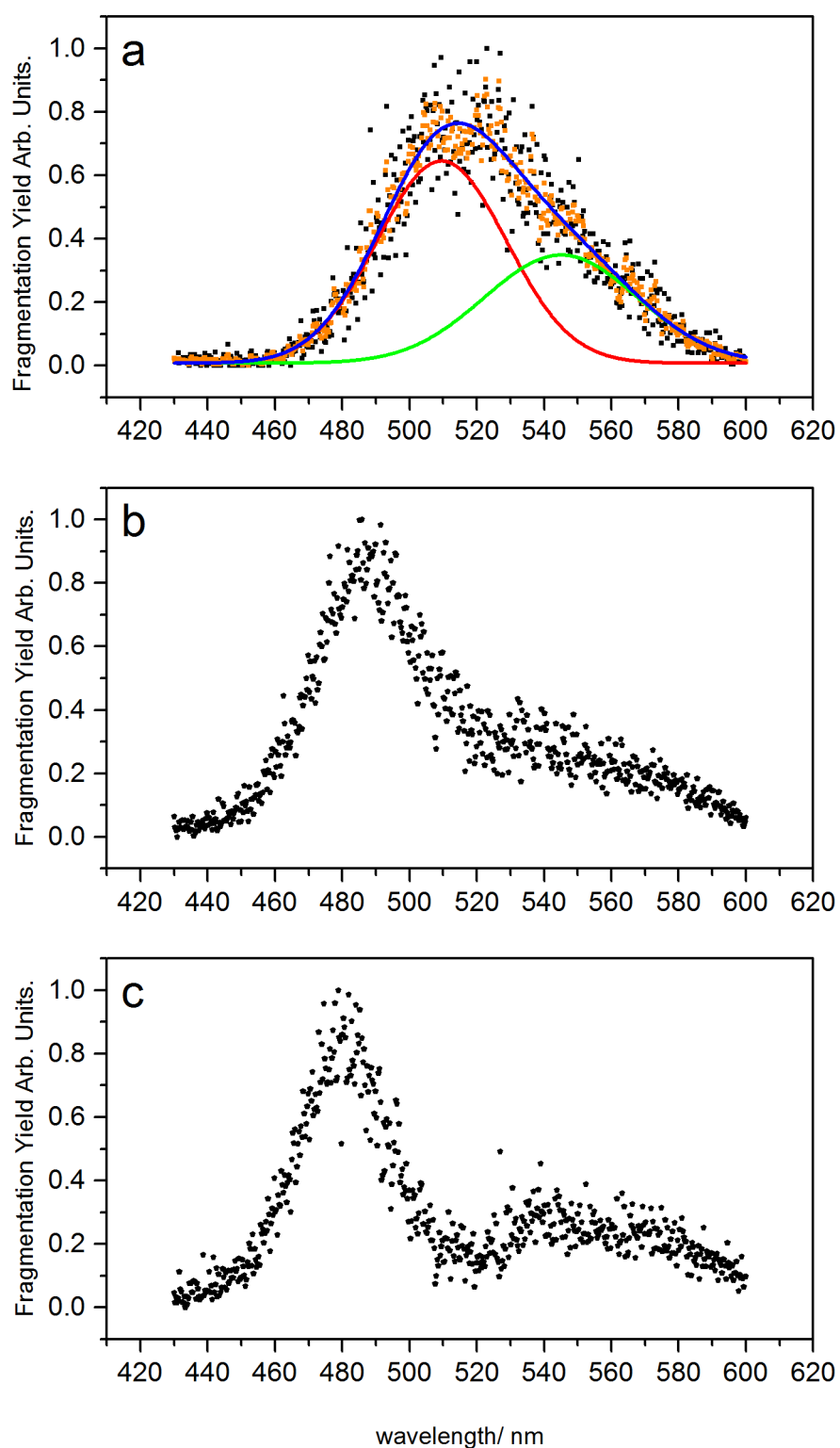


Figure 6.2.11. a) d-CA<sub>3</sub>DA<sub>3</sub>C-a (3-) normalized optical spectra reserved to the  $m/z$  625 specific photofragment (black), three point averaging (orange), b) loss of QSY9  $m/z$  980 c) loss of ATT0514  $m/z$  874.

In keeping with our previous convention, FRET efficiency is defined as  $A^{(505\text{ nm})}/A^{(545\text{ nm})}$ . It is important to understand that as the size of the studied molecular frameworks increases, there is increasing competition between IVR and the photofragmentation path route. As a consequence, the average LID-specific fragmentation intensity can be expected to decrease relative to the intensity of the statistical fragments. This rivalry in the relaxation route: IVR or photofragmentation will exist from onset that the energy is localized on the acceptor chromophore no matter the source of the energy: photofragmentation as a result of FRET or a direct excitation of the acceptor. Hence, if the FRET-mediated photofragmentation of the acceptor chromophore is normalized by direct photofragmentation, an IVR-independent quantification of action-FRET can be posited. This feasibility, as with previous studies on action-FRET is proven by comparing the peak areas of donor and acceptor absorptions. This ratio then serves to score a measure of FRET efficiency. See Table 6.2.4. Values of FRET efficiency were calculated for these species. This feedback provides the evidence that the short peptide fragment gives a relative 'high' FRET efficiency because and as expected the short peptide colocalises the chromophore dyes in close spatial proximity. Contrary to our expectation however is that the  $[\text{d-CA}_3\text{DA}_3\text{C-a}]^{3-}$  molecular framework yields more FRET efficiency than its minor charged homologue  $[\text{d-CA}_3\text{DA}_3\text{C-a}]^{2-}$ . Theories posited for explaining such results include that the higher charge state specimen holds a bent conformation that brings both FRET pairs in close spatial proximity and overcomes a certain coulombic repulsion. One also needs to take in that due to the high  $\pi$  character of the chromophores it is suggestive that  $\pi$ - $\pi$  stacking are at play. Furthermore, it is possible that auto-solvation effects, favored from the confinement of the analyte that, are in place that possibly acquire the molecular framework greater strength to take a close conformation and overcome coulombic repulsive interaction. This then supports the appraisal of the peptide and chromophores to bundle closely together and produce FRET. Another way to understand the results is that autofragmentation (the analogue to autofluorescence) is occurring, (*i.e.* the acceptor chromophore disintegrates) as a result of direct irradiation from the coherent light of the solid-state laser. Part of this study also aimed at taking the doubly grafting species in for IMS analysis. After first having checked their isolation in the LTQ Velos, the sample was taken to the IMS source for auscultation. Unfortunately the desired species, *i.e.*  $[\text{d-CA}_3\text{DA}_3\text{C-a}]^{3-}$  and  $[\text{d-CA}_3\text{DA}_3\text{C-a}]^{2-}$ , were not detected in sufficient spectral quality: no peak ticked up on the  $m/z$  spectrum. A meaningful signal of spectral quality was visualised however for  $[\text{Q9-CA}_3\text{DA}_3\text{C-Q9}]^{2-}$  and  $[\text{Q9-CA}_3\text{DA}_3\text{C-Q9}]^{3-}$  and their CCS spectra were acquired, Figure 6.2.12. Valuable information can be derived from this spectrum: their CCS values which indicate the size of the frameworks, if they are more globular or extended. It was noticed that the 2-charged species arrives after a longer drift time than the 3- charged species. The 3- charge state (both conformers) arrive more prematurely — at *ca.* 27.5ms and 32.5ms as they experience a higher electrical driving force than the 2- charged state species (drift time, *ca.* 40ms).

Comparing the top and bottom panel of the figure a second time, both charged species show subtle differences in the sizes of each of their conformers but stay grossly of same dimensionality. What transpires is that the lower charged state is marginally more compact ( $459\text{ \AA}^2$ ) to both 3- charged molecular conformations ( $464\text{ \AA}^2$ ,  $564\text{ \AA}^2$ ). Altogether, the data implicates that both species have the same conformational shape. It can then be implied that a FRET efficiency

for the CA<sub>3</sub>DA<sub>3</sub>C peptide would be relatively the same irrespective of charge state, no big change would be expected in FRET efficiency. Nevertheless, one could also estimate that this would not be the case, as it could be measured and checked by taking action-spectra of the acceptor donor CA<sub>3</sub>DA<sub>3</sub>C peptide that FRET efficiency does change considerably as a function of charge state.

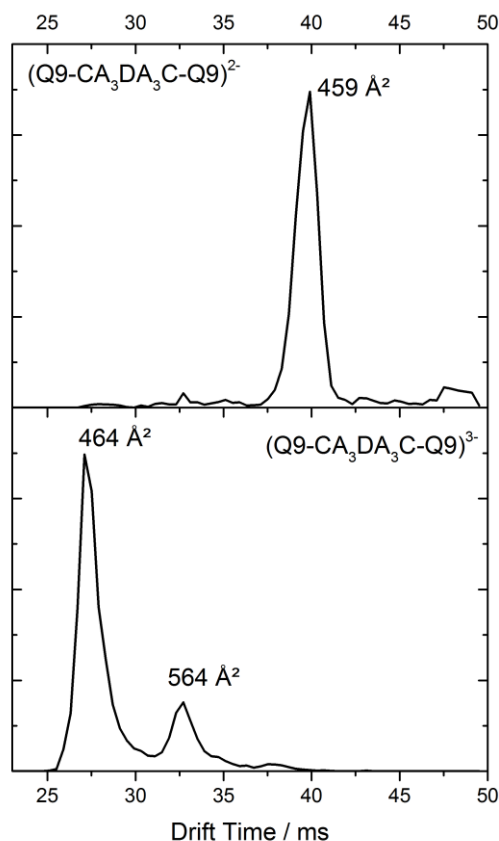


Figure 6.2.12. Mobility profiles for  $[Q9-CA_3DA_3C-Q9]^{2-}$  and  $[Q9-CA_3DA_3C-Q9]^{3-}$  conformers and their collisional cross section values.

Species	Donor			Acceptor			FRET efficiency
	$\lambda_{\text{max}}$	Height	Area	$\lambda_{\text{max}}$	Height	Area	
$[d-CAC-a]^{2-}$	499.8	0.68	30.4	545.4	0.44	25.8	1.18
$[d-CA_3DA_3C-a]^{2-}$	513.3	0.51	24.5	552.2	0.34	17.1	1.43
$[d-CA_3DA_3C-a]^{3-}$	509.5	0.64	30.8	545.1	0.34	19.6	1.58

Table 6.2.4. Peak position, height and area for donor and acceptor and the FRET efficiency scores.

### 6.2.3 Conclusion

It can be remarked that the global principal holds true, the emission spectrum of the fluorophore donor overlaps the absorption spectrum of the QSY acceptor. Upon laser irradiation this one disintegrates by direct transfer of energy into a specific photofragment among others. This can then be measured quantitatively so to gain an insight on the interdistance separating the chromophores and thus develop a structural description of the whole system. This technique has proven more rewarding in resolving proximity relationships than the previously discussed NBDmaleimide –Eosin donor-acceptor pair of frameworks but however remains inferior to the positive mode based action-FRET technique. The principal reason being that the donor chromophore does not dissociate during the photophysical interaction with laser irradiation as much.

### 6.3 Outline on encountered difficulties.

The task of establishing action-FRET as a technique remains difficult and is not always as straightforward, robust or reproducible in results as anticipated to be, negative mode action-FRET more so than action-FRET in the positive mode. As science progresses by corroboration there were times where false leads were being pursued or had the impression to be pursued. These difficulties were ausculted and in multiple cases emerged to be a combination of issues. These experienced pitfalls and observations that hampered the undertaking majorly all revolved around signal treatment and are summarized here and include:

- The operational setting of the MS tune to detect a given distribution of species.
- Intermittent loss of signal or severe signal fluctuation.
- Loss of the signal from specific LID fragmentation due to laser dissaligement.

Other encountered undesirables and challenges include:

- Laser power fluctuations.
- Weak response from the acceptor or/ and no observation of its fragmentation. Instead a total observation of its cleavage from the bonding site to where it was intended to permanently bind to, *i.e.* dissociation from the mercaptan group.
- The observation of electronic effects that induce major bathochromic shifts, changes to the optical properties of the molecular species.
- Variations in the form, quality of ordered compounds, and the principal substrate in building doubly labeled frameworks.
- Solubility and spraying of the compounds (experience of capillary fouling or even blockage).

## 6.4 References :

1. Baer T, Dunbar RC: **Ion Spectroscopy: Where Did It Come From; Where Is It Now; and Where Is It Going?** *Journal of the American Society for Mass Spectrometry* 2010, **21**:681-693.
2. Daly S, Kulesza A, Knight G, MacAleese L, Antoine R, Dugourd P: **Visible and Ultraviolet Spectroscopy of Gas Phase Rhodamine 575 Cations.** *Journal of Physical Chemistry A* 2015, **119**:5634-5641.
3. Daly S, Kulesza A, Knight G, MacAleese L, Antoine R, Dugourd P: **Visible and ultraviolet spectroscopy of gas phase rhodamine 575 cations.** *The journal of physical chemistry A* 2015, **119**:5634-5641.
4. Sassin NA, Everhart SC, Dangi BB, Ervin KM, Cline JI: **Fluorescence and Photodissociation of Rhodamine 575 Cations in a Quadrupole Ion Trap.** *Journal of the American Society for Mass Spectrometry* 2009, **20**:96-104.
5. Chingin K, Chen HW, Gamez G, Zenobi R: **Exploring Fluorescence and Fragmentation of Ions Produced by Electrospray Ionization in Ultrahigh Vacuum.** *Journal of the American Society for Mass Spectrometry* 2009, **20**:1731-1738.
6. Frankevich V, Chagovets V, Widjaja F, Barylyuk K, Yang ZY, Zenobi R: **Fluorescence resonance energy transfer of gas-phase ions under ultra high vacuum and ambient conditions.** *Physical Chemistry Chemical Physics* 2014, **16**:8911-8920.
7. GarzonRodriguez W, SepulvedaBecerra M, Milton S, Glabe CG: **Soluble amyloid A beta-(1-40) exists as a stable dimer at low concentrations.** *Journal of Biological Chemistry* 1997, **272**:21037-21044.
8. Ha T, Enderle T, Ogletree DF, Chemla DS, Selvin PR, Weiss S: **Probing the interaction between two single molecules: Fluorescence resonance energy transfer between a single donor and a single acceptor.** *Proceedings of the National Academy of Sciences of the United States of America* 1996, **93**:6264-6268.
9. Daly S, Poussigue F, Simon AL, MacAleese L, Bertorelle F, Chirot F, Antoine R, Dugourd P: **Action-FRET: Probing the Molecular Conformation of Mass-Selected Gas-Phase Peptides with Forster Resonance Energy Transfer Detected by Acceptor-Specific Fragmentation.** *Analytical Chemistry* 2014, **86**:8798-8804.
10. Arden J, Deltau G, Huth V, Kringel U, Peros D, Drexhage KH: **Fluorescence and lasing properties of rhodamine dyes.** *Journal of Luminescence* 1991, **48-9**:352-358.
11. Kulesza AJ, Titov E, Daly S, Wlodarczyk R, Megow J, Saalfrank P, Choi CM, MacAleese L, Antoine R, Dugourd P: **Excited States of Xanthene Analogues: Photofragmentation and Calculations by CC2 and Time-Dependent Density Functional Theory.** *Chemphyschem* 2016, **17**:3129-3138.
12. Rodriguez HB, San Roman E, Duarte P, Machado IF, Ferreira LFV: **Eosin Y Triplet State as a Probe of Spatial Heterogeneity in Microcrystalline Cellulose.** *Photochemistry and Photobiology* 2012, **88**:831-839.
13. Daly S, Kulesza A, Knight G, MacAleese L, Antoine R, Dugourd P: **The Gas-Phase Photophysics of Eosin Y and its Maleimide Conjugate.** *Journal of Physical Chemistry A* 2016, **120**:3484-3490.





## Chapter 7 Future developments.

### 7.1 Conclusion and general perspectives

#### 7.1.1 Conclusion

What this redaction looks to do is to transpose all of the experimental works and the results into writings and figures. By this way it is taken that the research on Action FRET: Probing the molecular conformation of gas phase proteins and protein assemblies. The dissertation's main research objective is to better understand the structure and conformations of peptides and proteins and how these are affected by their charge state. Towards this end, we have developed a coupled LASER mass spectrometry spectroscopy interface. This enables the use of laser spectroscopy to probe of the conformation of trapped ions. Gaseous ions are formed using electrospray ionization (ESI) and interact photo-physically through a pair of chromophores in a linear ion trap. With this setup, we can study the photophysics of the trapped ions, to select the species of interest and to isolate it by ejecting all others. This feature allows us to individually probe the peptides labelled with only the donor dye, only the acceptor or species with both dyes grafted on. It is then also possible to examine different charge states of a molecule if multiple charge states are produced in the electrospray.

The spectrometric evolution of the breakdown on the acceptor as a function of power and wavelength, what is coined as action-FRET was then monitored. This herein developed technique was taken to study a biomolecule of biological interest: first ubiquitin and then the amyloid beta protein. It has also provided real term answers to the structural arrangement of an amyloid protein segment in a host-guest interaction with a cyclodextrin molecule in gas isolation. Finally, efforts were laid to test and validate the action-FRET technique in the negative mode. The research of this undertaking has come across difficulties, mainly in the synthesis and isolation of the compounds of interest needed to generate the ion products of desired charge state in the mass spectrum with sufficient spectral quality to carry out experimental manipulations. In a nutshell, the aim of this dissertation has been to demonstrate and give results on isolated species in gas isolation which has the advantage to provide an overview study of the intrinsic properties and characteristics of the system without bias, without perturbations that would have been encountered in the condensed medium. The work carried out herein is important as action-FRET provides the development of a new quantitative tool that can glean new insight on biomolecules interesting to structural biology and biochemistry which are not accessible or not as directly available when using conventional biochemical approaches.

### 7.1.3 Future developments

While this thesis has demonstrated the potential of efficiently probing the molecular conformations of gas phase species, many opportunities for extending the scope of this thesis remain. This section presents some of these directions.

#### FRET experiments with LASER-IMS.

Finding the right IMS settings to isolate doubly grafted molecules of biological interest with a donor and acceptor chromophore and taking their conformational families to LASER-IMS studies is the next step and will enable new structural information on how conformational structure, collision cross section and FRET efficiencies relate to one another.

#### Transposing single molecule FRET (smFRET) to the gas phase.

Even though we do not do single ion measurements, a second future development that springs to mind consists of devising a way to find the equivalent of smFRET to the gas phase and the confines of a MS instrument. This way it would be possible to study even further the intrinsic phenomena that is FRET with even lesser bias as smFRET would discard any ensemble effects associated to recordings of experiments of ensemble of molecules and not single species.